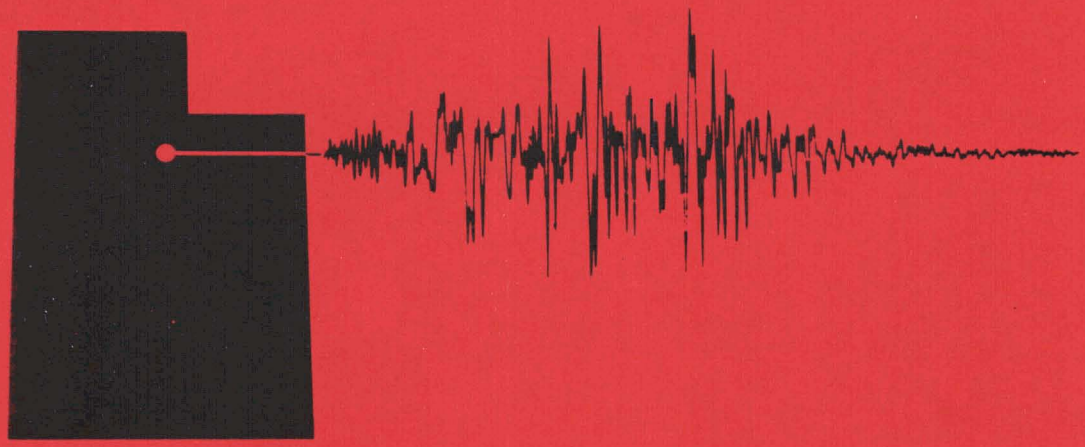

Seismotectonic Study

for
Jordanelle Dam and Reservoir Site
Central Utah Project, Utah

U. S. DEPARTMENT OF THE INTERIOR
BUREAU OF RECLAMATION
SEISMOTECTONIC SECTION
DENVER, COLORADO

SEISMOTECTONIC STUDY
FOR
JORDANELLE DAM
BONNEVILLE UNIT
CENTRAL UTAH PROJECT
UTAH

by

J. Timothy Sullivan
Richard A. Martin
Lucy L. Foley

with APPENDICES by:

Christopher K. Wood
Roland C. LaForge

SEISMOTECTONIC REPORT 88-6

Seismotectonic Section
Geologic Services Branch
Division of Geology
Denver Office
U. S. Bureau of Reclamation
Denver, Colorado

April, 1988

Prepared by:

J. Timothy Sullivan 4/14/88
Date

J. Timothy Sullivan
Geologist
Denver, Colorado

Richard A. Martin 4-14-88
Date

Richard A. Martin
Seismologist
Denver, Colorado

Lucy L. Foley 4-18-88
Date

Lucy L. Foley
Geologist
Denver, Colorado

Technical Approval by:

Dean Ostenaa 4/14/88
Date

D. A. Ostenaa
Head, Seismotectonic Section
Denver, Colorado

Reviewed by:

RB MacDonald 4-18-88
Date

R. B. MacDonald
Chief, Geologic Services Branch
Denver, Colorado

Approved by:

Steven D. Markwell 4/15/88
Date

S. D. Markwell
Chief, Division of Geology
Denver, Colorado

SUMMARY

Jordanelle damsite is located in the Wasatch Mountains within the ISB (Intermountain seismic belt) in north-central Utah. The ISB, a zone of contemporary seismicity extending from Arizona to Montana along the eastern margin of the Basin and Range province, is considered to have the highest level of earthquake risk in the contiguous United States outside of California and Nevada. Within the ISB, three historical earthquakes with magnitudes ranging from 6.6 to 7.5 have been accompanied by surface rupture on late Quaternary normal faults. Seismological evidence, largely based on network monitoring over the last 10 years by the University of Utah, demonstrates the pervasive occurrence of small- to moderate-magnitude earthquakes throughout the ISB in Utah. No clear pattern of spatial association of these events with faults that show evidence of late Quaternary (<130,000 years) surface rupture has emerged. Rather, it appears that most of this seismicity is occurring on "blind" faults with no surface expression. This conclusion is supported by aftershock studies of both the 1975 Pocatello Valley earthquake of magnitude 6.0 and the 1972 Heber Valley earthquake of magnitude 4.3 that occurred about 12 km (7.2 mi) southeast of Jordanelle damsite. Monitoring by the University of Utah's regional network, with the addition of a seismograph station installed in the vicinity of Jordanelle damsite in 1981, has not disclosed additional information regarding the occurrence of earthquakes in the immediate vicinity of the damsite.

As a part of a regional seismotectonic study of the northern Wasatch Mountains, Sullivan and others (1988) identified normal faults with evidence of late Quaternary surface displacements in the back valleys and presented data on the rates and sizes of surface-faulting events on those faults. Detailed investigations were conducted on faults for which evidence of late Quaternary surface displacements was preserved. The conclusions for these faults were then applied to other late Quaternary faults in the back valleys where detailed investigations were not conducted. Although back valley faults are present in Keetley Valley near the damsite and in Kamas Valley about 12 km east of the damsite, fault investigations have shown that no late Quaternary (<130,000 years) displacements have occurred on the principal faults in these valleys, or elsewhere in the central Wasatch Mountains within about 20 km (12 mi) of the damsite.

Keetley Valley is a 7-km-long, 2- to 3-km-wide back valley that forms the north arm of the reservoir. Mid-Quaternary and older basin fill deposits have been mapped from bore holes, trenches,

and seismic refraction profiles. Reservoir boreholes indicated that the basin fill reaches a maximum thickess of more than 150 m (450 ft) in the center of the valley. Boreholes also showed that the basin fill overlies early Tertiary volcanics and late Eocene andesite porphyry; in two holes gravel clasts enveloped by andesite porphyry suggest that at least the lower portion of the basin fill is older than the andesite porphyry and, therefore, is of early Tertiary age. Trenches in the basin fill revealed an interbedded sequence of fine-grained debris flows and channel deposits. Tephrastratigraphy, aminostratigraphy, paleomagnetism, and soil relative-age dating indicated that the upper portions of the basin fill are of mid-Quaternary age. Seismic refraction profiles across the valley do not show abrupt steps in the basin fill-bedrock contact that would be indicative of late Cenozoic faulting, except along the southwestern margin of the valley where the Bald Mountain fault was identified.

Although no fault-related scarps are present in the basin fill, review of aerial photography and comparisons with other back valleys suggested that a previously unrecognized normal fault, the Bald Mountain fault, was present at the base of a 2-km-long escarpment along the southwestern margin of the valley. Two trenches at the base of the escarpment exposed a N20^{o}E-striking, steeply east-dipping normal fault in early Tertiary and older bedrock. In one of these trenches, and in a third trench in an embayment in the escarpment, basin fill deposits with an estimated minimum age of 130,000 to 150,000 years overlie the fault. Therefore, in Keetley Valley, as in Kamas Valley about 12 km to the east, late Cenozoic normal faults bound one valley margin; but we have concluded that no surface displacements have occurred on these faults in at least the last 130,000 years.

West of Keetley Valley in the Park City Mining District, mineralization in Paleozoic sedimentary rocks and early Tertiary intrusives is associated with east-trending fault zones. One of these faults, the Cottonwood fault, is mapped in the immediate vicinity of the damsite. Previous mapping and USBR damsite investigations indicate that the Cottonwood fault is a northeast-trending, north-dipping reverse fault with more than 300 m (1000 ft) of displacement in Paleozoic and Mesozoic sedimentary rocks. Stratigraphy exposed in trenches near the right abutment of the dam shows that faults in unconsolidated early Tertiary deposits (F-series faults), interpreted to be related to the Cottonwood fault, are terminated by or merge with a shear zone along the boundary of an andesite porphyry intrusive, the Jordanelle stock. Trench evidence indicated that this bounding shear developed contemporaneously with the intrusion of the Jordanelle andesite porphyry. Radiometric ages for the andesite porphyry range from 36 to 40 million years

providing a minimum age for displacement on the F-series faults. In a trench exposure, mid-Quaternary basin fill deposits overlie the bounding shear on the margin of the andesite porphyry showing that there has been no displacement on that shear zone in at least the last 500,000 years. Therefore, we conclude that late Quaternary surface displacements have not occurred on mapped faults near the dam.

Sections across the dam foundation constrained by boreholes and mapping show that the foundation of Jordanelle Dam will be andesite porphyry and country rocks, including early Tertiary volcanic rocks and, possibly, Mesozoic sedimentary rocks. Although stratigraphic markers are lacking in the andesite porphyry that would allow us to preclude faults, the conclusion from extensive investigation is that no significant faults cross the dam foundation. Trenches, some bore holes, and geophysical surveys indicate that zones of shearing or fracturing are present in andesite porphyry in the foundation. These features are interpreted to be related to multiple episodes of intrusion of the Jordanelle andesite porphyry, because they are discontinuous and confined to the andesite porphyry. Final confirmation of the conclusion that no faults are present awaits detailed mapping of the foundation excavation.

Potential earthquake sources for damsites in the ISB are considered to be of two types: 1) large-magnitude earthquakes on faults with evidence of late Quaternary surface rupture and 2) a local random earthquake that occurs on "blind" subsurface faults. The most likely sources of significant ground motions in the region that could affect Jordanelle damsite are the Wasatch fault, faults in Round Valley, and the random earthquake. An MCE of magnitude 7 1/2 is assigned to the Wasatch fault at a distance of 30 km (18 mi) from the damsite. An MCE of magnitude 6 1/2 to 6 3/4 is assigned to the faults in Round Valley at a distance of 20 km from the damsite. An MCE of magnitude 6 to 6 1/2 is assigned to a local random earthquake source.

Geologic investigations have shown that late Quaternary surface displacements have not occurred on faults in the vicinity of the damsite. Therefore, we have concluded that there is no potential for significant coseismic surface rupture in the dam foundation. However, ground deformation has been associated with recent moderate-magnitude earthquakes that have occurred on blind faults in the ISB. Tectonic subsidence accompanying the 1975 Pocatello Valley earthquake of magnitude 6.0 suggests that a similar phenomenon could accompany a magnitude 6 to 6 1/2 earthquake on a blind fault in the vicinity of the dam.

Historic data and model simulations indicate that this tectonic subsidence would occur over a surface area on the order of 100 km^2. Horizontal displacement gradients of 20 cm/km and net tectonic subsidence of about 50 cm would result. The historical earthquake record suggests that this subsidence could be accompanied by ground cracking or secondary surface displacements. These displacements would be most likely to occur on favorably oriented, pre-existing faults in the dam foundation. In order to estimate the maximum size of these displacements, we assume that they are related to the maximum subsidence in the same way that subsidiary faulting accompanying a large-magnitude, scarp-forming earthquake is related to the maximum surface displacement. Thus, the maximum subsidiary displacement is estimated to be 30% of the maximum subsidence of 50 cm. This displacement of 15 cm could occur on favorably oriented faults in association with a moderate-magnitude earthquake. If available data indicating that no faults are present in the dam foundation are confirmed, then no potential for secondary displacements should be considered. However, if foundation mapping unexpectedly reveals favorably oriented faults, conservative judgment suggests that small displacements (<15 cm) on these faults should be considered in the design of the dam.

TABLE OF CONTENTS

page

SUMMARY

1.0 INTRODUCTION..... 1
1.1 Location and description of proposed structures..... 1
1.2 Purpose and scope of the report..... 1
1.3 Consultant Panels..... 1
1.4 Acknowledgements..... 2

2.0 REGIONAL SETTING..... 4
2.1 Igneous rocks in the central Wasatch Mountains..... 6
2.2 Late Cenozoic and late Quaternary faulting..... 7
2.2.1 Wasatch fault..... 8
2.2.2 Northern and southern Wasatch Mountains..... 9
2.2.3 Central Wasatch Mountains.....10
2.2.3.1 Parleys Park.....10
2.2.3.2 Kamas Valley.....10
2.2.3.3 Heber Valley.....11
2.3 Historical seismicity.....11
2.3.1 Intermountain seismic belt.....11
2.3.2 History of station operation in Utah and local seismicity.....12

3.0 CENOZOIC FAULTING IN AND NEAR KEETLEY VALLEY.....16
3.1 Stratigraphy.....16
3.1.1 Paleozoic and Mesozoic sedimentary rocks.....18
3.1.2 Keetley volcanics.....18
3.1.3 Tertiary porphyry stocks.....18
3.1.4 Tertiary and Quaternary basin fill deposits.....18
3.1.5 Upper Quaternary deposits.....22
3.1.6 Soil relative age-dating.....22
3.2 East-trending faults in the Park City mining district...29
3.2.1 Hawkeye-McHenry fault zone.....29
3.2.2 Mayflower-Pearl structural zone.....31
3.2.3 Cottonwood fault.....35
3.3 North-trending normal faults in the Park City mining district.....36
3.4 East Kamas fault.....38
3.5 Concealed normal faults in Keetley Valley.....38
3.5.1 Seismic Refraction Survey.....38
3.5.2 Bald Mountain fault.....39
3.5.2.1 Trench J-9.....39
3.5.2.2 Trench J-10.....42
3.5.2.3 Trench J-13.....44
3.5.3 Other normal faults.....46
3.6 Conclusions.....46

TABLE OF CONTENTS (continued)

page

4.0 SITE GEOLOGY....48
4.1 Stratigraphy....48
4.1.1 Jordanelle andesite porphyry....48
4.1.2 Keetley volcanics....49
4.1.3 Unconsolidated deposits....49
4.2 Faults and shears at the damsite....50
4.2.1 F-series faults....50
4.2.2 SZ1 and SZ2....51
4.2.3 A and B contacts....53
4.2.4 Discontinuous shearing beneath the Provo River floodplain....54
4.2.5 Conclusions....55

5.0 CONCLUSIONS....57
5.1 Earthquake sources in the ISB....57
5.2 Maximum credible earthquakes....58
5.2.1 Quaternary faulting in the vicinity of Jordanelle damsite....58
5.2.2 Wasatch fault....59
5.2.3 Round Valley....60
5.2.4 Random earthquake....60
5.3 Potential deformation at the damsite....62
5.3.1 Potential deformation of the dam foundation....62
5.3.2 Potential deformation of the outlet works tunnels...64
5.4 Reservoir-induced seismicity....65

6.0 REFERENCES....67

APPENDIX A - Seismic refraction survey of Jordanelle Reservoir site

APPENDIX B - An analysis of reservoir-induced seismicity in the back valleys of the Wasatch Mountains

APPENDIX C - Static ground deformation for design earthquakes

APPENDIX D -Paleomagnetism of Quaternary sediments from the Jordanelle Damsite and vicinity

FIGURES

Figure		page
1	Regional geology and late Quaternary faults in a part of the Wasatch Mountains	5
2	Epicenter map of all earthquakes located during the period July 1962 through September 1987	14
3	Epicenter map of seismicity in the near vicinity of Jordanelle damsite for the period September 1981 through September 1987	15
4	Cross section AA and logs of drill holes through basin fill deposits in Keetley Valley	21
5	Values for rubification and non-arid index for Keetley Valley soils	28
6	Principal faults in the Park City mining district	30
7	Location map of trench sites on the west side of Keetley Valley	33
8	Logs of trench J-8 and J-8E in basin fill deposits above the Cunningham Tunnel	34
9	Log of trench J-9 exposing the Bald Mountain fault	40
10	Log of trench J-10 exposing the Bald Mountain fault	43
11	Log of trench J-13 in basin fill deposits	45
12	Log of trench DT-29 in basin fill deposits near the right abutment of Jordanelle Dam	52

TABLES

Table		page
1	Quaternary stratigraphic units in Keetley Valley	17
2	Selected properties and laboratory data for soil profiles in Keetley Valley	24-26
3	Soil development indices and secondary clay and carbonate for Jordanelle soils	27
4	K-Ar dates for intrusives near Jordanelle	49
5	Slip rates and average return periods for surface displacements on the central segments of the Wasatch fault	59
6	Maximum credible earthquakes for Jordanelle Dam	61

PLATES

Plate		page
1	Geologic Map of Keetley Valley, 1" = 1000'	in pocket

1.0 INTRODUCTION

1.1 Location and proposed structures

The proposed Jordanelle Dam and Reservoir, located in the central Wasatch Mountains east of Salt Lake City, Utah, is part of the Bonneville Unit of the Central Utah Project. The dam is located on the Provo River about 10 km (6 mi) north of Heber City and about 25 km (15 mi) upstream of Deer Creek Dam. The rockfill dam will have an average structural height of 99 m (325 ft) reaching a maximum of 118 m (390 ft) above the buried channel. The dam will be about 500 m (1650 ft) long and it will impound a 300,000 acre-ft reservoir with a maximum water depth of 87 m (285 ft). Completion of construction is anticipated in 1992.

1.2 Purpose and Scope of the report

This report presents the results of a seismotectonic study for Jordanelle Dam. It defines seismic source areas and MCEs (maximum credible earthquakes) for the design and analysis of the dam, discusses other earthquake hazards to the dam, and updates earlier assessments presented to two panels of consultants convened in 1982-1983 and 1986 (Sullivan and others, 1986). Background data pertinent to the seismotectonic setting of Jordanelle damsite and the results of investigations of late Quaternary faulting in the region, reported in the Central Utah Regional Seismotectonic Study (Sullivan and others, 1988), are summarized in this report. The conclusions of this report are based on the following: 1) seismotectonic investigations in the back valleys of the Wasatch Mountains (Sullivan and others, 1988), 2) the site-specific seismotectonic investigations completed as a part of this study, and 3) damsite geologic investigations conducted principally by the Bonneville Construction Office (USBR, 1986). The conclusions of this report supersede those presented in all previous documents.

1.3 Consultant Panels

A panel of consultants consisting of the late Dr. Richard Jahns, Dr. Walter Arabasz, and Dr. Ralph Peck, was convened in November, 1982 to review USBR geologic investigations and dam design concepts to determine if a safe dam could be built at the proposed Jordanelle damsite. Geologic design data, conclusions regarding MCEs, and preliminary conclusions regarding the potential for surface displacement on foundation faults were presented in the Consultants Briefing Document (USBR, 1982) and in oral presentations at the meetings. In their report, the

Panel concluded that a safe dam could be built at Jordanelle damsite and they recommended additional work based on interpretations of the geology of the damsite presented at that time (Arabasz and others, 1983).

Subsequent investigations were conducted between 1983 and 1986 and the results were presented in a report which includes geologic design data for the proposed damsite, the final draft of the Jordanelle seismotectonic report, and preliminary conceptual designs for each of the dam types (USBR, 1986; Sullivan and others, 1986). This report was reviewed by a second panel of consultants convened in September, 1986. The members of this panel were: Dr. Ralph Peck, Dr. Glenn Tarbox, Dr. Walter Arabasz, and Dr. Douglas Campbell. This panel concurred with the MCEs recommended for design and analysis of the dam, offered comments on the draft seismotectonic report, and recommended limited additional studies (Peck and others, 1986). These additional studies are discussed in Sullivan and others (1988) and in this report.

1.4 Acknowledgements

The cooperation and support of the Bonneville Construction Office and the Seismoteconic section through more than 5 years of investigations at Jordanelle damsite contributed greatly to the completion of this report. The detailed mapping on the middle right abutment by geologists Richard Meyers and Robert Peoples of the Bonneville Construction Office and James Peterson and Tim Sullivan of the Engineering and Research Center provides the documentation for some of the conclusions of this report. The report has also greatly benefited from numerous discussions with geologists on the project staff over a period of years regarding evolving interpretations of the enigmatic damsite geology. The Geology Division, headed presently by Dennis Williams and previously by Gary Dow, and the Materials Branch, headed by Jerry Eller, provided the logistic support essential to the excavation, shoring, and restoration of backhoe trenches and soil pits in Keetley Valley.

This report also benefited from the contributions and reviews of present and former members of the Seismotectonics Section. Roland LaForge prepared this final version of sec. 5.4. Chris Wood contributed to this final version of sec. 5.3. Dean Ostenaa contributed to earlier versions of sec. 5.3. Alan Nelson described soils in Keetley Valley, assisted in the preparation of early drafts of this report, and participated in the 1982-3 Consultants meeting. Lucy Piety reviewed this final draft. Capable assistance in the mapping and logging of

trenches was provided by Edward Baltzer, Carol Krinsky, and Rebecca Stoneman. Discussions with Dean Ostenaa, Dennis Williams, and Alan Nelson were helpful throughout the study.

Pete Klein and Ed Monk from the Applied Sciences Branch at the Engineering and Research Center provided thin section descriptions and useful discussions about intrusive contacts.

Rolf Kihl and Vance Holiday (INSTARR, University of Colorado) and the Soil Testing Laboratory, Colorado State University provided detailed grain size, carbonate, and organic matter analyses. Gifford Miller (INSTARR) provided amino acid analyses with the help of Dan Goter.

2.0 REGIONAL SETTING

Three periods of deformation are recorded in the Wasatch Mountains. During the Sevier Orogeny that began in the Jurassic and culminated in the late Cretaceous, sheets of Mesozoic and Paleozoic sedimentary rocks were thrust eastward across the former continental margin into northeastern Utah (Armstrong, 1968). Drilling, mapping, and seismic reflection data generated for oil and gas exploration have shown that the "sole" portions of these imbricate thrusts are low angle and follow incompetent beds. The thrust faults ramp upsection at steeper angles in the competent rocks. These ramps often serve to localize later normal faults (Royse and others, 1975; Dixon, 1982). Middle Tertiary deformation in the central Wasatch Mountains is manifested as generally east- and northeast-trending normal and reverse faults that formed in association with the emplacement of intrusive and extrusive rocks during the late Eocene, Oligocene and early Miocene. Late Cenozoic and recent deformation in the back valleys of the Wasatch Mountains results from east-west extension as in the Basin and Range to the west.

Evidence of all three periods of deformation is found in the vicinity of Keetley Valley where the dam and reservoir will be located. Keetley Valley is a small sediment-filled, intermontane basin in the Keetley volcanic field that is similar to Kamas Valley and Parleys Park (fig. 1), which were earlier described as back valleys by Gilbert (1928). Mesozoic and older sedimentary rocks intruded by lower Tertiary calc-alkaline stocks are exposed on the margins of the Keetley volcanic field. The Mesozoic and Paleozoic sedimentary rocks are part of a sequence of rocks in the lower plate of the Charleston thrust fault (Baker, 1964). This fault is the basal detachment for a stack of imbricate, late Cretaceous thrust faults in the southern Wasatch Mountains. A similar stack of thrust faults with the Absoraka thrust as the basal detachment is present in the northern Wasatch Mountains. The central Wasatch Mountains form a reentrant in the north-trending thrust belt exposing the lower plate rocks (Beutner, 1977).

The position of this reentrant is related to the Uinta Arch, a Laramide-age west-trending fold that projects below the central Wasatch Mountains from the east. This fold is flanked by Eocene and older, west-trending normal and reverse faults including the North Flank and the South Flank faults (fig. 1). Hansen (1983) discusses late Cenozoic normal displacement of as much as 1500 m (4950 ft) on the North Flank fault in the eastern Uinta Mountains, but the fault does not displace the Keetley volcanics in the western Uinta Mountains. No late Cenozoic displacement

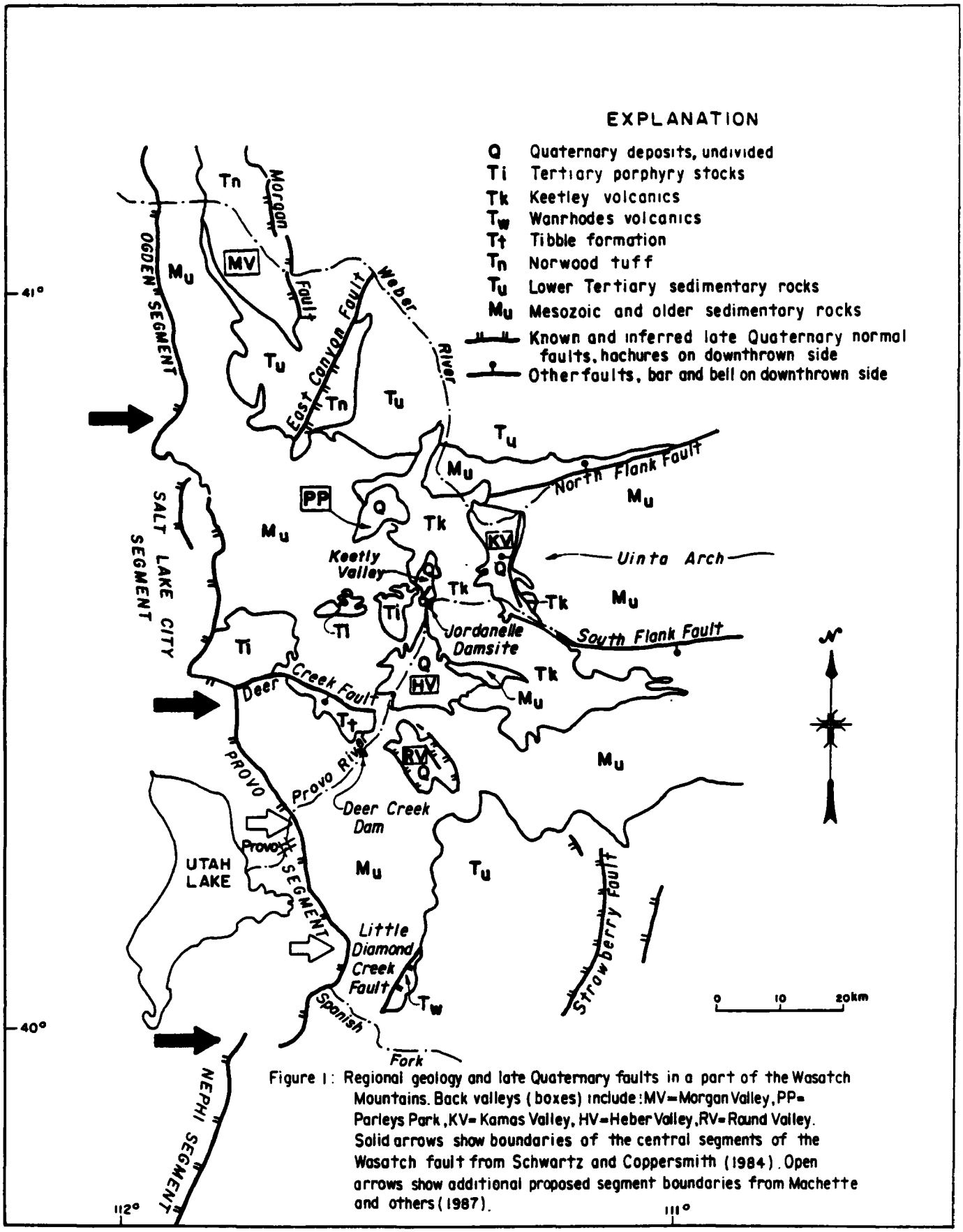

Figure 1: Regional geology and late Quaternary faults in a part of the Wasatch Mountains. Back valleys (boxes) include: MV=Morgan Valley, PP=Parleys Park, KV=Kamas Valley, HV=Heber Valley, RV=Round Valley. Solid arrows show boundaries of the central segments of the Wasatch fault from Schwartz and Coppersmith (1984). Open arrows show additional proposed segment boundaries from Machette and others (1987).

is indicated on the South Flank fault for it does not displace an erosion surface probably of early Tertiary age in the western Uinta Mountains (Martin and others, 1985).

Upper Cretaceous and lower Tertiary clastic sedimentary rocks with western provenance, largely derived from the thrust sheets, are exposed in the northern Wasatch Mountains. This sequence includes the Cretaceous Frontier, Current Creek, Echo Canyon, and Evanston Formations and the upper Tertiary Wasatch Formation (Mullens, 1971; Mann, 1974). These deposits are principally well-indurated conglomerates but they also include sandstone and shale. Although the Wasatch Formation reaches a maximum thickness of 3000 m (9900 ft) in Morgan Valley, similar Cretaceous or upper Tertiary sediments are almost entirely lacking in the central Wasatch Mountains in the vicinity of Keetley Valley. There, the lower Eocene Keetley volcanics typically lie unconformably on Jurassic and older sedimentary rocks, although locally preserved, unconsolidated gravels, as much as 200 m (660 ft) thick underlie the Keetley volcanics north of Keetley Valley. As discussed below we have documented the occurrence of similar, Tertiary, unconsolidated deposits in Keetley Valley.

2.1 Igneous rocks in the central Wasatch Mountains

In the central Wasatch Mountains, the emplacement of the thrust plates during the late Cretaceous was followed by the deposition of volcanic rocks, the coeval intrusion of calc-alkaline porphyry stocks, and the development of generally east-trending normal and reverse faults. The Keetley volcanics fill the structural saddle between the north-trending Wasatch Mountains to the west and the east-trending Uinta Mountains to the east. They are exposed over most of the eastern portion of the central Wasatch Mountains, including the vicinity of Jordanelle damsite. Bromfield and others (1970) and Bromfield and Crittenden (1971) have mapped andesite and rhyodacite flows, tuffs, volcanic breccias, and rhyodacite porphyries in the eastern portion of the Park City mining district. Woodfill (1972) in his petrographic and field study of the volcanic field describes volcanic breccias, flows, tuffs, lahars and intrusive rocks, which range in composition from quartz latite to trachyandesite.

A series of mid-Tertiary, calc-alkaline porphyry stocks (Ti on fig. 1) are aligned along the western projection of the Uinta axis and intrude the Keetley volcanics and older rocks (Stewart and others, 1977). Porphyritic and hypabyssal textures, strongly deformed host rocks, concordant intrusive contacts, and the lack of contact metamorphism indicate shallow emplacement

levels (<5 km [3 mi]) for the eastern stocks; discordant intrusive contacts, numerous dikes, wider metamorphic aureoles, and equigranular textures indicate deeper emplacement levels (>5 km [3 mi]) for the western stocks (Woodfill, 1972; Lawton and others, 1980). Isotopic ages indicate a short history of overlapping igneous events during the late Eocene and Oligocene that span 5 million years based on K-Ar (Potassium-Argon) dates on biotite, or at most 10 million years based on K-Ar dates on horneblende (Crittenden and others, 1973; Bromfield and others, 1977).

The Little Cottonwood stock is the largest and westernmost of these stocks. A radiometric age of 24 - 31 million years for the Little Cottonwood stock based on fission track and K-Ar dates is supported by local geologic relations (Crittenden and others, 1973). The Alta and Clayton Peak stocks are exposed further to the east and are not in contact with the Little Cottonwood stock. Geologic relations indicate that the Alta stock intrudes the Clayton Peak stock which is consistent with the radiometric ages of emplacement of 37-41 million years ago for the Clayton Peak stock and 32-33 million years ago for the Alta stock (Crittenden and others, 1973). The Alta magma was intruded in two pulses into pre-Triassic rocks at a depth of about 6.3 km (4 mi) (Wilson, 1961).

In the Park City mining district west of Keetley Valley, Boutwell (1912) mapped a large composite porphyry pluton later shown to consist of at least 6 separate intrusions: the Ontario, Mayflower, Glencoe, Valeo, Flagstaff, and Pine Creek stocks (Bromfield and others, 1970). East of the Park City mining district, volcaniclastic rocks and subordinate andesitic flows of the Keetley volcanics unconformably overlie Paleozoic and Mesozoic sedimentary rocks. These rocks are intruded by the Park Premier stock and the Indian Hollow plug that probably mark source vents for at least some of the volcanics (Bromfield and others, 1977; Bromfield and Crittenden, 1971; Bromfield and others, 1970; Woodfill, 1972).

2.2 Late Cenozoic and late Quaternary faulting

The principal late Quaternary fault in the region is the Wasatch fault which forms the physiographic boundary between the Basin and Range Province and the adjacent Colorado Plateau and Middle Rocky Mountains Provinces. Late Cenozoic normal faults are found east of the Wasatch fault on the margins of some of the back valleys of the Wasatch Mountains (fig. 1). Mapping, trenching, and comparison of the characteristics of bedrock escarpments have led to the conclusion that late Quaternary

displacements have occurred on some of these faults in the northern and southern Wasatch Mountains, but that late Quaternary displacement has not occurred on late Cenozoic normal faults in the central Wasatch Mountains (Sullivan and others, 1988).

In this report we refer to normal faults that displace late Eocene - Oligocene volcanic rocks and overlying unconsolidated basin fill in the Wasatch Mountains as late Cenozoic faults. In the back valleys of the northern Wasatch Mountains, the basin fill consists of late Eocene Norwood Tuff overlain by varying thicknesses of unconsolidated Tertiary and Quaternary sediments suggesting that displacement on the bounding normal faults commenced in the Eocene. In the central Wasatch Mountains, the late Eocene Keetley volcanics and overlying basin fill have also been displaced by back valley normal faults (Sullivan and others, 1988). This contrasts with the ages of basin fill sequences in Nevada which suggest that the most recent phase of extension in the Basin and Range commenced 10 to 17 million years ago (Stewart, 1978).

The focus of USBR seismotectonic studies in the back valleys has been to identify late Cenozoic faults that should be considered potential sources of large-magnitude earthquakes. These are faults that have experienced recurrent surface displacements recently enough to be of concern in the design of critical dams. For most of the faults in the back valleys, estimates of the actual or average recurrence intervals are not available. However, deposits with an estimated age of 130,000 to 150,000 years overlie some of the faults in the back valleys. Faults that displace deposits of this age or younger are referred to in this report as late Quaternary faults. Conversely, faults that do not displace deposits of this age probably have an average recurrence interval for surface displacements that is greater than 100,000 years. Physiographic or stratigraphic relations may indicate that these are late Cenozoic (post-Eocene) faults, but in this report they are not considered late Quaternary faults.

2.2.1 Wasatch fault

The Wasatch fault is the late Quaternary normal fault marking the abrupt physiographic boundary between the Basin and Range and Colorado Plateau provinces (fig. 1). The fault extends 370 km (222 mi) north from Gunnison, Utah to Malad City, Idaho. In most areas the most recently active trace is mapped near the base of the triangular facets that form the west face of the Wasatch Mountains. Late Quaternary surface displacements are

indicated by vegetation lineaments and scarps in lacustrine sediment of Lake Bonneville, in late Pleistocene (10,000 to 150,000 years old) moraines, and in Holocene alluvial and colluvial deposits along the trace of the fault. Schwartz and Coppersmith (1984) recognize six major segments of the Wasatch fault based on variability in timing of individual events, in scarp morphology, and in fault geometry. Smith and Bruhn (1984) demonstrate a coincidence between some segment boundaries and the location of lateral and sidewall ramps in thrust faults, and suggest that preexisting structure partly controls the position of segment boundaries of the Wasatch fault. They also present cross sections, based on seismic reflection profiles, that depict subsurface dips of the Wasatch fault that are less than the 60° to 80° dips of the surface scarps. Zoback (1983) reviews and tabulates dips measured at the surface for the Wasatch fault and adjacent faults as well as focal mechanism solutions. McKee and Arabasz (1982, p. 143) present a "sanitized" section across the Wasatch fault based on proprietary seismic reflection profiles which depicts the fault shallowing in dip in the subsurface and becoming subhorizontal at a depth of 6 to 7 km (3.6 to 4.2 mi).

The lack of spatial correlation between earthquake epicenters and the mapped traces of late Quaternary faults, particularly the Wasatch fault, has been a notable feature of the ISB in Utah since the initiation of earthquake monitoring. McKee and Arabasz (1982) have demonstrated that the lack of correlation between epicenters and the southern part of the Wasatch fault is not the result of epicentral location errors.

2.2.2 Northern and southern Wasatch Mountains

Late Quaternary normal faults have been identified in the northern and southern Wasatch Mountains (Sullivan and others, 1988). Trenches exposing the faults and displaced colluvial stratigraphy were used to interpret a history of late Quaternary surface displacements on the Strawberry fault in the southern Wasatch Mountains (Nelson and Martin, 1982), and on the Morgan and James Peak faults in the northern Wasatch Mountains (Sullivan and others, 1988) (fig. 1). Geologic mapping and comparisons of the characteristics of bedrock footwall escarpments were used to infer a history of late Quaternary surface displacements on other faults. Those closest to Jordanelle are the East Canyon fault (fig. 1), about 30 km (18 mi) north of Jordanelle, and faults bounding Round Valley (fig. 1), about 20 km (12 mi)south of Keetley Valley (Sullivan and others, 1988).

2.2.3 Central Wasatch Mountains

The upland surface of the central Wasatch Mountains is broken by a series of intermontane basins or back valleys, generally smaller than the back valleys of the northern and southern Wasatch Mountains. Heber Valley, Kamas Valley, and Parleys Park are back valleys that were originally described by Gilbert (1928). As in the northern and southern Wasatch Mountains, mapping, drilling, and geophysical studies have shown that some of the valleys are bounded by normal faults that displace lower Eocene and younger deposits (Sullivan and others, 1988). Although late Quaternary normal faults are present in the northern and southern Wasatch Mountains, none have been mapped in the central Wasatch Mountains. In the following sections we briefly summarize the conclusions for the back valleys of the central Wasatch Mountains that are discussed in detail in Sullivan and others (1988).

2.2.3.1 Parleys Park

Parleys Park and Richardsons Flat are irregularly-shaped valleys at the west edge of the Keetley volcanic field (fig. 1). They are filled with unconsolidated deposits which waterwell drilling has shown to vary in thickness from <50 to >200 m (<165 ft to >660 ft) (Sullivan and others, 1988). Mapping shows that these unconsolidated deposits underlie the Keetley volcanics on the margins of Parleys Park and are therefore of early Tertiary age, but the surficial deposits near the center of the valleys are of Quaternary age. The present drainage pattern and the slope of paleovalleys in the vicinity of Parleys Park show that this area was once a moderately-eroded fluvial terrane that sloped gently to the northeast. The subsequent disruption of this drainage system may be related to fluvial erosion or late Cenozoic displacement on concealed faults. No fault scarps in unconsolidated deposits were found in the area, and although some of the margins of Parleys Park may be bounded by short (<3 km long [1.8 mi]) normal faults with Quaternary displacement, no evidence was found for late Quaternary surface displacements (Sullivan and others, 1988).

2.2.3.2 Kamas Valley

Kamas Valley is a north-trending valley about 14 km (8.4 mi) long at the eastern edge of the Keetley volcanic field about 12 km (7.2 mi) east of Jordanelle (fig. 1). Gravity studies, drill hole logs, mapping, and the morphology of the escarpment in Paleozoic rocks suggest that the principal late Cenozoic fault in the valley is the East Kamas fault--a north-trending

concealed normal fault on the eastern margin of the valley (Sullivan and others, 1988). Well-developed soil profiles on alluvial fans that extend across the inferred trace of the East Kamas fault establish that there have been no surface displacements on this fault in at least the last 130,000 years (Sullivan and others, 1988).

2.2.3.3 Heber Valley

Heber Valley is a triangular-shaped valley drained by the Provo River about 10 km (6 mi) downstream of Jordanelle (fig. 1). No faults have been mapped previously on the margins of the valley, but gravity studies and drilling indicate that unconsolidated deposits in the valley are at least 100 m (330 ft) thick and may reach a thickness of 250 m (825 ft), suggesting that concealed normal faults may be present at or near the margins of the valley. Mapping and trenching in Heber Valley have shown that scarps in alluvial deposits in the valley result from erosion by the Provo River and its tributaries (Sullivan and others, 1988). In addition, the bedrock escarpments on the margins of the valley are sinuous and embayed in contrast to the linear, steep escarpments associated with other back valleys where late Quaternary surface displacements have been documented or inferred (Sullivan and others, 1988). Therefore, we have concluded that no late Quaternary displacements have occurred on faults in Heber Valley.

2.3 Historical seismicity

2.3.1 Intermountain seismic belt

Jordanelle damsite is located within the Intermountain seismic belt (ISB), a 100-km-wide (60 mi) zone of contemporary seismicity on the eastern margin of the Basin and Range. Centered approximately on the Wasatch fault in central Utah, the ISB is considered to have the highest level of earthquake risk in the United States outside of California and Nevada (Arabasz and Smith, 1979). Commonly observed features of earthquake occurrence within the ISB have been described by Smith and Sbar (1974), Smith (1978) and Arabasz and Smith (1981). Among these features are the following: 1) diffuse seismicity which shows only general correlation with late Quaternary faults, 2) an apparent lack of correlation between small- to moderate-magnitude earthquakes and mapped faults, 3) shallow focal depths (less than 20 km [12 mi]), 4) sporadic occurrence of earthquakes both spatially and temporally, and 5) a persistent pattern of normal faulting indicating predominantly east-west extension (Piety and others, 1986, p. 112). A discussion of earthquake

occurrence in the back valleys of the Wasatch Front, including the damsite region, is presented in Sullivan and others (1988). In the following section the seismicity in the the Jordanelle damsite region will be discussed briefly.

2.3.2 History of station operation in Utah and local seismicity

The historical earthquake record in the vicinity of Jordanelle damsite began with the settlement of the area following the influx of the Mormons to the Wasatch Front in 1847. Instrumental monitoring of earthquakes did not begin in Utah until a seismograph station was installed 40 km (24 mi) from the damsite in Salt Lake City in 1907. It was not until 1962 that earthquakes occurring on a state-wide basis could be reasonably located instrumentally. Coverage was slightly improved in 1970 when a seismograph was installed 28 km (17 mi) west of Jordanelle, and dramatically improved in 1974 when a regional array of high-gain, telemetered stations was installed throughout the Wasatch Front. With this new network, the damsite was surrounded by nine seismographs located between 20 and 50 km (12 and 30 mi) of the damsite.

In September, 1981, a vertical-component seismograph station (JLU) was installed about 1.6 km (1 mi) west of the damsite. This station was upgraded to four-components in July, 1986. The present station consists of a vertical and two horizontal-component, short-period seismometers that are operating at maximum gain to allow for the detection of the smallest possible earthquakes in the Jordanelle area. In addition, the vertical component seismometer is simultaneously being recorded at somewhat lower gains to facilitate the on-scale recording of larger-magnitude events. Also, in 1981 an accelerometer was installed at the damsite to record strong ground motion from large-magnitude events should they occur.

Since September 1981, the location threshold for earthquakes in the vicinity of the damsite has been about magnitude 1.0, although earthquakes smaller than this are routinely located in the area. During seismic exploration in the area of the proposed reservoir (Appendix A, this report), it was demonstrated that station JLU can detect seismic waves resulting from the detonation of explosives as small as 1 lb in the vicinity of the damsite. It is estimated that magnitude 0 or smaller earthquakes could be detected in the vicinity of the damsite should they occur. However, with the current station configuration it would not be possible to determine the locations of events of this size.

Figure 2 shows the distribution of currently operating seismograph stations providing coverage in the vicinity of the damsite together with the epicenters of all earthquakes (319) recorded during the 25+ year period from July 1, 1962 through September 30, 1987. Given this capability to detect microearthquakes, it is somewhat surprising that no earthquakes have occurred within 5 km (3 mi) of the damsite either before or after the installation of station JLU. Earthquake catalogs for the Utah region indicate that within 10 km (6 mi) of Jordanelle only 27 earthquakes have occurred since settlement began in 1847, 19 of these events since 1962, and all of these events were of small magnitude (University of Utah, 1987).

The most significant earthquake that occurred in the vicinity of Jordanelle damsite was the 1972 Richter magnitude 4.3 (body-wave magnitude 4.7) Heber City earthquake, which was located about 12 km (7.2 mi) southeast of Jordanelle along the eastern margin of Heber Valley (fig. 2). This earthquake was felt over a 6500 km^2 area with a maximum Modified Mercalli intensity of VI in the epicentral region. An aftershock study defined the probable causative structure to be a northeast-dipping, northwest-trending normal fault that is not expressed in the surface geology (Langer and others, 1979). Continuing seismicity in Heber Valley since 1972 has been associated with this event. Figure 3 is a larger scale plot of the seismicity that has occurred near Jordanelle since the installation of station JLU in 1981. Of the 78 earthquake epicenters shown on figure 3, 45 are located in the Heber City earthquake aftershock zone.

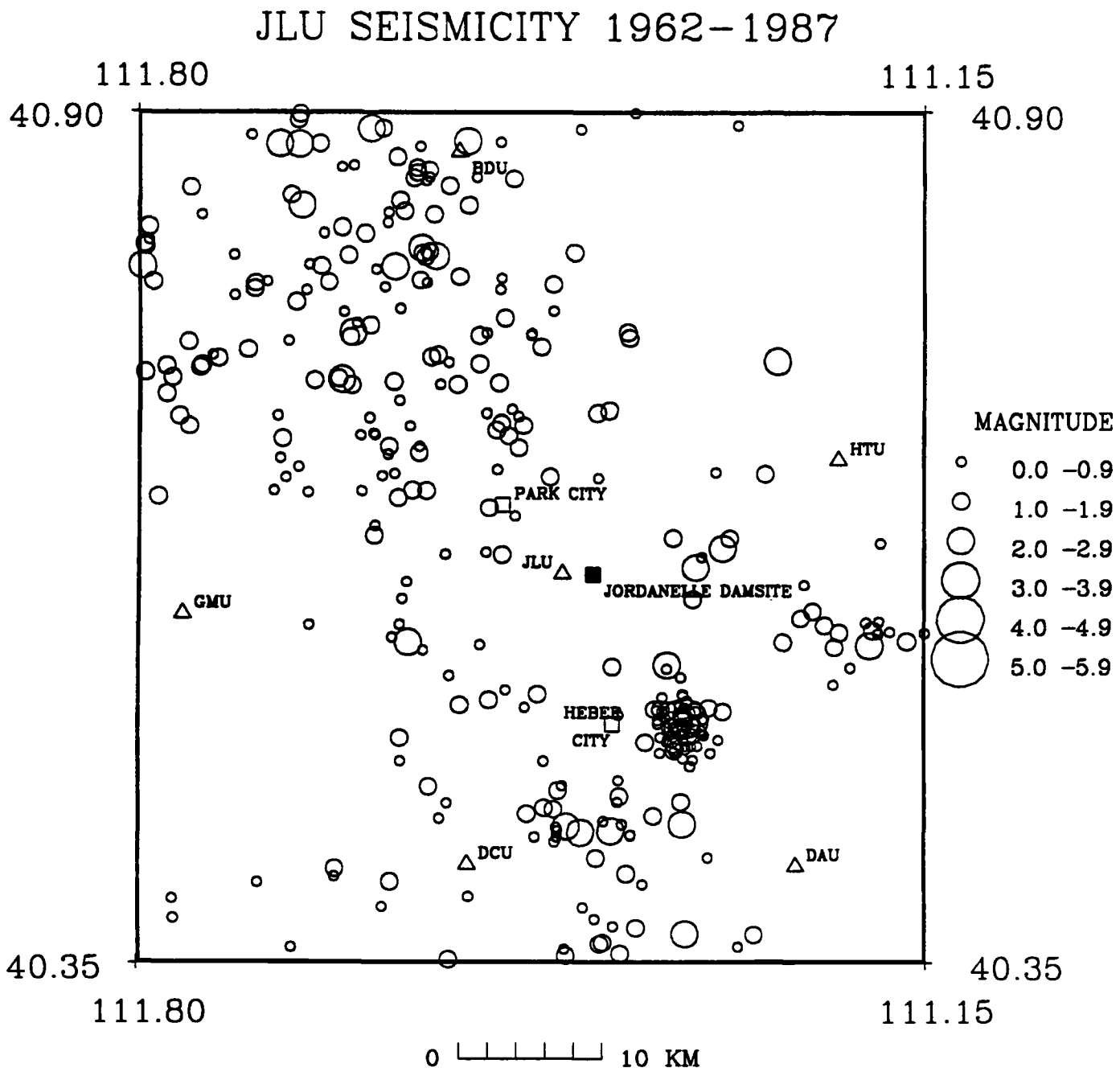

Figure 2. Epicenter map of all earthquakes located during the period July 1962 through September 1987. Also shown are the currently operating seismograph stations (triangles with three letter designators) relative to the location of Jordanelle damsite (solid square) and Heber and Park Cities (open squares). Cluster of epicenters east of Heber City includes a magnitude 4.7 event that occurred in 1972.

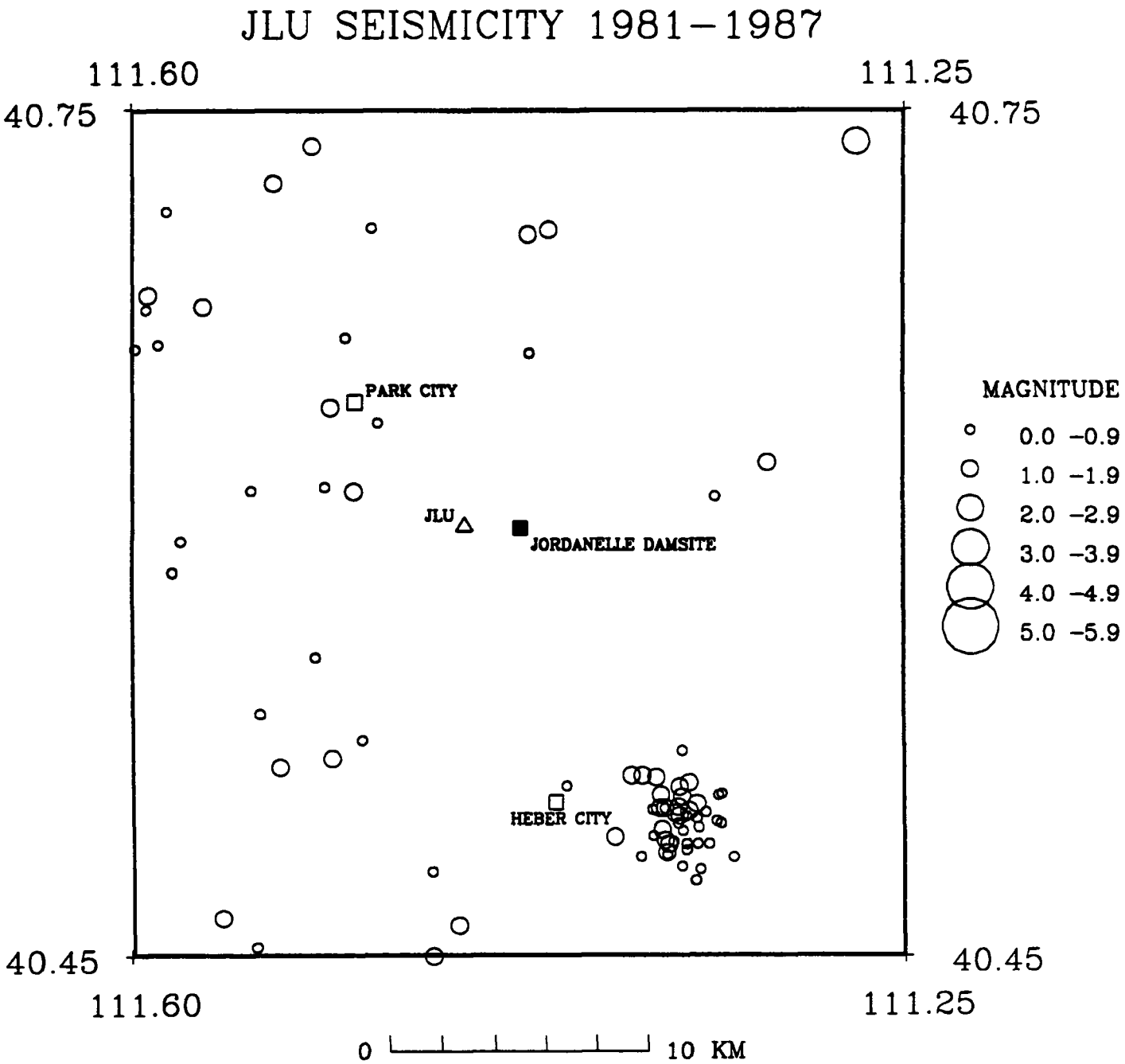

Figure 3. Epicenter map of seismicity in the near vicinity of Jordanelle damsite (solid square) for the period September 1981 through September 1987. Seismograph station JLU is indicated by a triangle. Heber City and Park City are shown as open squares.

3.0 CENOZOIC FAULTING IN AND NEAR KEETLEY VALLEY

Jordanelle Dam and Reservoir will be located on the east side of the Park City mining district, a district that has produced lead, zinc, silver and gold since 1869. The largest and most productive ore bodies in the district are of two types: bedded replacement ores, principally in limestones; and vein or lode deposits. Principal production is from lode deposits associated with fault zones in the district (Garmoe and Erickson, 1968).

The damsite is located at the south end of Keetley Valley (pl. 1), a north-trending topographic basin about 7 km (4.4 mi) long and 2 to 3 km (1.3 to 1.8 mi) wide that shares similar characteristics with other back valleys of the Wasatch Mountains. These characteristics include: 1) bedrock escarpments on the margins of the valley, 2) unconsolidated basin fill deposits as much as 142 m (465 ft) thick within the valley, and 3) post-Eocene normal faulting on at least one margin of the valley. This evidence was earlier interpreted as suggesting that concealed Cenozoic and possibly late Quaternary normal faults were present in Keetley Valley (USBR, 1982; Sullivan and Nelson, 1983). Subsequent investigations have shown that no late Quaternary displacements have occurred on faults in Keetley Valley.

Plate 1 is a geologic map of Keetley Valley. The Quaternary units on this map are described in Table 1. On pl. 1 they are divided into three categories: units that are dated either directly or indirectly as Pleistocene, those inferred to be Holocene on the basis of geomorphic position, and undifferentiated Quaternary deposits. Pleistocene deposits in Keetley Valley consist predominantly of older basin fill (Pao) of mid-Pleistocene age and older (>150,000 yrs), late Pleistocene (150,000 to 10,000 years old) alluvial fan deposits that overlie the basin fill around the margins of the valley (Pa/ao) including alluvium (Pa), and latest Pleistocene (30,000 to 10,000 years old) alluvium (Pay). Holocene units (10,000 years old to present) are inset into the Pleistocene deposits as fans around the valley margins (Haf) and as floodplain deposits along the valley axis and the Provo River drainage (Ha). The stratigraphy and age of the Quaternary deposits are discussed in the following sections.

3.1 Stratigraphy

The oldest rocks in the vicinity of Keetley Valley are Paleozoic and Mesozoic sedimentary rocks. This sequence is unconformably

Table 1. Quaternary stratigraphic units in Keetley Valley (pl. 1 and figs 6 and 7)

Map symbol	Age	Description
Ha	Holocene	**Floodplain alluvium of Ross Creek, the Provo River, and their tributaries:** clay, clayey sand, and gravelly clay 3 to 6 m (10 to 20 ft) thick overlying subrounded and subangular cobbles in a clay matrix along Ross Creek; clay with subangular to well-rounded gravel 1.5 m (5 ft) thick overlying well-rounded cobbles and boulders along the Provo River.
Haf	Holocene	**Alluvial fan deposits at the mouths of tributaries to Ross Creek:** silty sand, sandy clay, and gravelly clay with subangular gravels and cobbles.
Pay	Latest Pleistocene	**Younger alluvium of McHenry Creek:** silty and sandy gravels, cobbles, and boulders of subrounded and subangular quartzite and rounded and well-rounded granitic rocks that form a terrace 6 m (20 ft) above lower McHenry Creek and fill a channel formed in older basin-fill deposits (Pao). Rounded, imbricated quartzite and granitic gravels of ancient Ross Creek are exposed in a soil pit 6 m (20 ft) above the present creek bed and are included in this map unit.
Pa	Late Pleistocene	**Alluvium:** moderately sorted, subrounded cobbles and boulders of quartzite and partially grusified granitic rocks with a sandy clay matrix up to 10 m (30 ft) thick overlying bedrock in McHenry and Glencoe Canyons.
Pa/ao	Pleistocene	**Gravelly alluvium overlying basin fill:** moderately well-sorted, subrounded gravels and cobbles of orange sandstone and shale and rounded, gray, partially grusified granitic and volcanic rocks up to 1 m (3 ft) thick deposited in alluvial fans over stratified sand, silty clay, sandy clay, and clay of the basin fill (Pao). Because the basin fill is not exposed above elevation 1963 m (6440 ft), this elevation is used as an arbitrary upper limit for this map unit on pl. 1 and consists of a dashed contact with Qc mapped at higher elevations. On the west side of Keetley Valley, this unit consists of moderately sorted, subrounded quartzite gravels, cobbles, and boulders and well-rounded, grusified cobbles and boulders with a brown sandy clay matrix up to 6 m (20 ft) thick.
Pao	Mid-Pleistocene to early Tertiary	**Basin fill:** interbedded subangular and subrounded quartzite and rounded partially grusified granitic gravels, massive to laminated sand, gravelly silty clay and clay; up to 150 m (500 ft) thick in the center of the valley (drill hole R104) and exposed up to elevation 1963 m (6440 ft). Paleomagnetic, amino acid, and tephrostratigraphic data (sec. 3.1.4) indicate that these deposits are older than 600,000 years. Evidence from exposures near the damsite and in drill holes indicates that the lower part of the section is early Tertiary in age.
Qc	Quaternary	**Colluvium:** poorly to moderately sorted, angular and subangular gravels, cobbles, boulders with a fine-grained matrix which form a mantle more than 1.5 m (5 ft) thick over bedrock as recognized on air photos; also includes areas mapped as Quaternary alluvium (Qoa) by Bromfield and others (1970) and by Bromfield and Crittenden (1971).
Qc/Pao	Quaternary	**Colluvium overlying older basin-fill deposits:** interbedded moderately sorted, subangular quartzite gravels and cobbles, sandy silty clay and gravelly clay up to 4.5 to 6 m (15 to 20 ft) thick overlying basin-fill sediments (Pao).

overlain by the mid-Tertiary (upper Eocene and Oligocene) Keetley volcanics and younger basin fill deposits.

3.1.1 Paleozoic and Mesozoic sedimentary rocks

Jurassic to Pennsylvanian limestones, sandstones and shales are the oldest rocks exposed in the vicinity of Keetley Valley (pl. 1). On the west side of the valley these rocks generally dip to the east on the east limb of the Park City anticline and they are unconformably overlain and intruded by Tertiary igneous rocks. On the east side of the valley these rocks are only locally exposed as roof pendants on the porphyry stocks.

3.1.2 Keetley volcanics

Nearly horizontal lower Tertiary (upper Eocene and Oligocene) volcanic rocks unconformably overlie deformed Paleozoic and Mesozoic sedimentary rocks in the Keetley volcanic field. The volcanics consist of volcaniclastic breccias, tuffs and flows. Mapped units of roughly equivalent age include the Tuffs of Mountain Meadows and the Silver Creek Breccias that are exposed in the northern portion of Keetley Valley (Bromfield and Crittenden, 1971) and the Coyote Canyon Breccia and the rhyodacite porphyry near Jordanelle that are exposed in the southern portion of the valley (Bromfield and others, 1970). In exposures near the damsite the Coyote Canyon Breccia consists of andesite lava flows and debris flow deposits. The debris flow deposits are moderately to well-indurated volcanic breccias composed of subangular boulders, cobbles and pebbles of igneous rocks (principally andesite), and clasts of sedimentary rocks.

3.1.3 Tertiary porphyry stocks

Calc-alkaline stocks intrude the volcanics and older sedimentary rocks in the central Wasatch Mountains (pl. 1 and fig. 1). The Park Premier stock, described as a rhyodacite porphyry (Bromfield and others, 1970), is exposed on the eastern side of Keetley Valley (pl. 1). The Mayflower stock, described as a granodiorite porphyry (Bromfield and others, 1970), is exposed on the southwest margin of the valley. At the south end of the valley, an intrusive andesite porphyry is exposed along the Provo River at Jordanelle damsite.

3.1.4 Tertiary and Quaternary basin fill deposits

In Keetley Valley the unconsolidated basin fill consists of alluvial fan gravels and debris flows interbedded with silts and clays (Pao on plate 1 and table 1). These deposits are recognized in trench exposures and drill cores where they

overlie the Silver Creek member of the Keetley volcanics. Drill holes and seismic profiles show that the basin fill reaches its maximum thickness in the center of the valley (Appendix A).

Alluvial gravels and debris flows at the damsite are similar to basin fill deposits in Keetley Valley and are included in this map unit (Pao, pl. 1). Exposures at the damsite, described in Appendix B of (USBR, 1986), show that the lowermost portion of these deposits (Tg) overlies the volcanic breccia of Coyote Canyon (Tkcb), but that the Jordanelle andesite porphyry (Tkj) intrudes both units. This relationship establishes that at least part of the basin fill is early Tertiary in age. These Tertiary deposits consist of alluvium, colluvium and debris flows with clasts of andesite and quartzite in a matrix of silt and sand. The unconsolidated matrix of these deposits readily distinguishes them from the volcanic breccia of Coyote Canyon. Basin fill of Quaternary age at the damsite contain the same lithologies as the Tertiary deposits and are distinguishable only on the basis of stratigraphic position.

Another example of unconsolidated lower Tertiary deposits, similar to those in Keetley Valley, is the silt, clay, and gravel that is exposed a few kilometers to the north and east near Parleys Park. These deposits are locally exposed beneath the breccia of the Silver Creek member of the Keetley volcanics (Ttg of Bromfield and Crittenden, 1971), and unconformably overlie deformed Mesozoic and Paleozoic sedimentary rocks. Crittenden and Calkins (1966) suggest that these deposits are derived from the Eocene Wasatch Formation and that they are in part younger, in part older, and in part contemporaneous with the Keetley volcanics.

Several independent methods of age-dating, described in the following paragraphs, including tephrastratigraphy, aminostratigraphy, paleomagnetism, and soil relative-age dating, have been used in this study to establish the age of the basin fill in Keetley Valley. These different lines of evidence indicate that most of the basin fill is early and middle Pleistocene in age.

In the northeastern part of Keetley Valley, two tephra layers are present in the basin fill. These tephra layers occur in the fine-grained distal alluvial fan deposits that comprise the uppermost one meter (3 ft) of the basin fill. One of these tephras is exposed in soil pit JS-15 (pl. 1) and is correlated on the basis of petrographic characteristics with the Lava Creek B ash dated at about 620,000 years old (Ray Wilcox, USGS, 1983, written communication). Another tephra layer was found in the

basin fill exposed in a roadcut on the east side of highway U.S. 40, approximately 30 m (100 ft) west of soil pit JS-15 (pl. 1). On the basis of petrographic characteristics this tephra is correlated with the Bishop Ash, dated at about 730,000 years old (Ray Wilcox, USGS,1983, written communication).

At one locality in Keetley Valley, shells of the gastropod Gyralus sp. were preserved in the basin fill exposed in a test pit near the southern end of the proposed reservoir (TP-314 on pl. 1). The average amino acid ratio from three preparations is 0.66. Using kinetic models of amino acid racemization and temperature histories discussed in Sullivan and others (1988), this ratio yields a minimum age for the sample of approximately 800,000 to 1,000,000 years.

A paleomagnetic study of the basin fill in Keetley Valley was conducted to determine whether sampled sediments retained a well-defined reversed polarity component that would suggest that they were more than 730,000 years old. The report describing the results of these analyses is included as Appendix B to this report. Samples for paleomagnetic analysis were obtained from fine-grained units within the basin fill in drill cores, trenches, soil pits, and natural and man-made exposures throughout Keetley Valley (pl. 1). Samples from 6 of the 10 surface sites (JT-2, JT-7A, JT-7B, JT-11, J-13, J-16) in Keetley Valley contain a strong indication of a reversed component of magnetization, indicating that the basin-fill sediments at these localities were deposited prior to 730,000 years ago. These magnetically reversed samples are from the upper 3 m (10 ft) of the basin fill. Samples from lower in the stratigraphic section were obtained from drill cores (R101, R110, R111, R114, and R115). These samples were difficult to interpret due to the presence of secondary components of magnetization related to drilling, but, in spite of these difficulties, several samples contained unambiguous reversed components indicating a pre-mid Pleistocene age (>730,000 years old) for most of the basin fill. Figure 4 is a diagram showing the stratigraphy, the relative position, and the polarity of the paleomagnetic samples in these cores along a section from north to south in Keetley Valley.

In summary, the stratigraphy of the basin fill in Keetley Valley, interpreted from the drill cores and surficial excavations and extrapolated from exposures at the damsite, shows that the filling of the valley was initiated during the early Tertiary and continued into the mid-Quaternary (about 600,000 years ago). Upper Quaternary (<150,000 years old) deposits in Keetley Valley, discussed in the following paragraphs, consist of alluvial fans around the margins of the

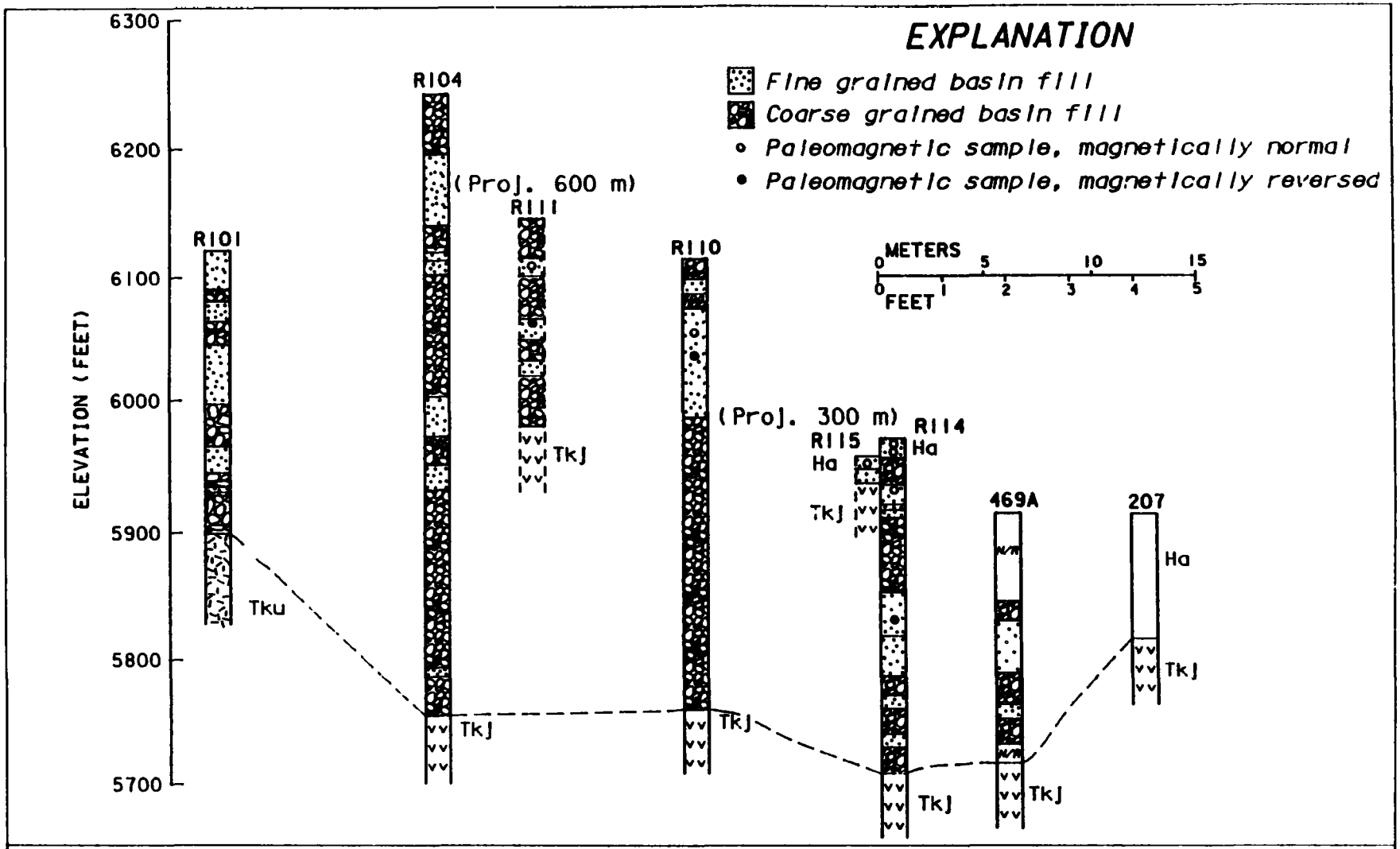

FIGURE 4: Cross section AA and logs of drill holes through basin fill deposits in Keetley Valley plotted on a north-south cross section with a vertical exaggeration of 10:1. Paleomagnetic samples from fine-grained deposits in the basin fill indicate both reverse and normal magnetization; see Appendix B for discussion. Heavy dashed line correlates bedrock surface in the deepest portion of Keetley Valley. Note bedrock elevation in drill holes in the center of the valley is lower than the bedrock elevation in the buried channel at at the damsite (207). Cross section and drill holes located on plate 1. Unit labels from plate 1.

102-CD-16

basin, colluvium on hillslopes, and alluvium inset into the basin fill along modern drainages.

3.1.5 Upper Quaternary deposits

At the northeast margin of Keetley Valley and at the mouth of McHenry Canyon, coarse alluvial gravels about 1 to 2 m (3 to 6 ft) thick (Pa on pl. 1 and table 1) were deposited in fans on the surface of the basin fill. These deposits consist of partially decomposed subrounded gravels that were derived from Keetley volcanics exposed in the highlands to the east and from Paleozoic sandstones and shales exposed to the west of Keetley Valley. In soil pit JS-15, these gravels unconformably overlie the Lava Creek ash and therefore are less than 620,000 years old. From this relationship and the relative degree of soil development on the surface, described in the following section, we infer that these fan gravels are late Pleistocene in age (150,000 to 10,000 years old).

On the west side of Keetley Valley, McHenry Creek has incised the basin fill (Pao) and the overlying fan gravels (Pa) to a depth of about 20 to 40 m (67 to 132 ft). An alluvial terrace 6 m (20 ft) above the present creek near the point where McHenry Canyon enters Keetley Valley (Pay on pl.1 and table 1) contains rounded gravels of quartzite and intrusive igneous rocks. Relative geomorphic position and soil development (discussed in the following section) suggest that these gravels date from the latest Pleistocene (30,000 to 10,000 years ago).

Alluvial deposits in the modern floodplain of Ross Creek and its tributaries that are inset into the basin fill about 30-50 m are inferred to have been deposited during the Holocene (<10,000 years old). Additionally, a veneer of active colluvium (Qc on pl. 1 and table 1) is present on the hillslopes surrounding Keetley Valley.

3.1.6 Soil relative-age dating

Eighteen soil profiles were described in trenches, soil pits, and natural and man-made exposures in Keetley Valley in order to assess the relative age of the surfaces on which they formed. The degree of development of the soils in Keetley Valley was compared with soils elsewhere in the back valleys of the Wasatch Mountains that have been assigned to one of four RAGs (relative age groups). The ages of these RAGS have been estimated based on correlation with Rocky Mountain glaciation and other independent age-dating criteria (Sullivan and others, 1988).

Eight of the Keetley Valley soil profiles (JS-1, 2, 3, 4, 5, 11, 13, 16) were described on the basin fill (Pao) and the data are compiled in tables 2 and 3. Soils on the surface of the basin fill are characterized by the presence of a 36- to 76-cm-thick argillic horizon with 1) an average of 33% estimated secondary clay, 2) thick and moderately thick clay films on ped faces, and 3) 5YR to 7.5YR hues. The presence of a Bk horizon with stage I or II carbonate is common in most profiles. Clasts of diorite, sandstone, and shale are strongly weathered (grusified) in some profiles (JS-5, 11). Seven profiles (JS-6, 7, 9, 14, 15, 17, 18) were described on surfaces containing a veneer (<1 m thick) of either colluvium (Qc) or alluvium (Pa) overlying basin fill. These soils are similar to those on the basin fill with the overlying colluvium and alluvium containing either the parent material for the A and B horizons in four profiles (JS-6, 7, 9, and 18), or the upper parts of the Bt and Bk horizons in three (JS-14, 15, and 17). Two profiles (JS-7, 9) on the Pleistocene alluvium (Pa) near the mouth of McHenry Canyon (pl. 1) lack carbonate horizons.

The soil profile (JS-8) on the surface of the younger Pleistocene alluvium (Pay) is less developed than the soils on the basin fill (Pao) or on the alluvium overlying the basin fill (Pa/ao). This soil contains a cambic horizon 13 cm (5.1 in) thick with 7.5 YR hue and thin clay films on clasts. About half of the igneous clasts in the profile are moderately weathered. There is no evidence for carbonate accumulation in the profile.

In order to quantitatively compare the degree of soil development among profiles in Keetley Valley with profiles elsewhere in the back valleys described in Sullivan and others (1988), soil development indices in table 3 were calculated for each profile using the methods of Harden (1982) and Harden and Taylor (1983). These indices give a measure of the degree of soil development for each profile using several field properties found to change with time as the age of the soil increases. Sullivan and others (1988) were able to distinguish four broad groups of soils of differing RAGs in the back valleys using plots of the non-arid profile index and the rubification index for 16 profiles. On figure 5 we have plotted the same soil parameters from the Keetley Valley sites to compare them with those described in Sullivan and others (1988). Indices for the soils on surfaces underlain by the basin fill plot within RAG 2 and RAG 3, suggesting a late Pleistocene age for the surface. Profiles JS-7 and JS-9 on the surface of the younger alluvium (Pa) are similar to soils in RAG 2 (10,000 to 130,000 years) in other back valleys. Profile JS-8 on the younger Pleistocene alluvium (Pay) at McHenry Canyon is similar to the soil in RAG 3

Table 2: Selected properties and laboratory data for soil profiles in Keetley Valley (continued on next two pages).

Map Unit (plate 1)	Profile	Horizon	Depth (cm)	Munsell color (dry)	Texture	------% Clasts >2 mm------ pebbles	cobbles	boulders	Carb. stage /1	% CO3 /2	% O.M. /3	% sand /4	% silt /4	% clay /4
Pao	JS-1	A1	0-10	7.5YR 4/3	sicl	2				n.d.	n.d.	n.d.	n.d.	n.d.
		A2	10-17	7.5YR 5/3	scl	2				n.d.	n.d.	n.d.	n.d.	n.d.
		BA	17-78	7.5YR 4/3	si	2				n.d.	n.d.	n.d.	n.d.	n.d.
		Bt	78-117	7.5YR 5/4	sicl	2			I	n.d.	n.d.	n.d.	n.d.	n.d.
		Bk	117-182	7.5YR 5/4	sicl	5			II	n.d.	n.d.	n.d.	n.d.	n.d.
Pao	JS-2	A1	0-14	10YR 6/2	sl	2				n.d.	n.d.	n.d.	n.d.	n.d.
		A2	14-25	10YR 5/3	sil	2				n.d.	n.d.	n.d.	n.d.	n.d.
		BA	25-37	7.5YR 6/3	scl	2				n.d.	n.d.	n.d.	n.d.	n.d.
		Bt	37-73	7.5YR 7/4	cl	1				n.d.	n.d.	n.d.	n.d.	n.d.
		C1	73-107	2.5YR 8/6	s	1				n.d.	n.d.	n.d.	n.d.	n.d.
		C2	107-195	2.5YR 8/4	s	15			I	n.d.	n.d.	n.d.	n.d.	n.d.
Pao	JS-3	A1	0-13	10YR 4/2	sil	1				n.d.	n.d.	n.d.	n.d.	n.d.
		A2	13-23	10YR 2/3	sicl	1				n.d.	n.d.	n.d.	n.d.	n.d.
		Bt	23-67	2.5Y 7/3	cl	1				n.d.	n.d.	n.d.	n.d.	n.d.
		BC	67-99	2.5Y 8/4	sicl	1			I	n.d.	n.d.	n.d.	n.d.	n.d.
		C1	99-126	2.5Y 8/4	sil	1			I	n.d.	n.d.	n.d.	n.d.	n.d.
		C2	126-185	2.5Y 8/3	l	1			I	n.d.	n.d.	n.d.	n.d.	n.d.
Pao (Trench J2)	JS-4	A1	0-10	7.5YR 5/3	sil	5				0.00	7.10	24.8	39.1	36.1
		A2	10-24	7.5YR 5/3	sicl	5				0.00	2.10	21.0	39.3	39.7
		Bt1	24-64	5YR 5/4	cl	5				0.00	0.84	19.0	27.1	53.9
		2Bt2	64-89	10YR 5/4	cl	2			I	0.50	0.33	19.5	33.0	47.5
		2Bk	89-122	10YR 7/3	sicl	2			II	28.14	0.54	24.5	33.4	42.1
		3Bk	122-158	10YR 7/3	sl	2			II	28.31	0.21	66.9	15.0	18.1
		4Bk	158-212	10YR 6/7	l	35			II	7.00	0.05	58.7	19.1	22.2
		5Bk	212-237	10YR 4/3	sicl	15			II	2.60	0.11	12.5	35.1	52.4
Pao	JS-5	A1	0-16	7.5YR 4/2	l	5				0.10	3.30	28.0	46.0	26.0
		A2	16-27	7.5YR 4/2	cl	8	2			0.10	2.70	26.4	42.6	31.0
		Bt1	27-40	5YR 5/3	c	10	2			0.10	1.70	22.1	37.3	40.6
		Bt2	40-63	5YR 5/4	c	20	5			0.20	1.10	20.6	36.7	42.7
		2Bt3	63-110	5YR 5/4	l	50	20			0.20	0.80	30.5	42.6	26.9
		3B	110-122	5YR 5/4	cl	5				3.80	0.50	21.0	54.4	24.6
		3Bk1	122-185	7.5YR 5/4	c	5			I	7.60	0.40	19.4	46.1	34.5
		3Bk2	185-210	5YR 5/4	c	5			I	1.00	0.30	9.80	46.4	43.8
Qc/Pao	JS-6	A1	0-5	10YR 3/2	l	2				1.00	5.90	27.0	48.3	24.7
		A2	5-17	10YR 5/2	cl	5				1.00	2.70	22.2	45.7	32.1
		A3	17-30	10YR 4/2	c	5				1.00	1.40	19.8	46.7	33.5
		2Bt1	30-80	7.5YR 4/4	sicl					1.00	0.40	14.2	46.6	39.2
		2Bt2	80-108	7.5YR 4/4	sicl					1.00	0.20	16.1	45.5	38.4
		2Bk1	108-145	7.5YR 4/4	sicl				I	4.90	0.20	16.5	49.7	33.8
		2Bk2	145-167	7.5YR 4/4	sicl	8			I	6.10	0.20	17.3	51.8	30.9
		3C	167-195	7.5YR 6/4	cl	70	10		I	7.90	0.10	32.8	36.7	30.5
Pa/ao	JS-7	A1	0-12	10YR 4/2	cl	5	5			1.0	5.4	21.3	50.7	28.0
		A2	12-30	10YR 4/2	cl	5	10			1.0	2.6	20.0	49.0	31.1
		2Bt	30-55	7.5YR 4/5	c	5	10			1.0	0.9	18.4	29.0	52.6
		3Bt	55-76	7.5YR 4/4	c	40	20			1.0	0.6	30.5	21.7	47.8
		3B	76-155	10YR 7/6	scl	60	30			1.0	0.4	46.0	21.9	32.1

/1 Maximum stage of carbonate development in the profile, terminology of Gile and others (1966) and Bachman and Machette (1977).
/2 Percent $CaCO_3$ by dilution with sulfuric acid and titration with sodium hydroxide using methods of Soltanpour and Workman (1981).
/3 Percent organic matter by wet titration using methods of Soltanpour and Workman (1981).
/4 Grain-size data are given in percent by weight of the less than 2 mm fraction: sand (>50um), silt (2-50um), clay (<2um). Sand fractions by dry sieve with prior removal of organic matter and $CaCO_3$. Silt fractions by pipette with prior removal of organic matter and $CaCO_3$.
n.d. No laboratory data available for these profiles.

Table 2, continued: Selected properties and laboratory data for soil profiles in Keetley Valley.

Map Unit (plate 1)	Profile	Horizon	Depth (cm)	Munsell color (dry)	Texture	% pebbles	% cobbles	% boulders	Carb. stage /1	% CO3 /3	% O.M. /4	% sand /5	% silt /5	% clay /5
Pay	JS-8	A	0-25	10YR 3/3	cl	15				0.1	4.8	30.7	50.6	18.7
		B1	25-38	10YR 4/3	l	30	30			0.1	1.6	37.6	44.5	17.9
		B2	38-82	7.5YR 6/4	sl	30	30	10		0.1	0.7	55.4	28.1	16.5
		B3	82-140	10YR 5/6	sl	20	50	10		0.1	0.4	70.0	19.9	10.1
		B4	140-170	10YR 6/8	sl	25	30	5		0.1	0.5	57.4	28.5	14.1
Pa/ao	JS-9	A	0-11	10YR 4/2	sil	20				0.0	5.4	22.0	51.1	26.9
		B1	11-37	10YR 4/2	l	20	20			0.0	3.9	29.2	47.3	23.5
		B2	37-65	10YR 4/2	l	20	40			0.0	2.0	30.0	43.9	26.1
		2Bt	65-110	5YR 4/6	sc	20	30	30		0.0	0.8	33.1	35.1	31.8
		2B	110-130	7.5YR 5/6	sl	20	30	30		0.0	0.4	58.0	23.7	18.3
		2C	130-180	7.5YR 5/5	sl	5	20	40		n.d.	n.d.	n.d.	n.d.	n.d.
Pa/ao	JS-10	A1	0-9	10YR 3/2	l	10				n.d.	n.d.	n.d.	n.d.	n.d.
		A2	9-25	10YR 2/2	cl	10				n.d.	n.d.	n.d.	n.d.	n.d.
		B	25-37	10YR 4/2	c	10				n.d.	n.d.	n.d.	n.d.	n.d.
		Bt	37-74	10YR 4/2	c	10				n.d.	n.d.	n.d.	n.d.	n.d.
		2Bt	74-112	2.5Y 7/3	sc	15				n.d.	n.d.	n.d.	n.d.	n.d.
		3Bt	112-136	2.5Y 7/2	c	10				n.d.	n.d.	n.d.	n.d.	n.d.
		4Bk	136-175	2.5Y 7/2	sl	40			I	n.d.	n.d.	n.d.	n.d.	n.d.
		4C	175-200	2.5Y 6/3	ls	25				n.d.	n.d.	n.d.	n.d.	n.d.
Pac	JS-11	A	0-17	7.5YR 4/2	sic	10				n.d.	n.d.	n.d.	n.d.	n.d.
		B	17-25	7.5YR 4/2	c	10	10			n.d.	n.d.	n.d.	n.d.	n.d.
		Bt1	25-61	7.5YR 6/4	c	10				n.d.	n.d.	n.d.	n.d.	n.d.
		Bt2	61-100	7.5YR 6/4	cl	10	10			n.d.	n.d.	n.d.	n.d.	n.d.
		2Bk	100-134	7.5YR 8/3	cl	30				n.d.	n.d.	n.d.	n.d.	n.d.
		3Bk	134-177	10YR 7/3	sl	5				n.d.	n.d.	n.d.	n.d.	n.d.
Pay	JS-12	A1	0-10	10YR 5/2	l	10				n.d.	n.d.	n.d.	n.d.	n.d.
		A2	10-18	10YR 4/2	cl	10				n.d.	n.d.	n.d.	n.d.	n.d.
		Bt1	18-35	10YR 5/3	cl	15				n.d.	n.d.	n.d.	n.d.	n.d.
		Bt2	35-68	7.5YR 6/4	cl	20				n.d.	n.d.	n.d.	n.d.	n.d.
		B1	68-82	10YR 5/3	scl	40	10			n.d.	n.d.	n.d.	n.d.	n.d.
		2B1	82-121	10YR 5/3	ls	60	30			n.d.	n.d.	n.d.	n.d.	n.d.
		2B3	121-160	10YR 5/3	ls	50	40			n.d.	n.d.	n.d.	n.d.	n.d.
		3C	160-200	7.5YR 6/4	cl	15				n.d.	n.d.	n.d.	n.d.	n.d.
Pac (Trench J7)	JS-13	A	0-15	7.5YR 5/3	cl	10				n.d.	n.d.	n.d.	n.d.	n.d.
		B	15-26	7.5YR 6/5	cl	7				n.d.	n.d.	n.d.	n.d.	n.d.
		Bt	26-90	10YR 6/3	c	1			I	n.d.	n.d.	n.d.	n.d.	n.d.
		2Bk1	90-116	2.5Y 7/2	c	1			II	n.d.	n.d.	n.d.	n.d.	n.d.
		2Bk2	116-131	2.5Y 5/3	c	1			II	n.d.	n.d.	n.d.	n.d.	n.d.
		2Bk3	131-148	2.5Y 7/2	c				III	n.d.	n.d.	n.d.	n.d.	n.d.
		3Bk	148-183	10YR 6/4	c	5			II	n.d.	n.d.	n.d.	n.d.	n.d.
		3C	183-212	10YR 8/2	c	65				n.d.	n.d.	n.d.	n.d.	n.d.

/1 Maximum stage of carbonate development in the profile, terminology of Bile and others (1966) and Bachman and Machette (1977).
/2 Percent $CaCO_3$ by dilution with sulfuric acid and titration with sodium hydroxide using methods of Soltanpour and Workman (1981).
/3 Percent organic matter by wet titration using methods of Soltanpour and Workman (1981).
/4 Grain-size data are given in percent by weight of the less than 2 mm fraction: sand (>50um), silt (2-50um), clay (<2um).
Sand fractions by dry sieve with prior removal of organic matter and $CaCO_3$. Silt fractions by pipette with prior removal of organic matter and $CaCO_3$.
n.d. No laboratory data available for these profiles.

Table 2, continued

Map Unit (plate 1)	Profile	Horizon	Depth (cm)	Munsell color (dry)	Texture	------% pebbles	cobbles	boulders	Carb. stage /1	% CO3 /3	% O.M. /4	% sand /5	% silt /5	% clay /5
Pa/ao	JS-14	A	0-19	10YR 4/2	sicl	5	5			0.1	3.3	47.1	34.3	18.6
		Bt1	19-36	7.5YR 4/3	l	30				0.1	1.1	45.9	24.7	29.4
		Bt2	36-79	7.5YR 5/4	l	60	10			0.1	0.8	56.8	20.6	22.6
		2Bt	79-107	10YR 7/3	cl	5				0.4	0.3	20.0	42.9	37.1
		2Bk1	107-148	10YR 8/2	cl	5			I	2.8	0.2	25.6	44.5	29.6
		2Bk2	148-173	10YR 8/2	l	5			I	3.7	0.1	33.4	39.7	26.9
Pa/ao	JS-15	A	0-23	10YR 4/2	l	40	10		II	n.d.	n.d.	n.d.	n.d.	n.d.
		Bk	23-34	10YR 7/3	l	10	40		II	n.d.	n.d.	n.d.	n.d.	n.d.
		2Bk	34-75	10YR 8/3	sl				II	n.d.	n.d.	n.d.	n.d.	n.d.
		3Bk	75-95	7.5YR 8/2	sicl				II	n.d.	n.d.	n.d.	n.d.	n.d.
		3C	95-122	7.5YR 8/2	sicl				I	n.d.	n.d.	n.d.	n.d.	n.d.
		4C	122-210	10YR 8/1	ls					n.d.	n.d.	n.d.	n.d.	n.d.
Pao (Trench J11)	JS-16	A	0-15	10YR 6/2	cl					n.d.	n.d.	n.d.	n.d.	n.d.
		Bt1	15-79	7.5YR 6/4	c	10				n.d.	n.d.	n.d.	n.d.	n.d.
		Bt2	79-91	10YR 7/4	c	5			II	n.d.	n.d.	n.d.	n.d.	n.d.
		2B	91-124	10YR 7/3	c	5			II	n.d.	n.d.	n.d.	n.d.	n.d.
		2C	124-157	2.5Y 6/3	c	20	5		I	n.d.	n.d.	n.d.	n.d.	n.d.
		3C	157-216	7.5YR 5/6	sc	20	5			n.d.	n.d.	n.d.	n.d.	n.d.
Qc/Pao (Trench J9)	JS-17	A1	0-12	7.5YR 5/3	sil	30	10			1.1	6.9	18.9	60.6	20.5
		A2	12-40	7.5YR 5/3	sil	30	10			0.4	2.8	20.9	57.5	21.6
		Bt1	40-55	7.5YR 7/4	sil	30	10			0.4	1.0	24.2	55.0	20.8
		Bt2	55-108	7.5YR 4/6	sicl	30	10			0.2	0.7	12.0	32.7	55.3
		C	108-128	7.5YR 7/4	l	30	10	2		0.0	0.4	36.0	48.1	15.9
		2Btb	128-192	5YR 7/4	sc	20	10			0.0	0.2	27.0	42.7	30.3
		2BC	192-265	7.5YR 7/4	l	30	10	2		0.0	0.4	47.1	39.1	13.8
		3C1	265-329	7.5YR 7/4	l	80	2			0.1	0.3	46.3	44.6	9.1
		3C2	329-369	7.5YR 7/4	l	50				0.1	0.2	46.4	39.0	14.6
		4C	369-467	10YR 7/8	scl					0.3	0.3	32.1	38.2	29.7
Qc/Pao (Trench J13)	JS-18	A1	0-14	7.5YR 5/3	sil	8				0.8	6.9	20.6	57.8	21.6
		A2	14-30	7.5YR 5/3	sil	8				0.8	3.0	20.8	56.0	23.2
		A3	30-80	7.5YR 6/4	sil	8				0.4	2.1	20.8	56.6	22.6
		Bt	80-104	7.5YR 7/4	sil	8	5			0.2	0.9	22.8	57.6	19.6
		2Bt	104-124	7.5YR 7/4	sicl	20	25			0.2	0.9	16.8	54.3	28.9
		2BC	124-155	7.5YR 7/4	l	20	25			0.2	0.6	32.7	49.8	17.5
		3Btb	155-252	5YR 5/6	c	20	8			0.2	0.4	19.9	32.7	47.4
		4Btb	252-309	7.5YR 5/6	c	3				0.4	0.3	13.6	31.3	55.1
		4BCb	309-329	7.5YR 6/6	sil	10	2			0.4	0.4	27.5	50.9	21.6
		5C	329-370	7.5YR 7/4	l	30	5			0.3	0.4	40.0	45.6	14.4

/1 Maximum stage of carbonate development in the profile, terminology of Gile and others (1966) and Bachman and Machette (1977).
/2 Percent $CaCO_3$ by dilution with sulfuric acid and titration with sodium hydroxide using methods of Soltanpour and Workman (1981).
/3 Percent organic matter by wet titration using methods of Soltanpour and Workman (1981).
/4 Grain-size data are given in percent by weight of the less than 2 mm fraction: sand (>50um), silt (2-50um), clay (<2um). Sand fractions by dry sieve with prior removal of organic matter and $CaCO_3$. Silt fractions by pipette with prior removal of organic matter and $CaCO_3$.
n.d. No laboratory data available for these profiles.

Table 3: Soil development indices and secondary clay and carbonate for Jordanelle soils

Profile	SOIL PROPERTIES /1								HARDEN INDICES /2			SECONDARY CLAY AND CARBONATE /3			
	RUBIFICATION	MELANIZATION	COLOR PALING	COLOR LIGHTENING	TEXTURE	STRUCTURE	DRY CONSISTENCE	CLAY FILMS	NON-ARID INDEX	ARID INDEX	ALL PROPERTIES INDEX	g/cm2 CLAY	g/cm3 CLAY	g/cm2 CARBONATE	g/cm3 CARBONATE
JS-1	15.66	14.24	0.00	10.56	25.00	131.33	43.20	116.38	56.85	54.41	58.79	n.d.	n.d.	n.d.	n.d.
JS-2	44.11	38.71	12.67	0.00	66.00	78.33	28.20	27.23	47.10	35.41	49.70	n.d.	n.d.	n.d.	n.d.
JS-3	5.53	35.53	15.50	0.00	58.78	94.25	33.40	22.00	41.58	37.32	47.99	n.d.	n.d.	n.d.	n.d.
JS-4	12.26	16.24	10.67	21.38	28.11	103.63	38.90	91.27	48.40	48.99	58.58	34.81	0.1268	37.42	0.1483
JS-5	28.55	10.59	13.50	13.78	32.44	69.75	2.30	73.31	36.16	34.18	44.10	16.14	0.0575	8.86	0.0242
JS-6	38.16	1.18	3.67	22.56	49.67	107.00	22.80	43.62	43.74	41.55	53.39	78.65	0.2691	7.30	0.2634
JS-7	35.29	13.88	14.08	29.63	26.56	44.33	19.00	84.62	37.28	36.37	42.87	9.02	0.0651	0.87	0.0080
JS-8	14.74	15.59	16.83	9.25	11.22	28.88	8.20	71.15	24.96	24.26	30.48	-0.23	0.0019	0.09	0.0006
JS-9	11.58	22.94	27.83	0.00	15.00	70.67	9.90	97.46	37.92	36.81	48.54	3.23	0.0121	0.00	0.0000
JS-10	0.32	19.41	27.00	12.63	32.89	65.25	20.10	71.62	34.93	38.25	41.90	n.d.	n.d.	n.d.	n.d.
JS-11	5.66	7.06	56.17	34.44	34.67	84.25	8.30	56.38	32.72	45.70	46.81	n.d.	n.d.	n.d.	n.d.
JS-12	8.55	3.65	6.00	9.13	17.33	48.25	3.30	94.38	29.24	29.73	37.00	n.d.	n.d.	n.d.	n.d.
JS-13	8.37	1.76	12.27	42.88	15.44	152.33	6.40	51.58	33.70	40.17	46.23	n.d.	n.d.	n.d.	n.d.
JS-14	8.34	9.71	17.33	33.69	40.56	77.38	6.90	69.73	27.30	32.97	38.02	16.79	0.0952	3.66	0.0195
JS-15	8.95	5.41	30.17	35.00	12.11	39.83	8.80	0.00	10.73	17.99	20.19	n.d.	n.d.	n.d.	n.d.
JS-16	22.00	7.06	0.00	16.63	48.44	84.17	20.20	73.62	36.50	34.72	41.79	n.d.	n.d.	n.d.	n.d.
JS-17	25.16	0.00	0.00	14.13	63.50	92.83	35.60	212.31	61.34	59.77	76.36	35.60	0.0653	0.30	0.0010
JS-18	10.21	25.88	10.00	3.75	97.11	154.00	59.40	170.15	86.13	82.40	115.18	67.69	0.1161	1.34	0.0040

/1 Numbers are calculated from field descriptions following the methods of Harden (1982) and Harden and Taylor (1983) and modified methods of Nelson and Taylor (1985).

/2 Properties used to calculate the non-arid index are rubification, melanization, texture, structure, dry consistence, clay films (Harden and Taylor, 1983). Properties used to calculate the arid index are color-paling, color lightening, texture, structure, dry consistence, clay films (Harden and Taylor, 1983). The all properties index was calculated from all of the properties tabulated for each profile.

/3 Secondary carbonate and clay in entire profile calculated according to methods described in Machette (1978, 1985). Bulk density estimated from texture (Rawls, 1983).

n.d. no data available

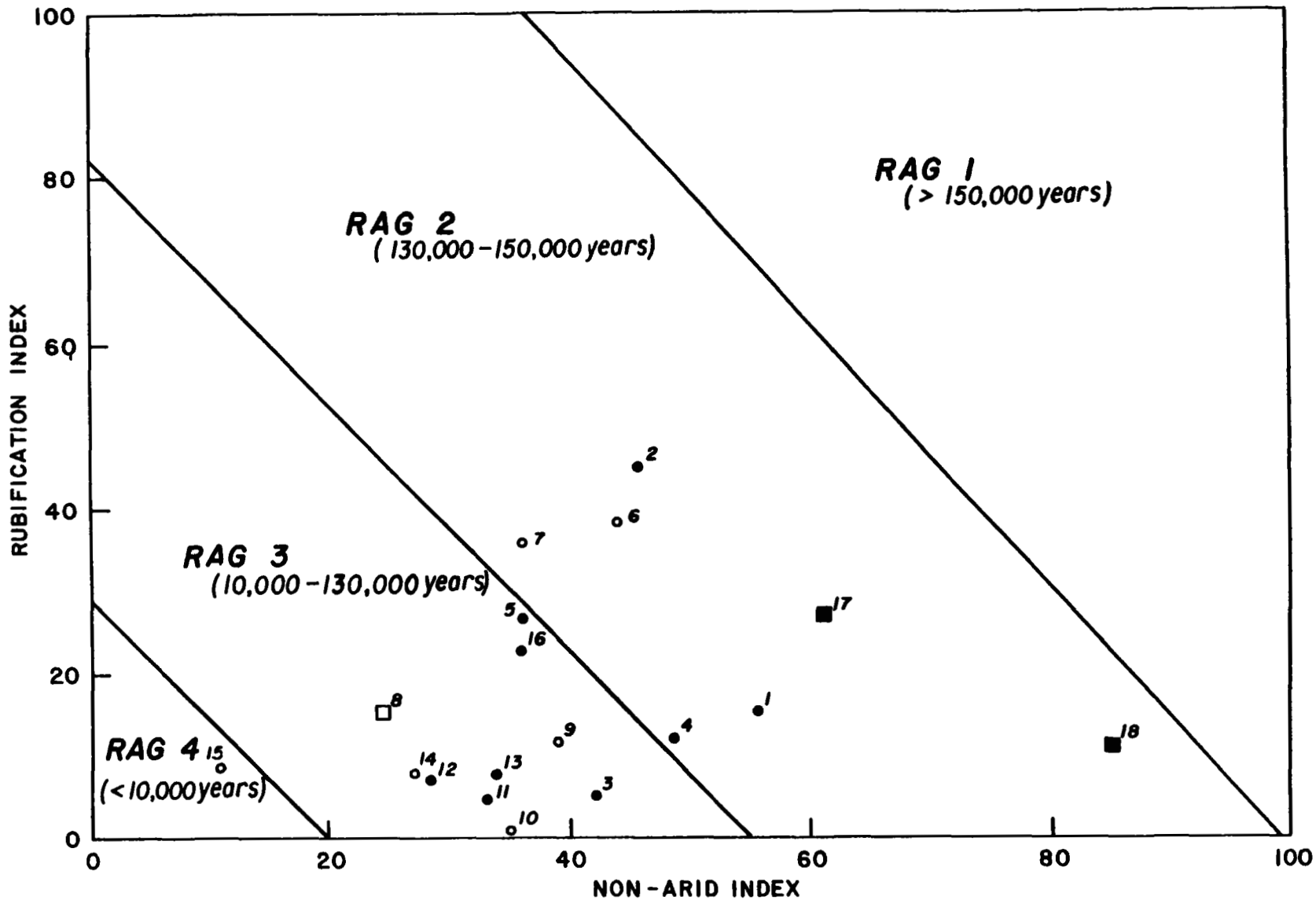

FIGURE 5: Values for rubification and non-arid index for Keetley Valley soils (JS1-JS18, Table 2) are plotted on a graph distinguishing relative age groups for soils in the back valleys (from Sullivan and others, 1988). Parent materials for the soils are Pao (•), Pa (○), Pay (□) and Qc (■) from Plate 1.

in other back valleys on deposits inferred to be 15,000 to 18,000 years old. Profile JS-15 appears younger than expected (RAG 4) because of the coarser texture of the parent material that is predominantly tephra.

In summary, the soil characteristics exhibited by the profiles on the surface of the basin fill are similar to those observed in profiles in other back valleys that are inferred to be at least 130,000 years old and probably are considerably older. This minimum age estimate for the surface on the basin fill is consistent with a pre-middle Pleistocene age for the deposits. The discrepancy between the estimated age of the parent material and the soil may indicate the surface of the basin fill was eroded prior to the onset of conditions favoring soil development. The younger Pleistocene alluvium (Pay) has a soil profile that is consistent with a latest Pleistocene age (30,000 to 10,000 years ago).

3.2 East-trending faults in the Park City mining district

Mineralization in the Park City mining district is associated with east-trending fault zones on the west side of Keetley Valley (fig. 6). The major mineralized structures are the Hawkeye-McHenry fault zone, its inferred extensions the Daly and Ontario veins, and the Mayflower structural zone. The Cottonwood fault is also a major, east-trending structure with minor mineralization.

3.2.1 Hawkeye-McHenry fault zone

The east-trending Hawkeye McHenry fault zone (fig. 6 and pl. 1) extends from the east limb of the Park City anticline east to the margin of Keetley Valley (Bromfield, 1968; Bromfield and Crittenden, 1971; Bromfield and others, 1970). At the surface Triassic sedimentary rocks and the overlying Keetley volcanics on the north are faulted against the Pennsylvanian Weber Quartzite on the south. In the subsurface, vein ore and bedded replacement deposits have been extensively mined along the fault zone. Mine maps show that the fault zone is complex, consisting of footwall and hanging wall strands that are hundreds of meters apart with an average dip of 45° to the north and stratigraphic displacement of at least 300 m (1000 ft) (Bromfield, 1968; Garmoe and Erickson, 1968). To the west, the fault is truncated by the north-trending #9 fault (fig. 6) (Garmoe and Erickson, 1968). Further west the highly productive east-trending Daly and Ontario Veins (fig. 6) are inferred to be the continuation of the Hawkeye-McHenry fault zone (Garmoe and Erickson, 1968). To the east the projection of the Hawkeye-McHenry fault is

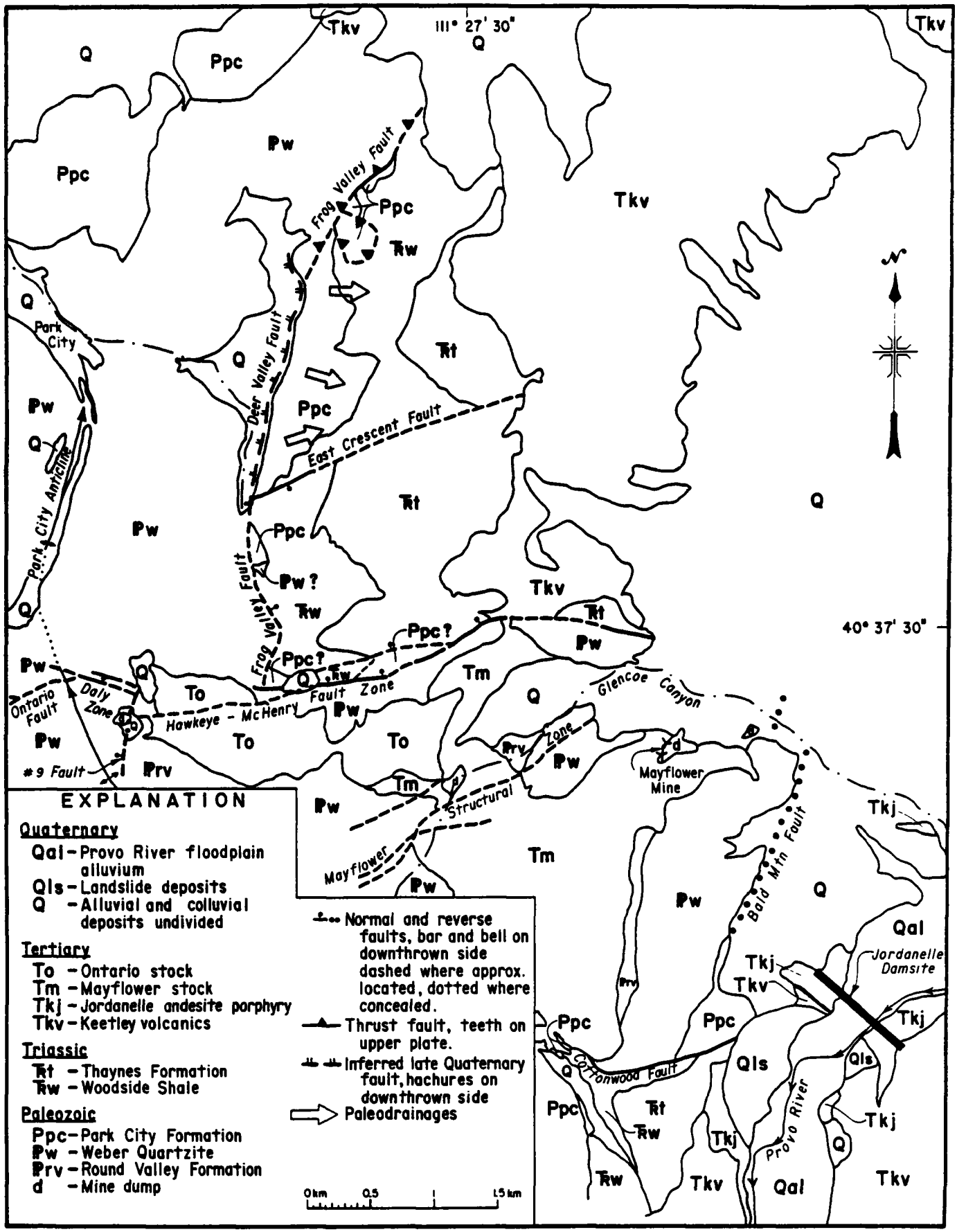

Figure 6 Principal faults in the Park City Mining District northeast of Jordanelle damsite from Bromfield and others (1970) and Bromfield and Crittenden (1971).

concealed by the basin fill in Keetley Valley. No topographic escarpment is present along the trace of the fault, and no scarps or lineaments are present in the valley on the projection of the fault.

Mine geologists and a USBR consultants map of the proposed reservoir (Bridges, 1984) infer that the fault continues with a southeast trend across the valley. Alternatively, the Hawkeye-McHenry fault has been modeled in resistivity traverses in Keetley Valley where it has been interpreted to turn and strike south along the southwest margin of the valley (Meiiji, 1980). Neither of these interpretations of the trend of an eastward extension of the Hawkeye-McHenry fault zone have been confirmed due, in large part, to the thick alluvial fill masking the projection of the fault.

Extensive mineralization of the fault zone and its subsequent offset by the barren #9 fault suggest that displacement on the fault largely predates or is contemporaneous with Tertiary mineralization in the Park City mining district. In addition the fault zone is offset by the #9 fault. This evidence, together with the lack of a bedrock escarpment or scarps and lineaments on in mid-Pleistocene basin fill the projection of the fault, indicate that no late Quaternary surface displacements have occurred on the fault.

3.2.2 Mayflower-Pearl structural zone

The Mayflower-Pearl structural zone (fig. 6 and pl. 1) is a zone of minor fracturing near the northern margin of the Mayflower stock that has localized silver, lead, zinc, gold and copper mineralization. The trend of this structural zone is irregular but has an average strike of N60^{o}E and an average dip of near vertical. It consists of a 60-m-wide zone of parallel, en echelon, braided and branching veins that pass from sedimentary rocks on the west into the Mayflower stock to the east (Quinlan and Simos, 1968). The maximum displacement on any individual fault in the zone is less than 3 m (10 ft) and the total displacement across the zone is estimated to be about 30 m (100 ft) with the north side down (Quinlan and Simos, 1968). East of the mapped trace of this structural zone (pl. 1), apparent left lateral offset of about 1000 m (3000 ft) of the Weber Quartzite-Round Valley Limestone contact has been interpreted as suggesting that substantial displacement has occurred on the fault zone (Jordanelle Task Force, 1982). As the west margin of the Mayflower stock is only offset about 30 m (100 ft) (Quinlan and Simos, 1968; Bromfield and others, 1970)

most of the displacement must predate or be related to the intrusion of the stock.

Mine maps of the Cunningham Tunnel (Jordanelle Task Force, 1982) show northeast-striking shears in unconsolidated deposits near the tunnel portal. To verify the existence of these shears and to investigate their origin and age, two trenches (J-8 and J-8E) were excavated in basin fill on the projection of the shears about 61 m (200 ft) west of the tunnel (fig. 7). The trenches (fig. 8) expose a stratified sequence of gravels (Pa on pl. 1) overlying clays and sand lenses of the basin fill (Pao on pl. 1) with a thin veneer of slope colluvium at the surface. The lithologies and near-horizontal contacts of the units are typical of the basin fill exposed elsewhere and indicate that these units were deposited prior to their incision by Big Dutch Pete Creek (pl. 1). Within the trenches overlapping stratigraphic contacts between units within the basin fill preclude displacement of the units since their deposition.

The age of these deposits is constrained by age estimates of the basin fill (Pao) in the vicinity. Paleomagnetic data from 11 samples at three separate locations within fine-grained units of the basin fill from trench J-8 (fig. 8) have a remnant magnetization dominated by a normal component. This indicates that the sediments were deposited during the last 730,000 years. Alluvial gravels (unit Pa on pl. 1) conformably overlie the basin fill in the trench (fig. 8). Soil profile JS-7 was described in a test pit in these deposits about 60 m (200 ft) northwest of trench J-8 (fig. 7 and pl. 1). The parent material for the soil consists of rounded pebbles and cobbles of quartzite, andesite porphyry, and sandstone with a matrix (<10%) of sandy clay. The soil has a strongly developed argillic horizon (table 2) and the igneous clasts are very strongly weathered throughout the profile. These soil characteristics suggest a correlation with RAG 2 deposits of Sullivan and others (1988), indicating a minimum age of at least 130,000 years for these gravels (sec. 3.1.5).

We conclude that the shear zones mapped in the unconsolidated deposits near the portal of the Cunningham Tunnel, if they exist, do not displace deposits with a mid-Pleistocene age. This evidence, together with the limited displacement of the Mayflower stock along the mapped trace of the fault and the lack of a topographic escarpment or scarps, indicates that no late Quaternary displacements have occurred on the Mayflower structural zone.

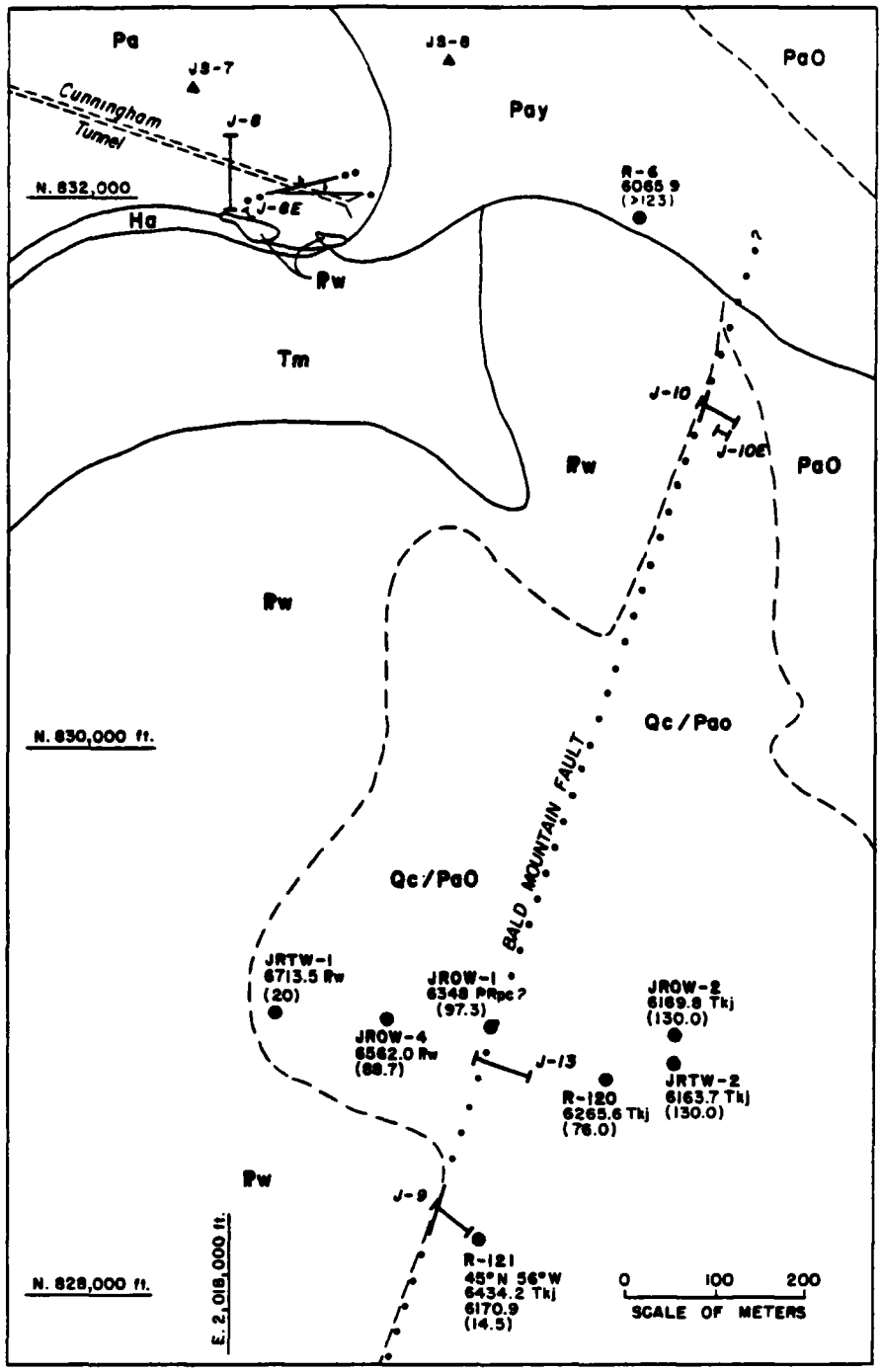

EXPLANATION

Ha	Holocene alluvium
Pay	Late Pleistocene alluvium
Pa	Mid-Pleistocene alluvium
PaO	Mid-Pleistocene and older basin fill
Qc	Colluvium
Tkj	Upper Eocene Jordanelle andesite porphyry
Tm	Upper Eocene Mayflower stock
PRpc	Permian Park City Formation
Pw	Pennsylvanian Weber Quartzite

— • •	Fault, solid where exposed, dotted where concealed
——	Shears mapped in Cunningham tunnel, arrows show dip direction
● R-120 6265.6 Tkj (76.0)	Drill holes showing elevation and lithology of bedrock in hole, and thickness of basin fill (ft)
⊢—⊣	Trenches
▲	Soil pits

Figure 7. Location map for trench sites on the west side of Keetley Valley. Shears in Cunningham tunnel from Jordanelle Task Force (1982); bedrock mapping from Bromfield and Crittenden (1971).

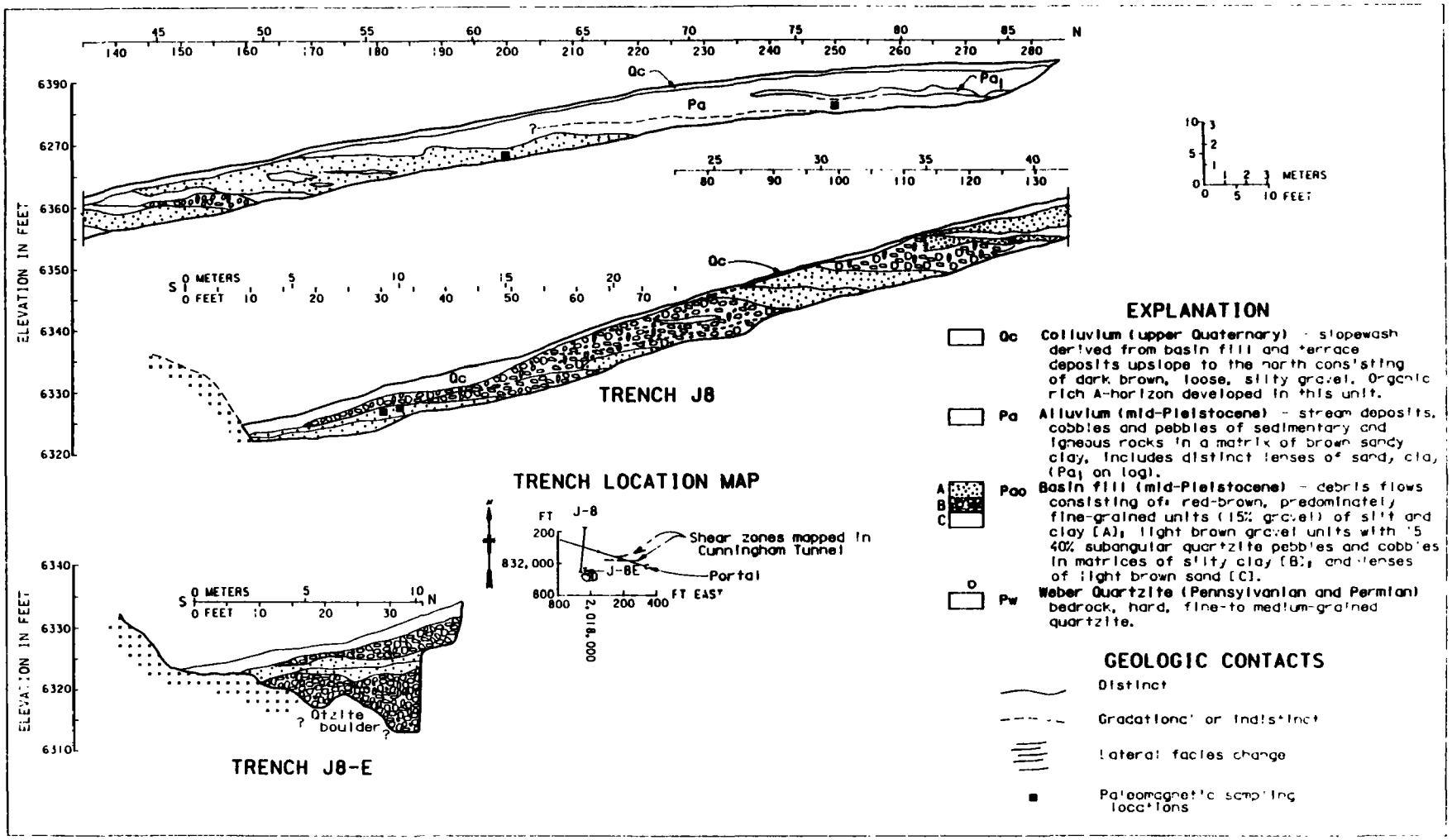

FIGURE 8 Logs of trenches J-8 and J-8E in basin fill deposits above the Cunningham Tunnel on the west side of Keetley Valley. The trenches are excavated on the projection of shears reported on mine maps in the Cunningham Tunnel portal (see location map). Mid-Quaternary basin fill deposits in the trench are undisplaced. See plate 1 and Fig. 7 for trench location.

3.2.3 Cottonwood fault

The principal mapped fault in the vicinity of the damsite is the Cottonwood fault (fig. 6 and pl. 1). The location, trend and character of the Cottonwood fault are interpreted from published geologic maps (Boutwell, 1912; Eardley, 1968; Bromfield, 1968; Bromfield and others, 1970), drill holes, trenching and mapping data developed by USBR (1986), and proprietary mining company maps of the Sphinx mine tunnels. The Cottonwood fault is a reverse fault that is mapped from the south margin of the Mayflower stock eastward and northeastward toward the damsite (Bromfield and others, 1970). Overturned Triassic Woodside Shale and Thaynes Formation form the footwall on the south; the Weber Quartzite and Park City Formation form the hanging wall to the north (Bromfield and others, 1970). The Weber Quartzite-Park City Formation contact has been offset laterally about 1000 m (3300 ft) along the fault (fig. 6). The overturning of footwall beds, the relative eastward displacement of beds in the hanging wall and the presence of the Mayflower stock in the hanging wall suggest that the fault formed during emplacement of the Mayflower stock (Bromfield, 1968; Bromfield and others, 1977). Proprietary mine tunnel maps depict a complex zone of east and northeast-trending faulting as much as 300 m (1000 ft) wide in Mesozoic rocks. This zone is described as horsetailing fault strands that generally dip to the north. Near the portal of the Sphinx Mine on pl. 1, the Cottonwood fault is exposed in USBR trench DT-13 (log included in USBR, 1986). In this exposure the fault zone is within the Woodside Shale, striking N63oE and dipping to the northwest. Further to the northeast the continuation of the fault zone is concealed by landslide deposits (fig. 6 and pl. 1).

Contrasting interpretations have been presented of the location and trend of the Cottonwood fault in the vicinity of the damsite. A Utah State Geologic map (Stokes and Madsen, 1961) depicts the fault as extending through the damsite to the east side of Keetley Valley, but a recent compilation (Hintze, 1980) shows the fault only on the southwest side of the valley as shown by Bromfield and others (1970). Based on proprietary mine maps the fault zone has been inferred to extend northeastward through Jordanelle damsite and across Keetley Valley to the Park Premier stock (Plate 5 and detail Plate B, Jordanelle Task Force, 1982). Seismic reflection records have been cited as supporting evidence for the continuation of the fault northeast into Keetley Valley (Grey, 1982). On these records the lack of coherent reflectors at the south end of Keetley Valley has been interpreted as evidence of a pervasive zone of east and northeast trending faulting 5 km (3.1 mi) to 10 km (6.2 mi) wide

beneath the valley that apparently is overlain by the "tuffaceous volcanic sequence" (Grey, 1982). However, incoherent reflectors and "noisy" records are commonly associated with areas overlain by volcanic rocks as in Keetley Valley.

This interpretation of the continuity of the fault through the damsite has not been confirmed by site investigations. Faults in mid Tertiary and older rocks in exposures near the right abutment of the dam are interpreted to be related to the Cottonwood fault. These faults can not be traced from the country rocks, along strike, into the Jordanelle andesite porphyry (USBR, 1986). The faults are terminated at the margin of the Jordanelle andesite porphyry indicating that displacement on the Cottonwood fault predates intrusion of the Jordanelle andesite porphyry.

The Cottonwood fault also lacks important characteristics of other late Quaternary faults in the region. Both seismologic and geologic data demonstrate that late Quaternary surface displacements and large-magnitude historical earthquakes in the ISB and elsewhere in the Basin and Range have occurred on normal faults with evidence of recurrent late Cenozoic normal displacements (Sullivan and others, 1988). Similarly, in the back valleys of the Wasatch Mountains, late Quaternary faults with Quaternary slip rates of 0.01-0.1 mm/yr are expressed as bedrock fault scarps that, locally, are associated with scarps in Quaternary deposits (Sullivan and others, 1988). In contrast, the Cottonwood fault is a reverse fault that lacks a bedrock escarpment or associated scarps or lineaments. Stratigraphic evidence suggests that displacement on the fault predates intrusion of the Jordanelle andesite porphyry during the late Eocene. We conclude that the Cottonwood fault is principally an early and middle Cenozoic fault. We find no evidence that late Quaternary displacements have occurred on the fault.

3.3 North-trending normal faults in the Park City mining district

North-trending normal and thrust faults are mapped west of Keetley Valley that are also known from mine workings in the Park City mining district. Two of the principal faults are the #9 fault and the Frog Valley thrust/Deer Valley normal fault.

In the northern part of the Park City mining district, the Frog Valley thrust fault is mapped along the east side of Deer Valley where Weber Quartzite is faulted over the Park City Formation

and Woodside Shale (Bromfield, 1968; Bromfield and Crittenden, 1971). Deer Valley is a small closed basin about 1.6 km (1 mi) long and 0.5 km (0.3 mi) wide that is located east of Park City, Utah (fig. 6). The north-northeast-trending basin is filled with unconsolidated deposits and bounded on the east by a linear escarpment in Paleozoic rocks. Although stratigraphic relations indicate reverse or thrust displacement on the Frog Valley thrust, a normal fault at the base of the 120-m-high (400 ft) escarpment is suggested by four, v-shaped, east-flowing stream valleys above the escarpment that appear to have been beheadeded. The most likely explanation for the disruption of these drainages is late Cenozoic or possibly Quaternary displacement on a normal fault at or near the base of the escarpment (Sullivan and Nelson, 1983). These geomorphic relations indicate that a reversal of the sense of displacement of the earlier thrust fault has occurred. The beheaded drainages deliver sediment to Keetley Valley about 3 km (2 mi) to the east. The mid-Quaternary age of the upper portion of these sediments in Keetley Valley suggests early and mid Quaternary displacement may have occurred on this fault.

The age of most-recent displacement on this inferred Deer Valley normal fault and its significance as a late Cenozoic or Quaternary fault are difficult to evaluate. The Frog Valley thrust fault has a mapped length of about 5 km (3.1 mi). At the south end it terminates against the Hawkeye-McHenry fault zone, and at the north end it is concealed by Quaternary deposits. The escarpment on the east side of Deer Valley has a length of only 1.6 km (1 mi). Holocene marsh sediments are found in the center of Deer Valley, but alluvium and colluvium around the margins of the valley have an estimated age of at least 50,000 years and probably >100,000 years (Sullivan and others, 1988). No fault scarps are found in these deposits, although if they formed at the base of the escarpment they could have degraded in a few thousand years. Therefore, the possibility that late Quaternary displacements have occurred on this inferred fault can not be precluded; however, the fault length is extremely short.

The #9 fault is a short north-trending normal fault known from mine workings where it truncates and offsets mineralization associated with the Ontario and Daly veins and the Hawkeye-McHenry fault zone (fig. 6) (Bromfield and others, 1970). This indicates that displacement on the fault may have occurred during the late Cenozoic. At the surface the fault is poorly exposed but has a mapped strike length of about 1 km (0.6 mi). The limited strike length of the fault and the lack of a topographic escarpment associated with the fault suggest that no

late Quaternary surface displacements have occurred on the fault.

3.4 East Kamas fault

Kamas Valley, located about 12 km east of Keetley Valley, is a back valley of the central Wasatch Mountains that is bounded by late Cenozoic normal faults. The principal fault is a north-striking, west-dipping normal fault mapped at the base of the bedrock escarpment on the eastern margin of the valley (Gilbert, 1928; Sullivan and others, 1988). A sequence of large alluvial fans of several ages have been deposited across the East Kamas fault (Sullivan and others, 1988, their fig. 5.6). The higher portions of the fans are the oldest; development indices for soils on these portions of the fans indicate a minimum age of 130,000 to 150,000 yrs for the deposits (Sullivan and others, 1988, sec. 5.8.2.1). There are no scarps in these alluvial fan deposits which cross the inferred trace of the East Kamas fault showing that there has been no surface displacement on the fault in at least the last 130,000 to 150,000 years.

3.5 Concealed normal faults in Keetley Valley

Although smaller than other back valleys of the Wasatch Mountains, the morphology of Keetley Valley is similar suggesting that north to northeast-trending concealed normal faults may be present in the valley, particularly along the southwest margin. In this section we present the results of investigations undertaken to determine whether concealed faults are present and if late Quaternary displacements have occurred on these faults. These investigations included seismic profiling, trenching, and drilling. These investigations have confirmed the presence of a previously unrecognized, concealed normal fault (the Bald Mountain fault) along the southwestern margin of the valley.

3.5.1 Seismic Refraction Survey

The seismic refraction method was used in Keetley Valley to determine if concealed north trending normal faults were present at or near Jordanelle damsite The results of this program are reported in Appendix A. The principal conclusions from the refraction program were the following: 1) boreholes along some of the lines confirm that the contact between bedrock and overlying basin fill was accurately mapped; 2) along the western margin of the basin the contact between the bedrock and the basin fill slopes gradually eastward to the deepest portion of the basin, a narrow channel-like feature north of the damsite; 3) high-angle normal faults related to the Bald Mountain fault

are interpreted from steps in the bedrock-basin fill contact in two locations near the western margin of the basin.

3.5.2 Bald Mountain fault

The location of a concealed normal fault on the southwest margin of Keetley Valley is indicated by a N20°E-trending, 3-km-long (2 mi) escarpment on the lower slope of Bald Mountain with a maximum height of 275 m (900 ft) (pl. 1). Overall, the escarpment has a linear trend, except for a 500-m-wide (1700 ft) embayment that has been eroded in the northern portion of the escarpment. The escarpment has formed in east-dipping Paleozoic sedimentary rocks, but drill holes (pl. 1) and trenches (discussed below) show that the basin fill east of the escarpment overlies Tertiary igneous rocks.

Linear bedrock escarpments form the footwalls of other Cenozoic and late Quaternary normal faults in the back valleys of the Wasatch Mountains (Sullivan and others, 1988). The Bald Mountain escarpment lacks triangular facets characteristic of late Quaternary faults, but its linear trend, together with the juxtaposition of stratigraphic units between the escarpment and the valley indicated by the drill holes, suggested that a normal fault was present at the base of the escarpment.

To verify the existence and location of the fault and to determine its age of most recent displacement, three trenches were excavated at the base of the escarpment (fig. 7). Trenches J-9 and J-10 verify the location and trend of the fault in bedrock; trenches J-9 and J-13 show that no late Quaternary displacements have occurred on the fault.

3.5.2.1 Trench J-9

The Bald Mountain fault is exposed at the west end of trench J-9 as a N20°E-striking, 80° east-dipping, 0.03 to 0.6 m-thick (0.1 to 2.0 ft) zone of red, plastic clay and quartzite breccia (fig. 9). The fault is coincident with the break-in-slope at the base of the escarpment at a point where the escarpment is about 150 m (500 ft) high. Intensely altered andesite porphyry is exposed in the hanging wall and Weber Quartzite is exposed in the footwall.

A 4 m-thick (12 ft) sequence of deposits, interpreted to be basin fill and younger colluvial deposits, overlies the Bald Mountain fault in trench J-9 (fig. 9). A surface horizon of clayey, cobbly colluvium (Qc) about 2 m (6 ft) thick extends the entire length of the trench. Below this colluvium a 2 m-thick (6 ft), wedge-shaped sequence of colluvium also overlies the

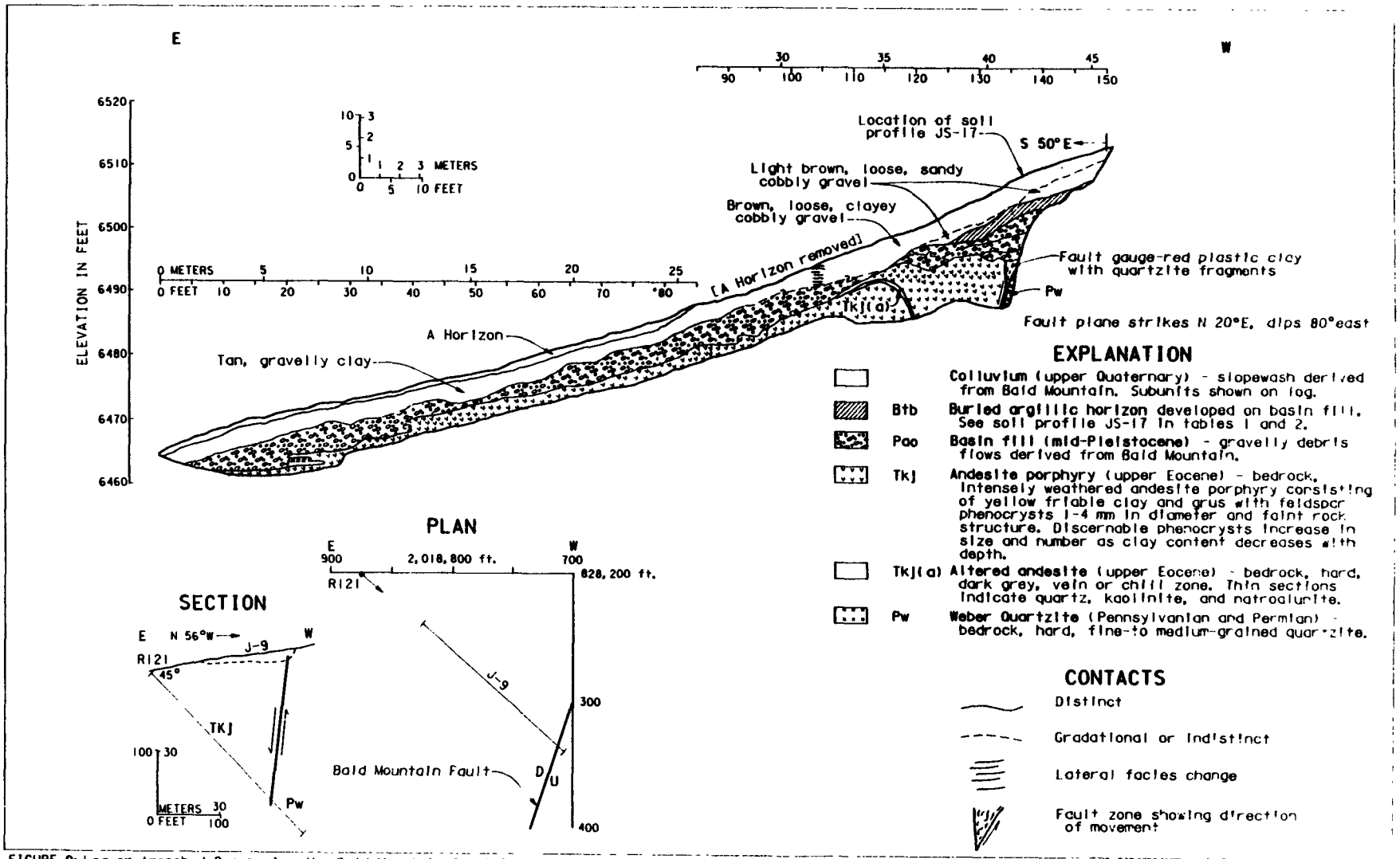

FIGURE 9. Log or trench J-9 exposing the Bald Mountain fault in middle Tertiary and older rocks at the base of an escarpment on the southwest margin of Beetle Valley. The argillic B-horizon preserved between st. 38 and 44 marks the top of the mid-Pleistocene basin fill sequence in the trench. This B-horizon and the overlying upper Quaternary colluvial deposits, both of which directly overlie the fault, are undisplaced. The position of the fault intercept in an angle drill hole shown on the section indicates that the Bald Mountain fault is a high-angle normal fault. See Plate 1 and fig. 7 for trench location.

fault. Due to the buried Bt horizon at the top of this sequence, we interpret these deposits to be equivalent in age to the mid-Pleistocene basin fill. At the base of this basin fill, a 0.3 m-thick (1 ft) bed of undeformed pebbly alluvium directly overlies the 0.6 m-wide (2 ft) fault zone, indicating that it was deposited after the latest movement on the fault. Careful inspection of the contacts of these units with the Weber Quartzite in the footwall of the fault showed that the contact was not planar, as in the case of the Morgan fault (Sullivan and others, 1988); no evidence of a shear fabric or fault gouge was found along the contact. The limited downslope extent of this wedge of colluvial units, together with the high-angle depositional contact of these units with the bedrock, suggest that the deposits have been locally derived from the footwall of the fault as scarp-derived colluvial deposits.

Between stations 0 and 36 m the surface on top of the andesite is irregular but has a slope of about 17° to the east, parallel to the ground surface, but from station 36 to 43 m this surface slopes only about 9° to the east. Although this difference in slope could be the result of erosion, it also could be the result of backtilting of the hanging wall associated with normal displacement on the Bald Mountain fault. Mid-Quaternary displacements are also suggested by the high-angle bedrock surface adjacent to the basin fill that appears to be a free face that developed as a result of surface displacements on the fault.

The age of the most recent displacement on the fault is constrained by the age of the deposits that overlie the Bald Mountain fault. Soil profile JS-17 was described in the deposits overlying the fault zone at station 41 m (fig. 9). The units comprising the uppermost 1.5 m (Qc) contain a soil with a 0.44 m-thick Bt horizon, slight evidence for translocated clay (no clay films visible), and a 7.5 YR hue (table 2). A buried soil 1.3 m (4.3 ft) deep on the top of the wedge of deposits interpreted to be basin fill contains a stronger Bt horizon (table 2) similar to that found in trench JS-13. The combined profile in trench J9 is within RAG 2 when comparing the rubification and non-arid profile indices with profiles elsewhere in the back valleys (fig. 5). The relative age of the soil profile suggests that the buried soil is mid-Pleistocene (>130,000 years old). This shows that the underlying deposits are at least this old, suggesting that they are coeval with portions of the basin fill in Keetley Valley. The trench also shows that no late Quaternary surface displacements have occurred on the fault at this location.

3.5.2.2 Trench J-10

The Bald Mountain fault is also exposed in trench J-10 at the break-in-slope at the base of the Bald Mountain escarpment (fig. 10). The trench is located at the north end of the escarpment about 1000 m (3300 ft) to the northeast of trench J-9 (pl. 1 and fig. 7). The trench site is on the south side of McHenry Creek where the escarpment is about 30 m (100 ft) high. In the trench the main fault is a steeply east-dipping zone of gouge and breccia up to 1.5 m (5 ft) thick that juxtaposes intensely weathered Tertiary volcanic rocks and Weber Quartzite. The west-dipping zone of gouge about 0.6 m (2 ft) thick is interpreted to be an antithetic fault.

Colluvial units (Qc) about 3 m thick (10 ft) also extend across the fault zones in trench J-10. These deposits are loose cobbly silts that include a 1-m-thick (3 ft) organic rich A-horizon that extends the entire length of the trench (stripped during excavation at upper end), and an underlying, brown loose cobble gravel. This lower unit decreases in thickness from about 3 m (10 ft) above the main fault to about 1.5 m (5 ft) as it grades laterally into the basin fill that overlies the Breccia of Silver Creek. Soil development in these colluvial units suggests that they are of Holocene age.

Below this sequence an older sequence of colluvial units are preserved in the hanging wall. Although no buried soil horizons are recognized within this sequence, they are interpreted to be mid-Pleistocene basin fill because the lithologies are similar to basin fill in trench J-9 and the units are in the same stratigraphic position as the basin fill in J-9. Samples from the basin fill in trench J-10E in a unit correlative with a unit at station 5 in J-10 have only a weak component of reverse magnetization indicating that they are <730,000 years old (Appendix B).

The steep east-dipping imbrication preserved in the basin fill at station 41 m, and the near vertical contact of the basin fill with the bedrock at station 44 m, suggest that these deposits are locally derived from the footwall of the fault. As in trench J-9, the contact between the basin fill and the volcanics between station 28 and 36 m appears to be backtilted into the fault in response to surface displacement on the fault. The lack of shear fabric along the near vertical contact between these units and the Weber Quartzite on the projection of the fault indicates that the basin fill not been displaced.

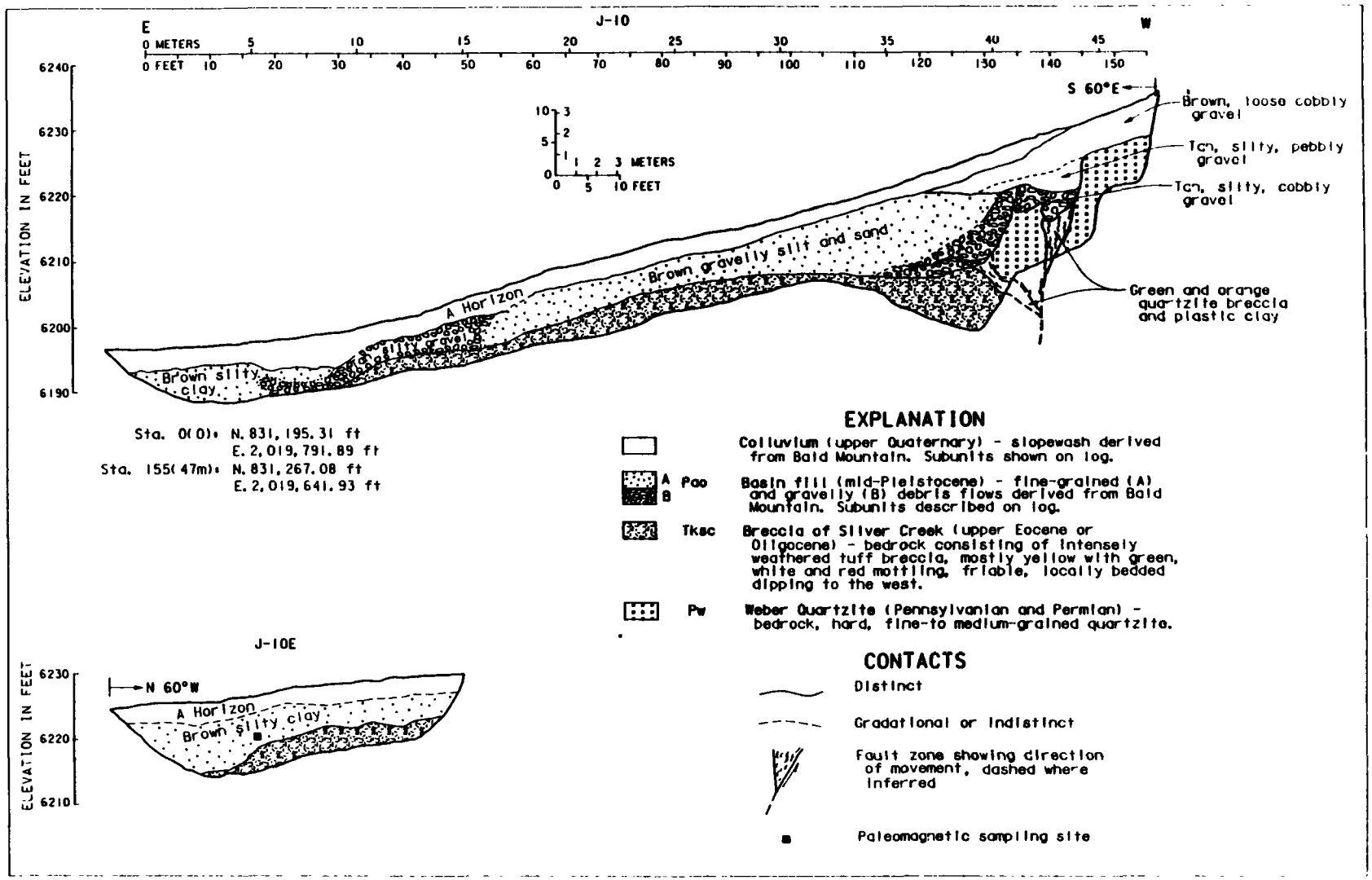

FIGURE 10. Log of trench J-10 exposing the Bald Mountain fault in middle Tertiary and older rocks at the base of an escarpment on the southwest margin of Keetley Valley. Although no buried argillic horizons were observed in the trench, the units overlying bedrock are interpreted to be mid-Pleistocene basin fill. As in trench J-9 the back-tilting of the contact between basin fill and bedrock in the hanging wall and the vertical contact between bedrock and basin fill and colluvium suggest mid-Quaternary displacements have occured on the fault. Upper Quaternary colluvial deposits overlying the fault are undisplaced. Inset shows an additional trench located 11 ft. (3.6 m) to the south. Paleomagnetic analysis of samples from the basin fill deposits in this trench have only a weak component of reverse magnetization indicating that the deposits are <730,000 years old. See plate 1 and fig. 5 for trench locations.

QSS-(102,521CD 20,3GN)

3.5.2.3 Trench J-13

Trench J-13 was excavated in the basin fill deposits in an area where no scarps or lineaments are present in the surficial deposits along the concealed trace of the fault (pl. 1 and fig. 7). Between trench sites J-9 and J-10 an embayment has been eroded into the Bald Mountain escarpment. The embayment was subsequently filled with basin fill at least 30 m (100 ft) thick (fig. 7). The position of the concealed trace of the Bald Mountain fault in the embayment can be accurately constrained by drill holes and by projection of the fault from trenches J-9 and J-10.

Projection of the strike of the Bald Mountain fault is constrained by trenches J-9 and J-10 and drill holes in the embayment (fig. 7): the fault is between drill holes JROW-1 and R120, for Paleozoic rocks were encountered in JROW-1 in the footwall of the fault and andesite porphyry was encountered in R120 in the hanging wall of the fault. Projection of the strike of the fault from trenches J-9 and J-10 indicates it is between 6 m (20 ft) and 42 m (220 ft) southeast of JROW-1. Trench J-13 was excavated beginning southwest of JROW-1 and extending southeast for a distance of 82 m (265 ft).

Undisplaced alluvial fan facies of the basin fill, overlain by colluvium, are exposed in trench J-13 (fig. 11). Surficial deposits in this area are mapped as colluvium overlying Pleistocene basin fill (fig. 7 and pl. 1). In the trench the colluvial deposits are represented by the upper 1 m (3 ft) of brown silt and light brown silty gravel (Qc). The soil in the colluvium contains a thick 0.8 m (2.6 ft) A horizon and a Bt horizon that is 0.44 m (1.4 ft) thick. The underlying basin fill deposits in the trench are debris flows and channel gravels (Pao). A buried soil in the debris flows has a 0.54 m-thick (1.8 ft) Bt horizon. The 33% increase in clay in this horizon (table 2) suggests that it required a period of approximately 130,000 - 150,000 years to form (see discussion of soil relative age dating in sec. 3.1.6). This buried soil extends from the upper end of the trench (st. 81 m) downslope to about station 30 m and is intermittently preserved to about station 17 m. The fault projects beneath the trench between stations 75 m and 20 m, and, therefore underlies the basin fill and the buried soil. The stratigraphy interpreted from trench J-13 indicates that the mid-Pleistocene basin fill has not been displaced by the Bald Mountain fault, showing that there has been no late Quaternary displacement on the fault.

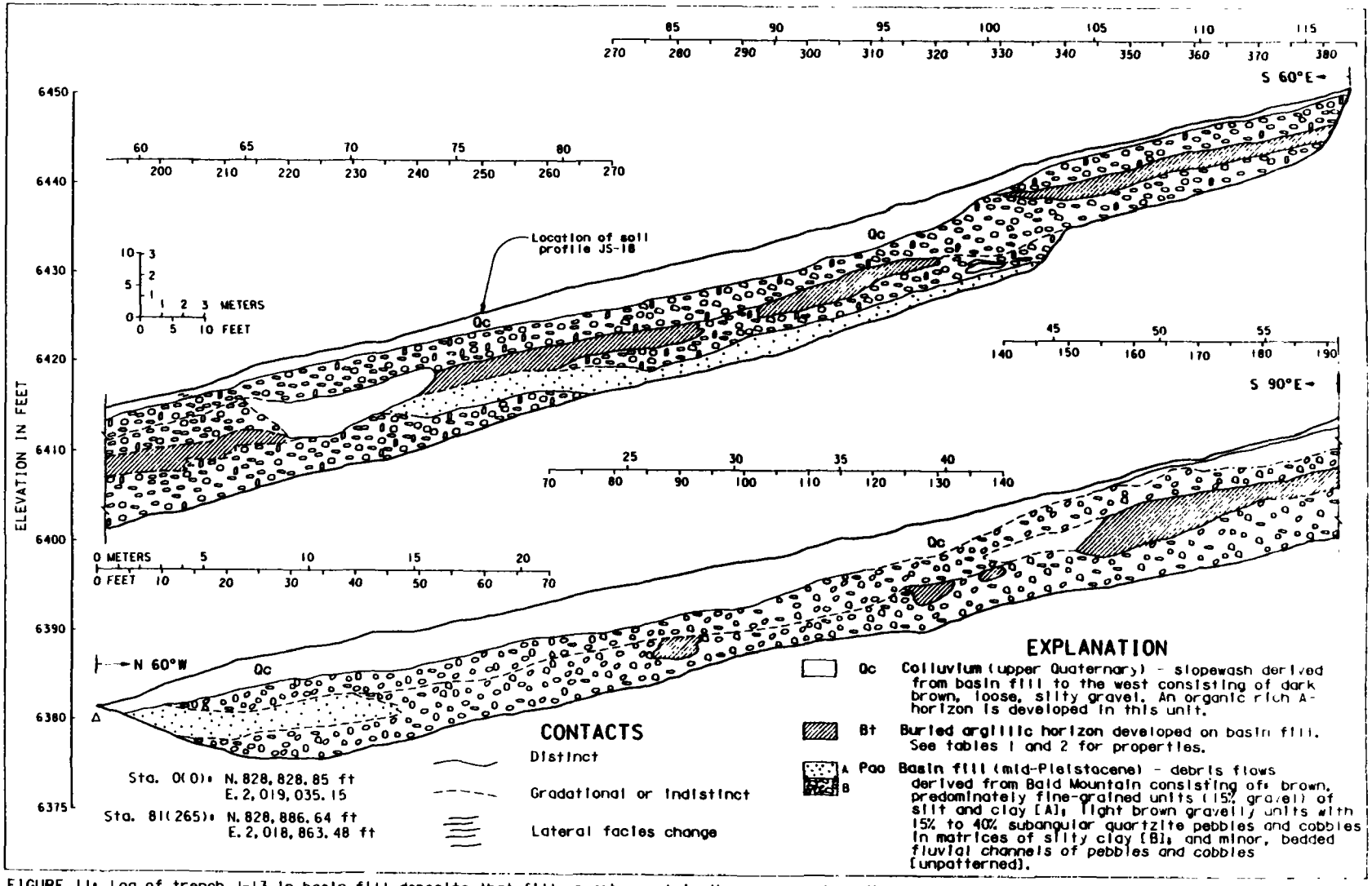

FIGURE 11: Log of trench J-13 in basin fill deposits that fill an embayment in the escarpment on the southwest margin of Keetley Valley. The Bald Mountain fault projects beneath the trench between stations 6 m and 70 m. A buried argillic B-horizon preserved in the trench marks the top of the mid-Pleistocene basin fill deposits. These deposits are undisplaced in the trench indicating that there has been no late Quaternary displacement on the Bald Mountain fault. See plate 1 and fig. 7 for trench location.

QS3-C102.S21CD130 DGN 1

3.5.3 Other concealed normal faults

Drill holes and the refraction lines indicate that the basin fill thickens eastward from the Bald Mountain fault reaching a maximum thickness of 60 to 108 m (200 to 354 ft) west of Drain Tunnel Creek. Boreholes in the floor of this creek and outcrops on its west bank also show that it flows on bedrock overlain only by a thin veneer of alluvium (pl. 1).

Faults were earlier inferred to bound the deepest portion of the north-trending trough of unconsolidated deposits that extends south from seismic lines S-14 and S-13 to line S-12 (see Appendix A, pl. 1).If present, the faults would define a narrow graben in the center of Keetley Valley; however, no scarps are present in the basin fill on the updip projection of the fault. Overlapping trenches in two locations (J-3 and J-11, J-1 and J-2 on pl. 1) above the projection of a N20oE-trending inferred fault on the west side of the trough expose undisplaced basin fill with a minimum age of 730,000 yrs (USBR, 1982). Additional seismic profiles indicate that the trough does not extend south to the damsite (Appendix A). In addition, cross sections across the dam foundation show no significant faults (USBR, 1986; 1987).

3.6 Conclusions

A previously unrecognized late Cenozoic normal fault has been identified in Keetley Valley. The mapped length of the fault on plate 1 is 2.4 km including the continuation of the escarpment south of trench J-9 (querried on pl. 1) where the existence of the fault is suspected but not confirmed. To the north, the escarpment ends at McHenry Canyon and no scarps or lineaments in the basin fill indicate its northern continuation. An abrupt step in the contact between bedrock and basin fill on a seismic profile along McHenry Canyon (Appendix A, pl. 1) is interpreted to be a down-to-the-southeast normal fault that is the en-echelon continuation of the Bald Mountain fault (Appendix A). If the fault is assumed to continue in the subsurface along the western margin of Keetley Valley, the length of the Bald Mountain fault would be 7.2 km.

The Bald Mountain fault is interpreted to be a high-angle normal fault on the basis of trench exposures and drilling. In trenches J-9 and J-10 the fault plane strikes N20^{o}E and dips 80° to 90° to the east. An angle drill hole (R121), collared near the east end of J-9 (fig. 9), intersects gouge and breccia between andesite porphyry and the Park City Formation (overturned) that is interpreted to be the Bald Mountain fault.

A cross section constrained by the angle hole and the position of the fault, both at the surface and at depth, establishes that the Bald Mountain fault is a steeply east-dipping normal fault (fig. 9).

Stratigraphic evidence from trenches shows that no surface displacements have occurred on the Bald Mountain fault in at least the last 130,000 to 150,000 years. Using published and unpublished geologic mapping and a review of aerial photos at multiple scales, we have identified or inferred other late Cenozoic faults in the central Wasatch Mountains in the vicinity of the damsite. The results of geologic investigations reported here and in Sullivan and others (1988) show that late Quaternary displacement has not occurred on any of the faults within 20 km of Jordanelle damsite.

4.0 SITE GEOLOGY

Mapping of the damsite by the USBR (1986) at a scale of 1 inch to 100 feet, together with detailed mapping at a scale of 1 inch to 20 feet of a portion of the right abutment of the dam where faults in Tertiary basin fill are exposed, form part of the basis for the conclusions in this section. The results of this mapping are generalized on plate 1.

4.1 Stratigraphy

Rocks exposed in the vicinity of the damsite include Mesozoic and Paleozoic rocks described in sec. 3.1.1 and USBR (1986), lower Tertiary (late Eocene or Oligocene) igneous rocks, and unconsolidated deposits of Tertiary and Quaternary age.

4.1.1 Jordanelle andesite porphyry

At the south end of Keetley Valley a porphyritic rock of andesitic composition (described as a granodiorite porphyry, Tkj, by Bromfield and others, 1970) is locally exposed over a roughly circular area with a diameter of about 1.6 km (1 mi). These rocks were originally interpreted to be flows within the Keetley volcanics, but mapping of trench exposures at Jordanelle damsite combined with drilling data and an analysis of aeromagnetic data have led to the interpretation of this andesite porphyry as a hypabyssal intrusive (USBR, 1986) as suggested by Woodfill (1972). The intrusive origin of the Jordanelle andesite porphyry has been established on the basis of contact relations with the host rocks. Although petrographic analysis of thin sections for indications of an intrusive or extrusive origin proved inconclusive, in exposures near the right abutment of the dam the andesite porphyry can be seen intruding each of the country rocks-- Paleozoic sedimentary rocks, Keetley volcanics, and Tertiary basin fill (USBR, 1986, Appendix B).

The Jordanelle andesite porphyry will be the predominant rock type in the dam foundation. The rock is a homogeneous grey andesite with an aphanitic groundmass and phenocrysts of plagioclase, biotite, and hornblende. The variable weathering and alteration of the rock in outcrops, excavations and drill holes has been characterized in maps and cross sections (USBR, 1986). Fracture density is light to moderate throughout the rock mass with zones of intense fracturing that have been mapped in exposures and logged in drill cores (USBR, 1986). The southern margin of the Jordanelle andesite porphyry extends east-west below the Provo River beneath the downstream shell of the dam.

Four radiometric dates were obtained from three unweathered drill core samples from depths of 54 to 132 m (180 to 439 ft) within the Jordanelle andesite porphyry. These dates, together with a published date on the Mayflower stock, suggest contemporaneous or slightly younger emplacement of the Jordanelle andesite porphyry (table 4).

Table 4 K-Ar dates for intrusives near Jordanelle

Intrusive	Drill hole depth (ft)*	Mineral	Age (million years)	Sample no.**
Jordanelle	DH-496 (206)	Horneblende	36.5 +/- 1.8	A-7482
	DH-491 (180)	Horneblende	36.3 +/- 1.8	A-7481
	DH-486 (439)	Hornblende	38.5 +/- 1.9	A-7480
	DH-486 (439)	Biotite	40.0 +/- 1.6	A-7480
Mayflower	surface	Hornblende	41.2 +/- 1.6***	

*for locations and logs see USBR (1986)
**Geochron Laboratories 1986
***from Bromfield and others (1977)

4.1.2 Keetley volcanics

The volcanic breccia of Coyote Canyon is the host rock for the Jordanelle andesite porphyry south and east of the damsite. These rocks consist principally of consolidated, poorly sorted, andesitic tuff breccias that were emplaced as debris flows in the vicinity of a volcanic vent (USBR, 1986; Best, 1986). The tuff breccias are described as 10 to 60 % ash to block sized fragments of andesite porphyry, tuff, sandstone, siltstone, shale, limestone and quartzite in an andesitic ash flow tuff or crystal tuff matrix (USBR, 1986).

4.1.3 Unconsolidated deposits

Unconsolidated alluvial and colluvial deposits of both Quaternary and Tertiary age have been mapped in exposures at the damsite. On the right abutment Tertiary alluvial and colluvial deposits are preserved in a fault block where they overlie the volcanic breccia of Coyote Canyon and the Paleozoic and Mesozoic sedimentary rocks. Exposures also show that they are intruded by the Jordanelle andesite porphyry establishing that they are of Tertiary age (USBR, 1986). This Tertiary-age sequence is

unconformably overlain by Quaternary landslide, alluvial and colluvial deposits (USBR, 1986, Appendix B).

Below the Provo River floodplain drill holes show that the alluvium varies in thickness from 9 to 30 m (30 to 98 ft). The alluvium consists of rounded cobbles and boulders in a matrix of sand which will be used as rockfill for the embankment. A study of the geomorphic history of the Provo River drainage conducted as part of the regional studies of the back valleys (Sullivan and others, 1988) indicates that these gravels are Holocene in age.

A thin veneer of slopewash and colluvium overlies the Jordanelle andesite porphyry and the volcanic breccia of Coyote Canyon on the steep slope above the Provo River in the area of the left abutment of the dam. Immediately downstream of the left abutment a rotational landslide involving a tabular, sill-like body of andesite porphyry and underlying volcanic breccia of Coyote Canyon is clearly expressed in the topography (USBR, 1986).

4.2 Faults and shears at the damsite

Detailed mapping of natural exposures and bulldozer excavations has disclosed evidence of faults and shears at the damsite (USBR, 1986). The faults include the Cottonwood fault that has been mapped in Paleozoic and Mesozoic rocks southwest of the damsite (discussed in sec. 3.4.3), and the F-series faults that have been mapped in Tertiary alluvial and colluvial deposits near the right abutment of the dam (pl. 1). Shear zones are defined as structural breaks that share the physical characteristics of faults--gouge, slickensides, and breccia--but lack continuity; often they are confined to a single rock unit (USBR, 1986). The principal mapped shears are SZ1 and SZ2, northwest-trending shear zones on the southern margin and within the Jordanelle andesite porphyry (pl. 1). Minor shears form discontinuous zones in the andesite porphyry in exposures and in drill holes. In this section we will summarize evidence for the location, age and origin of the faults and shears at the damsite. Detailed site geology maps at scales of 1 in = 100 ft and 1 in = 20 ft, trench logs, and logs of drill holes are included in USBR (1986).

4.2.1 F-series faults

Normal and reverse faults, referred to as the F-series faults, are exposed in trenches in unconsolidated lower Tertiary alluvial and colluvial deposits. These deposits are preserved below Quaternary alluvial deposits west of, and more than 100 m

(330 ft) above, the Provo River near the right abutment of the proposed Jordanelle Dam. It was earlier suggested that these faults represent evidence of late Quaternary displacements on the Cottonwood fault (Jordanelle Task Force, 1982). At that time it was assumed that these deposits were of Quaternary age. Subsequent detailed mapping of exposures created during 1985, reported in Appendix B of USBR (1986), has shown that the unconsolidated deposits in which the faults are exposed have been intruded by the Jordanelle andesite porphyry showing that they are of Tertiary age (USBR, 1986, Appendix B). The faults are terminated at the margin of the Jordanelle andesite porphyry; therefore, the faults also predate its emplacement 36 to 40 million years ago (table 4). Although landslide deposits and landslide-related faulting are mapped downstream, the F-series faults also displace the underlying volcanic breccia of Coyote Canyon and the locally overturned Triassic Woodside Shale indicating the F-series faults are not landslide-related. The location and timing of displacement on the faults suggest they are related to the Cottonwood fault (USBR, 1986).

4.2.2 SZ1 and SZ2

Shear zones characterized as zones of clay gouge and breccia have been mapped in exposures and logged in drill holes at the damsite. The principal mapped shear zone, called SZ1 in USBR (1986), was earlier referred to as the northwest structure (USBR, 1982). On the right abutment of the dam it is exposed in excavations over a distance of 360 m (1200 ft) from below DT-29 to DT-7 (pl. 1). The zone varies in thickness from 0.3 to 6 m (1 to 20 ft). It is characterized by clay gouge and rock fragments, moderate to intense alteration and weathering, and fluted, slickensided surfaces (USBR, 1986). In detail the zone is sinuous, but overall it strikes about N70°W. Drill holes indicate that the dip is nearly vertical, although in surface exposures its dip varies from moderate to steep. SZ1 follows the southern margin of the Jordanelle andesite porphyry. To the south the country rocks are Mesozoic sedimentary rocks. These rocks have been thrust eastward over early Tertiary unconsolidated deposits and volcanic breccia of Coyote Canyon along the Cottonwood fault and the F-series faults.

The F-series faults can not be traced across SZ1 indicating that SZ1 formed later than these faults; therefore, SZ1 is the youngest mapped structural feature at the site. However, between DT-32 and DT-7 exposures show that SZ1 is offset as much as 1.5 m (5 ft) by discontinuous, low-angle apparent thrust and normal faults that dip to the north and root in the Jordanelle andesite porphyry. These features are interpreted to represent

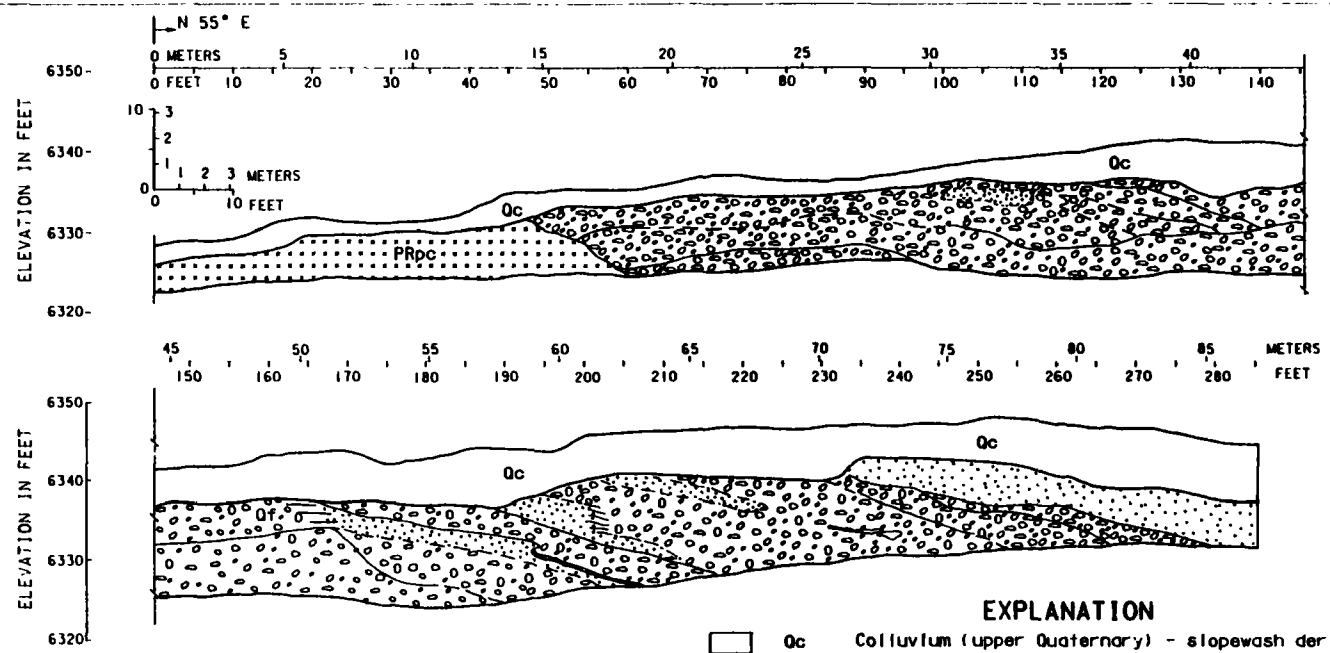

TRENCH LOCATION MAP

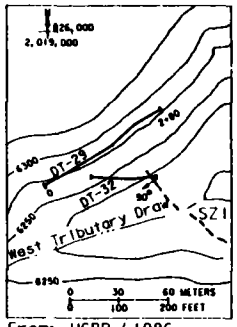

From: USBR (1986, Drawing 66-418-6396)

EXPLANATION

	Qc	Colluvium (upper Quaternary) - slopewash derived from basin fill upslope to the north consisting of dark brown, loose, silty gravel. An organic-rich A-horizon is developed in this unit.
A B	Pao	Basin fill (mid-Pleistocene and older) - debris flows derived from Bald Mountain to the west consisting of: dark brown or grey, predominately fine-grained units (15% gravel) of silt and clay [A]; light brown gravelly units with 15 to 40% subangular quartzite and granodiorite pebbles and cobbles in matrices of silty clay [B]; and minor, bedded channel deposits [unpatterned].
	PRpc	Park City Formation (Permian) - bedrock, tan sandstone.

CONTACTS

- Distinct
- Gradational or indistinct
- Lateral facies change

FIGURE 12: Log of trench DT-29 in basin fill deposits near the right abutment of Jordanelle Dam. SZ1, the youngest structural feature at the damsite, is exposed in trench DT-32 and projects beneath trench DT-29 (see inset). Mid-Quaternary basin fill deposits are undisplaced in the trench indicating that there has been no late Quaternary displacement on SZ1. See plate 1 and USBR (1986) for trench location.

near-surface adjustments to the final phases of emplacement of the andesite porphyry. These relationships indicate that SZ1 formed contemporaneously with or prior to emplacement of the andesite porphyry 36 to 40 million years ago.

Further investigations were directed toward evaluating whether there had been any late Quaternary reactivation of this shear zone. SZ1 is well exposed in DT-32 as a 4.5-m-wide (15 ft) shear zone between the Jordanelle andesite porphyry and sandstones of the Park City Formation (USBR, 1986, Drawing 66-418-6396). A thin aphanitic dike extending across most of the shear zone is displaced only about 0.15 m (0.5 ft). A 80 m-long (265 ft) sidehill cut, DT-29, was excavated in basin fill that overlies this shear zone (pl. 1). The basin fill exposed in the trench consists of debris flows with overlapping contacts that can be traced the length of the trench (fig. 12). No evidence of displacement of the debris flows was observed. The position of these deposits on a bench >100 m (330 ft) above the Provo River floodplain argues for an early Pleistocene age (>730,000 years), because Bull Lake terraces a few miles upstream are about 35 m (109 ft) above the river (Sullivan and others, 1988). We conclude that there has been no reactivation of SZ1 in at least the last 500,000 years.

SZ2 is a sheared contact between volcanic breccia of Coyote Canyon and andesite porphyry that strikes about N70^{o}W with a near vertical dip. It forms the southern and western margin of the andesite porphyry of the Flag Rock, a distinct unit of andesite porphyry within the Jordanelle andesite porphyry (shown as Tkj (fo) on Drawing 66-418-6396 in USBR, 1986). Detailed mapping has shown that this shear does not persist on strike into the country rocks; instead, at trench DT-7, it turns and follows the boundary of the Flag Rock intrusion (Drawing 66-418-6396, USBR, 1986). This, together with its short strike length and its vertical dip indicate that this shear zone, like SZ1, is also related to the intrusion of the andesite porphyry (USBR, 1986, Appendix C).

4.2.3 <u>A and B contacts</u>

On the east side of the Provo River, trench exposures and drilling have defined a tabular body of Jordanelle andesite porphyry, interpreted to be a sill, that extends south and east from the main body of the Jordanelle andesite porphyry (pl. 1) (USBR, 1986). Volcanic breccia of Coyote Canyon overlies this andesite porphyry in trench exposures on the left abutment above an overall near-horizontal, but locally vertical, sheared contact. This contact is referred to as the B-contact. The

shearing associated with the contact was earlier inferred to be related to a fault, referred to as the F-12 fault (USBR, 1982). Subsequent investigations have shown that the shearing can not be traced along strike beyond the contact zone; therefore, the shearing is interpreted to have resulted from the intrusion of the sill of andesite porphyry (USBR, 1986).

The sill is underlain by volcanic breccia of Coyote Canyon along a contact referred to as the A-contact. This contact is exposed in only one locality at river level on the left abutment of the dam. To the southeast it is concealed by landslide deposits; however, it can be traced in drill holes east of the river. Structure contours indicate that the contact strikes east-west and that it is near horizontal to north-dipping. Again, shearing in drill holes at the contact can not be traced to mapped shear zones at the surface.

4.2.4 Discontinuous shearing beneath the Provo River floodplain

Shear zones in the Jordanelle andesite porphyry have been logged in cores from drill holes in the central section of the dam foundation where it crosses the floodplain of the Provo River. Evaluating the origin and significance of these shear zones has resulted in the drilling of more than 50 core holes in the Provo River floodplain. The final phase of this investigation included the drilling of six angle holes recommended by consultants (Peck and others, 1986). The results of this investigation are reported in USBR (1987). They support the earlier conclusion that no significant faults are present in this portion of the dam foundation (USBR, 1986).

Faults can be precluded across most of this portion of the dam foundation by correlation of the A-contact in drill holes. This contact can be traced in drill holes from the margin of the landslide downstream of the left abutment, below the east side of the Provo River channel as a gently north-dipping, intermittently sheared contact (Drawing 66-418 6395, USBR, 1986; 1987). The continuity of this contact indicates that no faults are present below the eastern portion of the floodplain.

The apparent termination of the A-contact on the west side of the floodplain was earlier interpreted to be the result of faulting. This inferred fault was referred to as the F-10 fault (USBR, 1982); it was interpreted to trend N20^{o}E. Basin fill thicknesses of 60 m (200 ft) or more, preserved below the Provo River floodplain along the same trend in refraction lines and drill holes, was interpreted to have resulted from late Cenozoic displacement on this fault (USBR, 1982). However, subsequent

analysis of drill holes in the foundation along this trend shows no continuous, traceable zone of shearing (USBR, 1986); thus, there is no basis for a N20°E trending fault in this western portion of the floodplain.

Both the drill holes in the floodplain and geophysical data indicate discontinuous zones of shearing are present in the andesite porphyry below the Holocene Provo River floodplain deposits (USBR, 1986, Drawing 66-418-6396). East-trending magnetic lows together with mapped east trends of shears where exposed suggest that these concealed shears may form a zone with an east-west trend. However, individual shears can not be correlated between drill holes or into exposures beyond the margins of the floodplain (USBR, 1986).

There is no evidence that shearing in drill holes below the floodplain is related to late Quaternary faulting. Drilling has shown that this shearing is not related to the anomalous thickness of unconsolidated deposits below the flood plain north of the damsite. The shears appear to be concentrated on the margin of the main body of the andesite porphyry along the termination of the A-contact, suggesting that they are related to the emplacement of the Jordanelle andesite porphyry (USBR, 1986).

Closely-spaced drill holes across the Provo River floodplain show a nearly uniform thickness of about 9 m (30 ft) of alluvium is present on the western portion of the floodplain (USBR, 1986). Below the eastern portion of the floodplain the alluvium reaches a maximum thickness of about 30 m (100 ft) within a buried channel. This feature appears unrelated to faulting for: 1) drilling has established that the A-contact is undisplaced in the subsurface below this area, and 2) its sinuous path upstream and downstream of the dam axis suggest that it is an older channel of the Provo River (USBR, 1986).

4.2.5 Conclusions

The faults above the right abutment of the dam--the Cottonwood fault and the F-series faults--and the discontinuous shear zones within the andesite porphyry have developed nearly contemporaneously with the emplacement of the Mayflower stock and Jordanelle andesite porphyry 36,000,000 to 41,000,000 years ago. A trench in basin fill less than 100 m (330 ft) west of the dam shows that there has been no displacement on SZ1, the youngest structural feature at the damsite, in at least the last 500,000 years; thus there has been no late Quaternary reactivation of these faults or shears.

The base of the unconsolidated deposits in the narrow basin on line S-12 and drill hole R114 is at a lower elevation than the base of unconsolidated deposits at the damsite (pl. 1 and fig. 4). Earlier interpretations suggested that this difference in elevation resulted from late Cenozoic and possibly late Quaternary faulting (USBR, 1982). Drilling data (USBR, 1987) and seismic refraction studies (Appendix A) have shown that no faults are present below the Provo River floodplain to the north that project toward the damsite. Thus, available data indicate that no faults are present in the andesite porphyry that forms the foundation of the dam.

5.0 CONCLUSIONS

In this chapter we identify earthquake sources in the vicinity of Jordanelle Dam, estimate MCEs (maximum credible earthquakes) for these sources, and discuss the potential for surface displacement in the dam foundation.

5.1 Earthquake sources in the ISB

To account for observations of the characteristics of earthquake occurrence in the ISB, two separate earthquake sources are considered for seismotectonic hazard assessments: 1) large-magnitude earthquakes associated with potential surface rupture on late Quaternary faults, and 2) moderate-magnitude, random earthquakes that may be unrelated to faults mapped at the surface (Piety and others, 1986; Sullivan and others, 1988).

The association of surface displacements and large-magnitude earthquakes is indicated by the fault scarps that formed during three historic earthquakes that occurred in the ISB: the 1934 Hansel Valley earthquake of M 6.6 (Shenon, 1936), the 1959 Hebgen Lake earthquake of M 7.5 (Myers and Hamilton, 1964) and the 1983 Borah Peak earthquake of M 7.3 (Crone and Machette, 1984). Important characteristics common to these events are significant to the future occurrence of other large-magnitude earthquakes in the ISB. Doser (1985) concludes that large-magnitude earthquakes nucleate at or near the base of the seismogenic zone (about 15 km [9 mi]), rupture unilaterally to the surface along planar normal faults dipping 45° to 60°, and form fault scarps on the updip projection of the causative faults. Our current practice is to consider other faults with evidence for late Quaternary surface displacement as potential sources of large-magnitude earthquakes. The identification of the faults and the estimates of the associated MCEs, maximum surface displacements, and average return periods are based on geologic evidence from mapping and trenching studies.

Consideration of a moderate-magnitude, random earthquake source is dictated by network monitoring, aftershock studies, and detailed microearthquake studies in the ISB that indicate that small- and moderate-magnitude earthquakes show little or no spatial correlation with late Quaternary faults. Studies of recent moderate-magnitude earthquakes including the 1962 Cache Valley earthquake of M 5.7 (Westphal and Lange, 1966), the 1972 Heber earthquake of M_b 4.7 (Langer and others, 1979), and the 1975 Pocatello Valley earthquake of M 6.0 (Arabasz and others, 1981) indicate that aftershocks of these events occurred at depths of 8 to 12 km (5 to 7 mi) on faults that can not be

identified at the surface. Recent detailed microearthquake recording in the Basin and Range transition zone in central Utah also shows little correlation of earthquake activity with late Quaternary faults (McKee and Arabasz, 1982; Foley and others, 1986). These observations suggest that seismic slip manifested as background seismicity is occurring on moderate- to high-angle segments of blind faults that have no surface expression (Arabasz and Smith, 1981; Arabasz and Julander, 1986).

A moderate-magnitude earthquake source, referred to as the random earthquake, that is not necessarily associated with late Quaternary surface faults is considered for sites in the ISB to account for this contemporary small- and moderate-magnitude earthquake activity. Historical examples indicate that moderate-magnitude earthquakes occur on blind faults--faults that are unrecognized at the surface. Tectonic subsidence and ground cracking will occur in association with a moderate-magnitude earthquake. Ground cracking and "secondary" faulting are thought to result from adjustments of upper crustal blocks to the subsurface displacements on the causative fault, as in the "shattered glass" model of Arabasz and Smith (1981).

5.2 Maximum credible earthquakes

Both seismological and geological studies indicate that the principal mode of deformation in the ISB is normal faulting in response to east-west crustal extension. The MCEs discussed in this section are associated with generally north-trending normal faults and are assumed to be principally dip-slip earthquakes.

5.2.1 Quaternary faulting in the vicinity of Jordanelle damsite

Our regional investigations (Sullivan and others, 1988) together with investigations in the Keetley Valley and Jordanelle damsite areas (chapters 3 and 4) demonstrate that faults with evidence of late Quaternary surface displacement are not closer than 20 km (12 mi) to Jordanelle damsite. The closest late Quaternary fault to Jordanelle is in Round Valley, approximately 20 km (12 mi) south of the damsite (fig. 1). Other older, but possibly Quaternary, faults are present in Kamas, Keetley, and Deer Valleys at distances of <15 km (9 mi). Available data for these faults (Sullivan and others, 1988) suggest that while early to mid-Quaternary displacement is probable or likely, no late Quaternary (<130,000 years) displacement has occurred on these faults. This age of last displacement suggests recurrence intervals for surface displacements that are greater than 100,000 years and slip rates that are <0.01 mm/yr, more than an order of magnitude less than the estimated slip rate on the

faults in Round Valley. As a result of these considerations, no MCEs have been assigned to these faults.

5.2.2 Wasatch fault

The Wasatch fault is the principal source for large-magnitude earthquakes in the Utah portion of the ISB. It has experienced larger, Holocene, single-event surface ruptures with a shorter estimated average return period than other late Quaternary faults in the region.

Detailed geologic studies of the Wasatch fault, summarized by Schwartz and Coppersmith (1984), indicate that at least six individual segments of the Wasatch fault have ruptured independently. Jordanelle Dam is about 30 km (18 mi) from the closest approach of both the Provo and the Salt Lake segments of the Wasatch fault. The dam is about 45 km (28 mi) from the Ogden segment and 70 km (43 mi) from the Nephi segment (fig. 1). The slip rates and return periods for these segments are shown in table 5. Subsequent investigations summarized by Machette (1987) suggest that the Provo segment of Schwartz and Coppersmith (1984) may consist of as many as three segments as shown on fig. 1. More recent trench investigations of the central segments of the Wasatch fault yield slip rate and average return period estimates consistent with those in table 5 (Nelson and others, 1987; Personius and Gill, 1987; Machette and Lund, 1987).

Table 5 Slip rates and average return periods for surface displacements on the central segments of the Wasatch fault (from Schwartz and Coppersmith, 1984).

Wasatch fault Segment	Closest approach to Jordanelle (km)	Late Quaternary slip rate (mm/yr)	Average return period (yrs)
Ogden	45	1.1 to 1.8	2000
Salt Lake	30	.56 to 1.4	2400 to 3000
Provo	30	.85 to 1.0	1700 to 2600
Nephi	70	1.17 to 1.46	1700 to 2700

The largest historical earthquakes in the ISB, the 1959 Hebgen Lake earthquake with a magnitude of 7.5 and the 1983 Borah Peak earthquake with a magnitude of 7.3, are considered to be representative of the maximum magnitude earthquake expected in the ISB (Doser, 1984). These earthquakes are associated with surface displacements of > 2 m (6.6 ft) and surface rupture lengths of > 20 km (12 mi). In previous USBR studies we have estimated an MCE of magnitude 7 1/2 for late Quaternary faults in the ISB with surface rupture lengths greater than 20 to 30 km and/or evidence of maximum individual surface displacements of >2 m (6.6 ft) (Gilbert and others, 1983; Piety and others, 1986; Foley and others, 1986). Late Quaternary fault rupture lengths are 30 to 70 km (18 to 43 mi) and average surface displacement per event is > 2 m (6.6 ft) for the central segments of the fault in fig. 1. These rupture parameters suggest that paleoearthquakes with magnitudes of 6 3/4 to 7 1/2 have occurred on the Wasatch fault during the Holocene (Schwartz and Coppersmith, 1984). We concur with this interpretation and following previous practice we assign an MCE of magnitude 7 1/2 to the Wasatch fault (table 6). This MCE should be considered a dipslip earthquake that could occur on any of the segments of the Wasatch fault. The strikes of the individual segments vary from about N30°E to N20°W (fig. 1); all segments dip to the west.

5.2.3 Round Valley

An MCE of magnitude 6 1/2 to 6 3/4 has been estimated by Sullivan and others (1988) for late Quaternary normal faults in Round Valley about 20 km south of Jordanelle damsite (fig. 1). Lacking direct evidence of the late Quaternary displacement history of faults in Round Valley, Sullivan and others (1988) estimated that the late Quaternary slip rate on the faults is < 0.1 mm/yr, and that surface displacements have been no greater than those on the Morgan fault-- 0.5 to 1 m (1.6 to 3.3 ft). As indicated in table 6, the estimated return period for surface displacements on the faults in Round Valley, 25,000 to 100,000 years, is significantly greater than the return period for surface displacements on the Wasatch fault.

5.2.4 Random earthquake

A random earthquake is considered a potential seismic source for all sites within the ISB (Piety and others, 1986; Sullivan and others, 1988). As the threshold for surface faulting in the ISB appears to be within the magnitude range 6 to 6 3/4 (Doser, 1984; Piety and others, 1986; Sullivan and others, 1988, sec. 2.5.2), we assign an MCE of magnitude (M_L) 6 to 6 1/2 to this

random earthquake source (table 6). Based on calculations of probabilistic epicentral distances from geologic and seismologic data for central Utah, Sullivan and others (1988) concluded that for annual probabilities of occurrence of 1/50 000 to 1/100 000, an earthquake of magnitude 6 or greater could occur within 5 km (3 mi) of any site. We recommend that the random earthquake be considered a local event that could occur in the immediate vicinity of Jordanelle damsite.

Trench investigations have shown that no late Pleistocene surface displacements have occurred on the Bald Mountain fault in Keetley Valley; however, this evidence does not indicate whether moderate-magnitude earthquakes, without associated surface rupture, have occurred on the fault. The local, moderate-magnitude, random earthquake source accounts for the possible occurrence of a moderate-magnitude earthquake on the Bald Mountain fault in the vicinity of the damsite.

Table 6 Maximum credible earthquakes for Jordanelle Dam

Source	MCE (M_S)	Closest Approach (km)	Focal depth (km)	Average return period (yrs)
Wasatch fault#	7 1/2	30	10 to 15	400 to 666*
Round Valley faults	6 1/2 to 6 3/4	20	10 to 15	25,000 to 100,000
Random earthquake	6 to 6 1/2**	local	8 to 15	N/A***

#Each of the segments in table 5 should be considered a separate seismic source zone with an MCE of M 7 1/2 for any risk analyses conducted for Jordanelle Dam.
*average recurrence interval for surface faulting on the entire fault (Schwartz and Coppersmith, 1984)
**M_L
***for an annual probability of occurrence of 1/50,000 to 1/100,000 (Sullivan and others, 1988)

5.3 Potential deformation at the damsite

No faults or shears with a potential for coseismic surface rupture have been identified in the vicinity of the dam. This conclusion is based on 1) the lack of faults near the site with late Quaternary (<130,000 years) displacement and 2) the structural relationships of faults above the right abutment (discussed in chapter 4) that indicate displacement on the mapped faults occurred prior to intrusion of the andesite porphyry during the late Eocene. The conclusion of the first Board of Consultants regarding potential surface displacements in the dam foundation was that the "zero displacement option was indefensible" (Arabasz and other, 1982). This conclusion was based on earlier interpretations of the site geology indicating that a north-tending normal fault was present in the dam foundation (USBR, 1982), and the need to consider the potential for surface deformation associated with the nearby occurrence of a moderate-magnitude earthquake.

Mapping and trenching have shown that no north-trending faults are present on the abutments of the dam; subsequent subsurface investigations have found no evidence of a north-trending high-angle fault in the floodplain portion of the dam (USBR, 1987). However, a portion of the dam foundation in the floodplain is underlain by andesite porphyry that lacks continuous stratigraphic markers that would preclude faults. Trenches, some boreholes, and geophysical surveys indicate that discontinuous zones of fracturing are present in the andesite porphyry. These zones can not be traced between adjacent boreholes or related to surface exposures. Therefore, it was concluded that they formed during the emplacement of the andesite porphyry. We do not consider these features to be potential sites for coseismic surface displacements. Excavation and mapping of the foundation will provide the final interpretations regarding the presence of faults in the dam foundation. If our conclusion that no north-trending faults are present is confirmed, then potential surface displacements in the foundation should not be considered in the design of the dam.

5.3.1 Potential deformation of the dam foundation

In response to the recommendation of the recent Consulting Board (Peck and others, 1986), we have completed modelling studies of the elastic surface deformation associated with slip on buried faults. The results of these studies are reported in Appendix C.

Our model for the occurrence of a "random" earthquake within the Regional Study area assumes that these events do not produce large, recurrent surface ruptures. If such ruptures were occurring, geologic evidence should be preserved. Historical earthquakes such as the 1975 Pocatello Valley event demonstrate that surface deformation, such as tectonic subsidence and ground cracking, can occur in association with moderate-magnitude earthquakes. Geologic evidence of similar prehistoric surface deformation is beyond the resolution of our regional studies. Likewise, small differential displacements (<<0.5 m)) which might occur in association with this subsidence would likely lack continuity, degrade rapidly, and be difficult to observe in the geologic record.

Although there is limited data on tectonic subsidence recorded for this type of event, the results of the model simulations reported in Appendix C suggest that a reasonably conservative portrayal of the surface deformation associated with the occurrence of a magnitude 6 to 6 1/2 earthquake in the vicinity of the dam would include the following elements: 1) the event would likely be predominantly normal faulting on a plane with moderate to steep dip, striking within 30° of north; 2) the fault plane would be 10 km to 20 km long and 5 to 10 km wide; 3) rupture could be as shallow as 2 km (1 mi) and extend to a depth as great as 15 km (9 mi); 4) no discernible primary surface rupture would be identifiable; 5) geodetically observable tectonic subsidence would extend over 100 km^2 (36 mi^2) or more with net tectonic subsidence of 0.5 m (1.6 ft) and a maximum horizontal gradient of 20 cm/km; and 4) abundant ground cracking would occur within the subsided area, especially in areas of thicker alluvium, possibly with small, localized displacements occurring along favorably-oriented, preexisting faults. None of the three magnitude 6 to 6 1/2 historical non-surface faulting earthquakes for which geodetic data are available indicate maximum tectonic subsidence of greater than 15 cm, or maximum horizontal gradient greater than about 4 cm/km.

If an earthquake of magnitude 6 to 6 1/2 occurred in the vicinity of the dam, the horizontal gradient of 20 cm/km estimated for the tectonic subsidence would produce an elevation change of as much as 10 cm distributed uniformly across the 500-m-long dam.

Of greater engineering significance than tectonic subsidence would be the potential for small localized displacements on preexisting faults in the dam foundation. These displacements would likely occur on faults and shears with orientations

favorable to reactivation in the contemporary stress field, i.e., structures with moderate to steep dips and strikes within 30° of north. We would interpret these as the most likely sites for small displacements.

Bonilla (1982, p. 10), in his evaluation of potential surface faulting associated with large-magnitude earthquakes, defines secondary faults as subsidiary faults that are entirely separate from the main fault at the surface. Based on about 100 documented historical examples of subsidiary faulting, he concludes that an estimate that the displacement will be about 30% of the maximum displacement on the main fault is appropriate. Lacking other data, we use this relationship to estimate the maximum subsidiary displacement that could occur on favorably oriented faults as a result of tectonic subsidence. Modelling studies suggest tectonic subsidence of 50 cm; therefore, maximum subsidiary displacement are estimated to be 15 cm. Any favorably oriented faults mapped in the dam foundation should be considered capable of displacement of as much as 15 cm. The final determination of the sites of potential surface displacements, if any, will be made as the foundation mapping is completed.

5.3.2 Potential deformation of the outlet works tunnels

Small surface displacements associated with the occurrence of the local MCE at Jordanelle have been described as secondary ruptures that may be expected to occur on pre-existing faults with favorable orientations and strike lengths of at least a few km. Both the recent drilling across the Provo River floodplain upstream of the Jordanelle Dam axis (USBR, 1987) and cross sections of the left abutment (USBR, 1986) reveal no evidence of significant faults that could trend through the outlet works tunnels located upstream of the left abutment. Shears are present both in the drill holes and outcrops, but they are discontinuous features apparently related to the intrusion of the andesite porphyry. Although shears should also be anticipated in the outlet works tunnel, available evidence precludes significant faults of any orientation; therefore, no potential displacements should be considered in the design of the outlet works tunnels.

If an earthquake of magnitude 6 to 6 1/2 occurred in the vicinity of the dam on a blind fault oriented nearly normal to the the alinement of the tunnels, the horizontal gradient of 20 cm/km estimated for the tectonic subsidence would produce an elevation change of as much as 12 cm distributed uniformly over the 600 m length of the tunnels. This is a very conservative

conclusion because other, more likely, relative orientations would produce smaller horizontal gradients.

5.4 Reservoir-induced seismicity

RIS (reservoir induced seismicity) refers to the occurrence of small- and moderate-magnitude earthquakes during or after the impoundment of reservoirs. These earthquakes are thought to be naturally occurring events that are triggered prematurely by the presence of the reservoir. Empirical correlations, discussed in Appendix B, suggest that large, deep reservoirs in the vicinity of young faults are the most susceptible to RIS.

A detailed analysis of historic seismicity in the vicinity of the 13 USBR reservoirs in the back valleys of north-central Utah (Appendix B) showed no clear evidence for RIS near any of the reservoirs. A statistical analysis showed no seasonal fluctuations in seismicity that could be correlated with normal seasonal changes in reservoir level. However, at 99 m Jordanelle Dam will be the highest in north-central Utah. A reservoir depth of 90 m appears to be a threshold for a significant increase in the liklihood of RIS (Packer and others, 1980).

Baecher and Keeney (1982) developed statistical techniques for estimating probabilities of RIS occurrence that are conditioned on various states of five reservoir characteristics: depth, volume, crustal stress state, presence of active faults under the reservoir, and rock type underlying the reservoir. They examined 234 reservoirs, 29 of which were judged to have caused RIS. Utilizing their techniques, we have calculated the probabilities of RIS at Jordanelle Reservoir. Using their terminology, Jordanelle Reservoir was classified as deep, with small volume, within an extensional stress regime, with active faults in the reservoir, and with igneous rocks underlying the reservoir. A probability of .07 of RIS occurrence conditioned on the above attributes was computed by the "independent discrete" method, and a probability of .06 was computed based on the "dependent discrete" method. The latter method assumes dependence between depth and volume; the "independent discrete" method does not. Thus, the probability for RIS at Jordanelle Reservoir, based on these calculations,is about 6% - 7%. While Baecher and Keeney (1982) acknowledge that the probabilities of RIS estimated from their methodologies are not very precise, we feel that this estimate is reasonable.

Geologic evidence demonstrates that surface rupture and accompanying large-magnitude earthquakes have not occurred in or

near the reservoir in at least the last 130,000 years. The largest MCE originating in or near the reservoir is a magnitude (M_L) 6 to 6 1/2 random earthquake. As RIS appears to be a triggering event for naturally occurring events, we would not expect induced earthquakes to exceed magnitude (M_L) 6 to 6 1/2, nor would we expect surface ruptures to accompany RIS.

If RIS does occur at Jordanelle, its identification will be greatly facilitated by the 14+ year, pre-impoundment record of local seismicity. Seismic monitoring in the vicinity was enhanced by the deployment of a vertical component seismograph near the damsite in 1981. The addition of two horizontal components and another lower-gain, vertical component in 1986 currently allows for the location of earthquakes of magnitude 1 or less in the reservoir area (sec. 2.3.2). With this monitoring capability in the vicinity of the damsite, the statistical study of the region presented in Appendix B provides a baseline for evaluating RIS at Jordanelle Reservoir.

6.0 REFERENCES

Arabasz, W. J., Smith, R. B., and Richins, W. D., 1979, Earthquake studies along the Wasatch Front, Utah: Network monitoring, seismicity, and seismic hazards, in Arabasz, W. J., Smith, R. B., and Richins, W. D., eds., Earthquake studies in Utah 1850 to 1978: University of Utah Seismograph Stations, Department of Geology and Geophysics, University of Utah, Salt Lake City, Utah, p. 253-285.

Arabasz, W. J., and Smith, R. B., 1979, Introduction: What you've always wanted to know about earthquakes in Utah in Arabasz, W. J., Smith, R. B., and Richins, W. D., eds., Earthquake studies in Utah 1850 to 1978: University of Utah Seismograph Stations, Department of Geology and Geophysics, University of Utah, Salt Lake City, Utah, p. 1-14.

Arabasz, W. J., and Smith, R. B., 1981, Earthquake prediction in the Intermountain seismic belt -- an intraplate extensional regime, in Simpson, D. W. and Richards, P. G., eds., Earthquake prediction, an international review: Washington, D. C., American Geophysical Union, Maurice Ewing Series 4, p. 803-826.

Arabasz, W. J., Richins, W. D., and Langer, C. J., 1981, The Pocatello Valley (Idaho-Utah border) earthquake sequence of March to April, 1975: Bulletin of the Seismological Society of America, v. 71, no. 3, p. 803-826.

Arabasz, W. J., Jahns, R. H., and Peck, R. B., 1983, Review and analysis of geologic, seismotectonic, and design data for the proposed Jordanelle Dam, Bonneville Unit, Central Utah Project, Utah [unpublished report]: Joint Consultant Review Report to the U. S. Bureau of Reclamation, Engineering and Research Center, Denver, Colorado dated February, 1983, 87 p.

Arabasz, W. J., and Julander, D. R., 1986, Geometry of seismically active faults and crustal deformation within the Basin and Range-Colorado Plateau transition in Utah, in Mayer, L., ed., Extensional tectonics of the Basin and Range province: A perspective: Geological Society of America Special Paper no. 208.

Armstrong, R. L., 1968, Sevier orogenic belt in Nevada and Utah: Geological Society of America Bulletin, v. 79, p. 429-459.

Bachman, G. O., and Machette, M. N., 1977, Calcic soils and calcretes in the southwestern United States: U. S. Geological Survey Open-File Report 77-794.

Baecher, G. B., and Keeney, R. L., 1982, Statistical examination of reservoir-induced seismicity: Bulletin of the Seismological Society of America, v. 72, no. 2, p. 553-569.

Baker, A. A., 1964, Geology of the Aspen Grove Quadrangle, Utah: U.S. Geological Survey Geologic Quadrangle Map GQ-239, scale 1:24,000.

Best, M. G., 1986, Review of the Geology of the Middle Right Abutment of the Jordanelle, Utah damsite in Technical Review Document for Consultant Review, vol. II, Appendix IB -- Structural and stratigraphic relationships for the middle right abutment, Jordanelle damsite [unpublished report]: submitted to the U. S. Bureau of Reclamation, Bonneville Construction Office, dated August 22, 1986.

Beutner, E., 1977, Causes and consequences of curvature in the Sevier orogenic belt in Utah and Montana: Wyoming Geological Association Guidebook, 29th Annual Field Conference, p. 353-366.

Bonilla, M. G., 1982, Evaluation of potential surface faulting and other tectonic deformation: U.S. Geological Survey, Open-File Report 82-732.

Bonilla, M. G., Mark, R. K., and Lienkaemper, J. J., 1984, Statistical relations among earthquake magnitude, surface rupture length, and surface fault displacement: Bulletin of the Seismological Society of America, v. 74, p. 2379-2411.

Boutwell, J. M., 1912, Geology and ore deposits of the Park City district, Utah: U.S. Geological Survey Professional Paper 77, 231 p.

Bridges, R. L., 1984, Geologic Report, Jordanelle Reservoir [unpublished report]: Provo, Utah submitted to U. S. Bureau of Reclamation, Bonneville Construction Office, dated August, 1984.

Bromfield, C. S., 1968, General Geology of the Park City region, Utah, in Erickson, A. J., Phillips, W. R., and Garmoe, W. J., eds., Guidebook to the geology of the Park City district: Utah Geological Association Guidebook no. 22, p. 10-29.

Bromfield, C. S., Baker, A. A., and Crittenden, M. D., Jr., 1970, Geologic map of the Heber quadrangle, Wasatch and Summit counties, Utah: U.S. Geological Survey Geologic Quadrangle Map GQ-864, scale 1:24,000.

Bromfield, C. S., and Crittenden, M. D., Jr., 1971, Geologic map of the Park City East quadrangle, Summit and Wasatch counties, Utah: U.S. Geological Survey Geologic Quadrangle Map GQ-852, scale 1:24,000.

Bromfield, C. S., Erickson, A. J., Jr., Haddadin, M. A., and Mehnent, H. H., 1977, Potassium-argon ages of intrusion, extrusion and associated ore deposits, Park City mining district, Utah: Economic Geology, v. 72, p. 837-848.

Bucknam, R. C, 1976, Leveling data from the epicentral area of the March 27, 1975, earthquake in Pocatello Valley, Idaho: U. S. Geological Survey Open-file Report 76-52, 6 p.

Bucknam, R. C., Algermissen, S. T., and Anderson, R. E., 1980, Patterns of late Quaternary faulting in western Utah and an application in earthquake hazard evaluation, in Proceedings, Conference X, Earthquake hazards along the Wasatch and Sierra Nevada frontal fault zones: U. S. Geological Survey Open-File Report 80-801, p. 291-314.

Crittenden, M. D., Jr., and Calkins, F. C., 1966, Geologic map of the Park City West quadrangle, Utah: U.S. Geological Survey Geologic Quadrangle Map GQ-535, scale 1:24,000.

Crittenden, M. D. Jr., Stuckless, J. S., Kistler, R. N., and Stern, T. W., 1973, Radiometric dating of intrusive rocks in the Cottonwood area, Utah: U.S. Geological Survey Journal of Research, v. 1, p. 173-178.

Crone, A. J., and Machette, M. N., 1984, Surface faulting accompanying the Borah Peak earthquake, central Idaho: Geology, v. 12, no. 5, p. 292-295.

Dixon, J. S., 1982, Regional structural synthesis, Wyoming salient of the western overthrust belt: American Association of Petroleum Geologists Bulletin, vol. 66, no. 10, p. 1560-1580.

Doser, D. I., 1984, Source parameters and faulting processes of the August 1959 Hebgen Lake, Montana, earthquake sequence [Ph. D. thesis]: Salt Lake City, University of Utah, 165 p.

Doser, D. I., 1985, The 1983 Borah Peak, Idaho and 1959 Hebgen Lake, Montana, earthquakes : Models for normal fault earthquakes in the Intermountain seismic belt, in Stein, R. S. and Bucknam, R. C., eds., Proceedings of Workshop XXVIII on the Borah Peak, Idaho earthquake: U. S Geological Survey Open-File Report 85-290, v. A, p. 368-384.

Eardley, A. J., 1968, Regional geologic relations of the Park City district, in Erickson, A. J., Phillips, W. R., and Garmoe, W. J., eds., Guidebook to the geology of the Park City district: Utah Geological Association Guidebook no. 22, p. 3-9.

Foley, L. L., Martin, R. A., and Sullivan, J. T., 1986, Seismotectonic study for Joes Valley, Scofield, and Huntington North Dams, Emery County and Scofield Projects, Utah [unpublished report]: Denver, Colorado, U. S. Bureau of Reclamation, Seismotectonic Study report 86-7, 167 p.

Garmoe, W. J, and Erickson, A. J., 1968, Ore deposits of the Park City District, in Erickson, A. J., Phillips, W. R., and Garmoe, W. J. eds., Guidebook to the Geology of the Park City district: Utah Geological Association Guidebook no. 22, p. 30-38.

Gilbert, G. K., 1928, Studies of Basin and Range structure: U. S. Geological Survey Professional Paper 153, 89 p.

Gile, L. H., Peterson, F. F., and Grossman, R. B., 1966, Morphological and genetic sequences of carbonate accumulation in desert soils: Soil Science, v. 101, p. 347-360.

Gilbert, J. D., Ostenaa, D., and Wood, C., 1983, Seismotectonic study for Jackson Lake Dam and Reservoir, Minidoka Project, Idaho-Wyoming [unpublished report]: Denver, Colorado and Pacific Northwest Regional Office, Boise, Idaho, U. S. Bureau of Reclamation, Seismotectonic Study report 83-3, 123 p.

Grey, E., 1982, Seismic interpretation of the Jordanelle damsite area, in Consultant Review Briefing Document for the proposed Jordanelle damsite and Reservoir, Bonneville Unit, Central Utah Project, Appendix A [unpublished report]: Salt Lake City, Utah, Jordanelle Task Force.

Hansen, W. R., 1983, Post-Laramide tectonic history of the eastern Uinta Mountains, Utah, Colorado, and Wyoming: The Mountain Geologist, v. 21, no. 1, p. 5-29.

Harden, J. W., 1982, A quantitative index of soil development from field descriptions: examples from a chronosequence in central California: Geoderma, v. 28, p. 1-28.

Harden, J. W. and Taylor, E. W., 1983, A quantitative comparison of soil development in four climatic regimes: Quaternary Research, v. 20, p. 342-359.

Hintze, L. F., 1980, Geologic map of Utah: Utah Geological and Mineral Survey, scale 1:500,000.

Jordanelle Task Force, 1982, Consultant Review Briefing Document for the proposed Jordanelle damsite and Reservoir, Bonneville Unit, Central Utah Project [unpublished report]: Park City Utah, United Park City Mines.

Kaliser, B. N., 1975, Ground cracks resulting from the Pocatello Valley earthquake: Geological Society of America Abstracts with Programs, v. 7, no. 7, p. 1137.

Langer, C. J., Keller, G. R., and Smith, R. B., 1979, A study of aftershocks of the October 1, 1972, m_b = 4.7, Heber City, Utah earthquake, in Arabasz, W. J., Smith, R. B., and Richins, W. D., eds., Earthquake studies in Utah 1850 to 1978: University of Utah Seismograph Stations, Department of Geology and Geophysics, University of Utah, Salt Lake City, Utah, p. 383-394.

Lawton, T. F., 1980, Petrography and structure of the Little Cottonwood stock and metamorphic aureole, central Wasatch Mountains, Utah [Ph.D. thesis]: Stanford University, California.

Lawton, T. F., John, D. A., and Moore, W. J., 1980, Levels of emplacement of mid-Tertiary plutons in the central Wasatch Mountains, Utah: Geological Society of America, Abstracts with Programs, v. 12, no. 6, p. 278.

Machette, M. N., 1985, Calcic soils of the southwestern United States, in Weide, D. L., ed., Soils and Quaternary geology of the southwestern United States: Geological Society of America Special Paper 203, p. 1-23.

Machette, M. N., 1987, Recent studies of the late Quaternary history of the Wasatch fault zone, Utah--a review: Geological Society of America, Abstracts with Programs v. 19, no. 5, p. 317.

Machette, M. N., and Lund, W. R., 1987, Late Quaternary history of the American Fork segment of the Wasatch fault zone, Utah: Geological Society of America, Abstracts with Programs, v. 19, no. 5, p. 317.

Mann, D. C., 1974, Clastic Laramide sediments of the Wasatch Hinterland, northeastern Utah [M.S. thesis]: University of Utah, Salt Lake City, Utah, 112 p.

Martin, R. A., Jr., Nelson, A. R., Weisser, R. R., and Sullivan, J. T., 1985, Seismotectonic study for Taskeech Dam and Reservoir Site, Upalco Unit, and Upper Stillwater Dam and Reservoir site, Bonneville Unit, Central Utah Project, Utah: U. S. Bureau of Reclamation Seismotectonic Report 85-2.

McKee, M. E., and Arabasz, W. J., 1982, Microearthquake studies across the Basin and Range-Colorado transition in central Utah, in Nielson, D. L., ed., Overthrust Belt of Utah: Utah Geological Association Publication no. 10, p. 137-149.

Meiiji, 1980, Results of a geophysical survey of the Jordanelle damsite and reservoir [unpublished report]: prepared by Meiiji Resource Consultants for the U.S. Bureau of Reclamation, Provo, Utah.

Mullens, T. E., 1971, Reconnaissance study of the Wasatch, Evanston, and Echo Canyon Formations in part of northern Utah: U. S. Geological Survey Bulletin 1311-D, 31 p.

Myers, W. B., and Hamilton, W., 1964, Deformation accompanying the Hebgen Lake earthquake of August 17, 1959, in The Hebgen Lake, Montana earthquake of August 17, 1959: U. S. Geolgical Survey Professional Paper 435, p. 55-98.

Nelson, A. R., and Martin, R. A., 1982, Seismotectonic report for Soldier Creek Dam, Central Utah Project, Utah: U. S. Bureau of Reclamation Seismotectonic Report 82-1, 115 p.

Nelson, A. R., and Taylor, E. M., 1985, Automated calculation of soil profile development indices using a microcomputer and integrated spreadsheet: Geological Society of America Abstracts with Programs, v. 17, no. 4, p. 258.

Nelson, A. R., Klauk, R. H., Lowe, M., and Garr, J. D., 1987, Holocene history of displacement on the Weber segment of the Wasatch fault zone at Ogden, northern Utah: Geological Society of America, Abstracts with Programs, v. 19, no. 5, p. 322.

Packer, D. R., Lovegreen, J. R., and Born, J. L., 1977, Reservoir-induced seismicity in Earthquake evaluation studies for Auburn Dam, Woodward-Clyde Consultants, vol. 6: NTIS report PB-283 531/2GA,PC A15/MF A01.

Peck, R. B., Arabasz, W. J., Tarbox, G. S., and Campbell, D. D., 1986, Joint Report of Architect-Engineer Consulting Group for Jordanelle Dam [unpublished report]: Denver, Colorado, U. S. Bureau of Reclamation, dated December 3, 1986, 43 p.

Personius, S. F., and Gill, H. E., 1987, Holocene displacement on the Brigham City segment of the Wasatch fault zone near Brigham City, Utah: Geological Society of America, Abstracts with Programs, v. 19, no. 5, p. 326.

Piety, L. A., Wood, C. K.,Gilbert, J. D., Sullivan, J. T., and Anders, M. H., 1986, Seismotectonic Study for Palisades Dam and Reservoir, Palisades Project, Idaho [unpublished report]: Denver, Colorado, U. S. Bureau of Reclamation, Seismotectonic Study report 86-3, 198 p.

Pitt, A. M., Weaver, C. S., and Spence, W., 1979, The Yellowstone Park earthquake of June 30, 1975: Bulletin of the Seismological Society of America, v. 69, no. 1, p. 187-205.

Platt, L. B., 1975, Recent faulting at Samaria Mountain, southeastern Idaho: Geological Society of America Abstracts with Programs, v. 7 no. 7, p. 1229-1230.

Quinlan, J. J., and Simos, J. G., 1968, The Mayflower Mine, in Erickson, A. J., Phillips, W. R., and Garmoe, W. J., eds., Guidebook to the geology of the Park City district: Utah Geological Association Guidebook no. 22, p. 40-55.

Rawls, W. J., 1983, Estimating bulk density from particale size analysis and organic matter content: Soil Science, v. 135, no. 2, p. 123-125.

Royse, Frank Jr., Warner, M. A., and Reeves, D. L., 1975, Thrust belt structural geometery and related stratigraphic problems -- Wyoming, Idaho, and northern Utah: Rocky Mountain Association of Geologists Symposium -- Deep Drilling Frontiers of the Rocky Mountains, pp. 41-54.

Royse, F., 1983, Extensional faults and folds in the Foreland Thrust Belt, Utah, Wyoming, and Idaho: Geological Society of America Abstracts, v. 15, no. 5, p. 295.

Schwartz, D. P., and Coppersmith, K. J., 1984, Fault behavior and characteristic earthquakes -- examples from the Wasatch and San Andreas fault zones: Journal of Geophysical Research, v. 89, no. B7, p. 5681-5689.

Shenon, P. J., 1936, The Utah earthquake of March 12, 1934, (extracts from an unpublished report), in Newman, F., United States Earthquakes, 1934: U. S. Coast and Geodetic Survey Serial 4593, p. 43-48.

Smith, R. B., 1978, Seismicity, crustal structure, and intraplate tectonics of the interior of the western Cordillera: Geological Society of America Memoir 152, p. 111-144.

Smith, R. B., and Sbar, M. L, 1974, Contemporary tectonics and seismicity of the Intermountain seismic belt: Geological Society of America Bulletin v. 72 p. 151-172.

Smith, R. B., and Bruhn, R. L., 1984, Intraplate extensional tectonics of the eastern Basin and Range: Inferences on structural style from seismic reflection data, regional tectonics, and thermal-mechanical models of brittle-ductile deformation: Journal of Geophysical Research, v. 89, p. 5733-5762.

Soltanpour, P. N., and Workman, S. M., 1981, Soil-testing methods used at Colorado State University Soil Testing Laboratory: Colorado State University Experiment Station of Fort Collins Technical Bulletin 142, 22 p.

Stein, R. S., and Barrientos, S. E., 1985, The 1983 Borah Peak, Idaho earthquake: Geodetic evidence for rupture on a planar fault: U. S. Geological Survey Open-File Report 85-290, p. 459-484.

Stewart, J. H., Moore, W. J., and Zeitz, I., 1977, East-west patterns of igneous rocks, aeromagnetic anomalies, and mineral deposits, Nevada and Utah: Geological Society of America Bulletin, v. 88, p. 67-77.

Stewart, J. H., 1978, Basin-range structure in western North America: a review: Geological Society of America Memoir 152, p. 1-32.

Stokes, W. L., and Madsen, J. H., Jr., 1961, Geologic map of Utah - northeast quarter: Utah Geological and Mineral survey, scale 1:250,000.

Sullivan, J. T., and Nelson, A. R., 1983, Late Cenozoic faulting in Heber and Keetley Valleys, northeastern Utah, in Crone A. J. ed., Paleoseismicity along the Wasatch Front and adjacent areas, central Utah, in Geological excursions in neotectonics and engineering geology in Utah, Geological Society of America, Fieldtrip Guidebook for Rocky Mountain and Cordilleran Section Meeting - Part IV: Utah Geological and Mineral Survey Special Studies 62, p. 55-62.

Sullivan, J. T., Foley, L. L., and Martin, R. A., Jr., 1986, Draft seismotectonic study for Jordanelle Dam, Central Utah Project, Utah, in Technical Review Document for Consultant Review, vol. II [unpublished report]: Denver, Colorado and Bonneville Construction Office, Provo, Utah, U. S. Bureau of Reclamation, dated September, 1986.

Sullivan, J. T., Nelson, A. R., LaForge, R. C., Wood, C. K., and Hansen, R. A., 1988, Central Utah regional seismotectonic study for USBR Dams in the Wasatch Mountains of north-central Utah [unpublished report]: Denver, Colorado, U. S. Bureau of Reclamation Seismotectonic Study report 88-5, 270 p.

University of Utah, 1987, Utah Preliminary Epicenters [computer tape]: Seismograph Station, Department of Geology and Geophysics, University of Utah, Salt Lake City, Utah.

U. S. Bureau of Reclamation, 1982, Consultants Briefing Document for 1982 Meeting [unpublished report]: Denver, Colorado, U. S. Bureau of Reclamation.

U.S. Bureau of Reclamation, 1986, Draft Geologic Report for Jordanelle damsite and Reservoir, Bonneville Unit, Central Utah Project, Utah, in Technical Review Document for Consultant Review, vol. I [unpublished report]: Bonneville Construction Office, Provo, Utah, U. S. Bureau of Reclamation, dated September, 1986.

U. S. Bureau of Reclamation, 1987, Draft Geology Report -- Results of Jordanelle damsite Angle Hole Drilling Program proposed by the 1986 Consultant Group [unpublished report]: Bonneville Construction Office, Provo, Utah, U. S. Bureau of Reclamation, dated July, 1987.

Westphal, W.H., and Lange, A. L., 1966, Local seismic monitoring-final technical report: Stanford Research Inst. Report, 242 p.

Wilson, J. C., 1961, Geology of the Alta stock, Utah [Ph.D. thesis]: Pasadena, California, California Institute of Technology.

Woodfill, R. D., 1972, A geologic and petrographic investigation of a northern part of the Keetley volcanic field, Summit and Wasatch Counties, Utah [Ph.D. thesis]: Purdue University, 168 p.

Wyss, M., 1979, Estimating maximum expectable earthquakes from fault dimensions: Geology, v. 7 p. 336-340.

Zoback, M. L., 1983, Structure and Cenozoic tectonism along the Wasatch fault zone, Utah, in Tectonic and Stratigraphic studies of the eastern Great Basin: Geological Society of America Memoir 157, p. 3-27.

APPENDIX A

Seismic Refraction Survey of Jordanelle Reservoir Site

Bonneville Unit

Central Utah Project

by

Richard A. Martin
and
J. Timothy Sullivan

September 1987

Introduction

The seismic refraction method has been used at the south end of Keetley Valley in the area of the proposed Jordanelle Reservoir to aid in the assessment of earthquake hazards for Jordanelle Dam. The primary objective of this refraction program was to map the contact between the bedrock and overlying basin fill for the purpose of identifying abrupt changes in bedrock elevation that may be the result of young faulting. This information was then incorporated in the seismotectonic analysis.

Survey Description

The seismic refraction survey was conducted in three phases. Phase I involved the acquisition of about 17700 ft of data along 10 different lines (seismic lines S-1 through S-10) in Keetley Valley. The goals of phase I were (1) to test the applicability of the method and determine the appropriate field parameters required to successfully use this exploration tool in this area, and (2) to get a general idea of the sub-alluvial topography and basin fill thickness in a variety of locations both in the middle of the basin and along its western margin. The field work for phase I was conducted during the summer of 1982 and followed by preliminary processing and analysis of the resulting data. Information from this analysis was used to refine the field parameters and to plan phase II. Phase II involved the acquisition of 6900 ft of data along two lines (lines S-11 and S-12) in the flood plain of the Provo River immediately north of the damsite. The data for phases I and II were acquired by geophysicists from the E&R Center, processed by geophysicists from the USGS (U. S. Geological Survey) during the fall and winter of 1982, and used to plan phase III of the study.

Phase III involved detailed data collection along two long lines that traversed the basin in directions that were either perpendicular (line S-13) or somewhat parallel (line S-14) to the general strike of the basin. The data acquisition, processing, and analysis for phase III were performed by the USGS during 1983.

During phases I and II, two 12-channel digital seismographs were used to record data, and in phase III a 48 channel system was used. All data were stored on magnetic tape and played out at the USGS Oil and Gas Branch seismic data processing center. For seismic lines S-1, S-2, S-6, S-62, S-11, and S-12 the geophone separation was 20 ft. Lines S-4, S-5, S-7, S-9, S-10, S-13, and S-14 had jug separations of 50 ft. Line S-3 had 40-ft

geophone spacings. Shot sizes varied between 0.33 and 5.0 lb of Kinepac or gelatin dynamite, and shot depth ranged from about 3 to 10 ft.

Processing and Analysis Methodology

The data were processed by geophysicists from the Geophysics Branch of the USGS using interactive computer methods developed by Ackermann and others (1982; 1983). These methods were designed specifically for use with multiple shotpoint locations for each spread providing a large quantity of overlapping data, as done on this survey. The resulting subsurface p-wave velocity sections satisfied the initial data with a high degree of accuracy.

The data are processed as discrete layers. Line S-8 on plate 2, for example, consists of five layers. The upper boundary of each layer will be referred to as an interface. Each interface represents a seismic ray which has followed a minimum time path between shotpoint and receivers. Thus the art of processing consists of mapping minimum time paths, and in that respect is unrelated to the geology. The velocity of a ray may vary laterally, thus each layer may vary in thickness, depth, and velocity. Rays may follow or track geologic or hydrologic interfaces, but not necessarily so. Rays at times may cut across such boundaries, or may even propagate within geologic units. Thus each ray or interface may or may not correspond to a geologic or hydrologic boundary.

The art of interpretation consists of making geologic sense from the processed velocity sections. This requires an understanding of the geologic framework of the surveyed area and the relationship between geologic units and their velocity. Frequently, drill hole results agreed remarkably well with the processed refraction sections and the drill hole data could be confidently extrapolated along the seismic section. On the other hand, apparent discrepancies between drill hole data and velocity sections did occur.

Results

The primary objective of the refraction program was to map the top of bedrock in the vicinity of the reservoir. Bedrock is late Eocene Jordanelle andesite porphyry (Tkj). The overlying basin fill deposits consist of unconsolidated, interbedded, fine-grained and coarse-grained alluvial fan deposits. Little data on

the thickness of the basin fill within the reservoir area, and no data on the seismic velocities were available prior to phase I. Information gained from phase I indicated that relatively large offsets and long profiles were necessary to acquire information about the bedrock topography in the deeper portions of the basin. Data from lines S-1, S-2, S-3, S-4, S-7, S-9, and S-10 revealed information only about the basin fill deposits, and were of no value in assessing the nature of possible faults in the bedrock. However, these lines provide velocity information about the basin fill and minimum depths to bedrock. Line S-5 was an attempt to acquire data along the paved road that ascends the western portion of the basin, but because of the many curves in the road, the data produced uninterpretable results. Because of the limited value of lines S-1, S-2, S-4, S-5, S-9, and S-10 in assessing bedrock depths, they will not be discussed further in this report. Velocity sections for lines S-3 and S-7, however, are presented.

The locations of seismic lines S-3, S-6, S-62, S-7, S-8, S-11, S-12, S-13, and S-14 are indicated on plate 1. The numbers accompanying the ends of each line correspond to horizontal distances measured in feet with 0 indicating the beginning of each line. These end-points match the velocity sections for each line which are included in this report as plates 2 through 11. Two sets of velocity sections are presented. The sections shown on plate 2 are for all the lines where bedrock was encountered and are at a scale that represents the topography of the bedrock surface with a vertical exaggeration of 1.5 to 1. The sections shown on plates 3 through 11 have vertical exaggerations of 5 times the horizontal scale (either 1 in = 200 ft or 1 in = 400 ft) thus making it possible to include velocity information for all the layers.

The bedrock interface with the overlying basin fill is interpreted from the velocity sections in plate 2. On plate 2 for all the the velocity sections the horizontal scale is 1 in equals 400 ft, the vertical exaggeration equals 1.5 times horizontal scale, and the indicated p-wave velocities are in kft/sec (kilofeet per second). Each section shows several discrete layers over a half-space. The seismic interface separating the half-space from the overlying layers is interpreted to be the contact between the bedrock and the basin fill on all the sections shown on plate 2 with the exception of line S-13 where a refractor within the andesite is evident along a portion of the profile. These interfaces are divided into sections delineated by vertical lines based on changes in the seismic velocity of the upper portion of bedrock. Because the vertical exaggeration was limited to 1.5, there was generally

insufficient space at the chosen scale to include on these sections velocity data for the alluvial layers.

Velocity information for all layers is indicated on plates 3 through 11. On these plates the layers below the first layer are subdivided by numbers that depict the velocity of each layer from that point to the next number in a left to right sense. For example layer 2 on line S-3 (plate 3) has a velocity of 3.9 kft/sec from station -600 to about station 200 where the velocity changes to 3.2 kft/sec for the next 720 ft. From station 920 to the western end of the line the velocity of layer 2 is 2.8 kft/sec.

The velocities of the individual layers above bedrock are everywhere less than about 8.6 kft/sec, vary both laterally and vertically, and increase in value with depth. Up-hole shooting in boreholes DH-469 and DH469a (on S-12), however, indicate the velocity of the basin fill is more complicated than the simple layered models shown on plates 3 through 11, and include low velocity zones or hidden layers. The interval velocity and corresponding geologic logs for DH-469 and DH-469a, which are within 10 ft of each other along line S-12, are shown on figure 1. Average interval velocities range from about 1.5 kft/sec for the unsaturated near surface layer, to 7.64 kft/sec for the deeper alluvium. Where low velocity layers exist in the basin fill the depth to bedrock may be misrepresented by the seismic sections, but the general shape of the bedrock surface should be relatively unaffected. The effect of these low velocity layers on estimates of bedrock depths is greater where the basin fill is relatively thin.

The average velocity of the upper 27 ft of bedrock (Tkj) in DH-469a was measured at about 11.0 kft/sec. The velocity of the bedrock as determined by the seismic refraction data ranged from about 8.0 kft/sec for a small portion of line S-62 to 18.4 kft/sec for part of line S-11. Sections of the lines where the velocity of the bedrock is less than 10.0 kft/sec are quite limited with the great majority of bedrock having seismic velocities greater than about 11.0 kft/sec. The variation in bedrock velocities is due primarily to changes in the fracture density and degree of weathering of the rock. The sections of the lines where the velocity is in the 8.0 to 9.0 kft/sec range may be the result of faulting, although it is not possible to conclude this with the available data. If these low velocity zones do correspond to faulting, the faults are not associated with obvious steps in the bedrock-basin fill interface. This suggests that the faults do not displace the basin fill and, therefore, predate its deposition.

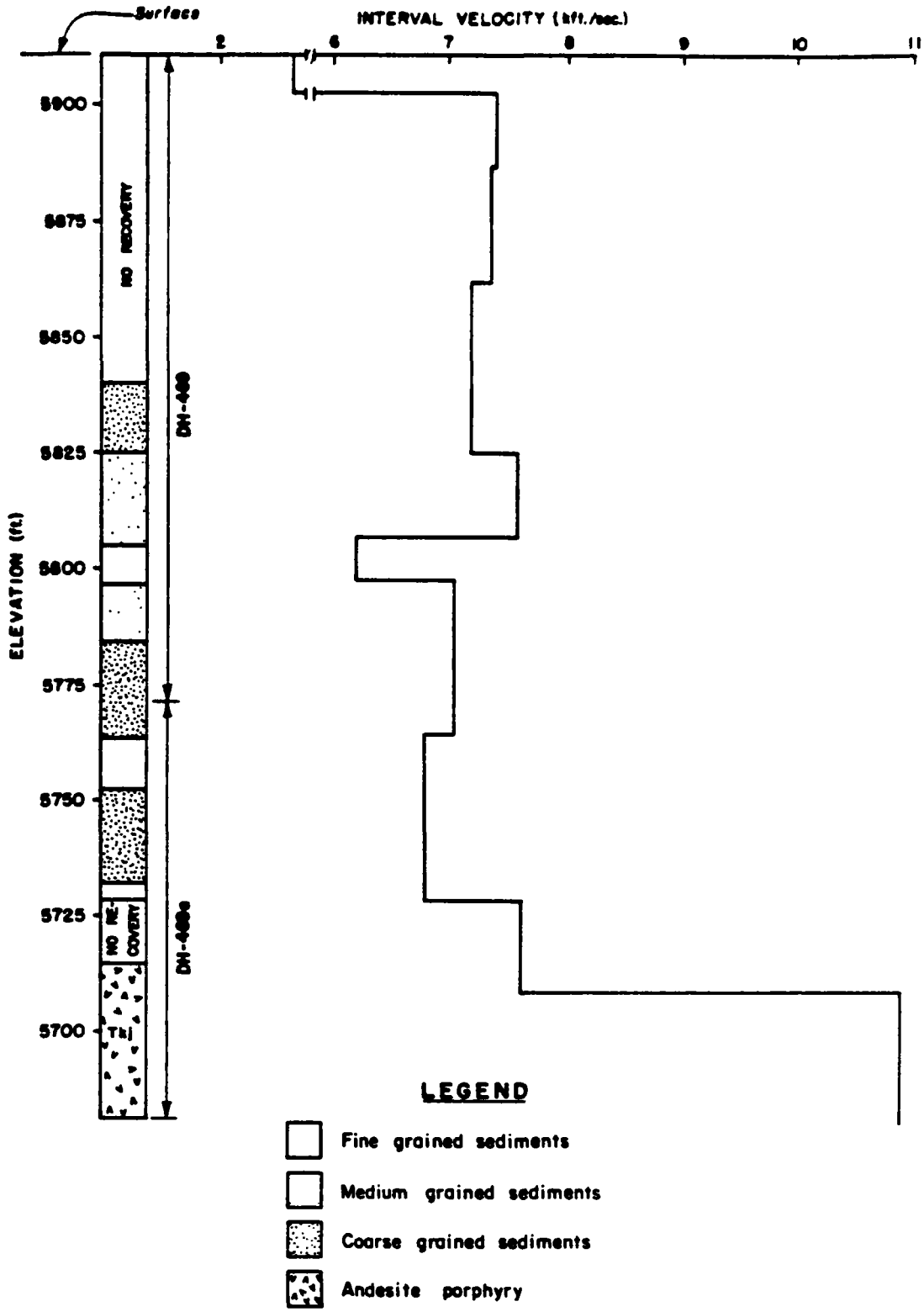

Figure A-1. Interval velocity and geologic logs of DH-469; 469a.

Borehole data are indicated on the seismic sections where available. The bottom of the borehole indicates the depth at which the bedrock was encountered in all cases with the exception of DH-511 which bottomed in alluvium. Boreholes that were not located directly on the seismic lines are shown at their perpendicular projection with the distance and direction of projection noted on the sections. The borehole data indicate that there is general agreement in the calculated and true depths to bedrock in many locations, and that the refraction data are valuable in revealing the topography and general shape of the bedrock surface.

Line S-13 gives the best picture of the overall shape of the western portion of Keetley Valley. S-13 was processed in terms of seven layers. The upper five layers represent alluvium, and the velocity increase with depth is due to water saturation and the increase in density with depth. Some of the alluvial layers pinch out against a bedrock high at about station 4000.

The velocities in each layer show a high degree of variability indicative of the laterally varying nature of the subsurface materials. At the west end of the section the water table is probably represented by the interface between layers a12 and a13. Here, its velocity decreases from 4.6 to 4.2 kft/sec at about station 2800. East of this point, the water table probably crosses seismic layer three (a13), and beyond about station 2300 it is represented by the interface where the velocity varies between 5.3 and 6.3 kft/sec.

The shape of the bedrock interface suggests a cross section of a basin with the deepest point at about station 1500. Bedrock velocity varies from about 9.2 to 13.7 kft/sec. The velocity of the bedrock is greatest in the deepest portion of the basin. The projected bedrock surface from borehole R-114 about 135 ft north of the seismic line is about 40 ft deeper than the bedrock surface shown on plates 2 and 10. Borehole R-115 encountered bedrock within a few feet of the bedrock indicated on the velocity section. Thus, it can be assumed that the shape of the bedrock surface interpreted from the refraction data is correct.

Between shotpoints SP-2 and SP-3, the bedrock surface was processed assuming no hidden layers in the thick section between the 6.3 to 7.4 kft/sec interface and bedrock. The fact that the bedrock depth agrees well with borehole R-114 validates this assumption. If there had been a severe mistie, velocities above the bedrock would have been adjusted in terms of hidden layers to provide a better fit.

The deepest seismic layer (layer 7) originates within bedrock. The interface between layer 6 (bedrock) and layer 7 probably represents the base of a weathering profile that does not occur within the deepest part of the basin where bedrock velocities are already quite high (13.7 kft/sec).

With a vertical exaggeration of about 1.5, plate 2 provides a more realistic portrayal of the true shape of the bedrock surface than plate 10. With a possible exception near station 3800, abrupt steps in the bedrock-basin fill interface can be ruled out by the smooth profile of the bedrock interface. Therefore, except near station 3800, we conclude that no significant high-angle normal faults are present that displace the basin fill. This, however, does not rule out the possibility that faults do exist within the basin, but they do not occur with high-angle fault planes or large displacements. Near station 3800 a high-angle normal fault is inferred from the seismic data. Its location is indicated in cross section on plates 2 and 10, and the surface projection of this inferred fault is indicated on plate 1.

Line 14 in some respects yielded results quite similar to line 13. The water table corresponds to the top of layer 4 with velocities in the range of 5.0 to 5.6 kft/sec. The bedrock profile is constrained by borehole R-110, located about 1050 ft northeast of the line near station 2000. This bore hole encountered bedrock at elevation 5757 ft which agrees well with the 5725 ft elevation of the bedrock surface at the perpendicular projection onto the line. Thus it can be concluded that in the vicinity of station 2000 bedrock depths remain fairly constant to the northeast. On the other hand, borehole R-4, located about 1060 ft southwest of the line near station 2700, encountered andesite at an elevation of 5977 ft. Where this hole projects onto the seismic line an elevation of about 5750 ft is indicated, with a resulting difference of almost 230 ft. This discrepancy probably reflects differences in basin fill thickness related to the original basin shape and/or subsequent erosion of the bedrock surface. Profiles S-13 and S-14, and boreholes east of the Bald Mountain fault, indicate that the bedrock surface slopes north and east toward the center of Keetley Valley. Assuming that the bedrock begins to rise abruptly to the southwest of the seismic line, the gradient of the bedrock surface is almost equivalent to the gradient of the northeast-sloping bedrock surface between shot points SP-5 and SP-7 on line S-13.

An alternative explanation for this discrepancy is an offset in the bedrock surface due to a fault with an east or southeast

trend, parallel to line S-14. Although no north-south seismic profiles are available to assess this possibility, the similar elevations of the bedrock surface in boreholes R114 and R110 on either side of an eastward projection of such a fault offset do not support this interpretation..

Line 14 also shows some unusual complexity northwest of shot point SP-8 in that there is a thick 8.0 to 8.5 kft/sec layer that terminates abruptly at about station 4400. The true depth and velocity of this layer is poorly constrained due to a lack of complete seismic coverage on it. Thus, it must be assumed that the actual depth and velocity of this layer are only approximately correct, but for all practical purposes its velocity must be less than about 9.0 kft/sec. The velocity of 8.0 to 8.5 kft/sec is high for saturated basin fill, but too low for bedrock. This layer probably represents a partially indurated alluvial wedge. The abrupt termination of the 8.0 to 8.5 kft/sec layer suggests that it may be the expression of a fault. This inferred fault is indicated on both the seismic sections for line S-14 and on the base map of plate 1. We interpret this inferred fault to be the en-echelon continuation of the Bald Mountain fault.

There is an apparent discrepancy at the east end of Line S-14 where the bedrock crops out at the base of a small hill, whereas the seismic data indicates the bedrock interface occurs at a depth of 70 to 80 ft. The seismic data preclude an error of 50 ft or more to a 10.0 to 14.0 kft/sec layer at such a shallow depth. It is more likely that the andesite that comprises this hill is extremely weathered and fractured and may have velocities as low as 3.5 to 4.0 kft/sec within the upper 50 ft. In fact, such low velocities have been frequently measured to considerable depths beneath elevated and exposed igneous and sedimentary rocks and, therefore, encountering this this condition here is not considered to be anomalous or unusual.

Line S-6 runs north from the damsite, where andesite crops out, along the old U.S. Highway 40 to the point where the road begins to curve east near borehole DH-518. Line S-6 is modeled as three seismic layers over a half-space. Determined velocities in the half-space range from 8.5 kft/sec on the north end of the line to 12.2 kft/sec at the southern end. A shallow undulating bedrock surface is indicated across the entire line. There is some doubt, however, as to whether the northern section of 8,500 ft/sec material is bedrock. Refraction data at the ends of the lines tend to be less reliable due to limited coverage and should not be relied on heavily. The original line S-6 continued along the curve to the east end of line S-62. Because of the effects

of the curve, the portion of the line from DH-518 to the beginning of line S-62 was not usable, and the original line S-6 was divided into two sections with the eastern part being designated as line S-62.

Line S-12 trends east-west across the flood plain north of the damsite and is about 2700 ft long. This line is modeled as a thin layer of unsaturated alluvium over a relatively thick section of saturated basin fill, which in turn overlies a bedrock surface showing substantial relief. Boreholes DH-469a and DH-470 are on the line whereas DH-511 is projected about 115 ft from the north. Depth to bedrock was accurately determined from the refraction data for that portion of the line near DH-469a, but was overestimated near DH-470. Seismic velocities of the bedrock varies from a low of 8.8 kft/sec to a high of 16.4 kft/sec.

Line S-12 and borehole DH-469a identify a channel beneath the Provo River flood plain deposits with a maximum depth of about 200 ft. The bedrock beneath line S-6 slopes to the east into the channel. The channel is the narrower southern continuation of the deepest portion of the basin cross section shown on lines S-13, S-14, and S-8, and confirmed by boreholes R-114 and R-110.

Line S-11 extends northeast from the damsite along new U.S. Highway 40 for about 4200 ft. Where lines S-11 and S-12 cross, the depth to bedrock ties to within 5 ft. This profile shows an undulating bedrock surface, but the lowest elevation of the bedrock surface is everywhere greater than 5800 ft, and the maximum thickness of unconsolidated deposits is <100 ft. Thus, line S-11 shows that the deep channel does not continue south to the damsite.

Line S-62 is modeled as three layers of alluvium over andesite. Bedrock is mapped in an easterly direction only as far as station 600. At this point the velocity of the lowest interface reduces to 8.2 kft/sec and then finally to 5.8 and 6.3 kft/sec. The bedrock at station 600 probably begins to deepen and was not mapped due to inadequate coverage at the end of the line.

Line S-8 was processed in terms of five layers and shows a relatively uniformly sloping bedrock surface. The northern portion of the basin, therefore, appears to be very similar to that seen along lines S-12 and S-13 to the south. Borehole R-110, projected 350 ft south, indicates bedrock is within about 15 ft of that indicated on the seismic section.

Velocity sections for lines S-3 and S-7 are shown on plates 3 and 6, respectively. Borehole R-110, which was right on line,

shows that bedrock is about 130 ft deeper than the lowest interface detected on line S-3. Line S-7 also failed to map the bedrock-alluvium contact, in part because of the presence of the relatively high 8.2 to 8.6 kft/sec alluvial layer 5. Larger shot point offsets are required to see through to the bedrock when the velocities of overlying units begin to approach the velocity of the intended target of interest.

Conclusions

The seismic refraction method has been shown to be a valuable tool in mapping the bedrock surface beneath basin fill deposits in the area of the proposed Jordanelle Reservoir. However, in order to sample the bedrock in the deeper portions of the basin, it is necessary to have long offsets and overlapping coverage. Despite low velocity layers in the basin fill which preclude precise calculation of depths to bedrock uniformly throughout the study area, boreholes on or near the seismic lines show that the seismic data represents the general configuration of the bedrock surface. The velocity of the andesite porphery is seen to vary as a function of weathering and fracture density. Low velocity zones in the bedrock with velocities of 8000 to 10000 ft/sec may be coincident with zones of shearing, though it is not possible to prove this with the available data. These low velocity zones were not very prevelent and were only observed in about 10 locations. On the remaining portions of the lines the bedrock p-wave velocity was greater than 10000 ft/sec, and usually greater than 12000 ft/sec.

The profiles provide cross section of the valley that suggest that it has the shape of a basin. The deepest portion of the basin is mapped from seismic profiles constrained by boreholes. An unusual feature of the profiles is that the broad deeper portion of the basin in the center of Keetley Valley narrows to a channel-like feature at the south end of the Valley then disappears north of the damsite.

Evidence for obvious steps in the bedrock which may be indicative of faulting are present in only two locations. These inferred faults are shown on the seismic sections for lines S-13 and S-14 on plate 2 and also on plates 10 and 11. The surface projections of these inferred faults are indicated on plate 1. The bedrock step shown on line S-14 is interpreted to be a high-angle normal fault displacing the basin fill that is the en echelon continuation of the north-trending Bald Mountain fault. The bedrock step shown on line S-13 is interpreted to be a high-angle normal fault displacing the basin fill that strikes parallel to

the Bald Mountain fault. No other faults displacing the basin fill can be identified with the available data.

References

Ackermann, H. D., Pankratz, L. W., and Dansereau, D. A., 1982, A comprehensive system for interpreting seismic refraction arrival-time data using interactive computer methods: U. S. Geological Survey open-file report 82-1065, 268 p.

Ackermann, H. D., Pankratz, L. W, and Dansereau, D. A., 1983, Computer program modifications of open-file report 82-1065; A comprehensive system for interpreting seismic refraction arrival-time data using interactive computer methods: U. S. Geological Survey open-file report 83-0604, 3 p.

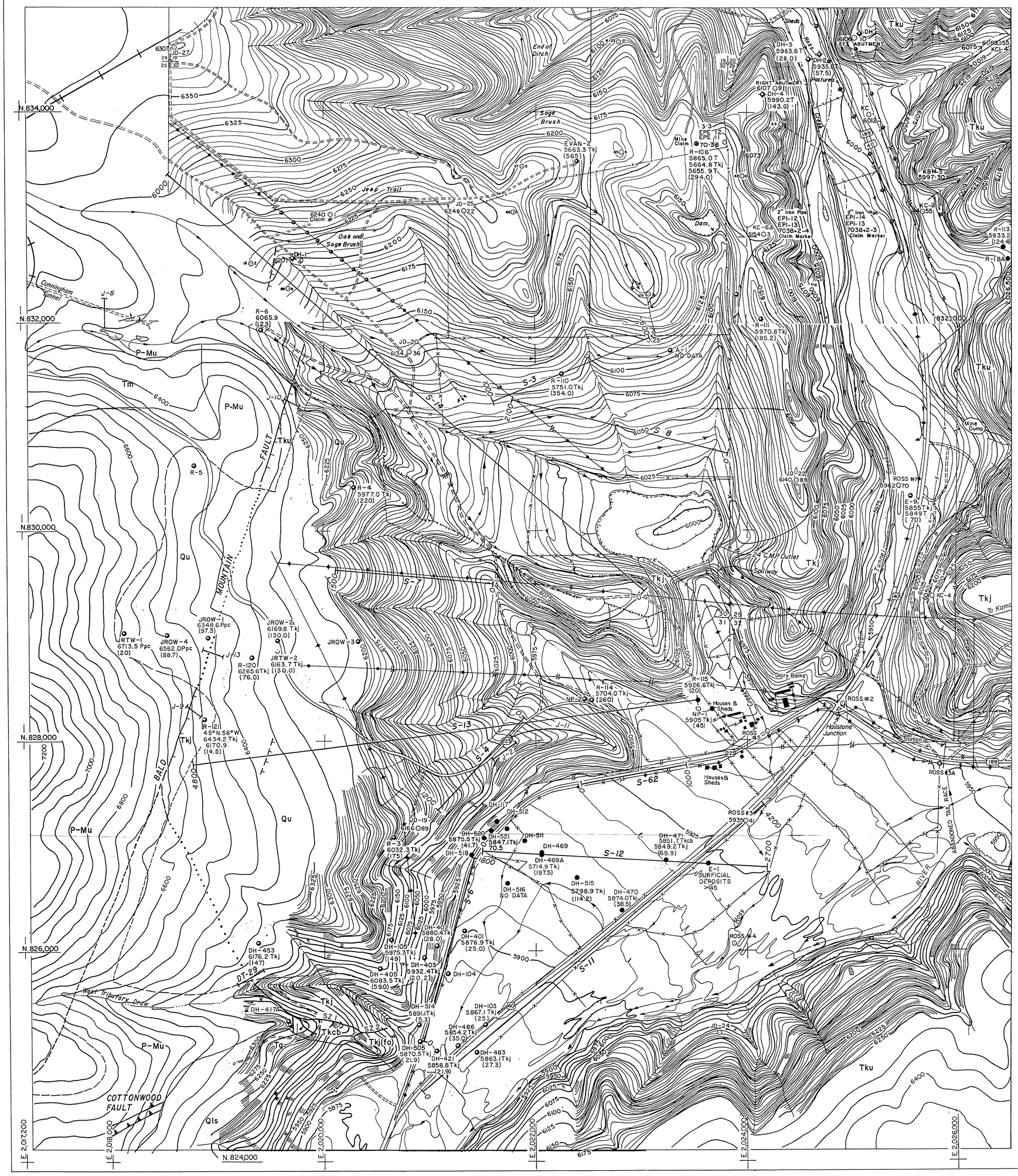

EXPLANATION

QUATERNARY

Qls – Landslide deposits

Qu – Quaternary alluvial and colluvial deposits, undivided, not shown where known or inferred to be < 10 feet thick along Bald Mountain fault

TERTIARY

Tkj – Jordanelle stock

Tm – Mayflower stock

Tg – Alluvial and colluvial deposits

Tkcb – Coyote Canyon volcanic breccia

Tku – Keetley volcanics undivided, includes intrusive and extrusive rocks

PRE-TERTIARY

P-Mu – Paleozoic and Mesozoic sedimentary rocks, undivided

Late Cenozoic normal fault-dashed where inferred from geomorphic evidence, dotted where concealed, hachures on downthrown side

Late Cenozoic normal fault-inferred from seismic refraction profiles, hachures on downthrown side

Cenozoic reverse fault-dashed where approximately located, teeth on upthrown side

Cenozoic normal fault-bar and ball on downthrown side

Shear zones

Geologic contacts-dashed where approximately located

S-12 Seismic refraction profiles

J-9 Trenches

● DH-103 Drillholes, with elevation and thickness of unconsolidated deposits shown, if the hole reached bedrock the lithology is shown

400 0 400 800 1200

SCALE OF FEET

JORDANELLE SEISMOTECTONIC STUDY

PLATE I FAULT MAP OF SOUTHERN KEETLEY VALLEY WITH LOCATIONS OF SEISMIC REFRACTION PROFILES AND TRENCHES

APPENDIX A

LINE S-13

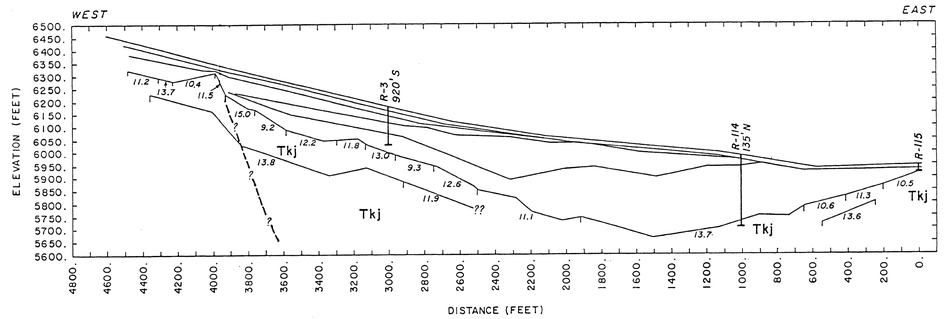

LINE S-14

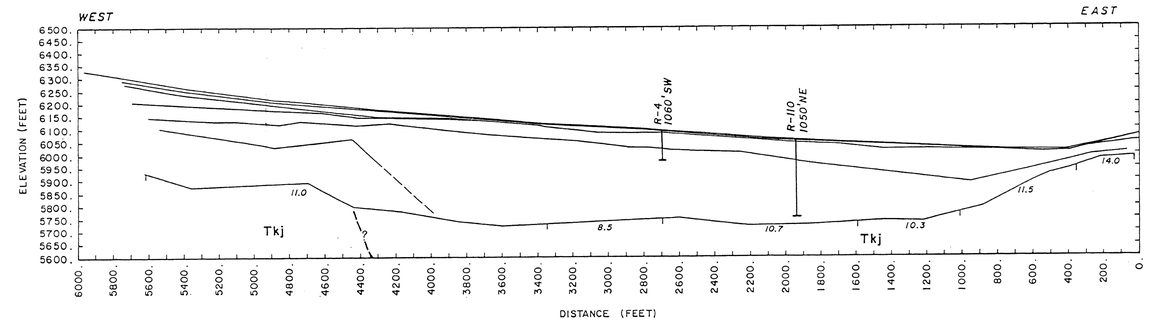

LINE S-11

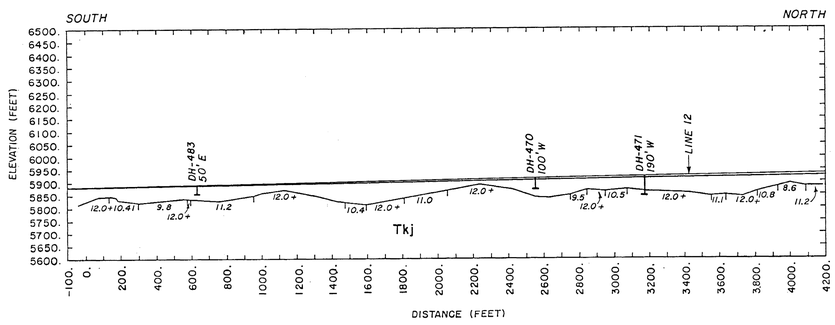

LINE S-12

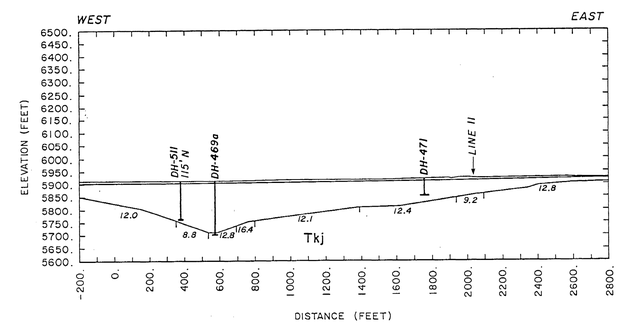

LINE S-6

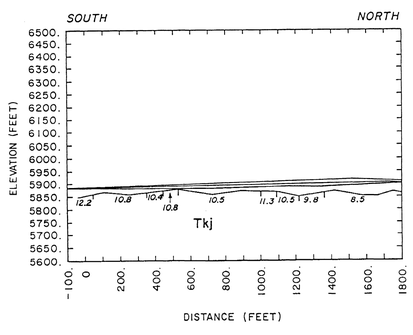

LINE S-8

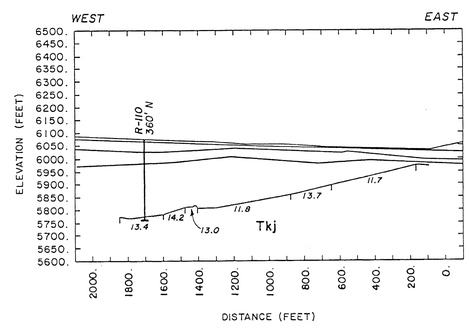

LINE S-62

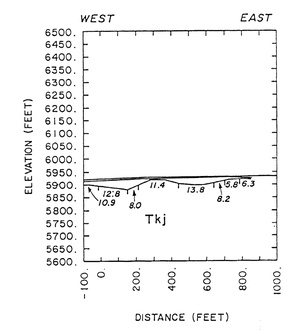

JORDANELLE SEISMOTECTONIC STUDY	
PLATE 2 - SEISMIC REFRACTION PROFILES	
	APPENDIX A

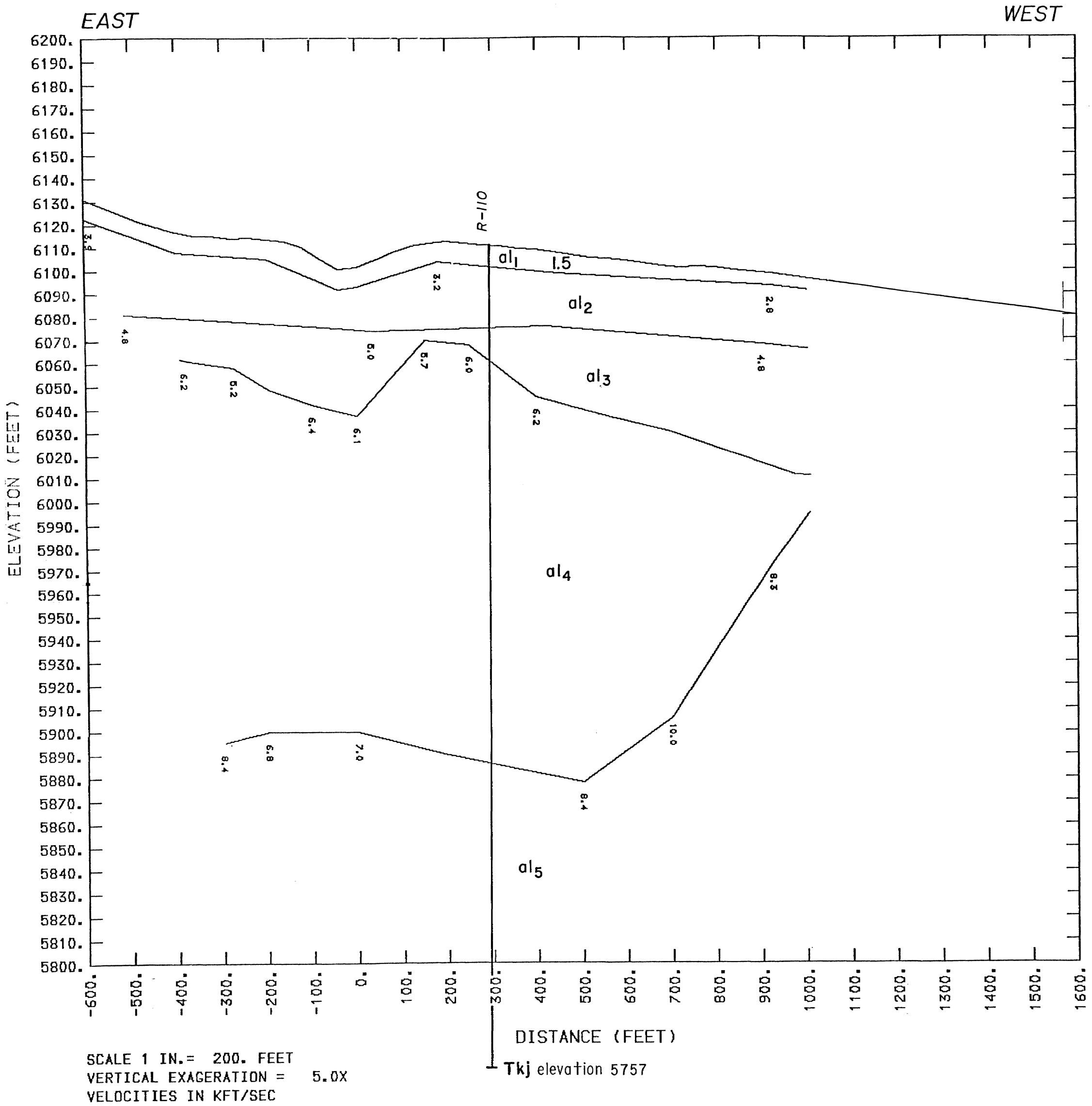

JORDANELLE SEISMOTECTONIC STUDY	
PLATE 3 - LINE S-3	
	APPENDIX A

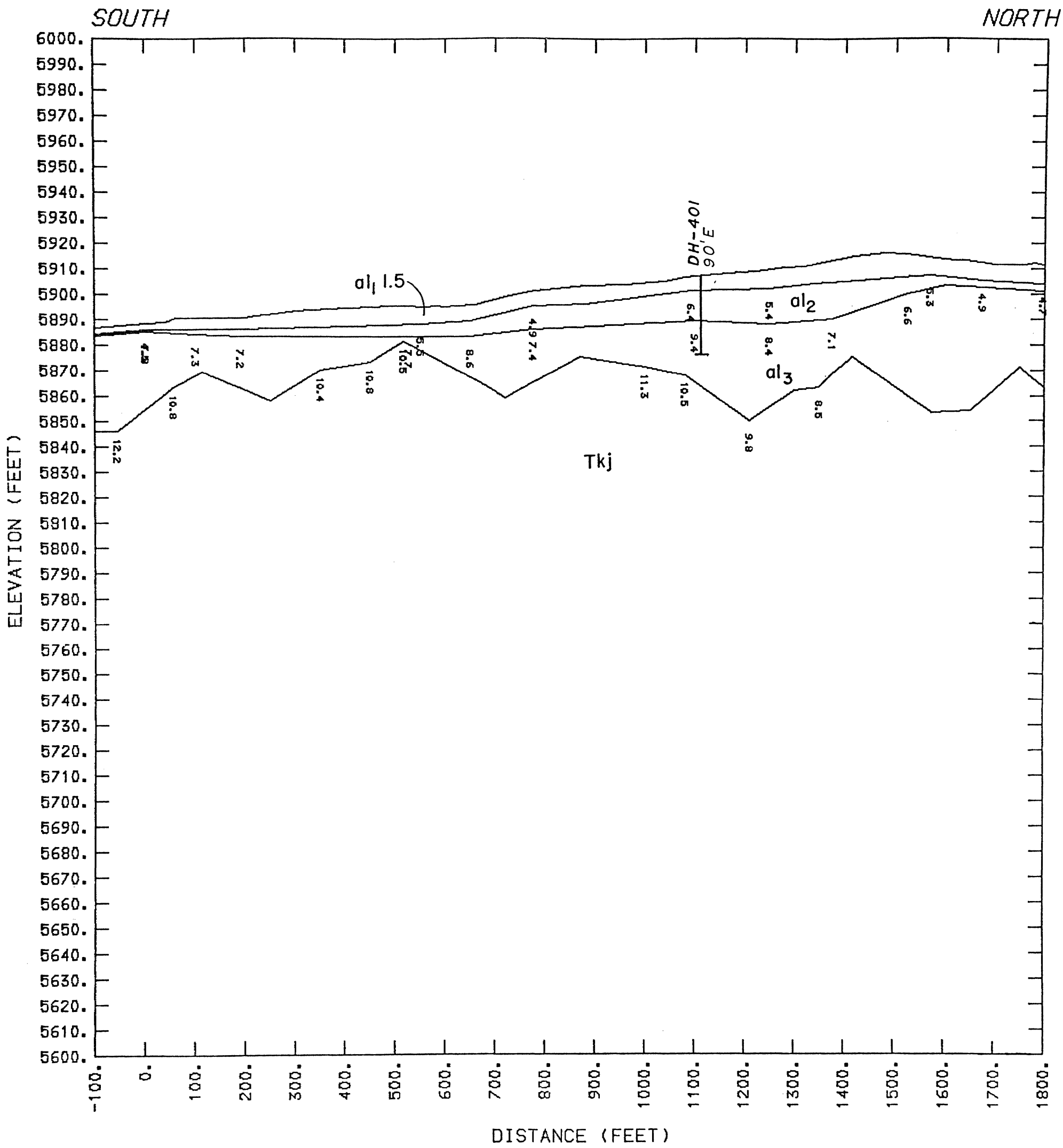

SCALE 1 IN.= 200. FEET
VERTICAL EXAGERATION = 5.0X
VELOCITIES IN KFT/SEC

JORDANELLE SEISMOTECTONIC STUDY	
PLATE 4 - LINE S-6	
	APPENDIX A

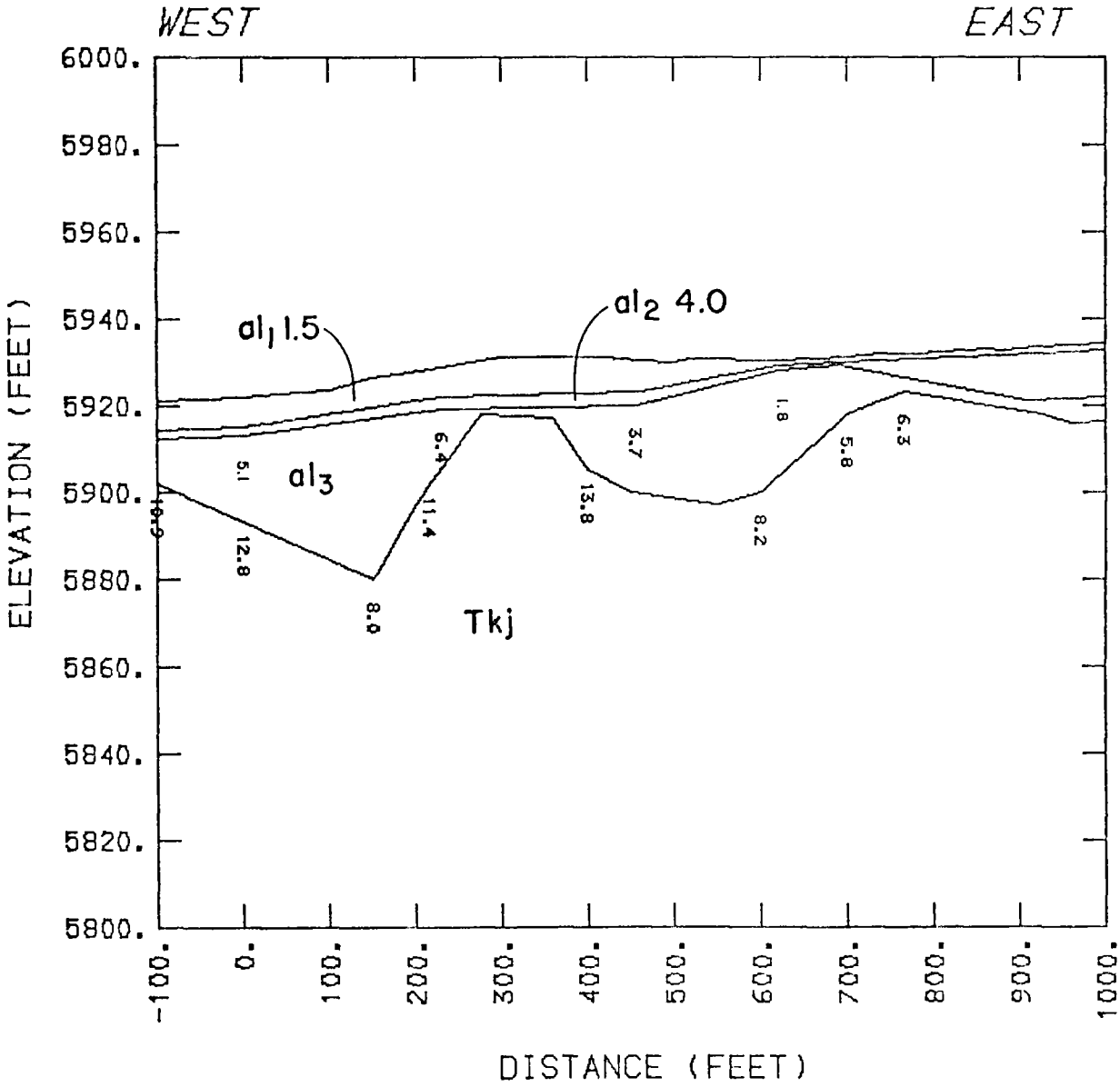

SCALE 1 IN.= 200. FEET
VERTICAL EXAGERATION = 5.0X
VELOCITIES IN KFT/SEC

JORDANELLE SEISMOTECTONIC STUDY	
PLATE 5 - LINE S-62	
	APPENDIX A

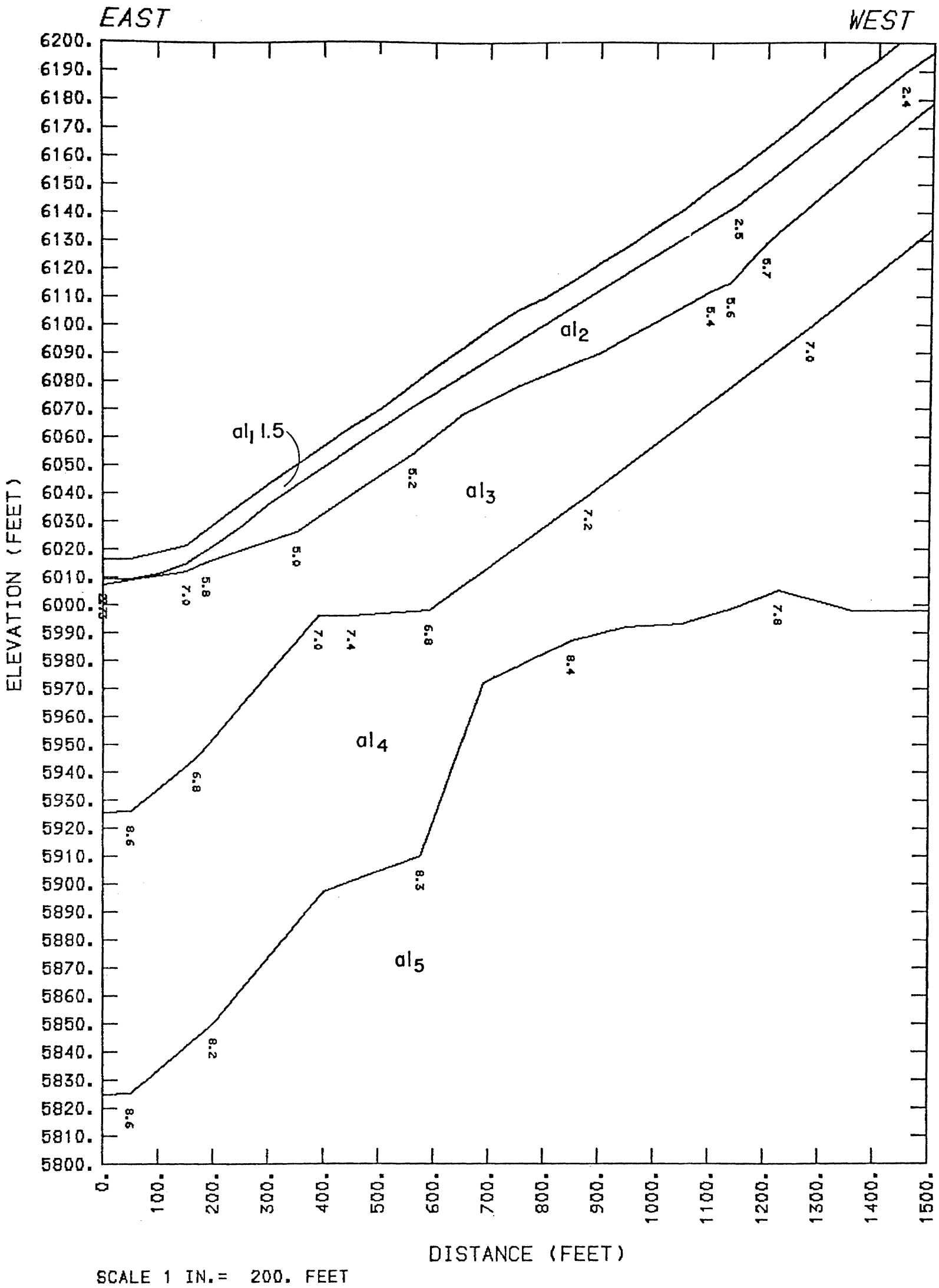

SCALE 1 IN.= 200. FEET
VERTICAL EXAGERATION = 5.0X
VELOCITIES IN KFT/SEC

JORDANELLE SEISMOTECTONIC STUDY	
PLATE 6 - LINE S-7	
	APPENDIX A

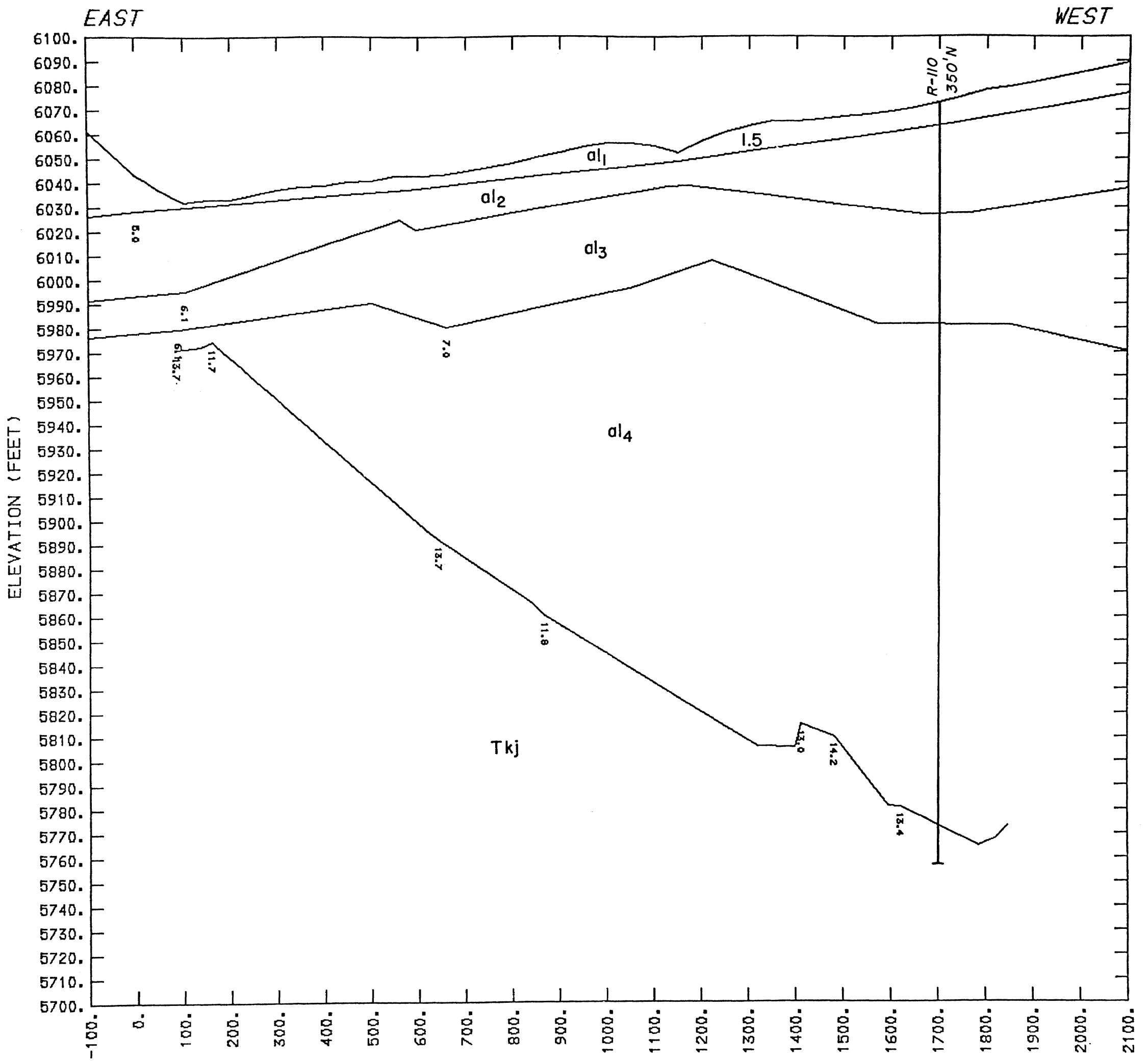

SCALE 1 IN.= 200. FEET
VERTICAL EXAGERATION = 5.0X
VELOCITIES IN KFT/SEC

JORDANELLE SEISMOTECTONIC STUDY	
PLATE 7 - LINE S-8	
	APPENDIX A

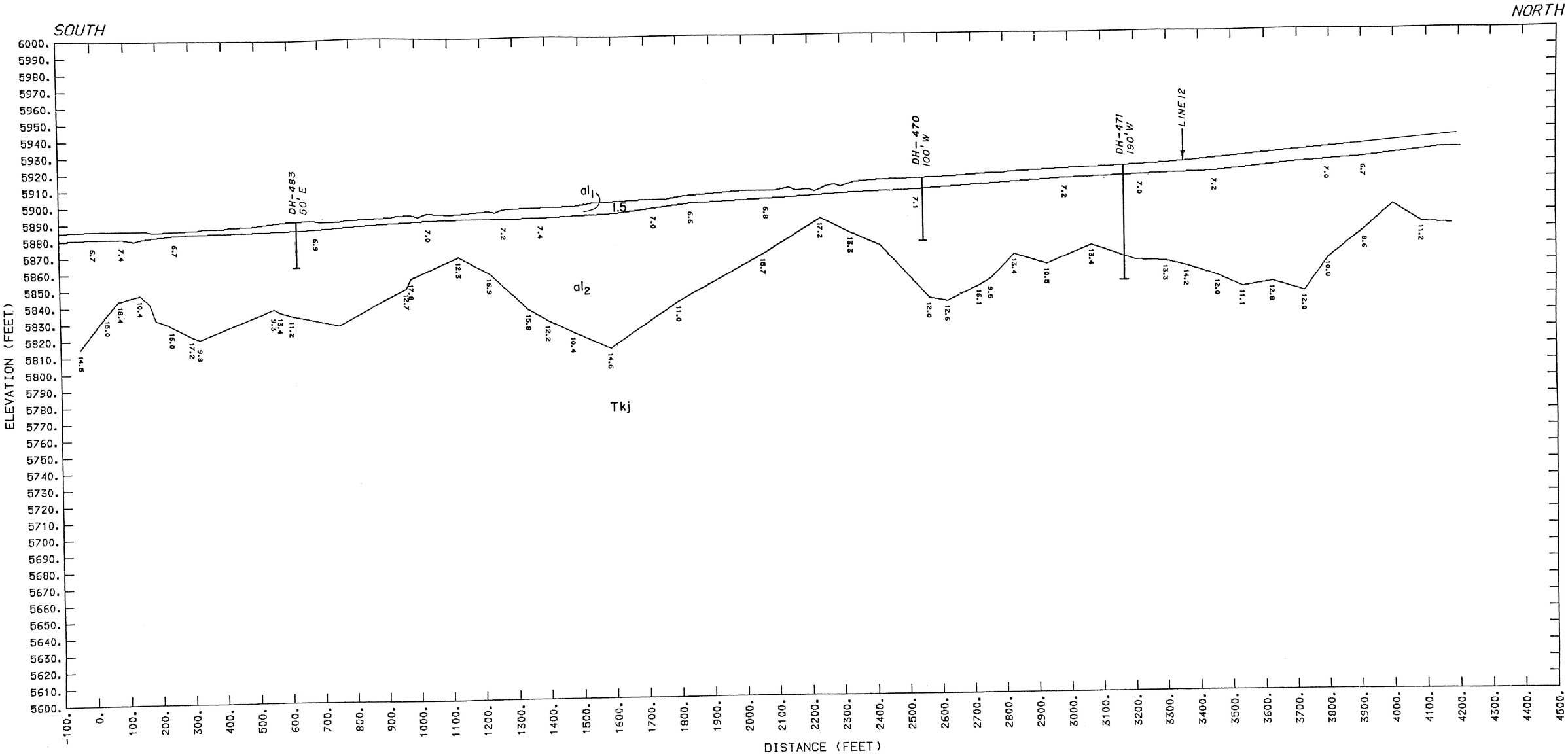

SCALE 1 IN.= 200. FEET
VERTICAL EXAGERATION = 5.0X
VELOCITIES IN KFT/SEC

JORDANELLE SEISMOTECTONIC STUDY	
PLATE 8 - LINE S-11	
	APPENDIX A

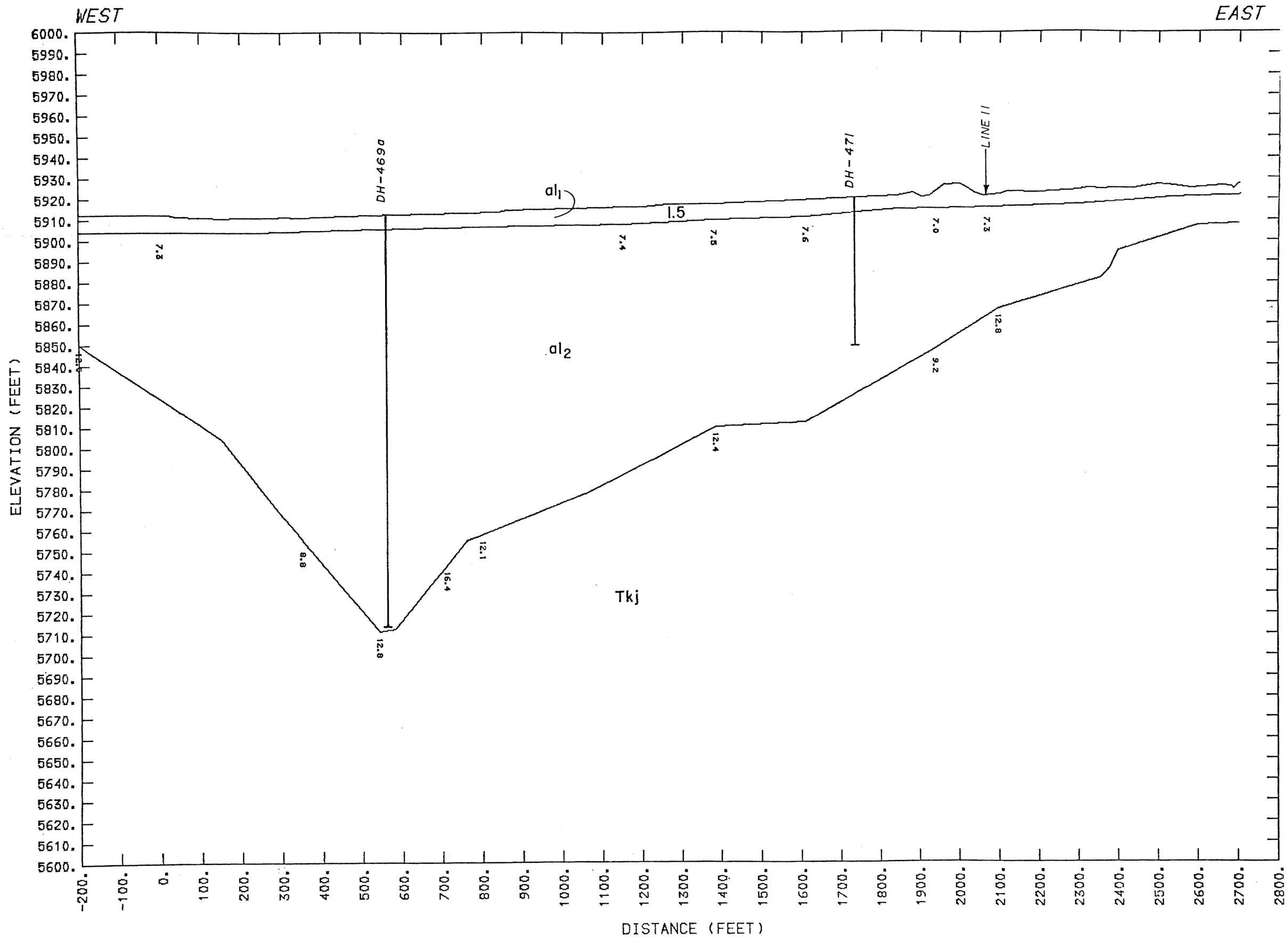

SCALE 1 IN.= 200. FEET
VERTICAL EXAGERATION = 5.0X
VELOCITIES IN KFT/SEC

JORDANELLE SEISMOTECTONIC STUDY

PLATE 9 - LINE S-12

APPENDIX A

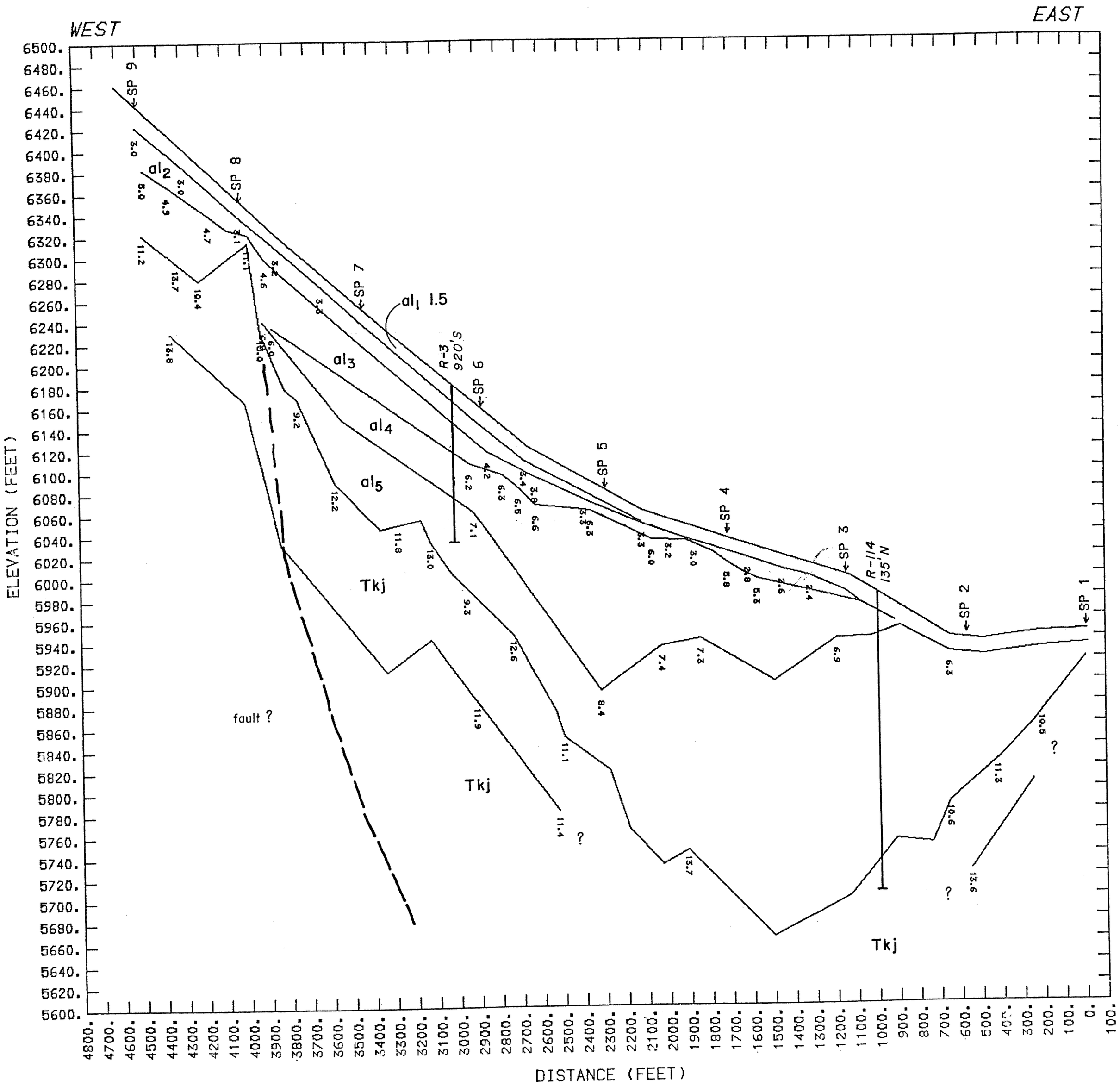

SCALE 1 IN.= 400. FEET
VERTICAL EXAGERATION = 5.0X
VELOCITIES IN KFT/SEC

JORDANELLE SEISMOTECTONIC STUDY	
PLATE 10 - LINE S-13	
	APPENDIX A

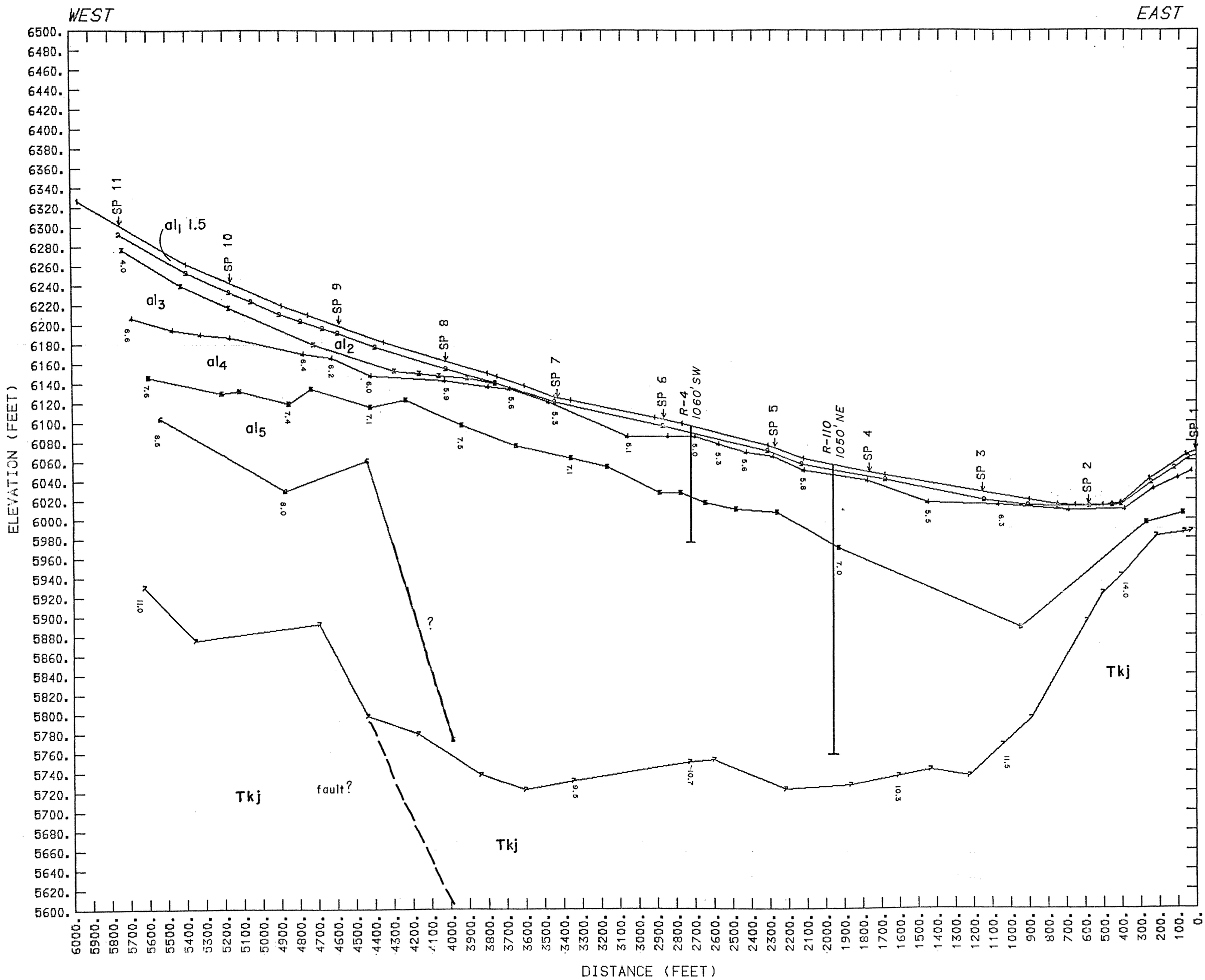

SCALE 1 IN.= 400. FEET
VERTICAL EXAGERATION = 5.0X
VELOCITIES IN KFT/SEC

JORDANELLE SEISMOTECTONIC STUDY	
PLATE II - LINE S-14	
	APPENDIX A

APPENDIX B

AN ANALYSIS OF RESERVOIR-INDUCED SEISMICITY IN THE BACK VALLEYS OF THE WASATCH MOUNTAINS

by

Roland C. LaForge

An Analysis of Reservoir Induced Seismicity in the Back Valleys of the Wasatch Mountains

by

Roland C. LaForge

B.1.0 Introduction

Reservoir induced seismicity (RIS), the occurrence of earthquakes caused by the artificial storage and regulation of impounded water, is a phenomenon that is generally acknowledged to have occurred in a number of cases. In specific cases, however, RIS has proven very difficult to define, observe, and predict (Meade, 1982). Early reviews of RIS include those by Rothé (1970), Simpson (1976), and Stuart-Alexander and Mark (1976). Packer and others (1977) list 16 "accepted" and 35 "questionable" cases of RIS worldwide. The most destructive induced earthquake appears to be the 1967 magnitude 6.5 Koyna, India event. This quake killed 200 persons and injured 1500 others, and caused significant damage to the dam (Gupta and Rastogi, 1976). Other notable examples include activity at Hoover Dam, Nevada (Carder, 1945), Nurek reservoir in the Soviet Union (Simpson and Negmatullaev, 1981), and Lake Kariba in Rhodesia (Gough and Gough, 1970).

Proposed mechanisms for the physical causes of RIS are presented by Kisslinger (1976) and Simpson (1986). It is generally agreed that two main effects are responsible for the phenomenon: elastic stresses transmitted to the underlying crust due to the weight of the impounded water, and the effect of increased pore pressure on fault planes at depth. In both cases the state of stress on a fault must be very near that required for rupture, so that the impounded water in effect acts as a triggering mechanism. Factors that appear to be important include the volume and depth of the reservoir, the type of rock underlying the reservoir, its permeability, the existence of pre-existing faults, and the magnitude and orientation of the crustal stress field. Packer and others (1980) found that the great majority of RIS events occurred within 5 years of initial impoundment, and all but one occurred within 10 years. It has been suggested (Simpson, 1986; Leith, 1984) that the two main mechanisms described above influence the delay time between initial impoundment and the RIS event. Whereas initial compaction due to the water weight would cause the event to occur within several weeks or months, pore pressure changes due to the downward percolation of water could take several years to manifest as failure of a fault plane. Gupta and others (1972) found that RIS is influenced by the rate of increase of water level, the duration of loading, and the period of time during which high water levels are maintained.

To our knowledge, the only suggested case of RIS in the ISB is at Palisades Reservoir, Idaho (e.g., Smith and Sbar, 1974; Schleicher, 1975). These suggestions, however, are based on the detection of swarms near the reservoir during brief (less than one month) recording periods. Bones (1978), in discussing the results from a 3-week microearthquake survey, disputed Schleicher's (1975) suggestion. Piety and others (1987), during a 3-month microearthquake survey, found swarms lasting several days to be pervasive in the area, and unrelated to fluctuations in reservoir level. Continuous monitoring over several years would be necessary to resolve the question of RIS at Palisades Reservoir.

In this study we analyzed historical seismicity to detect possible RIS occurrence associated with the 13 USBR reservoirs in north-central Utah. The study consists two parts. In the first, a search for an increase in activity following initial reservoir impoundment is made. In the second, the more recent network data are examined statistically to search for consistent seasonal increases in seismic activity that may be related to the normal yearly fluctuations in reservoir level. At the end of this section, the potential for RIS in north-central Utah will be discussed based on the results of this study, published observations of RIS elsewhere, and theoretical studies.

B.2.0 Statistical Analysis of RIS in North-central Utah

This section describes a statistical analysis of earthquake occurrence around USBR dams in north-central Utah. The purpose of the study was to try to determine whether RIS occurred upon initial filling, or has occurred on a seasonal basis in the vicinity of the subject dams. The procedure for the analysis was as follows:

(1) Earthquakes from the entire historic record occurring within 15 km of the 13 subject dams were extracted from the University of Utah catalog. These were plotted in map view in order to examine their spatial distribution, relation to regional seismicity patterns, and relation to mapped faults.

(2) The earthquakes for each dam were plotted in histogram form to show the number of events per year, and detect any significant increases in local earthquake occurrence following initial water impoundment.

(3) A statistical analysis was performed on more recent data (1974-1986) to search for seasonal biases in seismicity levels around the subject reservoirs. A test was made to see if monthly variations in activity in the vicinity of each dam differed significantly from variations in the regional data. Then, the data were grouped into 3-month periods to detect increases in seasonal proportions between the local and regional data sets.

(4) The evidence for RIS around each dam was then discussed in light of the above evidence, and additional factors such as significant changes in network configuration and other sampling problems were considered.

Table B-1 lists the 13 USBR dams that are the subject of this study. Information regarding the location, year of initial filling, and reservoir capacity are listed for each dam. The structural height of the dam is tabulated, and is taken as a reasonable estimate of maximum reservoir depth. The locations of the dams are plotted on Plates 1a, 1b, and 1c.

Earthquakes taken from the University of Utah catalog that occurred within 15 km of the dams are plotted in figure B-1(a-m). This distance is somewhat arbitrary, but was judged to be a reasonable value considering such factors as the size of the reservoirs, the closeness of induced events to reservoirs in documented cases, and the location errors of earthquakes in the catalog. The plotted symbols are scaled to magnitude, and faults are drawn as mapped on Plate 1 on each figure. In contrast to the epicenters plotted on plate 1, those in figure B-1 encompass the entire historical extent of the catalog. In the figure for Joe's Valley dam (B-1f), the cluster of events in the box are the result of mining activity (Smith and others, 1974; Foley and others, 1986; Williams and Arabasz, 1988) and were not used in further analyses.

Histograms that display the epicenters plotted on figure B-1 as number of events per year are shown in figure B-2(a-m). The year of initial reservoir filling is indicated by an arrow. In figures

without arrows, seismicity within 15 km of the dam was not recorded until a number of years after initial filling. Note that scales differ between figures, and that due to the record length at some damsites the histograms may extend for two or three pages. In most of the figures, an increase in activity is evident in the mid-1970's. This is largely due to the installation of a dense, high-magnification network of seismograph stations in central Utah, which allowed for the detection and location of larger numbers of smaller magnitude events. A significant problem with graphs of this type is that changes in detection capabilities sometimes occur within the time span of the displayed data set. In order to compensate for the increase in detection in 1974, earthquakes that occurred between 1962 and 1986 with magnitude greater than or equal to 2.3 are plotted in figure B-2 as solid portions of the histogram. Since Arabasz and others (1980) assert completeness for the Wasatch front area for magnitude 2.3 since 1962, the solid representations give a more accurate picture, from the standpoint of a uniform detection level, of earthquake occurrence around the dams. A discussion of changes in instrumentation and detection capabilities in the study area can be found in section 4.2 in the main body of this report.

Table B-3 summarizes post-impoundment activity in the vicinity of the reservoirs. The largest post-impoundment earthquake within two different radii, 15 and 25 km, is tabulated from a point estimated to be the center of the reservoir. Δt refers to the number of years after initial filling the event occurred, and the length of the observation period is noted in the last column. Simpson (1986) observed that RIS due to pore pressure changes can occur up to 20 km from the reservoir. The 25 km distance was chosen to conform to this distance, and to take into account such variables as irregularities in reservoir outline and epicentral errors.

The purpose of the statistical analysis was to compare monthly seismicity rates between local samples near the reservoirs (figure B-1) and rates recorded in the central Utah region as a whole, in order to detect possible seasonal biases that may be attributable to RIS. The "central Utah region" as defined for this analysis extends from latitude 39.0N - 42.0N, and from longitude 111.0W - 112.5W, and is therefore equivalent to the area shown in Plate 1. Because of uncertainties in catalog completeness before installation of the dense high-gain network, only data recorded since November 1, 1974 are used in the analysis. The catalog was complete through June, 1986 at the time of this study. Although Arabasz and others (1978) state that this catalog can be considered complete only for events of magnitude 1.5 and above, all magnitudes were utilized. While a greater number of events lends greater credence to the statistical conclusions, the danger exists that a change in the station distribution in the vicinity of a specific site can significantly alter the detection capability in that area, and therefore give a biased estimate of the seismicity rate. To account for this possibility, yearly station location maps have been drawn (figure B-3). These, along with knowledge of the operating histories of individual stations, were used to help determine whether significant changes in activity were real or could be attributed to changes in detection capability.

Due to practical considerations, aftershocks and swarms events were not deleted from the catalog before carrying out the statistical analysis. While over a large region these phenomena may occur randomly and frequently enough to not bias the data, for local samples the occurrence of either is bound to signal aberrations in seismicity not necessarily due to RIS. Ideally, it would be preferable for earthquake occurrence to approximate a Poisson process, where events occur independently in time and space. Since it does not for this case, we were forced to identify the effects of aftershocks and swarms on a case by case basis when discussing statistically significant results.

The first statistical test considered was to see whether or not the monthly proportions of events at a given site can be said to differ significantly from those in the region. This "goodness of fit" test has an approximately χ^2 distribution (e.g., Waldpole and Myers, 1985), and was calculated with the statistic

$$\chi^2 = \sum_{i=1}^{12} \frac{(o_i - e_i)^2}{e_i} \tag{1}$$

where o_i = the observed number of events that occurred around the reservoir in month i, and e_i = the expected number of local events in month i, given the proportion of events that occurred in the central Utah region (as defined above) during that month. Tabulations of the number of events occurring in each month of each year, for the region and for the area around each dam, are presented in table B-2. In this and the following test, the events occurring around the reservoir were subtracted from the number of regional events, so that the two samples were independent.

An important limitation to the effectiveness of this statistical test is the small sample size around many of the reservoirs. A number of statistics textbooks (e.g. Waldpole and Meyers, 1985) state that equation (1) should not be used when e_i is less than 5. This means that low confidence should be placed in the analysis of damsites where the earthquake sample size is less than about 50. Table B-2 shows that about half of the dams have sample sizes below this number. However, χ^2 values have been computed for all dams, and problems associated with sampling deficiencies will be discussed later for each case.

The calculated χ^2 values are presented in table B-4. Here we tested the hypothesis that the monthly proportion of activity around a particular reservoir did not differ significantly from that in the region as a whole. Examining the χ^2 table with $n-1 = 11$ degrees of freedom, we find that the χ^2 value is significant at the 95% level if it exceeds 19.675. It can be seen in table B-4 that the χ^2 values for Deer Creek, Echo, Hyrum, Newton, and Wanship Dams exceeded this value. The analysis therefore pointed to these dams as subjects for further examination.

The next step in the process was to isolate the particular month or season that gave anomalous statistical results in individual cases, and see if an annual periodicity in anomalous behavior was evident. For this test the rates for each month were summed into 3-month quarters in order to detect rate changes in a "seasonal" time frame. This grouping is based on the presumption that water level changes responsible for RIS also occur at roughly "seasonal" intervals. Every possible consecutive 3-month combination was utilized, so that if indeed a cause and effect relationship existed, a phase shift of 1 or 2 months would not go undetected. This staggering of quarters was also effective in isolating single months of anomalous activity, as will be seen in the discussion of the results.

In this case we were interested in comparing the quarterly proportions of activity in the area surrounding the dam to that in the region, to see if a significant difference could be detected. For this purpose we used the statistic

$$z = \frac{\frac{x_1}{n_1} - \frac{x_2}{n_2}}{\left[\hat{p}(1-\hat{p})(\frac{1}{n_1} + \frac{1}{n_2})\right]^{\frac{1}{2}}}, \tag{2}$$

$$where\ \hat{p} = \frac{x_1 + x_2}{n_1 + n_2},$$

x_1 is the number of events per quarter around the dam, n_1 is the total number of events around the dam, and x_2 and n_2 are the same values, respectively, for the region. z is a random variable having approximately the standard normal distribution.

In formalizing this problem, our null hypothesis, H_o, was that the local quarterly proportion did not significantly differ from the regional quarterly proportion. Where we set the critical z-value for a given significance level depended on whether the alternative hypothesis, H_1, was that the local proportion was greater than or less than the regional proportion, or whether it was only greater. For the purposes of this study, we chose the second option (with a critical value of 1.645), on the reasoning that for engineering purposes we are only interested in identifying an increased hazard due to possible RIS effects. The first alternative, however, assumes interest in decreased activity as well, and has implications for the physical causes of the fluctuations. This will be discussed further in section B.3.0.

The computed values are shown in table B-5 with values greater than 1.645 marked. The table shows that quarters with abnormally high rates appeared to be distributed equally among the spring, summer, and autumn months. There was no dam around which activity could be characterized as unusually high during the winter months. In no quarter were there more than four dams that exhibited anomalous activity, and thus the evidence does not suggest a regional seasonal preference for abnormally high activity.

B.2.1 Results

In examining the question of whether RIS has occurred at any of the major dams in the CUP region, each dam and reservoir will be discussed in terms of seismicity occurrence upon initial filling, seismicity occurrence in the vicinity of the reservoir and its relation to regional patterns, and results of the statistical analysis. If the analysis showed significantly higher activity during particular periods than that observed in the region, table B-2 was examined to see if the anomaly was due to an isolated swarm or mainshock-aftershock sequence, or if it was caused by consistently higher activity in all or most of the years of record. Because the number of earthquakes varied greatly from sample to sample, there were cases where the occurrence of a small number of events during a given period gave rise to a misleadingly high statistic. These cases were identified where they arise.

Causey Reservoir, filled in 1966, lies on the eastern edge of the north-south trending back valley seismicity trend (plate 1a). Two local (within 15 km of the dam) events were recorded in 1967; then none until 1971 (figure B-2a). The z-test showed one period that slightly exceeded the 95% confidence limit. This anomaly can be traced to a swarm of events that

occurred in September 1978 (table B-2b).

Deer Creek Reservoir, filled in 1941, lies in a zone of sparse activity near Round Valley (plate 1b). No local events were recorded until 1953, 12 years after initial impoundment. The chi-square test (table B-2) shows a significant deviation from the regional norm, which also appears in columns 4,5, and 6 of table B-5. An examination of the monthly event counts (table B-2c) shows June and July to have had a high number of events relative to the rest of the year. Further examination of the table, however, reveals that 17 of 23 monthly readings, or 74%, had zero events, and 9 of the 23 events, or 40%, occurred during only 2 periods. Thus it does not appear that June and July exhibit consistently increased activity.

East Canyon Reservoir, filled in 1966, lies within the back valley seismic trend northeast of Salt Lake City (plate 1b). Local seismicity was negligible in the 8 years following initial impoundment (figure B-2c). While the chi-square test was negative (table B-2), the z-test shows two anomalously high late summer-autumn quarters (table B-5). This observation can be traced to the occurrence of a swarm of small ($M_L < 1.5$) events in September and October of 1976, which is seen in figure B-1c as a cluster about 10 km northeast of the dam. Figure B-3 shows a stable station distribution about this site during the entire recording period. To draw a possible correlation between this swarm and the East Canyon fault is beyond the scope of this study. Aside from the swarm, activity during September and October in all other years appears normal.

Echo Reservoir is located about 20 km east of East Canyon Reservoir. Although the reservoir was filled in 1930, no local earthquakes were documented until 1964 (figure B-2d). The z-values show anomalously high periods in the autumn. This results from the same 1976 swarm that was responsible for high values for East Canyon Reservoir, and aside from that year activity during those months appears normal.

Hyrum Reservoir, filled in 1935, is located about 50 km north of Ogden, several km west of the back valley seismic trend (plate 1a). No anomalous activity was recorded following initial filling of the reservoir (figure B-2e). The statistical tests show anomalously high activity rates in spring and late fall (table B-5). These can be traced to a swarm of 19 small ($M_L < 1.0$) events on June 12, 1982, and a week-long swarm of 25 somewhat larger ($M_L < 2.0$) earthquakes in late December, 1983 (table B-2f). The 1982 swarm can be seen if figure B-1e about 5 km southeast of the dam; the 1983 swarm is part of the cluster on the east side of the East Cache fault. Aside from these two isolated swarms, activity during those months appears normal. Figure B-3 shows that station distribution around the reservoir has been dense and stable since 1978.

Joes Valley Reservoir, filled in 1966, is located on the Wasatch Plateau (plate 1c), in an area of low-level, diffuse seismicity. The dense cluster of activity outlined in figure B-1f has been related to coal mining activity (Smith and others, 1974; Foley and others, 1986; Williams and Arabasz, 1988), and was deleted prior to analysis. No anomalous activity was recorded following initial reservoir filling (figure B-2f). The statistical analysis (table B-5) shows a high quarter during the spring. An examination of actual activity, however, (table B-2g) shows that 12 of the total of 27 events occurred during this period. Given this small total number, and the fact that most of the entries during March, April, and May show zero events, the high z-value computed for this period should be attributed to the small sample size. Sampling problems due to uneven station distribution about the site are also suggested by figure B-3.

Lost Creek Reservoir, also filled in 1966, is located in a region of very low seismicity about 40 km east of Ogden (plate 1a). No unusual activity was recorded following initial reservoir

filling. Although one anomalously high quarter was noted by the statistical analysis (table B-5), arguments presented above regarding the validity of the analysis when small sample sizes are involved apply to this case also.

Newton Reservoir, filled in 1945, is located in a relatively quiet zone about 20 km northeast of Logan (plate 1a). No local activity was recorded until 12 years after initial filling. The statistical analysis shows 3 summer quarters of high activity, which can be traced in table B-2i to a high total number for the month of July. However, since only 3 of the 11 years are responsible for the anomaly, this cannot be considered a consistent seasonal trend.

Pineview Reservoir, located several km east of Ogden (plate 1a), was first filled in 1937, and raised to its current dimensions in 1957. No anomalous activity was noted during the decade following either year (figure B-2i). A high z-value is noted during January, February, and March in table B-5. This is due to 5 swarm events that occurred on February 11, 1976.

Scofield Reservoir, filled in 1946, is located on the Wasatch Plateau in a region of low seismicity (plate 1c). No local activity was noted until 21 years after initial filling. Although seismicity during the months of March, April, and May are noted in table B-5 as being high, the small sample size (30 total events) preclude this from being labeled significant. This site has also suffered from uneven and sporadic station coverage (figureB-3).

Soldier Creek Reservoir is located in a relatively quiescent zone about 30 km east of Provo (plate 1b). Although the dam was constructed in 1973, filling did not begin until 1984. Because filling is not yet complete, the reservoir outline has not been drawn on figure B-1k. Figure B-2k indicates no increase in activity since 1984. Because only 5 local events have been recorded for this site, statistical analyses are probably meaningless. Figure B-3, however, shows that station coverage in this area has always been poor, and an examination of the 5 events shows that none have a magnitude less than 1.2. Therefore it is likely that smaller earthquakes are missing from the sample, and that the low activity rate is somewhat misleading.

Strawberry Reservoir, located a few km west of Soldier Creek Reservoir, was filled in 1913. No local events were recorded until 1971 (figure B-2l). Since the local seismicity sample numbers only 12 events, a statistical analysis, as for Soldier Creek, is probably meaningless. The discussion on station coverage presented in the previous paragraph also applies to this site.

Wanship Dam (Rockport Reservoir), is located on the east side of the back valley seismic trend about 30 km east of Salt Lake City (plate 1b). The reservoir was filled in 1957, and no local activity was recorded until 1970 (figure B-2m). The statistical analysis points to anomalously high activity during the fall months (table B-2,B-5). Table B-2n shows the numbers of events to be fairly well distributed throughout the years, except for a swarm of 4 events that occurred during December 8-10, 1978. The removal of these events would lower the number of anomalous periods. The sample size for this site is relatively small (45 events). Aside from these considerations, two additional observations argue against RIS occurrence at this site. The first is that the anomalous period is during the autumn months, when reservoir levels are generally low and stable. An examination of table B-2n shows that the statistical anomaly is due to heightened activity during the months of October, November, and December. Simpson (1976) and Simpson and Negmatullaev (1981) point out that induced earthquakes seem to occur when the water level is at or near maximum, and also when abrupt decreases in water level or rapid decreases in the rate of filling occur. Considering the normal seasonal water level cycles for reservoirs in the study area, these conditions and level changes are very unlikely to occur during the months of October, November,

and December. The second is that the local seismicity pattern seen in figure B-1m clearly appears to be part of the larger regional pattern seen in plate 1b. We would therefore argue against RIS occurrence at Rockport Reservoir, although the evidence is not conclusive.

B.3.0 Discussion

The results of the statistical analysis show no clear evidence for RIS at any of the 13 USBR dams. However, the limitations of this study require that these results should not be considered conclusive. Earthquake detection capabilities at the dates when many of the reservoirs were initially filled were poor by today's standards, and it is therefore possible that smaller magnitude induced events occurred that were not detected. The University of Utah seismograph network was not designed with the documentation of RIS as a primarily goal, and coverage around a number of the reservoirs has been poor or uneven. Thus it is possible that RIS has occurred in the study area, but that evidence for it is not obtainable from the available data. Also, the statistical analysis looked at only one parameter, number of earthquakes. The examination of other parameters, such as moment release, could yield different results. The possibility that the statistical models used do not adequately approximate the earthquake occurrence process also exists.

Baecher and Keeney (1982) attempted to draw statistical correlations between documented cases of RIS and attributes such as reservoir depth and volume, bedrock type, stress field, and presence of active faulting in the reservoir. They found that of all the characteristics, depth and volume best correlated with RIS occurrence. Specifically, it was found that reservoirs deeper than 92 m or greater than 12 x 10^8 m^3 in volume showed the highest probabilities of exhibiting RIS. A weak correlation between depth and volume, given RIS occurrence, was noted. Reservoirs with parameters less than these values were judged to have probabilities of RIS of close to zero. Other preferred attributes were found to be sedimentary bedrock beneath the reservoir, and active faulting present prior to reservoir impoundment, although the statistical correlation for these characteristics was not as strong as that for depth and volume. Probabilities for RIS were presented given various single and combined attributes. For example, looking only at reservoirs exceeding 92 m in depth gives an RIS frequency of about .14.

A stress field in which extensional or shear faulting predominates appears to be the most conducive for RIS occurrence, based on theoretical studies (Simpson, 1986) and observed cases (Baecher and Keeney, 1982). A sizable body of evidence (section 2.4) indicates that the CUP region is currently experiencing crustal extension. In-situ stress measurements conducted near the Jordanelle damsite (discussed in section 2.4) indicate stress levels that may be close to failure. The measurements also indicated low pore pressures, which would tend to maximize the potential for induced failure on a fault due to water seeping down from a reservoir. Simpson (1986), however, points out that uncertainties in this type of measurement may be large compared to the stress required to initiate failure.

In the description of the statistical analysis, it was mentioned that there was a choice between a one-sided test and a two-sided test when using equation (2) in section B.3.0, depending on whether we were interested in identifying both increases and decreases in activity, or only increases. For the purposes of this study, only increases were noted. In table B-5, there are 27 quarters in which the regional rate was exceeded at the 95% confidence level. It is interesting to note, however, that there were 25 quarters in which the local rate was lower than the regional rate at the same confidence level (i.e., z-value less than -1.645). This implies that if there is one specific mechanism causing the local fluctuations, it has the effect of both raising and lowering the rate of local seismic activity.

Although the great majority of documented RIS cases record an increase in activity due to reservoir related effects, two cases have been described in which a decrease in seismicity has been attributed to effects associated with water impoundment. In the first, a gap in seismicity along the Calaveras fault in central California is postulated by Bufe (1976) to be caused by stable sliding (creep) along the fault due to increased pore pressure, resulting from downward percolation of water from Anderson Reservoir. Bufe (1976) implied that this effect occurs at shallow (less than 5 km) depths, and for small earthquakes on faults already prone to creep. The second case involves Tarbela Dam in Pakistan. Jacob and others (1979) noted a reduction in seismicity during initial reservoir filling, which they attributed to increased loading in a compressional tectonic environment. While the data for this case were not well supported statistically, good theoretical arguments exist for their hypothesis (Simpson, 1976). None of the specialized conditions involved in these two cases appear to exist in north central Utah. Regional stresses are clearly extensional, not compressional, and to our knowledge fault creep has not been shown to play a significant role in tectonic movements. We would therefore expect reservoir related effects to manifest as an increase in activity in the CUP region. The fact that an approximately equal number of periods of decreased as opposed to increased activity were observed argues against RIS as the causative mechanism of the abnormal periods identified in table B-5.

Packer and others (1980), in examining 42 "accepted" RIS cases, tabulated the time between initial filling and the occurrence of the largest suspected RIS event. It was found that 37 of the total, or 88%, occurred within 5 years of initial impoundment, and all but two, or 95%, occurred within 10 years. In examining the case for dams in north-central Utah in table B-3, for only 2 of the 13 dams (excluding Soldier Creek reservoir, which has not been completely filled) did the largest local event occur less than 10 years before initial filling. The two exceptions are a magnitude 3.7 event seen 13 km WSW of Causey dam in figure B-1a, and a magnitude 2.6 event seen at the center of Joes Valley reservoir in figure B-1f. Neither earthquake appears to stand out from the regional seismicity pattern, and neither is unusually large.

The largest earthquake that appears to have been induced by water impoundment is the 1967 Koyna, India event. The actual magnitude of this event, however, varies from source to source in the literature, and the magnitude scale is rarely noted. The magnitude is stated as "magnitude 7.0" in Guha (1977), "magnitude 6.0" in Gupta and Combs (1976), and "M 6.5" in Gupta and Rastogi (1976). Rothé (1973) uses values of "magnitude 6.3" and "magnitude 6.4" in different places in the same article. The only mentions of magnitude scales found by this author were by Gupta and others (1972) ("magnitude 6.0 on Karnik's $L_G H$ scale"), and an M_S 6.3 noted by Gupta and others (1980). The scale preferred by the USBR for magnitudes in this range for use in strong motion analysis is the M_L scale. While it is apparent that no Wood-Anderson seismographs were operating within a favorable distance of the 1967 event, the M_S reading gives some insight into an equivalent M_L value. Based on a comparison between M_S and M_L for 24 western U.S. earthquakes, Nuttli (1979) calculated a regression between the two scales which equates M_S 6.3 to M_L 6.2. This relation should be considered very tenuous, however, because of the fact that there were only three magnitudes greater than 6 in Nuttli's analysis, and also because frequency filtering characterics of the crust in India may be quite different from those in the western U.S. Faced with the necessity of estimating a value for the maximum induced event for central Utah, however, we will assume an M_L 6.5 earthquake to be a reasonable, conservative value for such an event. This value also coincides with the estimated magnitude of the maximum random (i.e., non-surface rupturing) earthquake for the intermountain seismic belt.

Based on observations of RIS worldwide, one may conclude that the CUP region is a favorable environment for RIS occurrence based on the presence of a moderately active, extensional stress field. However, all but one of the USBR dams considered here are smaller and shallower than those considered by Baecher and Keeney (1982) as having a greater than negligible probability of exhibiting RIS. The lone exception, Soldier Creek reservoir, would be classified as shallow (81 m) but has a projected volume of 13.65 x 10^8 m^3. The depth of this reservoir, however, has to date

not exceeded 63 m, and the current volume is 7.821 x 10^8 m^3. This is below the threshold value of 12 x 10^8 m^3 proposed by Baecher and Keeney (1982). In summary, although to the best of our knowledge RIS has not occurred in north-central Utah, reservoirs that have existed to date in the region have not been as large as those for which RIS is considered to have a greater than negligible probability.

B.4.0 Conclusions

(1) Within the resolution of available data, no increase in activity upon initial filling was noted at any of the subject dams. However, all but one of the reservoirs were filled prior to 1967, before the installation of the current seismograph network. Therefore this conclusion must be qualified by the regional detection thresholds discussed in section 2.1 of the main report.

(2) The statistical tests proved useful in isolating seasonal periods of anomalously high seismic activity. In all but one case, however, the anomalous activity was traceable to swarms during specific years and not to consistently higher activity during all of the years. Inadequate sample sizes also provided justifications for questioning the validity of anomalous values. The fact that comparable numbers of anomalously high and low values were identified argues against RIS as the causative mechanism of the fluctuations.

(3) Based on the statistical analysis performed in this report, there is no evidence for the occurrence of RIS at all but one of the 13 USBR reservoirs. While the analysis pointed to possible RIS at Rockport Reservoir (Wanship Dam), further considerations lead us to conclude that RIS was not responsible for the statistical anomaly.

(4) Based on theoretical studies and observed cases of RIS worldwide, the CUP region shares a number of attributes that appear to be conducive to RIS. However, the depths and volumes of the reservoirs analyzed in this report are lower than those for which the probability of RIS occurrence has been judged to have a greater than negligible value. For deeper and larger volume reservoirs, RIS probabilities may be assignable based on the work of Baecher and Keeney (1982).

B.5.0 Acknowledgements

Comments on this appendix furnished by Bill Astle, Mathematics Department, Colorado School of Mines, are greatly appreciated. Dr. Walter Arabasz of the University of Utah made several good suggestions which were incorporated into the final manuscript.

Table B-1 Dam and Reservoir Parameters

Dam	Latitude	Longitude	Year Completed	Capacity ($x 10^8 m^3$)	Structural Height (m)
Causey	41.298	111.592	1966	.084	66
Deer Creek	40.400	111.533	1941	1.84	72
East Canyon	40.920	111.600	1966	.593	79
Echo	40.963	111.432	1930	.911	48
Hyrum	41.625	111.875	1935	.189	35
Joe's Valley	39.288	111.270	1966	.678	59
Lost Creek	41.185	111.400	1966	.247	76
Newton	41.900	111.983	1945	.067	31
Pineview	41.250	111.833	1937	.543	32
Pineview			1957	1.359	42
Scofield	39.789	111.125	1946	.812	38
Soldier Creek	40.153	111.015	1973,1983*	13.650	81
Strawberry	40.157	111.114	1913	3.330	22
Wanship	40.790	111.403	1957	.751	53

*filling began in 1983;
reservoir depth is at 63 m, volume is at 7.821 x 10^8 m^3 (March, 1988)

Table B-2a. Monthly event counts for study region.

NORTH-CENTRAL UTAH

YEAR	JAN	FEB	MAR	APR	MAY	JUN	JUL	AUG	SEP	OCT	NOV	DEC
1974											16	29
1975	21	12	12	15	10	16	26	14	21	40	17	30
1976	24	33	44	24	29	24	49	45	31	33	50	55
1977	39	42	19	19	28	21	25	17	20	19	18	16
1978	32	13	21	7	14	22	14	15	31	21	39	23
1979	53	33	15	24	34	14	21	30	9	15	13	34
1980	24	13	21	28	20	10	30	16	33	12	12	22
1981	19	10	10	41	21	6	5	15	15	19	16	15
1982	5	10	21	15	23	51	15	21	32	26	45	28
1983	14	19	16	27	25	37	21	30	22	36	22	48
1984	6	4	12	3	7	40	17	23	29	38	15	30
1985	23	15	13	14	22	15	10	17	14	17	12	9
1986	18	13	37	17	10	18						
TOTALS	278	217	241	234	243	274	233	243	257	276	275	339

TOTAL NUMBER OF EVENTS = 3110

Table B-2b. Monthly event counts for Causey Dam.

CAUSEY DAM

YEAR	JAN	FEB	MAR	APR	MAY	JUN	JUL	AUG	SEP	OCT	NOV	DEC
1974											1	0
1975	0	1	0	0	1	0	1	0	1	0	1	1
1976	1	1	1	0	0	1	4	2	0	0	1	1
1977	1	0	0	0	2	0	1	2	1	0	1	0
1978	0	0	1	0	0	2	0	2	8	5	1	3
1979	10	1	1	0	0	0	0	1	0	0	0	1
1980	0	0	0	1	0	0	0	1	2	1	2	2
1981	0	1	1	1	1	0	0	1	0	0	1	0
1982	0	0	0	1	0	1	0	3	0	1	0	0
1983	0	4	2	2	0	0	0	1	2	2	0	0
1984	0	0	2	0	0	1	0	0	0	0	0	1
1985	1	0	1	0	0	0	2	0	0	0	1	1
1986	3	0	1	0	0	4	0					
TOTALS	16	8	10	5	4	9	8	13	14	9	9	10

TOTAL NUMBER OF EVENTS = 115

Table B-2c. Monthly event counts for Deer Creek Dam.

DEER CREEK DAM

YEAR	JAN	FEB	MAR	APR	MAY	JUN	JUL	AUG	SEP	OCT	NOV	DEC
1974											1	1
1975	0	0	0	0	0	3	1	1	1	1	0	0
1976	1	0	0	0	0	0	0	0	0	0	1	1
1977	0	0	1	0	0	0	4	0	0	0	0	0
1978	0	0	0	1	1	0	0	0	0	0	0	0
1979	1	1	0	2	0	0	0	0	0	0	0	0
1980	0	0	0	0	0	0	0	0	0	0	0	0
1981	1	0	0	0	1	0	0	0	0	0	0	1
1982	0	0	0	0	0	5	0	3	0	1	1	0
1983	0	0	0	0	0	0	0	0	0	0	0	0
1984	0	0	2	1	0	3	3	1	0	0	0	1
1985	0	0	0	0	1	2	2	0	2	0	0	0
1986	1	0	0	1	0	0						
TOTALS	4	1	3	5	3	13	10	5	3	2	3	4

TOTAL NUMBER OF EVENTS = 56

Table B-2d. Monthly event counts for East Canyon Dam.

EAST CANYON DAM

YEAR	JAN	FEB	MAR	APR	MAY	JUN	JUL	AUG	SEP	OCT	NOV	DEC
1974											0	1
1975	3	0	0	0	1	0	1	1	4	2	0	4
1976	1	0	1	0	0	0	4	3	6	10	1	2
1977	2	2	0	3	3	1	1	1	1	3	1	0
1978	0	0	0	0	0	1	0	0	1	0	0	5
1979	0	1	1	1	0	0	0	0	0	0	1	0
1980	0	2	0	0	0	0	0	1	3	0	1	0
1981	2	0	0	0	0	0	0	1	0	0	0	1
1982	0	0	1	0	0	2	0	1	1	0	1	1
1983	1	2	0	0	0	0	0	0	0	0	1	0
1984	0	0	0	0	0	3	1	0	0	0	1	0
1985	0	1	1	0	0	1	0	0	0	0	0	0
1986	1	1	0	0	0	0						
TOTALS	10	9	4	4	4	8	7	8	16	15	7	14

TOTAL NUMBER OF EVENTS = 106

Table B-2e. Monthly event counts for Echo Dam.

ECHO DAM

YEAR	JAN	FEB	MAR	APR	MAY	JUN	JUL	AUG	SEP	OCT	NOV	DEC
1974											0	0
1975	0	0	0	0	0	0	0	0	2	1	0	5
1976	1	0	0	1	0	0	4	4	6	9	3	3
1977	1	0	0	2	0	3	3	2	2	2	2	0
1978	1	0	0	0	0	1	0	0	1	0	1	1
1979	0	1	0	1	0	0	0	0	0	0	0	2
1980	0	0	0	0	0	0	0	0	0	0	1	0
1981	2	0	0	0	0	0	0	1	0	0	0	1
1982	0	0	0	0	0	1	0	0	0	0	0	0
1983	1	0	0	0	0	0	0	1	0	0	0	0
1984	0	0	0	0	0	3	0	0	0	0	1	0
1985	0	1	0	0	0	0	0	0	0	0	0	0
1986	0	0	0	0	0	0						
TOTALS	6	2	0	4	0	8	7	8	11	12	8	12

TOTAL NUMBER OF EVENTS = 78

Table B-2f. Monthly event counts for Hyrum Dam.

HYRUM DAM

YEAR	JAN	FEB	MAR	APR	MAY	JUN	JUL	AUG	SEP	OCT	NOV	DEC
1974											0	0
1975	0	0	3	0	0	0	1	1	0	2	0	1
1976	1	1	1	2	4	1	0	1	0	1	0	1
1977	2	1	0	0	0	0	0	0	0	0	0	0
1978	1	0	1	0	1	1	0	1	1	1	2	1
1979	1	2	0	1	0	0	0	0	0	0	0	0
1980	0	1	3	0	2	0	0	0	2	0	2	0
1981	0	0	1	0	0	0	1	0	1	0	0	1
1982	0	1	1	0	0	21	0	0	0	1	8	5
1983	0	0	0	0	7	7	1	1	3	1	0	26
1984	0	0	0	0	0	2	0	2	1	0	3	2
1985	0	0	0	2	4	0	0	1	0	1	2	0
1986	0	0	1	0	0	0						
TOTALS	5	6	11	5	18	32	3	7	8	7	17	37

TOTAL NUMBER OF EVENTS = 156

Table B-2g. Monthly event counts for Joes Valley Dam.

JOE'S VALLEY DAM (MINING EVENTS DELETED)

YEAR	JAN	FEB	MAR	APR	MAY	JUN	JUL	AUG	SEP	OCT	NOV	DEC
1974											0	0
1975	0	0	0	0	0	0	1	0	0	0	0	0
1976	0	0	1	0	0	0	0	0	0	0	1	0
1977	0	0	2	0	0	0	0	0	0	0	0	0
1978	0	0	0	0	0	0	0	0	2	0	0	0
1979	0	1	0	0	0	0	0	0	0	0	0	1
1980	0	0	0	2	1	0	0	1	0	0	0	1
1981	0	0	0	0	0	0	0	0	0	0	0	0
1982	0	0	0	0	0	0	0	0	0	0	0	0
1983	1	1	0	1	3	0	1	0	0	0	0	2
1984	0	0	0	0	0	0	0	0	0	0	1	0
1985	0	0	0	0	0	0	0	0	0	1	0	0
1986	0	0	0	2	0	0						
TOTALS	1	2	3	5	4	0	2	1	2	1	2	4

TOTAL NUMBER OF EVENTS = 27

Table B-2h. Monthly event counts for Lost Creek Dam.

LOST CREEK DAM

YEAR	JAN	FEB	MAR	APR	MAY	JUN	JUL	AUG	SEP	OCT	NOV	DEC
1974											1	0
1975	0	0	0	0	0	0	0	0	1	0	0	0
1976	0	1	0	0	0	0	2	0	1	1	1	0
1977	0	0	0	0	0	0	0	0	0	2	0	0
1978	1	0	0	0	0	0	0	0	2	0	0	0
1979	1	0	0	1	0	0	0	0	0	0	0	0
1980	0	0	0	0	0	0	0	0	0	0	0	0
1981	0	0	0	0	0	0	0	0	0	0	2	0
1982	0	0	0	1	0	0	0	0	0	0	1	0
1983	1	1	0	0	0	0	0	1	0	0	0	0
1984	0	0	0	0	0	0	0	0	0	0	0	0
1985	0	0	0	0	0	0	0	0	0	0	0	0
1986	1	0	0	0	0	0						
TOTALS	4	2	0	2	0	0	2	1	4	3	5	0

TOTAL NUMBER OF EVENTS = 23

Table B-2i. Monthly event counts for Newton Dam.

NEWTON DAM

YEAR	JAN	FEB	MAR	APR	MAY	JUN	JUL	AUG	SEP	OCT	NOV	DEC
1974											0	1
1975	0	0	0	0	1	0	0	0	0	0	0	0
1976	1	0	0	0	0	1	4	0	0	0	1	1
1977	1	0	0	0	0	0	0	0	0	0	0	0
1978	1	1	1	0	0	0	6	0	0	0	0	0
1979	0	0	0	0	0	0	0	0	0	0	0	0
1980	1	0	0	0	0	0	9	0	0	0	0	0
1981	0	0	0	0	0	0	0	0	0	0	0	1
1982	0	0	0	0	0	0	0	0	0	0	1	1
1983	0	1	2	2	0	1	0	0	0	0	0	0
1984	0	0	0	0	0	2	0	0	1	0	0	0
1985	0	0	0	1	0	0	1	0	0	0	0	0
1986	0	0	0	1	0	0						
TOTALS	4	2	3	4	1	4	20	0	1	0	2	4

TOTAL NUMBER OF EVENTS = 45

Table B-2j. Monthly event counts for Pineview Dam.

PINEVIEW DAM

YEAR	JAN	FEB	MAR	APR	MAY	JUN	JUL	AUG	SEP	OCT	NOV	DEC
1974											1	0
1975	0	0	0	0	0	0	1	0	1	0	1	1
1976	2	5	1	0	0	2	3	2	0	0	3	1
1977	3	0	0	0	2	0	0	0	1	0	0	1
1978	1	0	1	0	0	0	0	0	2	1	0	0
1979	4	1	0	0	0	0	0	0	0	0	0	0
1980	0	0	0	0	0	0	0	1	2	3	3	0
1981	0	0	0	1	1	0	0	0	0	0	0	0
1982	0	0	0	0	0	0	0	2	0	1	0	0
1983	0	1	2	0	0	0	0	0	0	1	0	0
1984	0	0	0	0	0	0	0	0	0	0	0	1
1985	1	0	0	0	0	0	1	0	0	0	1	0
1986	1	0	0	0	1	4						
TOTALS	12	7	4	1	4	6	5	5	6	6	9	4

TOTAL NUMBER OF EVENTS = 69

Table B-2k. Monthly event counts for Scofield Dam.

SCOFIELD DAM

YEAR	JAN	FEB	MAR	APR	MAY	JUN	JUL	AUG	SEP	OCT	NOV	DEC
1974											0	2
1975	1	0	0	0	0	0	0	0	0	2	0	0
1976	1	0	0	0	0	0	0	1	0	0	0	0
1977	0	0	0	0	0	0	0	0	1	0	1	0
1978	0	0	0	0	3	0	1	0	0	0	0	0
1979	0	0	0	2	0	0	0	1	1	1	0	0
1980	0	0	2	1	2	0	0	0	1	1	0	0
1981	0	0	0	0	0	0	0	1	0	1	0	0
1982	0	0	0	0	0	0	0	0	0	0	0	0
1983	0	0	0	0	0	0	0	0	0	0	0	0
1984	0	0	0	0	0	0	0	0	0	0	0	0
1985	0	0	2	0	0	0	0	0	0	0	0	1
1986	0	0	0	0	0	0						
TOTALS	2	0	4	3	5	0	1	3	3	5	1	3

TOTAL NUMBER OF EVENTS = 30

Table B-2l. Monthly event counts for Soldier Creek Dam.

SOLDIER CREEK DAM

YEAR	JAN	FEB	MAR	APR	MAY	JUN	JUL	AUG	SEP	OCT	NOV	DEC
1974											0	0
1975	0	0	0	0	0	0	0	0	0	0	0	0
1976	0	0	0	0	0	0	0	0	0	1	0	0
1977	0	0	0	0	0	0	0	0	0	0	0	1
1978	0	0	0	0	0	0	0	0	0	0	0	0
1979	0	0	0	0	0	0	0	1	0	0	0	1
1980	0	0	0	0	0	0	0	0	0	0	0	0
1981	0	0	0	0	0	0	0	0	0	0	0	0
1982	0	0	0	0	0	0	0	0	0	0	0	0
1983	0	0	0	0	0	0	0	0	0	0	0	0
1984	0	0	0	0	0	0	0	0	0	0	0	0
1985	0	0	0	0	1	0	0	0	0	0	0	0
1986	0	0	0	0	0	0						
TOTALS	0	0	0	0	1	0	0	1	0	1	0	2

TOTAL NUMBER OF EVENTS = 5

Table B-2m. Monthly event counts for Strawberry Dam.

STRAWBERRY DAM

YEAR	JAN	FEB	MAR	APR	MAY	JUN	JUL	AUG	SEP	OCT	NOV	DEC
1974											0	1
1975	0	0	0	0	0	0	0	0	0	0	0	0
1976	0	1	0	0	0	0	0	0	0	1	0	0
1977	0	0	0	0	0	0	0	0	0	0	0	2
1978	0	0	0	0	0	0	0	0	2	0	0	0
1979	0	0	0	0	0	0	0	1	0	0	0	1
1980	0	0	0	0	0	0	0	0	0	0	0	0
1981	0	0	0	0	0	0	0	0	0	0	0	0
1982	0	0	0	0	0	0	0	0	0	0	0	0
1983	0	0	0	0	0	0	0	0	0	0	0	0
1984	0	0	0	0	0	0	0	0	0	0	0	1
1985	0	0	0	0	1	0	0	0	0	0	1	0
1986	0	0	0	0	0	0						
TOTALS	0	1	0	0	1	0	0	1	2	1	1	5

TOTAL NUMBER OF EVENTS = 12

Table B-2n. Monthly event counts for Wanship Dam.

WANSHIP DAM

YEAR	JAN	FEB	MAR	APR	MAY	JUN	JUL	AUG	SEP	OCT	NOV	DEC
1974											1	0
1975	0	0	0	0	0	0	1	1	0	1	0	1
1976	0	2	0	0	0	0	0	0	0	1	0	0
1977	0	0	0	1	0	0	1	0	0	1	2	0
1978	0	0	0	0	0	1	0	0	1	2	1	5
1979	0	1	0	1	0	0	0	0	0	3	1	0
1980	2	0	0	0	0	0	0	0	0	0	0	0
1981	0	0	0	0	1	0	0	1	0	0	1	1
1982	0	0	0	0	2	0	0	0	0	1	0	1
1983	0	0	0	0	0	0	1	0	0	0	2	0
1984	0	0	0	0	0	0	0	0	0	0	0	0
1985	0	2	0	0	0	0	0	1	0	0	0	0
1986	0	0	0	0	0	0						
TOTALS	2	5	0	2	3	1	3	3	1	9	8	8

TOTAL NUMBER OF EVENTS = 45

Table B-3 Largest Post-Impoundment Earthquakes

Dam	Year Filled	M_{max} r=15 km	Δt (yrs)	M_{max} r=25 km	Δt (yrs)	Years Since Initial Filling
Causey	1966	3.7	1	**		20
Deer Creek	1941	5.0	17	**		45
East Canyon	1966	2.7	12	2.8	17	20
Echo	1930	2.8	28	3.7	25	56
Hyrum	1935	4.1	29	4.3	11	51
Joes Valley	1966	2.6	9	3.1	16	20
Lost Creek	1966	2.8	17	3.6	20	20
Newton	1945	3.1	33	3.1	17	41
Pineview	1937	3.7	30	**		49
Pineview	1957	3.7	10	**		29
Scofield	1946	2.7	39	2.9	37	40
Soldier Creek*	1983	2.6	2	**		3
Strawberry	1913	2.8	72	4.0	50	73
Wanship	1957	2.7	21	2.7	25	29

*filling not completed
**M_{max} at r=15 km exceeds M_{max} at r=25 km

Table B-4 Computed χ^2 Values

Dam	χ^2
Causey	13.528
Deer Creek	30.240*
East Canyon	18.864
Echo	25.698*
Hyrum	88.676*
Joe's Valley	11.734
Lost Creek	17.855
Newton	104.268*
Pineview	13.315
Scofield	13.715
Soldier Creek	9.757
Strawberry	16.574
Wanship	23.620*

*exceeds 95% level

Table B-5 Computed z-values

Dam	3-Month Period					
	Jan Feb Mar	Feb Mar Apr	Mar Apr May	Apr May Jun	May Jun Jul	Jun Jul Aug
Causey	1.515	-.513	-1.704	-2.164	-1.490	.510
Deer Creek	-1.688	-1.123	-.618	2.361*	3.945*	4.575*
East Canyon	-.487	-1.566	-2.927	-2.211	-1.511	-.586
Echo	-2.823	-3.132	-3.813	-1.827	-1.017	1.129
Hyrum	-2.885	-2.513	-.395	3.335*	2.962*	.849
Joe's Valley	-.178	1.845*	2.644*	1.123	-.228	-1.384
Lost Creek	.273	-.563	-1.645	-1.736	-1.733	-1.244
Newton	-.584	-.367	-.852	-.651	4.972*	4.621*
Pineview	1.828*	-1.041	-2.056	-1.633	-.527	-.244
Scofield	-.476	.142	2.208*	.327	-.527	-1.385
Soldier Creek	-1.246	-1.197	-.164	-.216	-.214	-.214
Strawberry	-1.253	-1.162	-1.216	-1.281	-1.279	-1.279
Wanship	-1.290	-1.089	-1.921	-1.704	-1.349	-1.349

Table B-5 (Cont'd)

Dam	3-Month Period					
	Jul Aug Sep	Aug Sep Oct	Sep Oct Nov	Oct Nov Dec	Nov Dec Jan	Dec Jan Feb
Causey	1.766*	1.602	.458	-1.034	.676	.676
Deer Creek	1.524	-1.239	-2.015	-2.098	-1.511	-1.833
East Canyon	-1.399	2.864*	2.355*	1.237	.128	1.018
Echo	2.056*	3.056*	2.805*	2.454*	.918	-.239
Hyrum	-3.636	-3.215	-1.600	2.970*	2.587*	1.141
Joe's Valley	-.622	-1.223	-.889	-.312	-.319	-.106
Lost Creek	.778	1.093	2.874*	.656	1.111	-.080
Newton	3.676*	-3.550	-2.977	-2.286	-.966	-.702
Pineview	-.143	-.132	.744	-.010	1.581	1.425
Scofield	-.032	1.489	.503	.167	-1.058	-1.262
Soldier Creek	-.189	.778	.306	1.553	.560	.665
Strawberry	.116	.672	.581	2.281*	1.635	1.815*
Wanship	-1.277	.613	2.159*	4.026*	1.689*	.993

*exceeds 95% confidence level

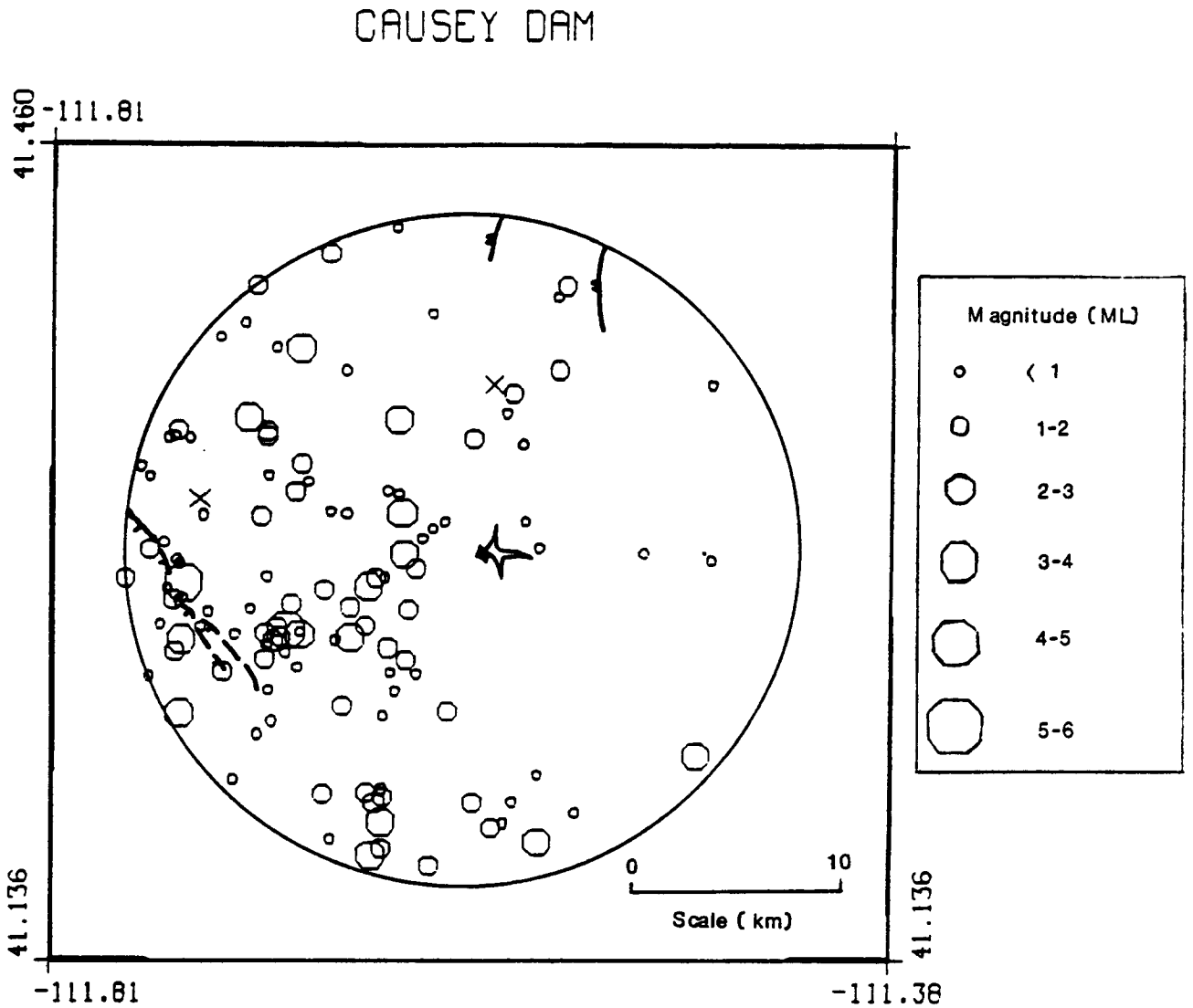

Figure B-1a Seismicity within 15 km of Causey Dam, through 6/86. Symbols scaled for magnitude; x signifies magnitude not computed. Faults plotted as on plate 1. Reservoir area outlined.

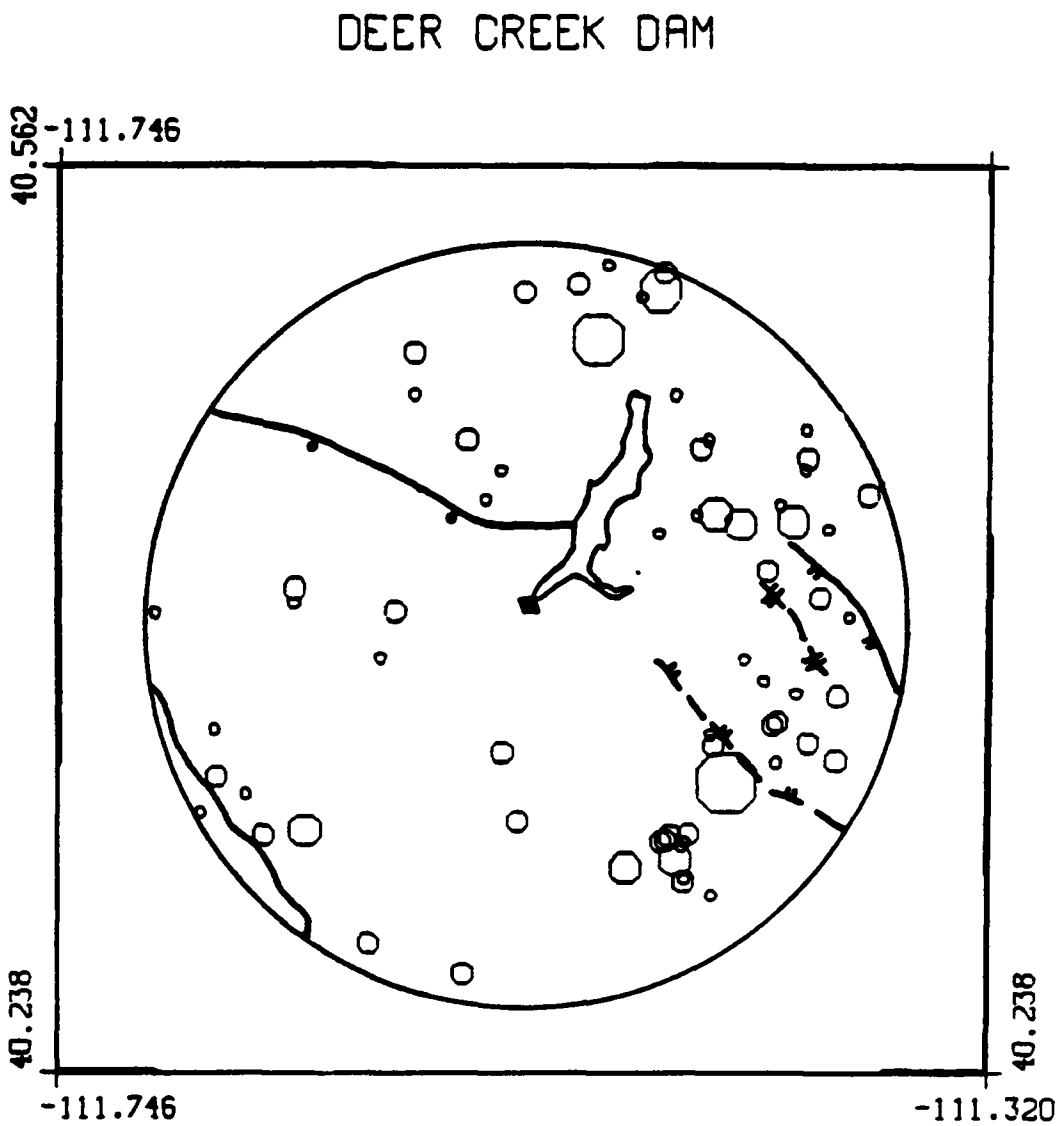

Figure B-1b Seismicity within 15 km of Deer Creek Dam, through 6/86. Symbols scaled for magnitude; x signifies magnitude not computed. Faults plotted as on plate 1. Reservoir area outlined.

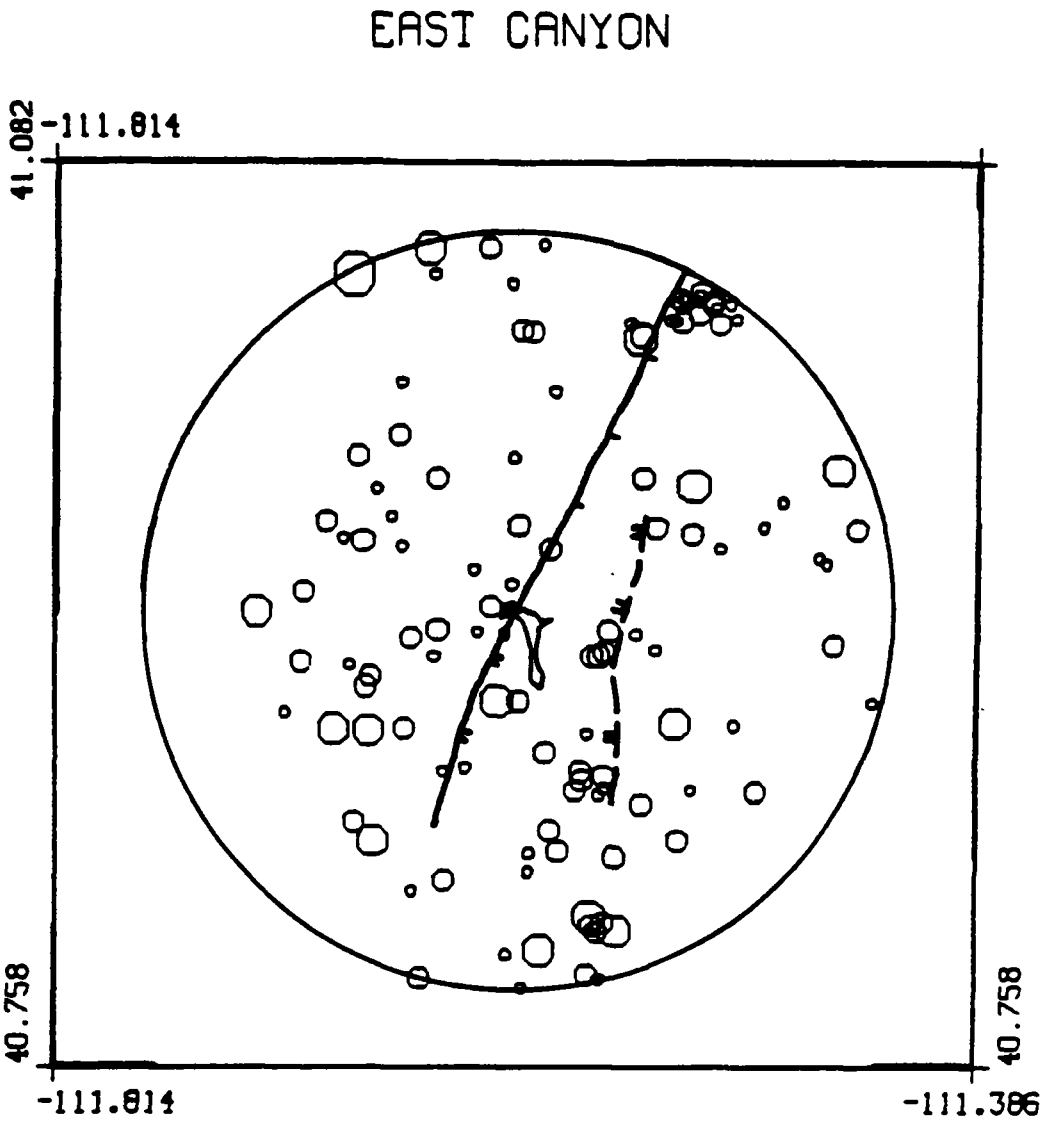

Figure B-1c. Seismicity within 15 km of East Canyon Dam, through 6/86. Symbols scaled for magnitude; x signifies magnitude not computed. Faults plotted as on plate 1. Reservoir area outlined.

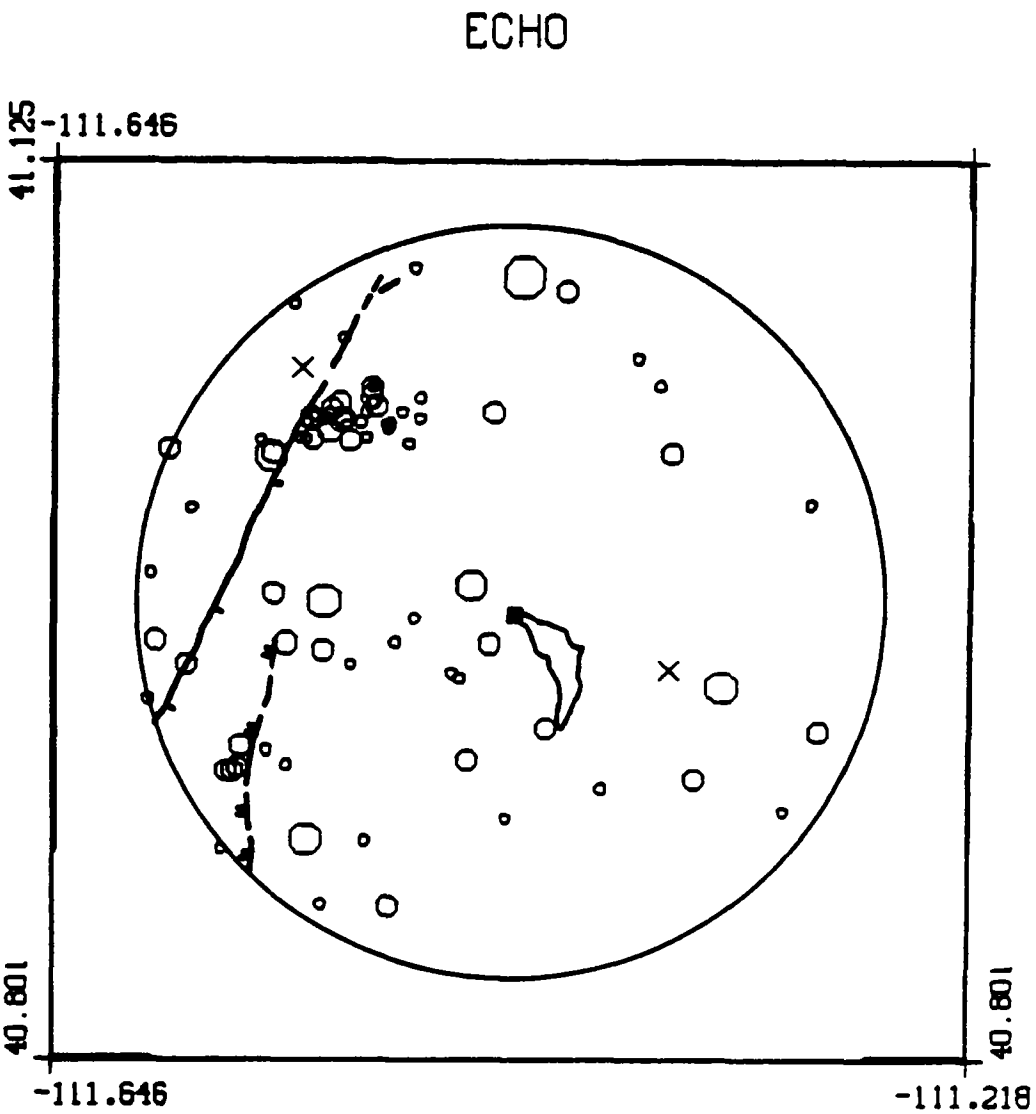

Figure B-1d. Seismicity within 15 km of Echo Dam, through 6/86. Symbols scaled for magnitude; x signifies magnitude not computed. Faults plotted as on plate 1. Reservoir area outlined.

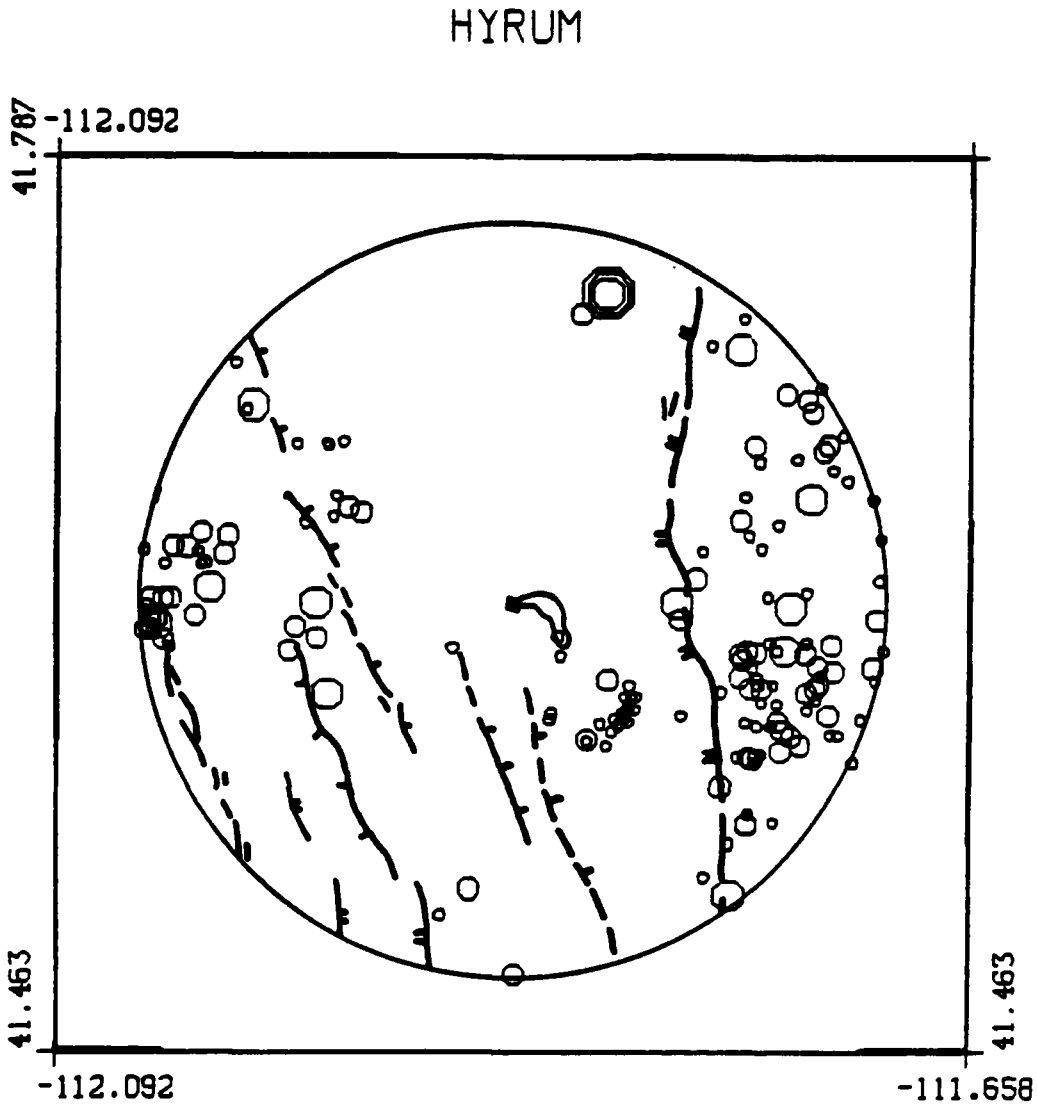

Figure B-1e. Seismicity within 15 km of Hyrum Dam, through 6/86. Symbols scaled for magnitude; x signifies magnitude not computed. Faults plotted as on plate 1. Reservoir area outlined.

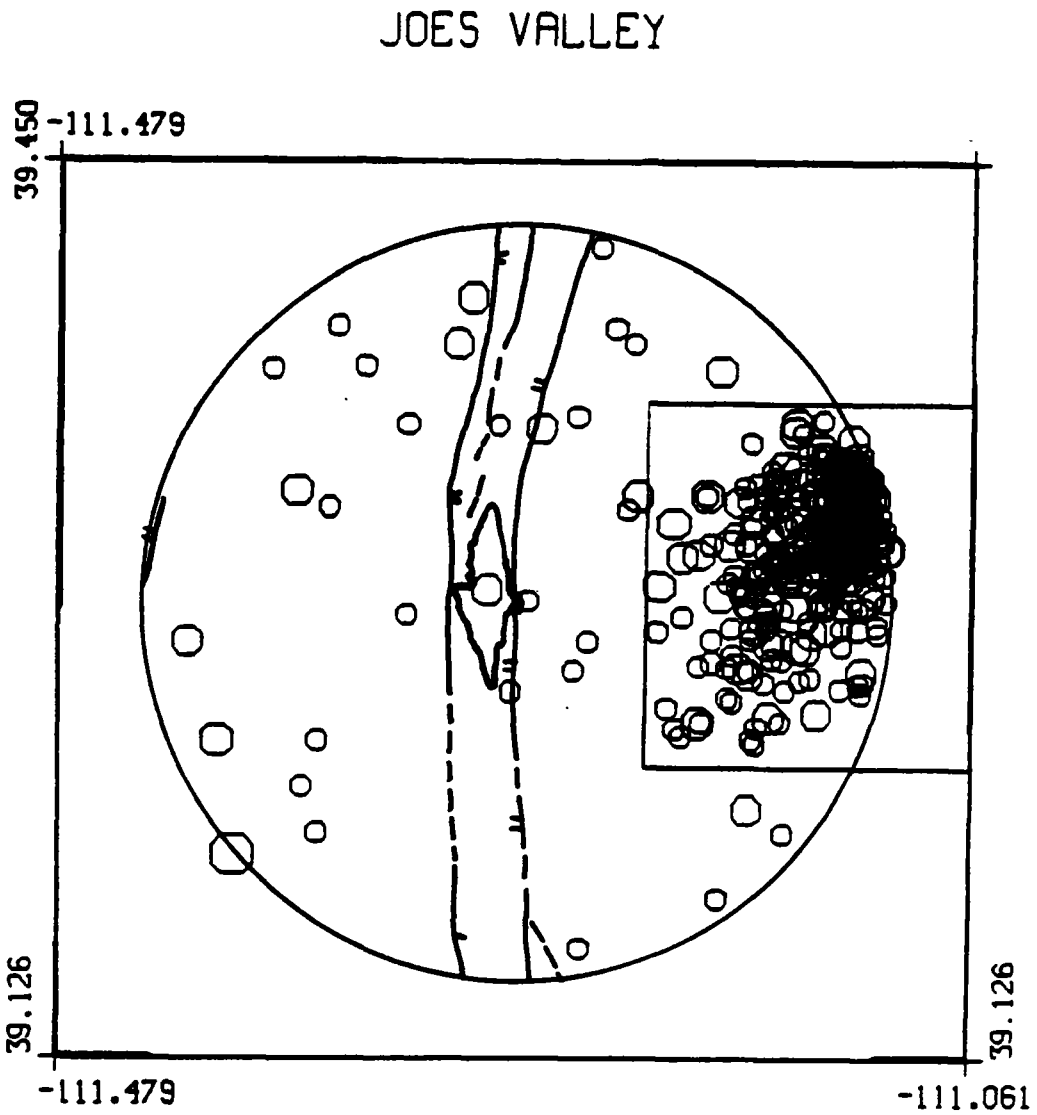

Figure B-1f. Seismicity within 15 km of Joes Valley Dam, through 6/86. Symbols scaled for magnitude; x signifies magnitude not computed. Faults plotted as on plate 1. Reservoir area outlined.

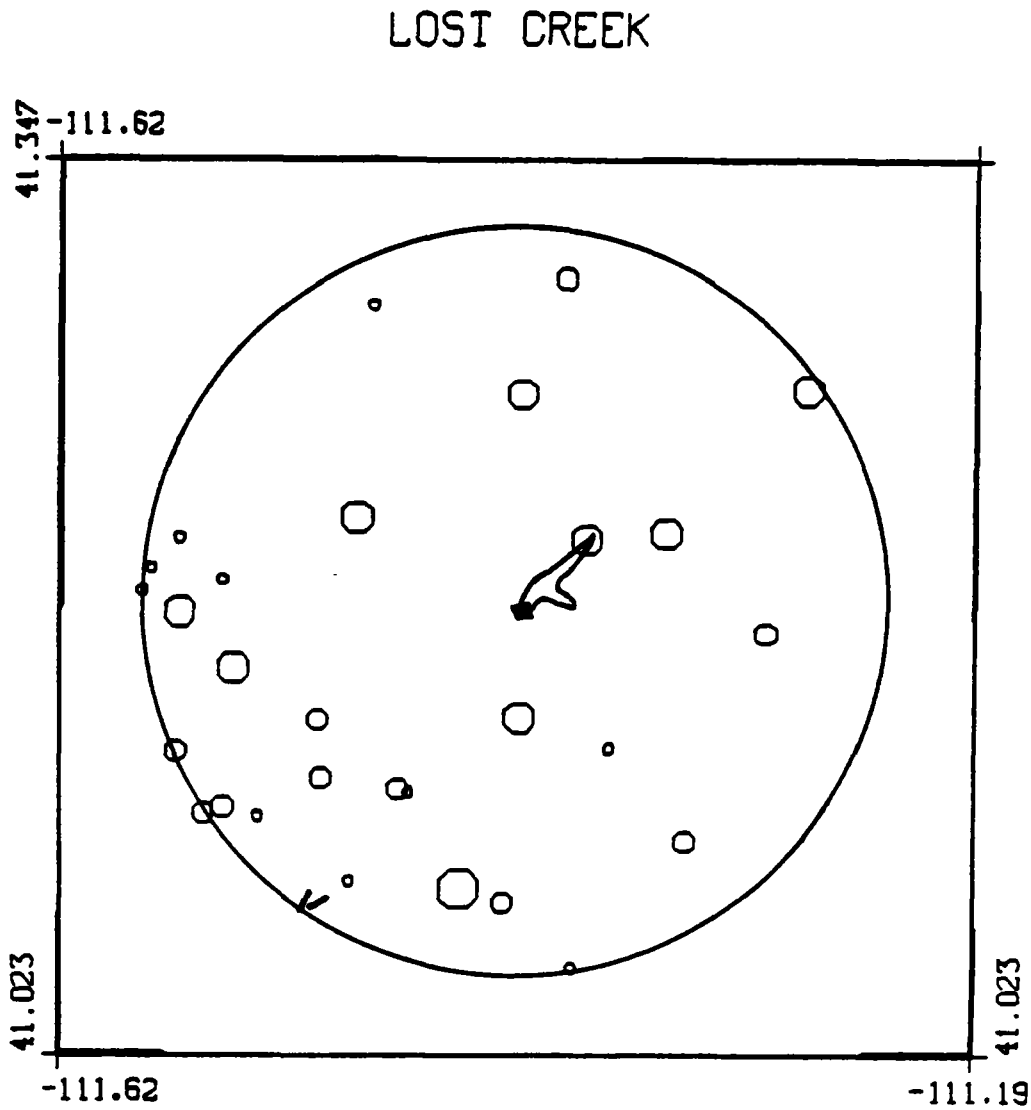

Figure B-1g. Seismicity within 15 km of Lost Creek Dam, through 6/86. Symbols scaled for magnitude; x signifies magnitude not computed. Faults plotted as on plate 1. Reservoir area outlined.

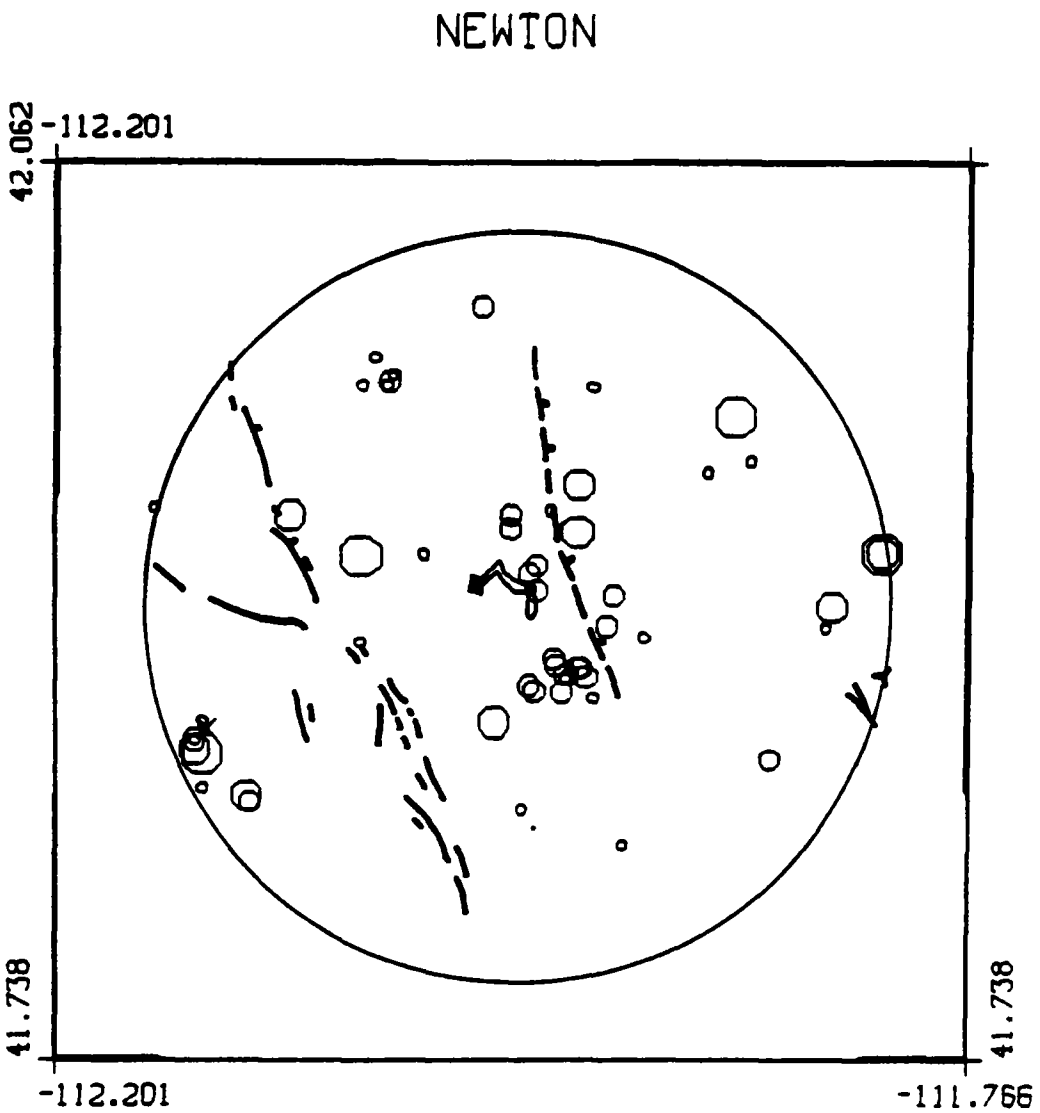

Figure B-1h. Seismicity within 15 km of Newton Dam, through 6/86. Symbols scaled for magnitude; x signifies magnitude not computed. Faults plotted as on plate 1. Reservoir area outlined.

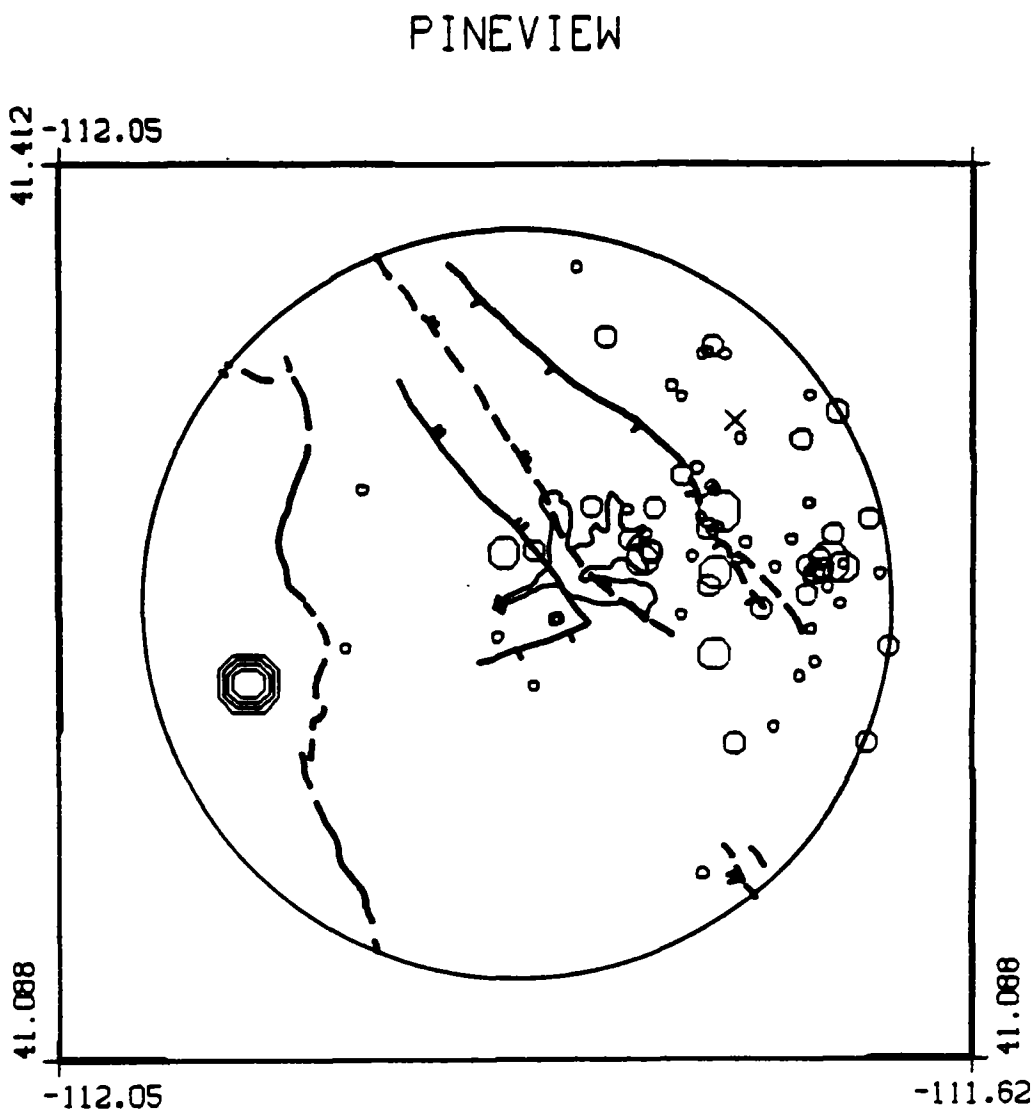

Figure B-1i. Seismicity within 15 km of Pineview Dam, through 6/86. Symbols scaled for magnitude; x signifies magnitude not computed. Faults plotted as on plate 1. Reservoir area outlined.

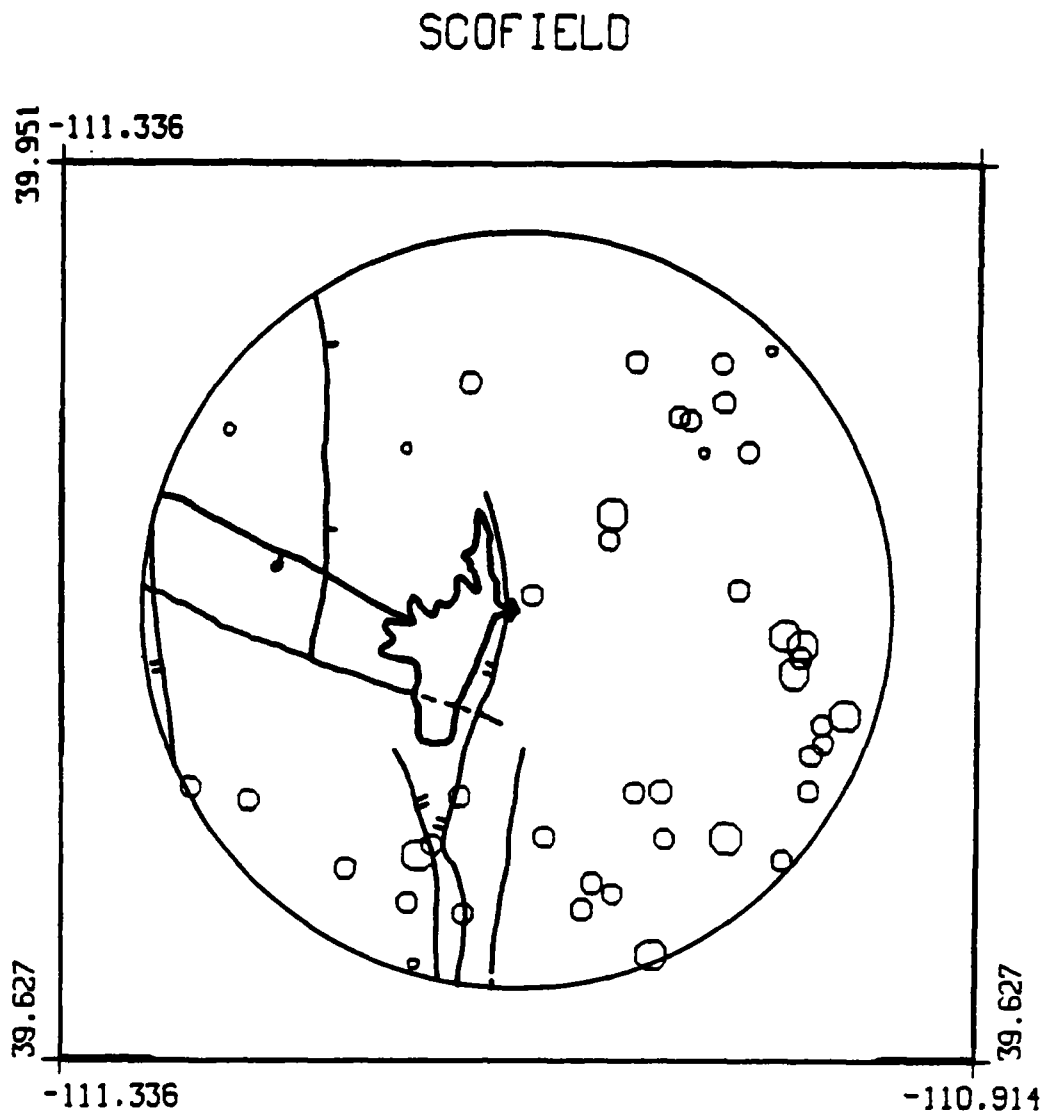

Figure B-1j. Seismicity within 15 km of Scofield Dam, through 6/86. Symbols scaled for magnitude; x signifies magnitude not computed. Faults plotted as on plate 1. Reservoir area outlined.

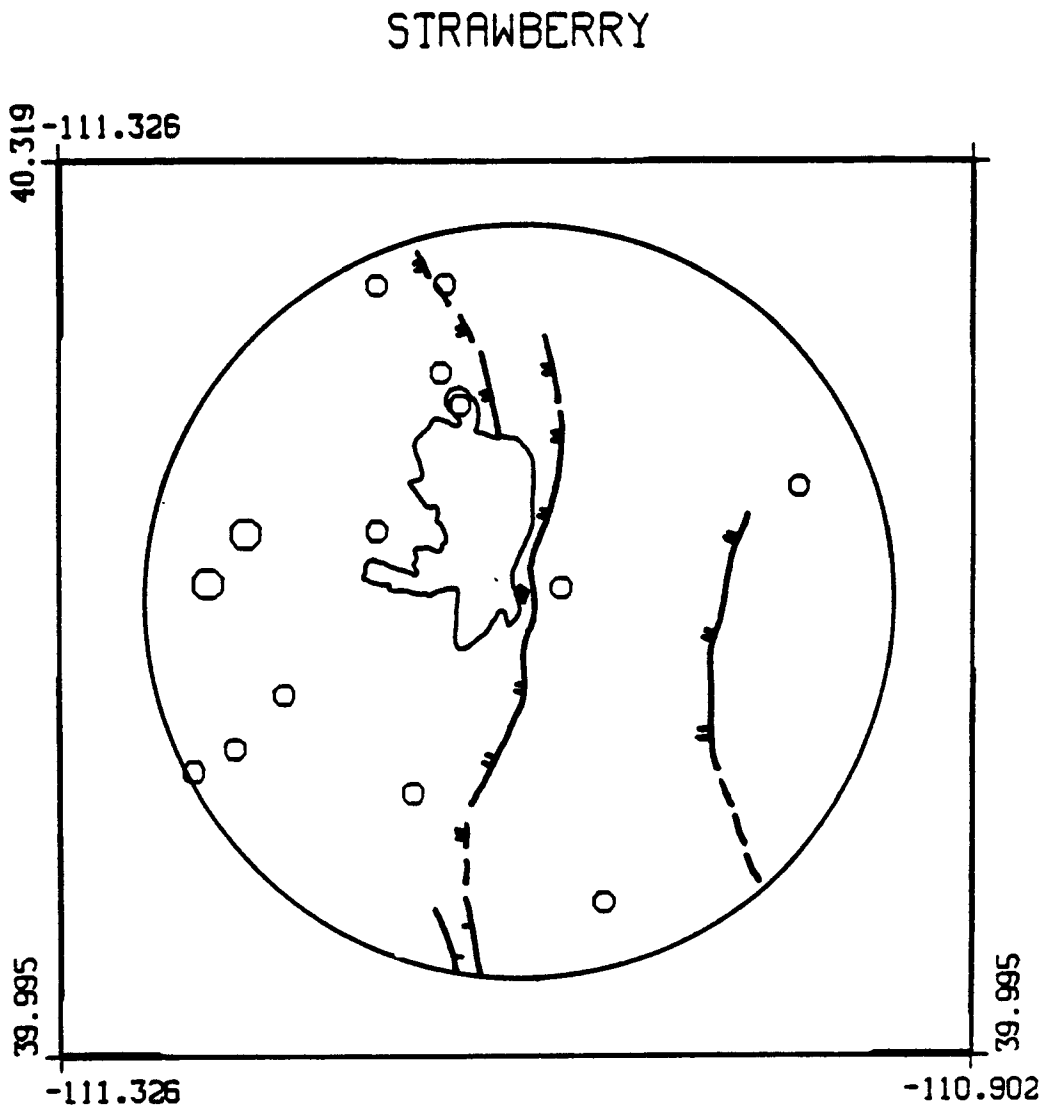

Figure B-1k. Seismicity within 15 km of Strawberry Dam, through 6/86. Symbols scaled for magnitude; x signifies magnitude not computed. Faults plotted as on plate 1. Reservoir area outlined.

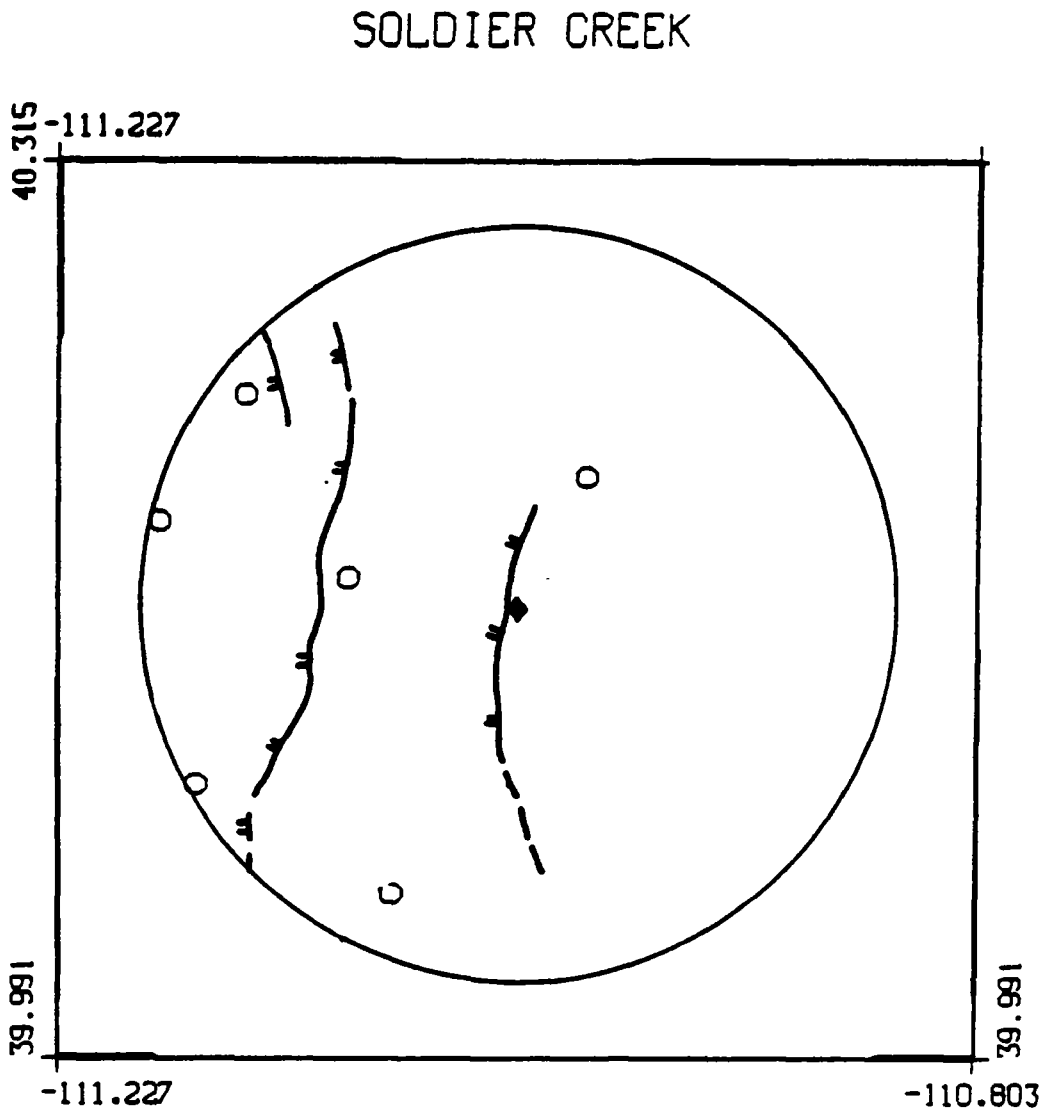

Figure B-11. Seismicity within 15 km of Soldier Creek Dam, through 6/86. Symbols scaled for magnitude; x signifies magnitude not computed. Faults plotted as on plate 1.

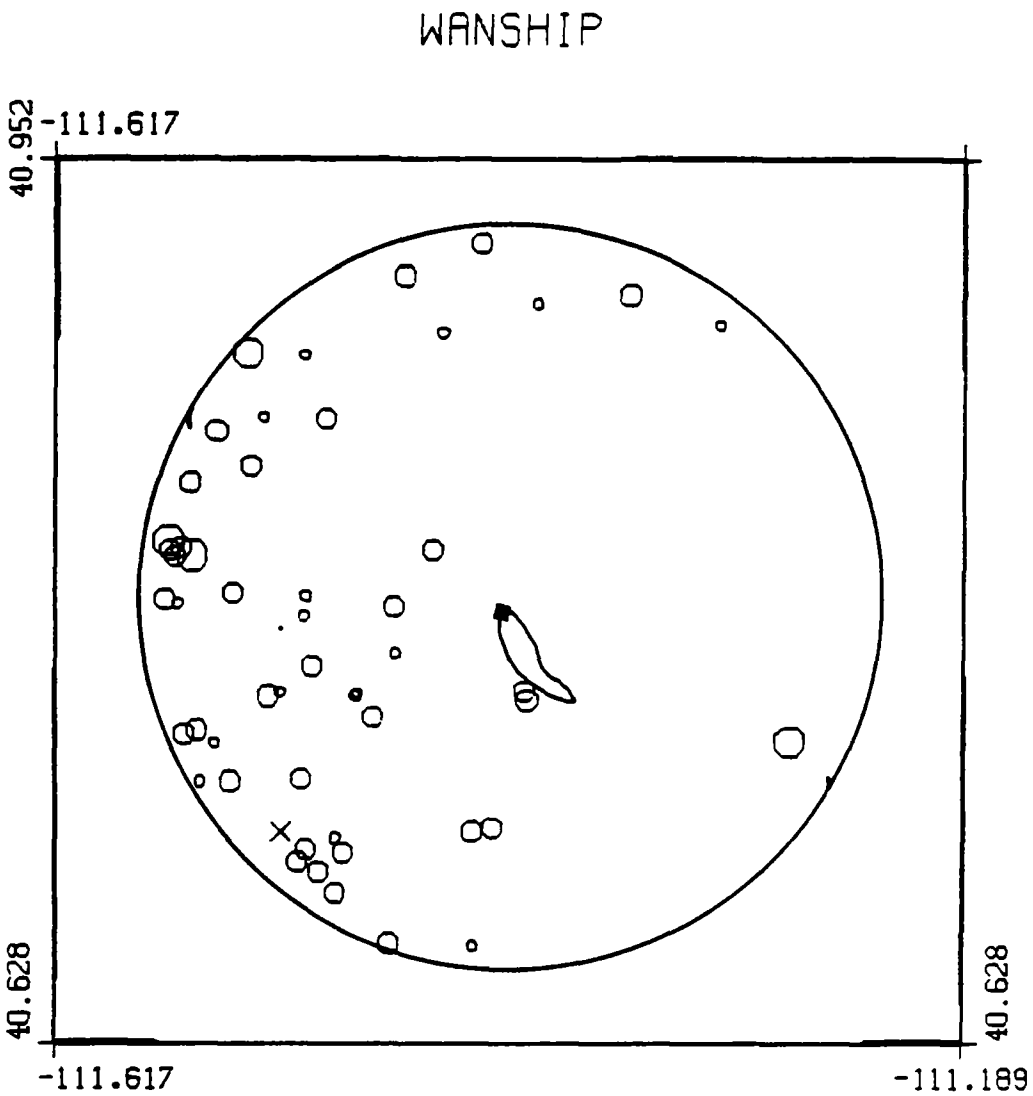

Figure B-1m Seismicity within 15 km of Wanship Dam, through 6/86. Symbols scaled for magnitude; x signifies magnitude not computed. Faults plotted as on plate 1. Reservoir area outlined.

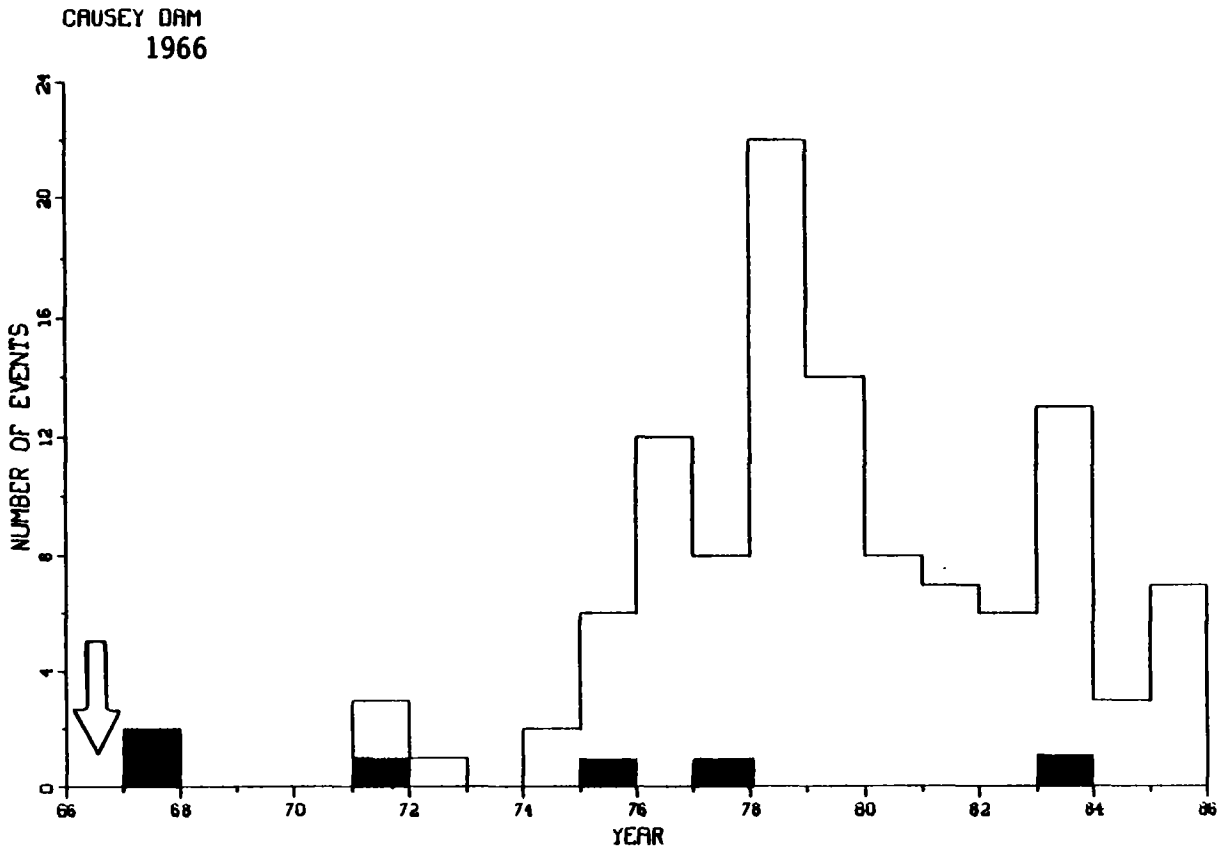

Figure B-2a. Yearly event count for Causey Dam. Arrow signifies year of initial reservoir filling. Solid portions indicate events $\geq$ magnitude 2.3.

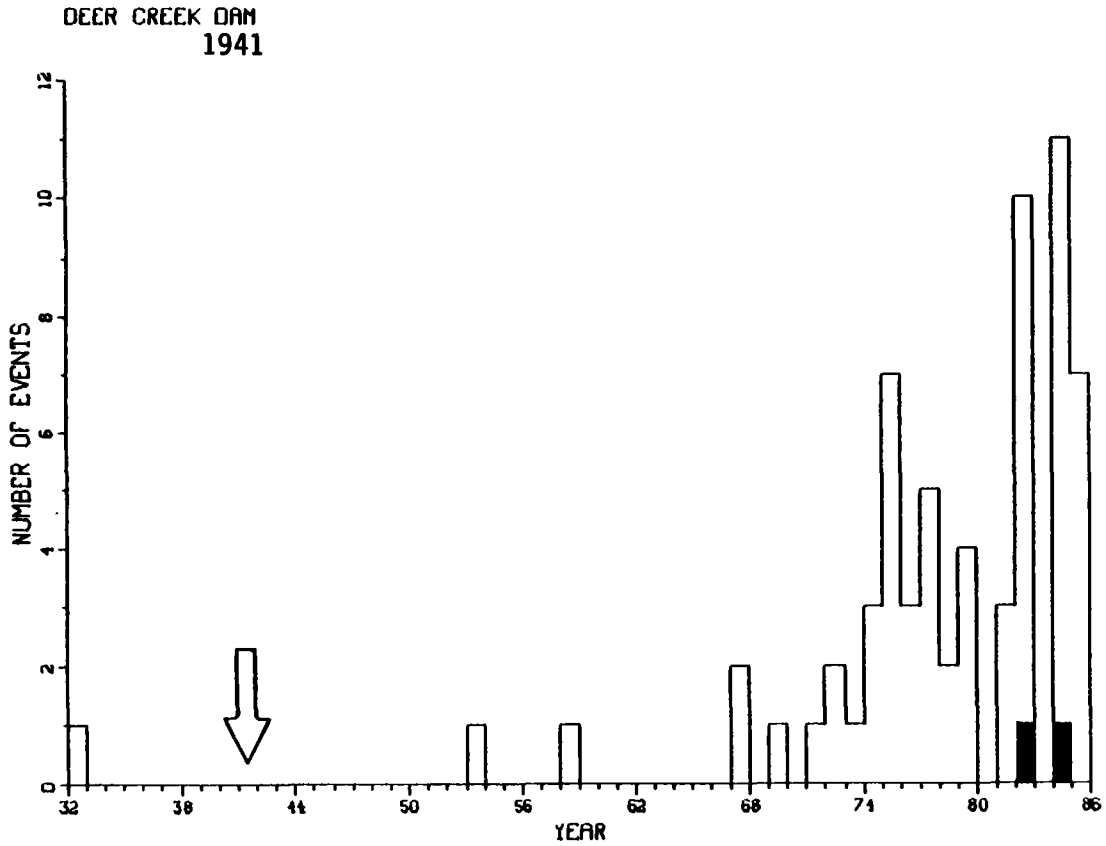

Figure B-2b. Yearly event count for Deer Creek Dam. Arrow signifies year of initial reservoir filling. Solid portions indicate events $\geq$ magnitude 2.3.

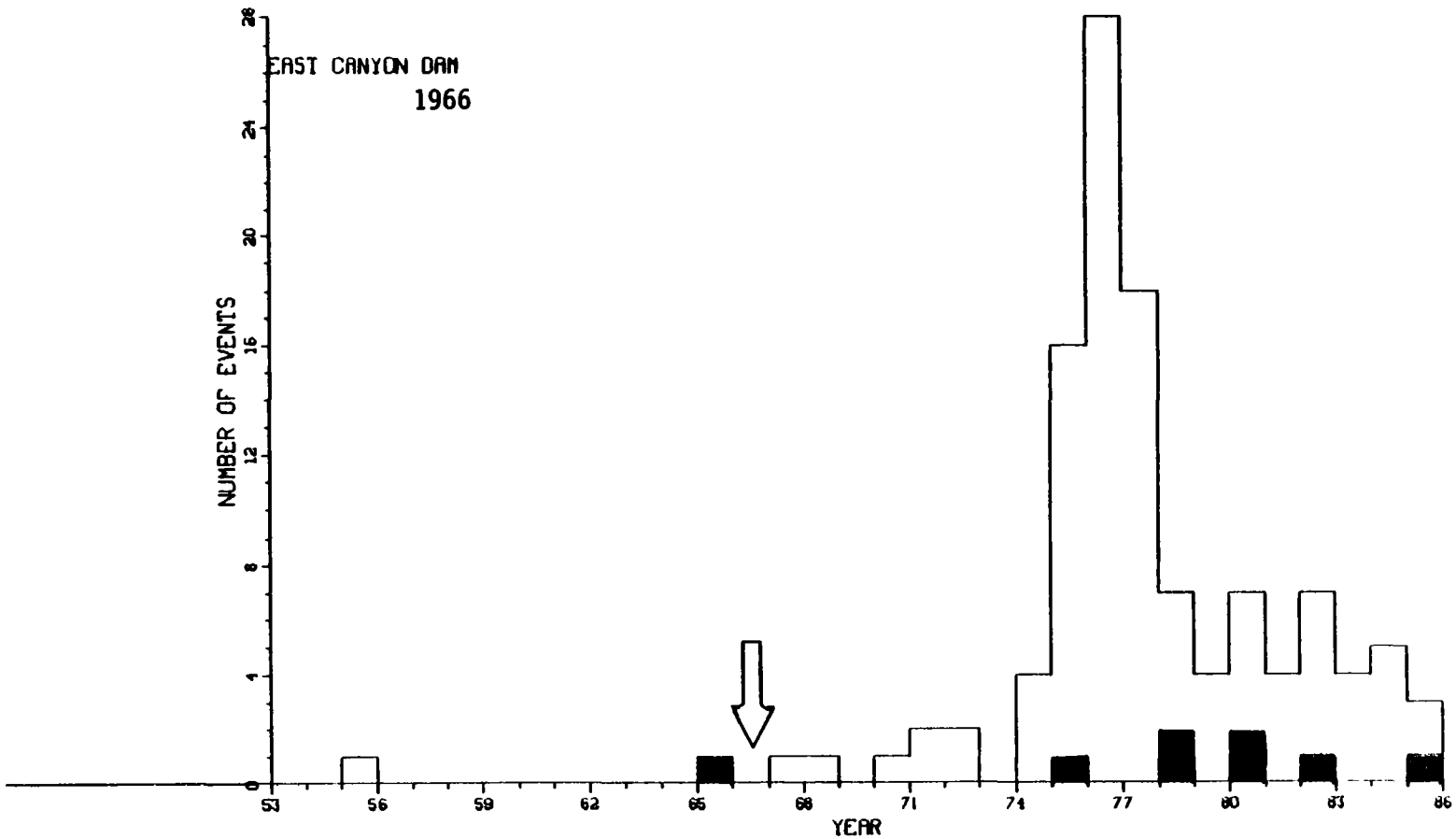

Figure B-2c. Yearly event count for East Canyon Dam. Arrow signifies year of initial reservoir filling. Solid portions indicate events $\geq$ magnitude 2.3

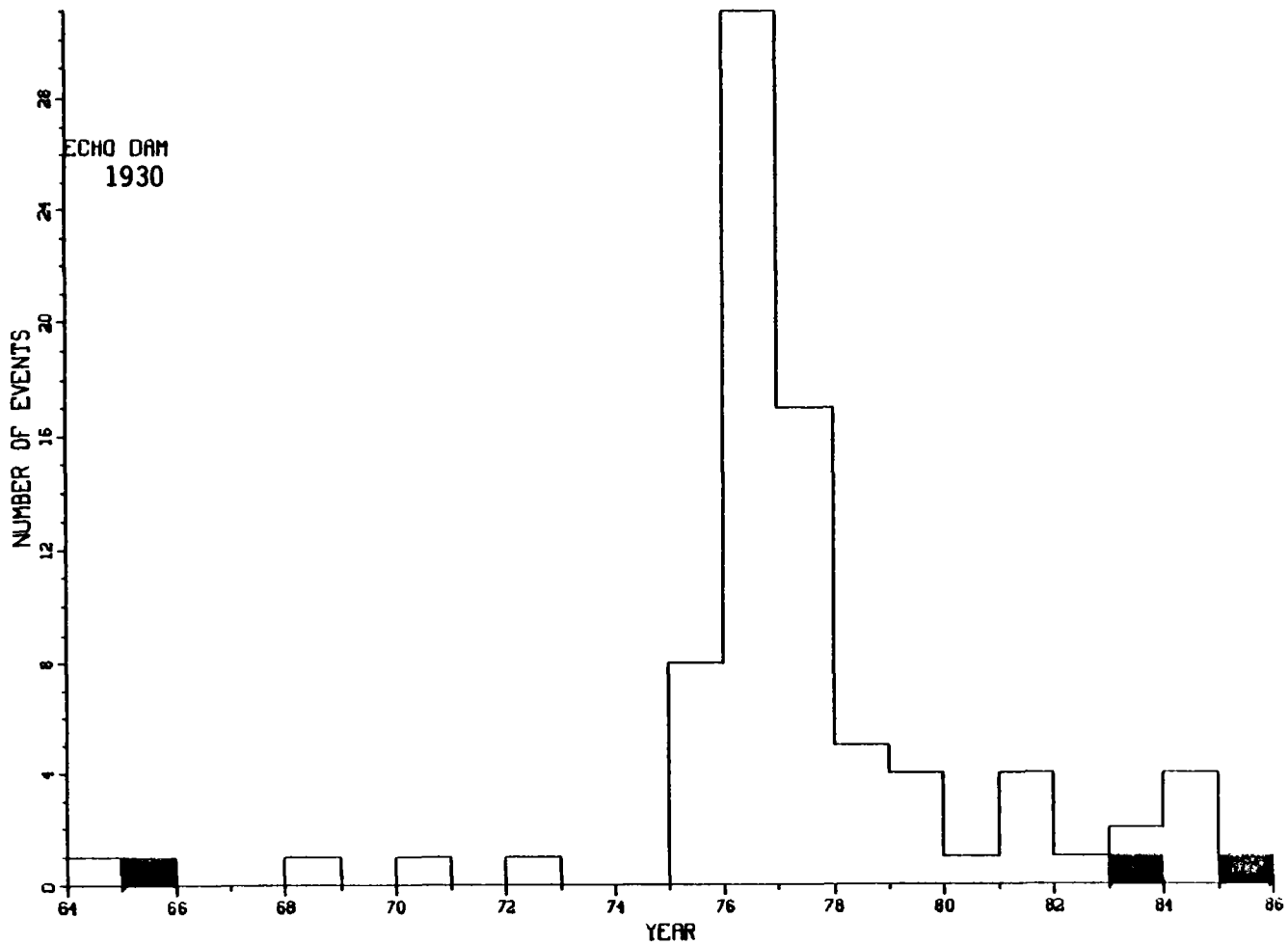

Figure B-2d. Yearly event count for Echo Dam. Arrow signifies year of initial reservoir filling. Solid portions indicate events $\geq$ magnitude 2.3.

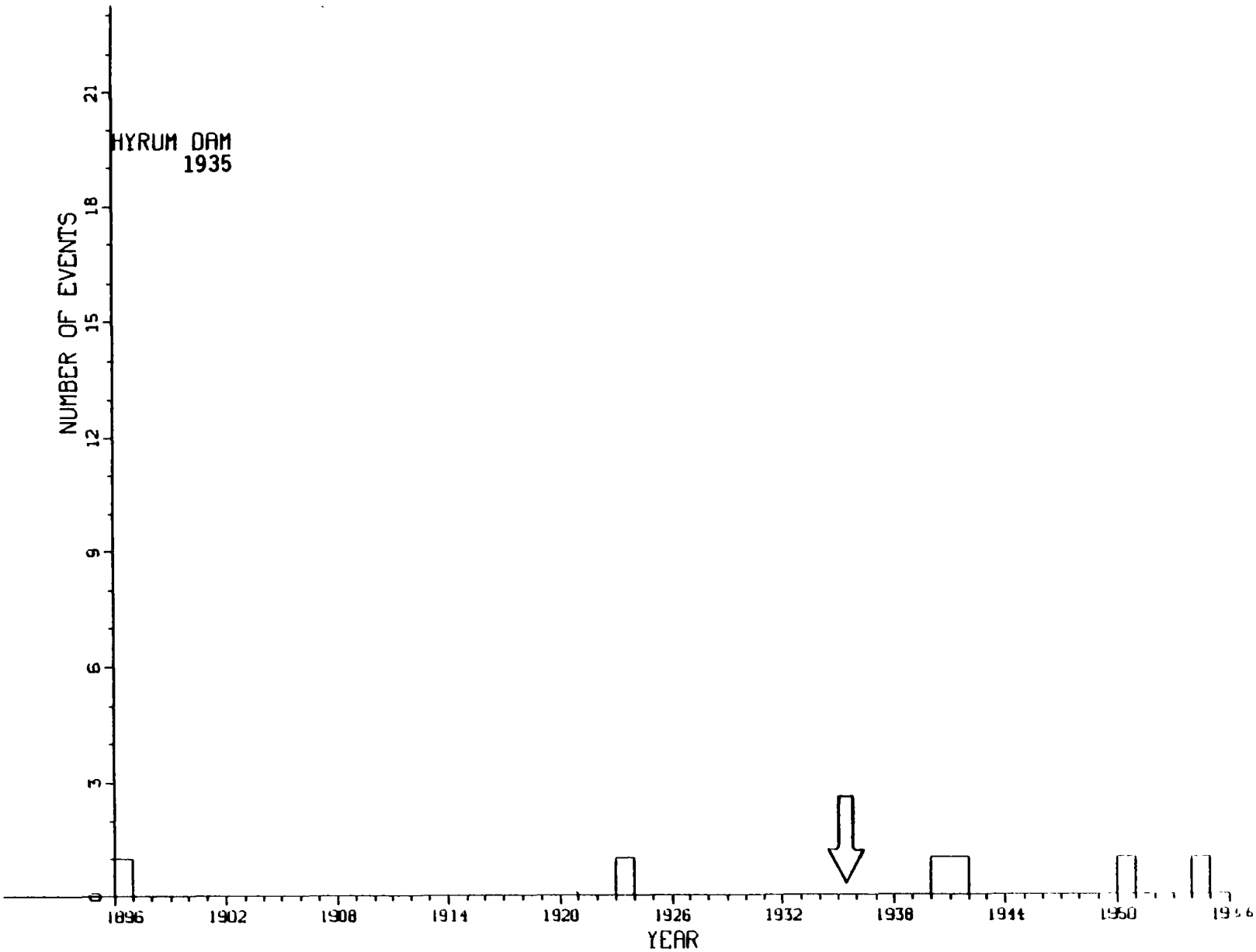

Figure B-2e. Yearly event count for Hyrum Dam. Arrow signifies year of initial reservoir filling.

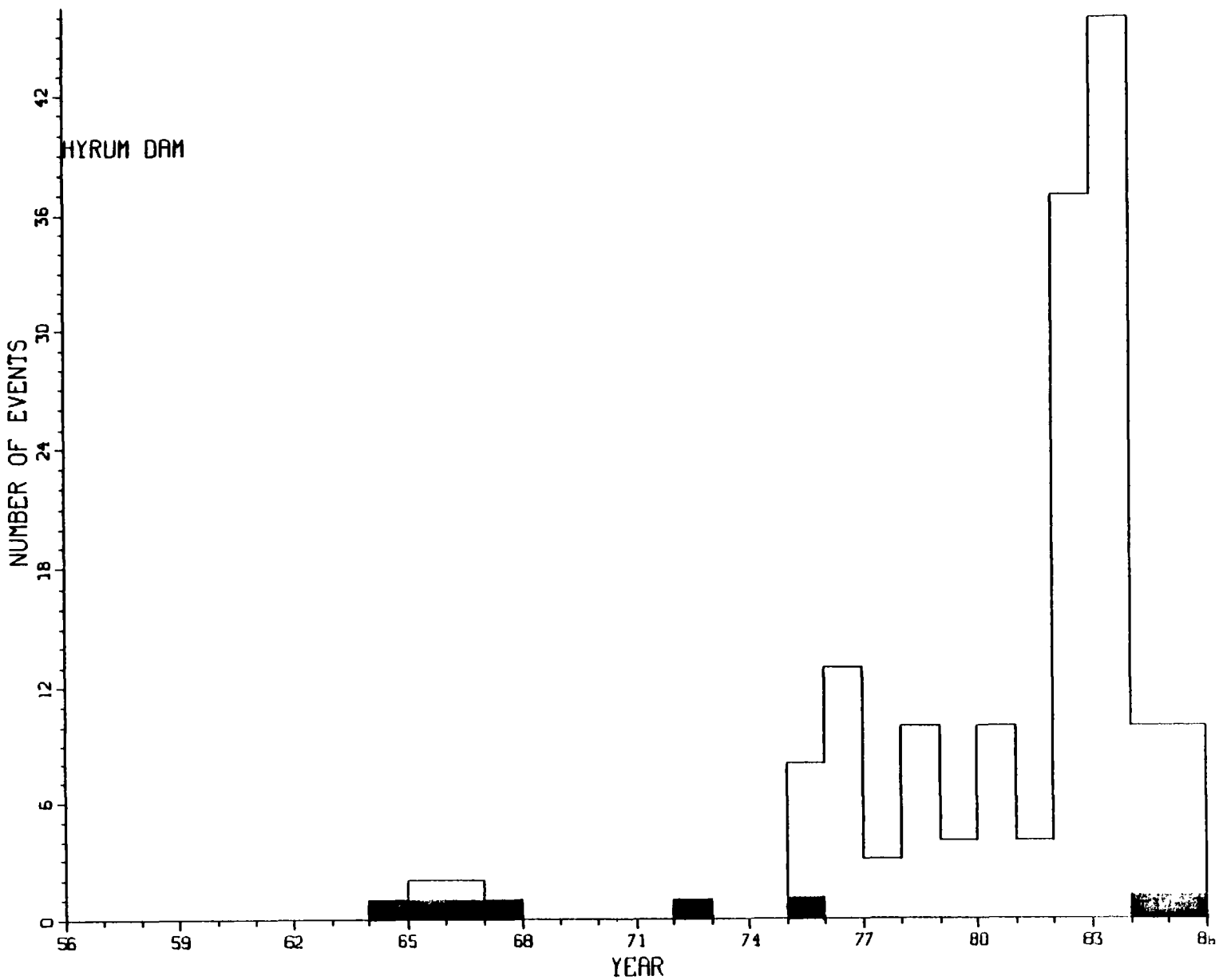

Figure B-2e (Cont'd) . Solid portions indicate events ≥ magnitude 2.3.

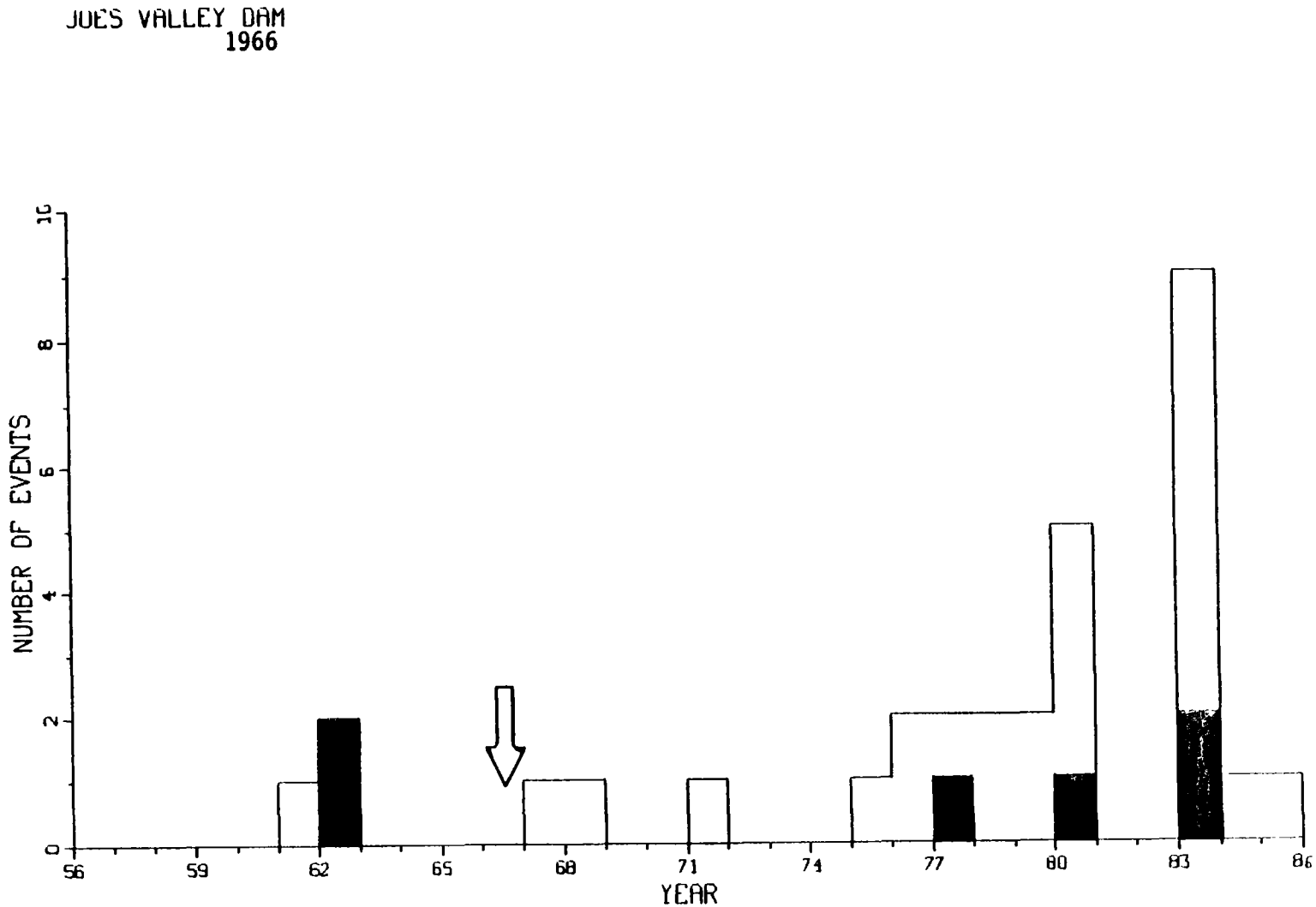

Figure B-2f. Yearly event count for Joes Valley Dam. Arrow signifies year of initial reservoir filling. Solid portions indicate events ≥ magnitude 2.3.

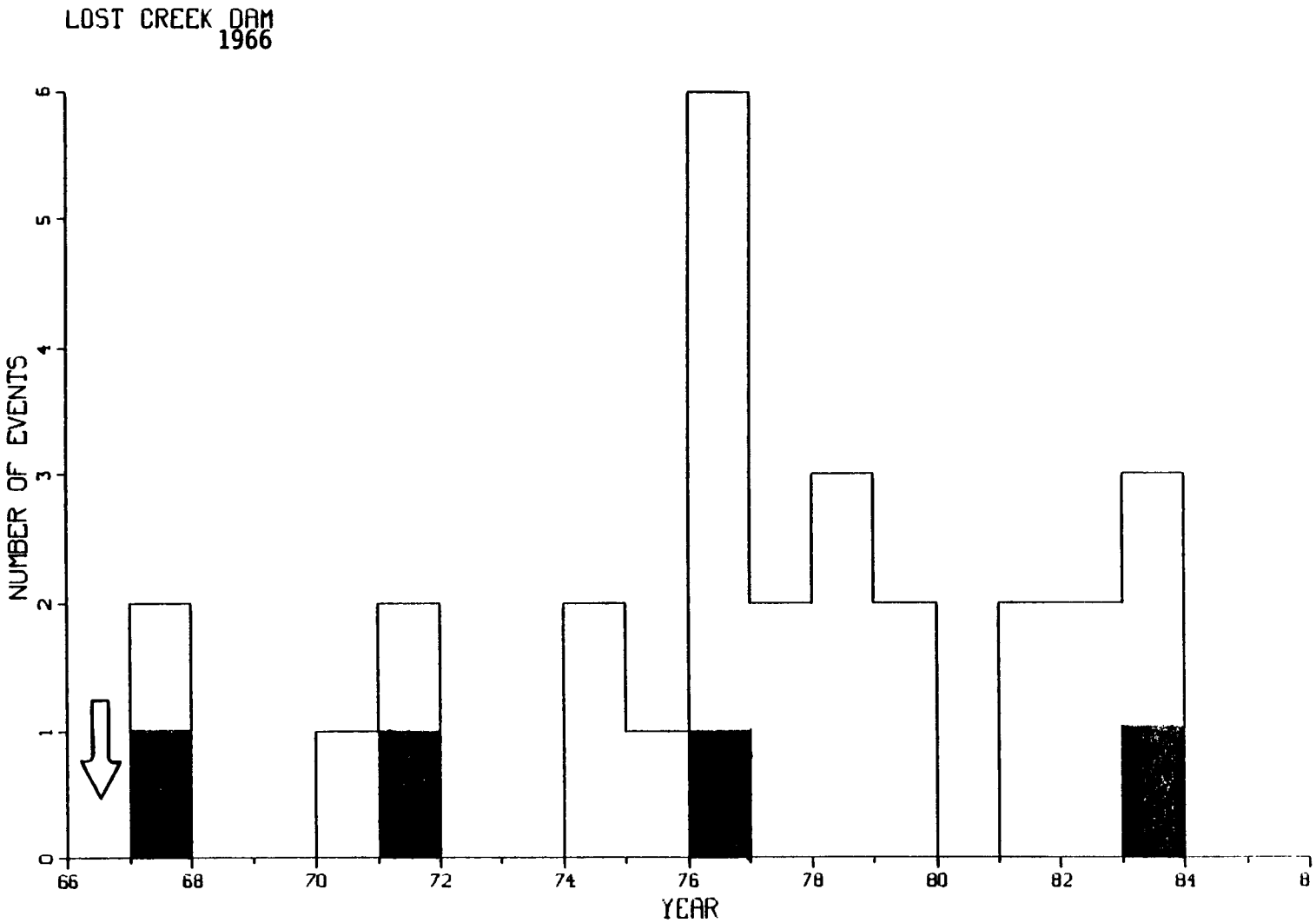

Figure B-2g. Yearly event count for Lost Creek Dam. Arrow signifies year of initial reservoir filling. Solid portions indicate events ≥ magnitude 2.3.

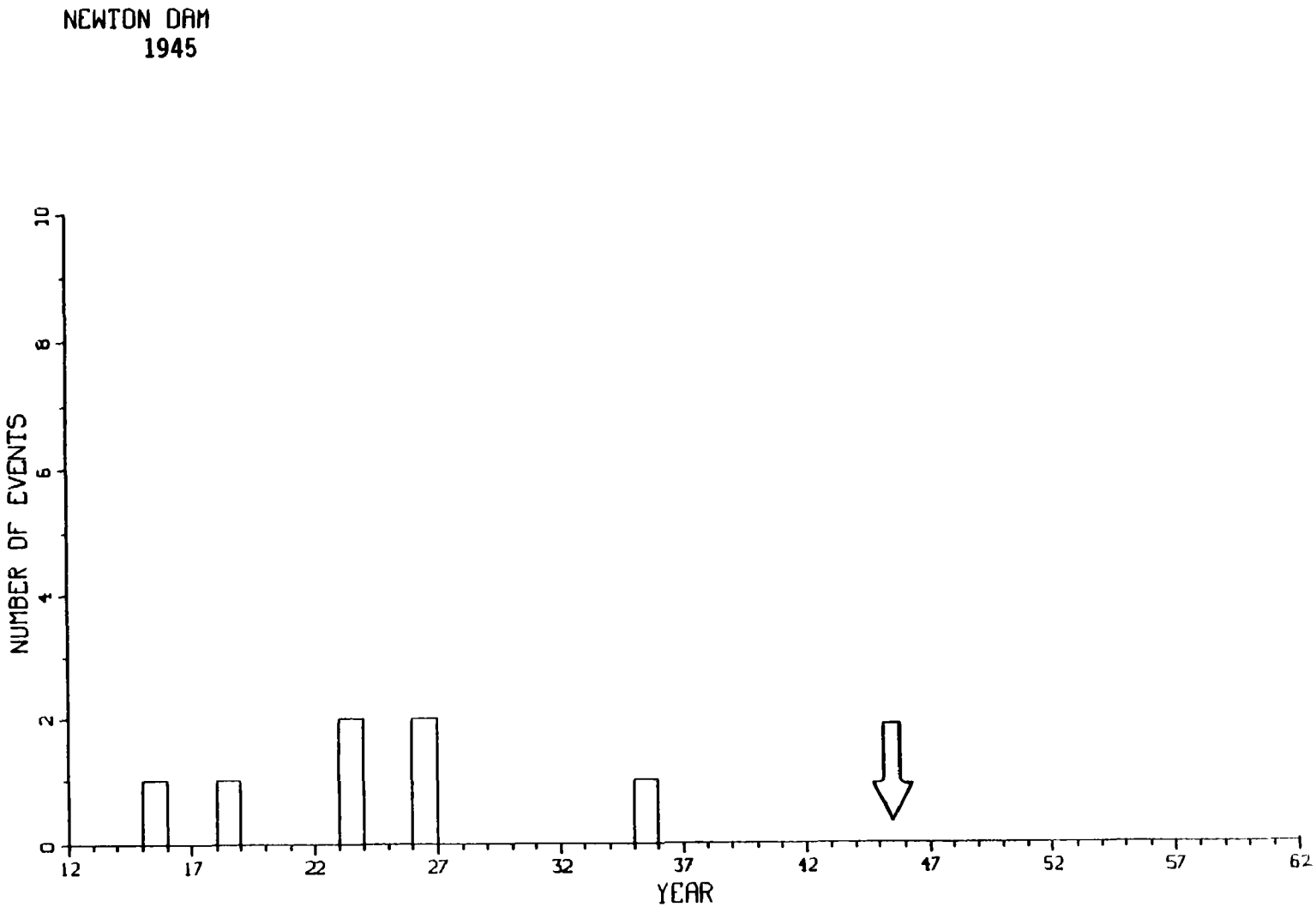

Figure B-2h. Yearly event count for Newton Dam. Arrow signifies year of initial reservoir filling.

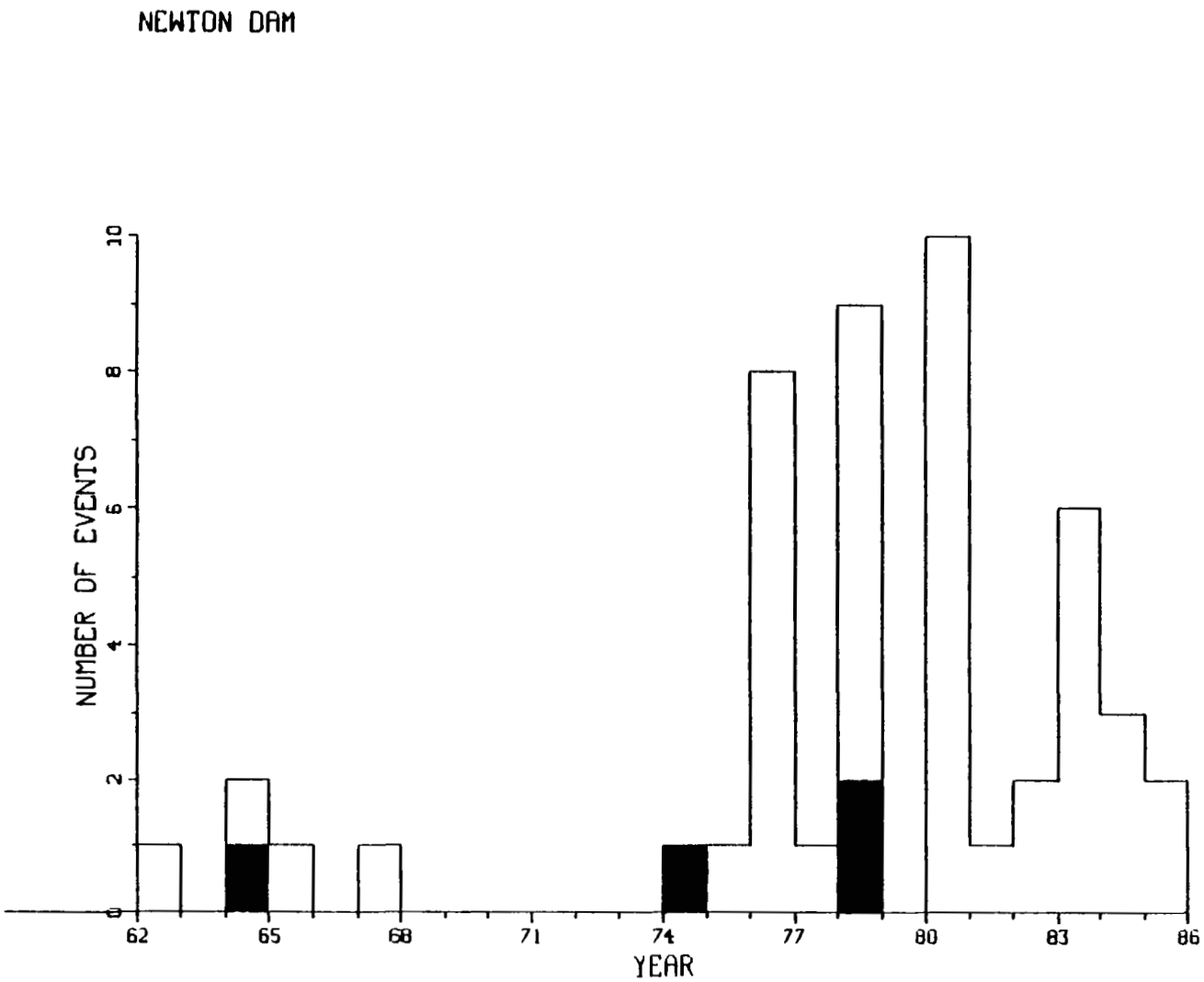

Figure B-2h (Cont'd). Solid portions indicate events ≥ magnitude 2.3.

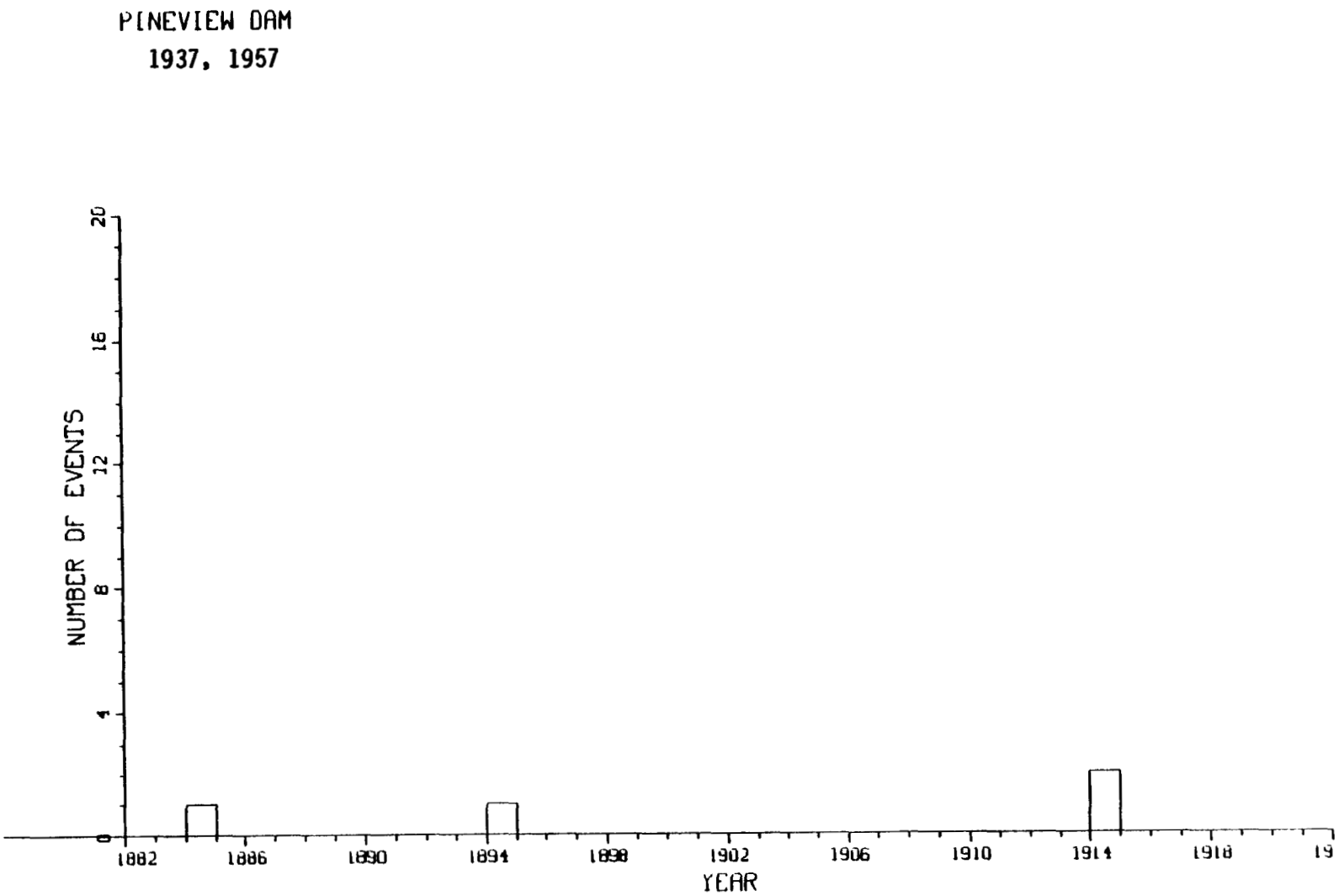

Figure B-2i. Yearly event count for Pineview Dam. Arrow signifies year of initial reservoir filling.

PINEVIEW DAM

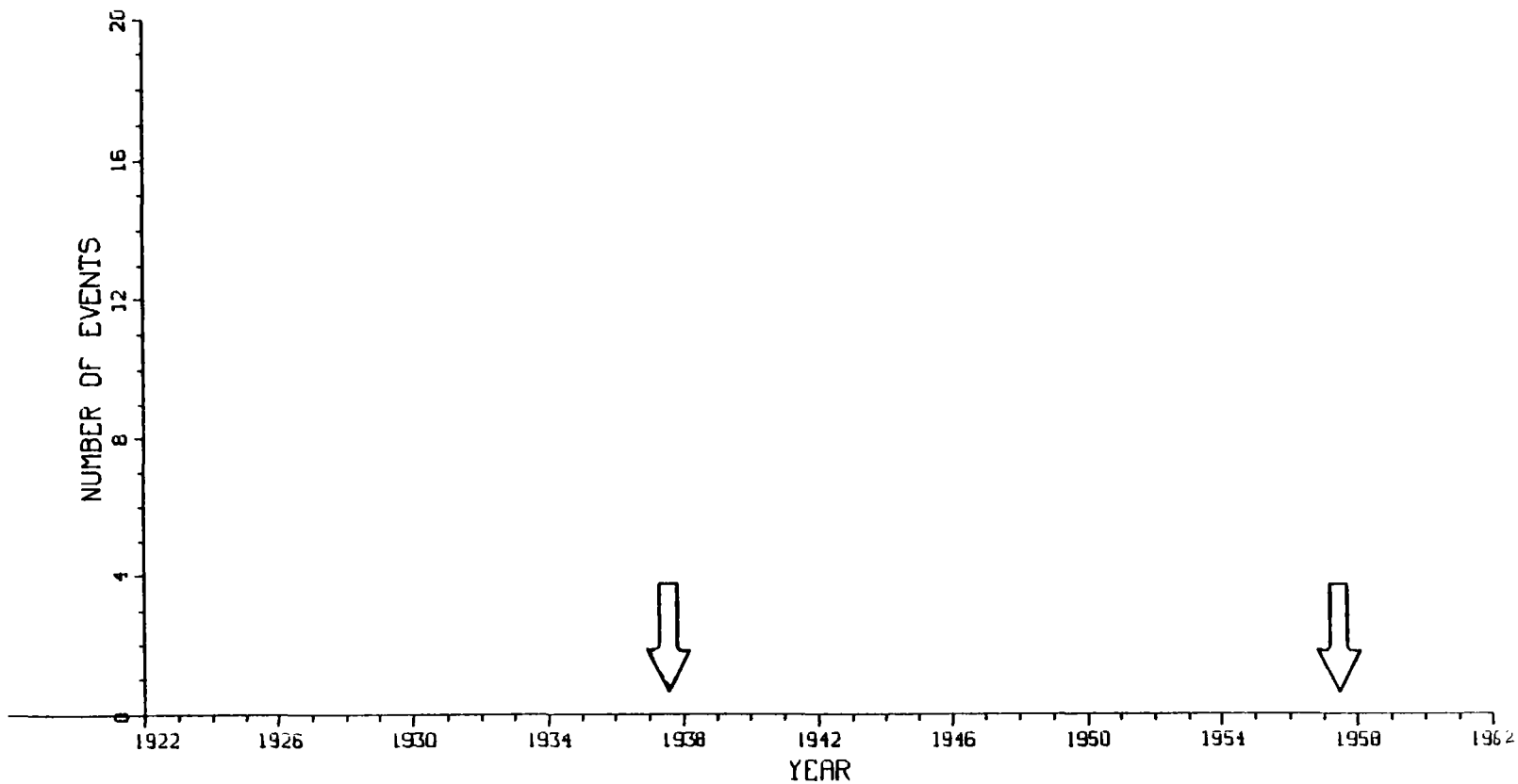

Figure B-2i (Cont'd)

PINEVIEW DAM

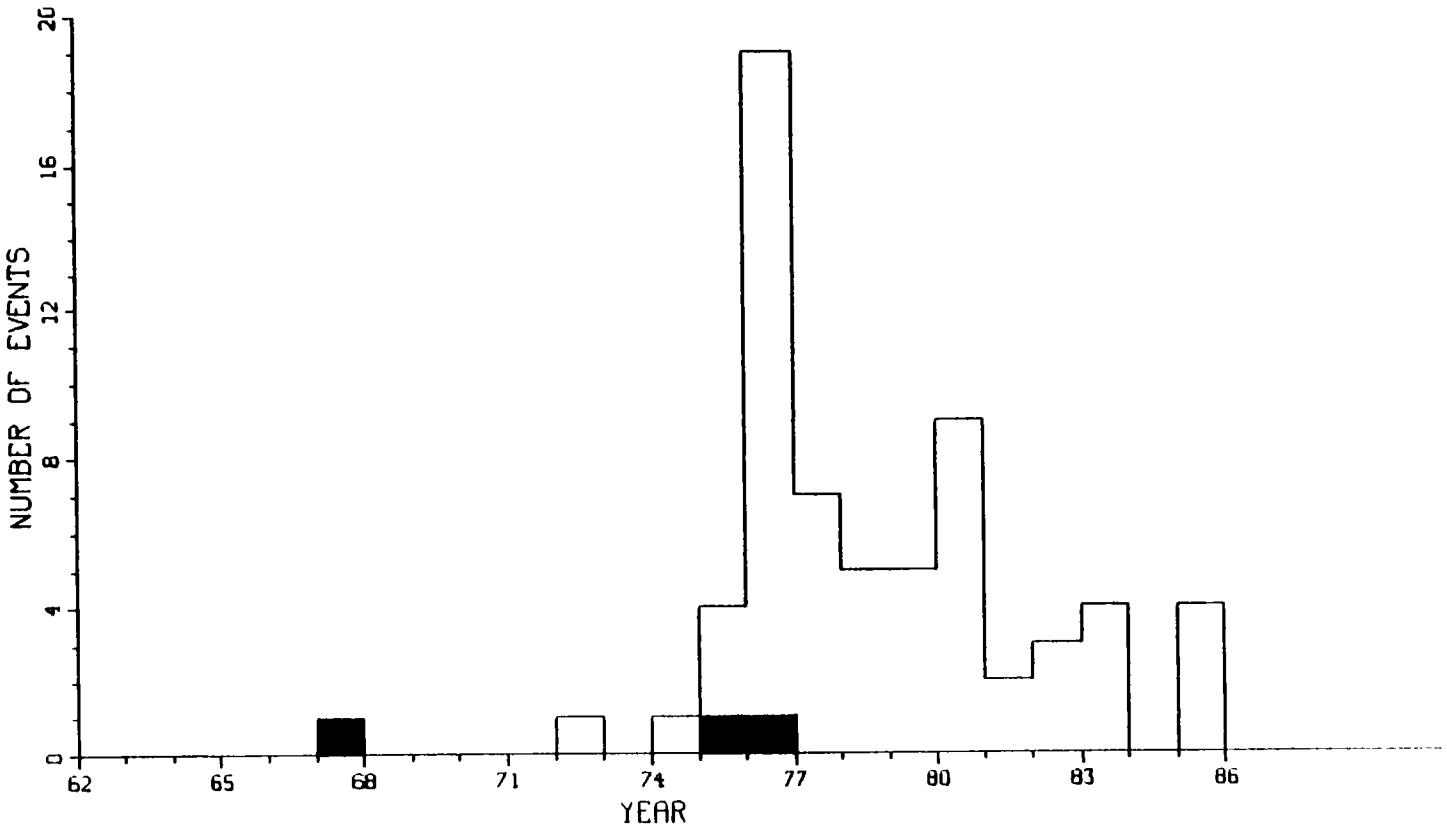

Figure B-2i (Cont'd)

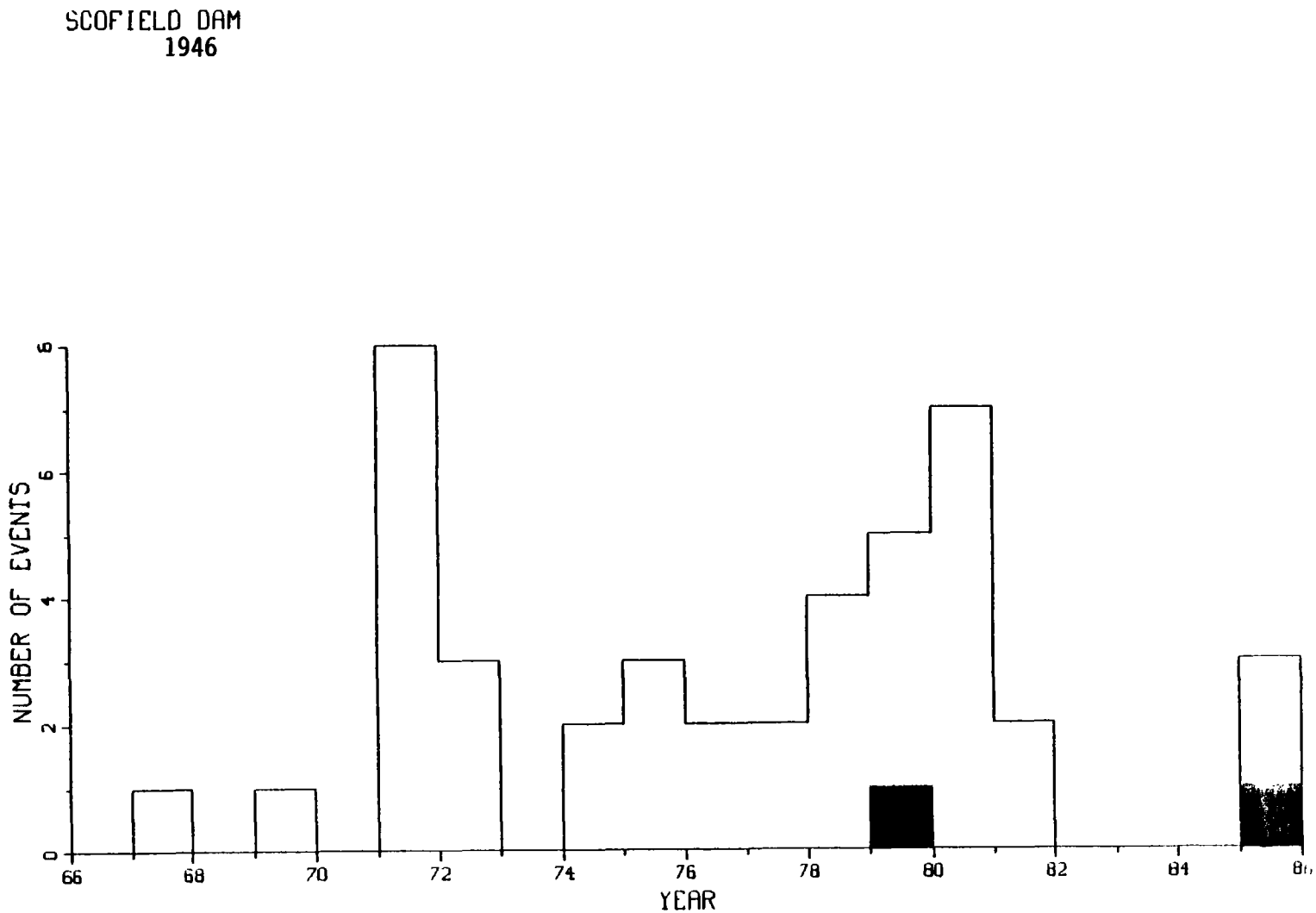

Figure B-2j. Yearly event count for Scofield Dam. Arrow signifies year of initial reservoir filling. Solid portions indicate events $\geq$ magnitude 2.3.

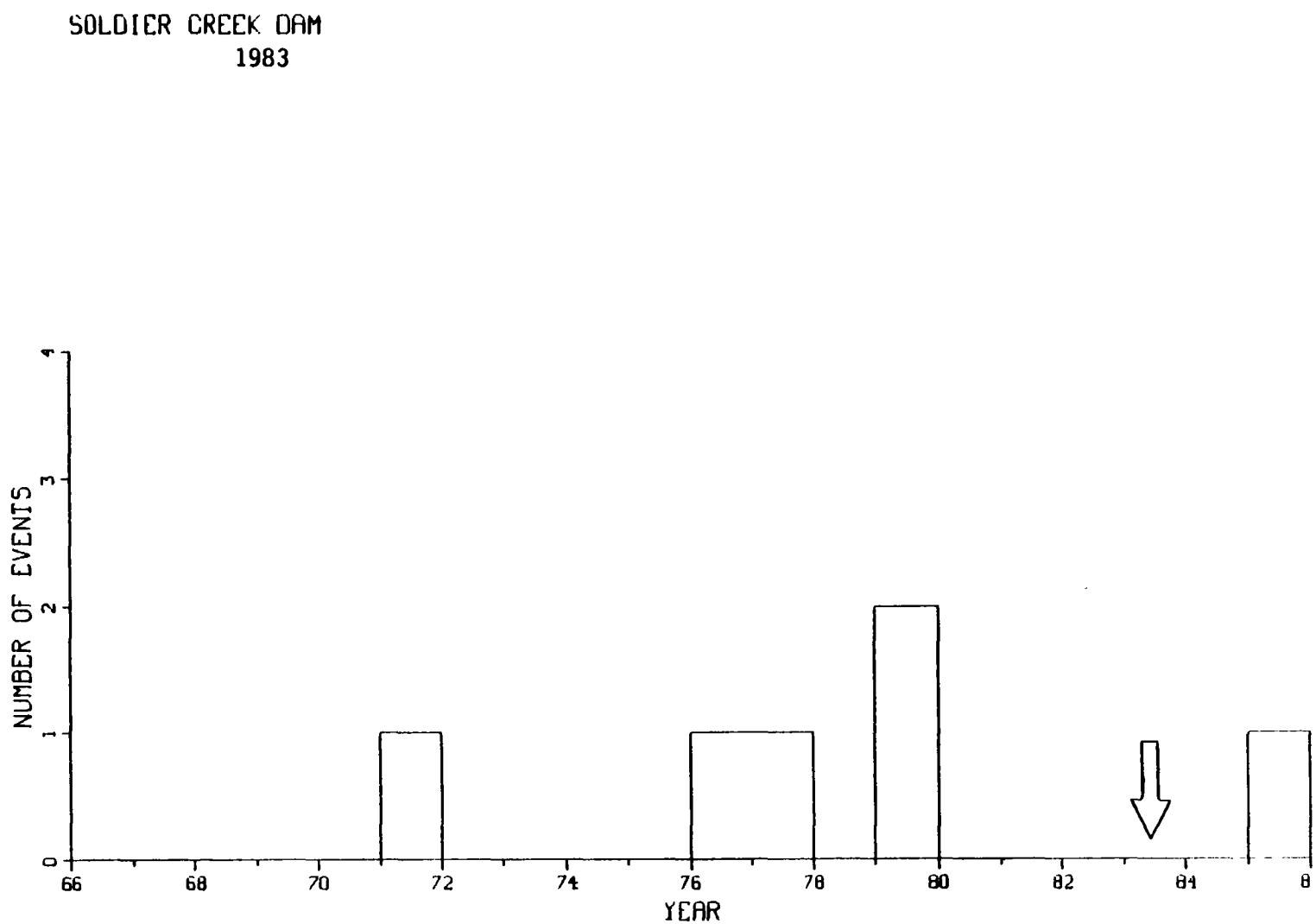

Figure B-2k. Yearly event count for Soldier Creek Dam. Arrow signifies year of initial reservoir filling.

STRAWBERRY DAM
1913

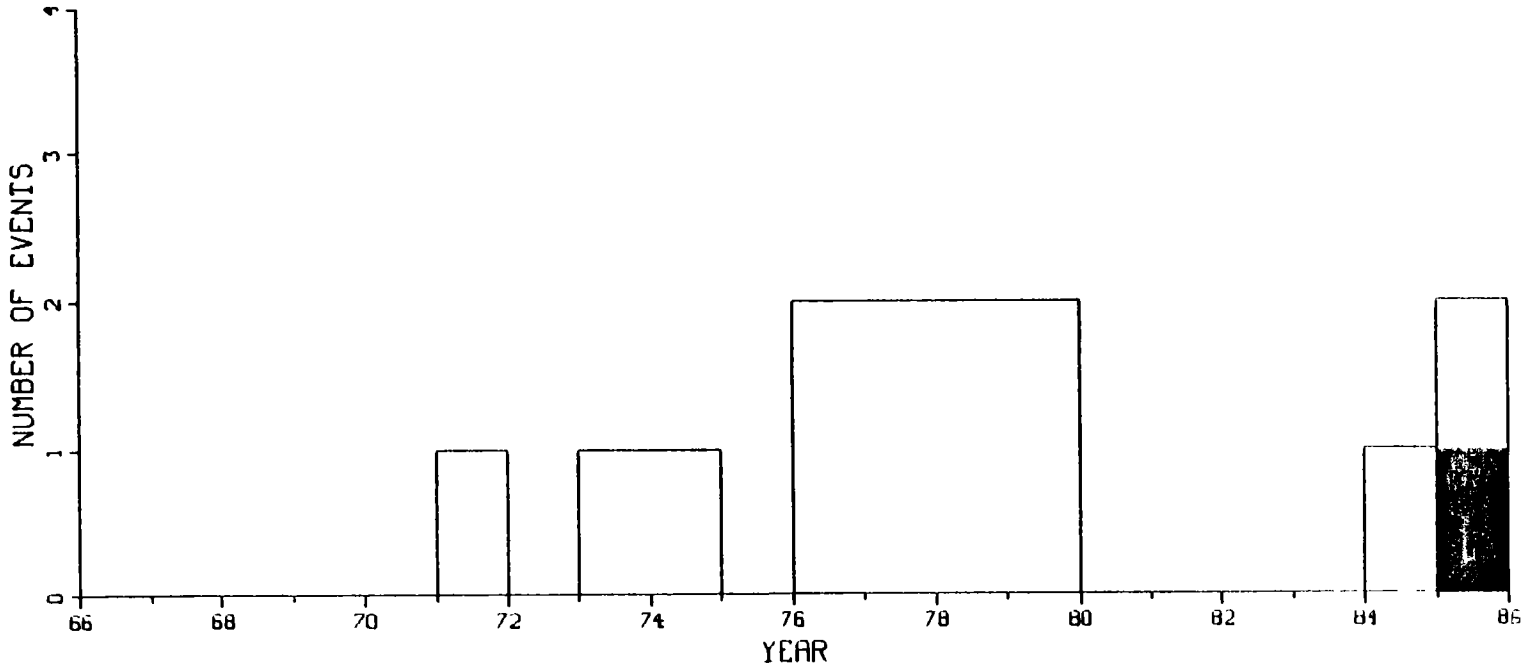

Figure B-21. Yearly event count for Strawberry Dam. Arrow signifies year of initial reservoir filling. Solid portions indicate events $\geq$ magnitude 2.3.

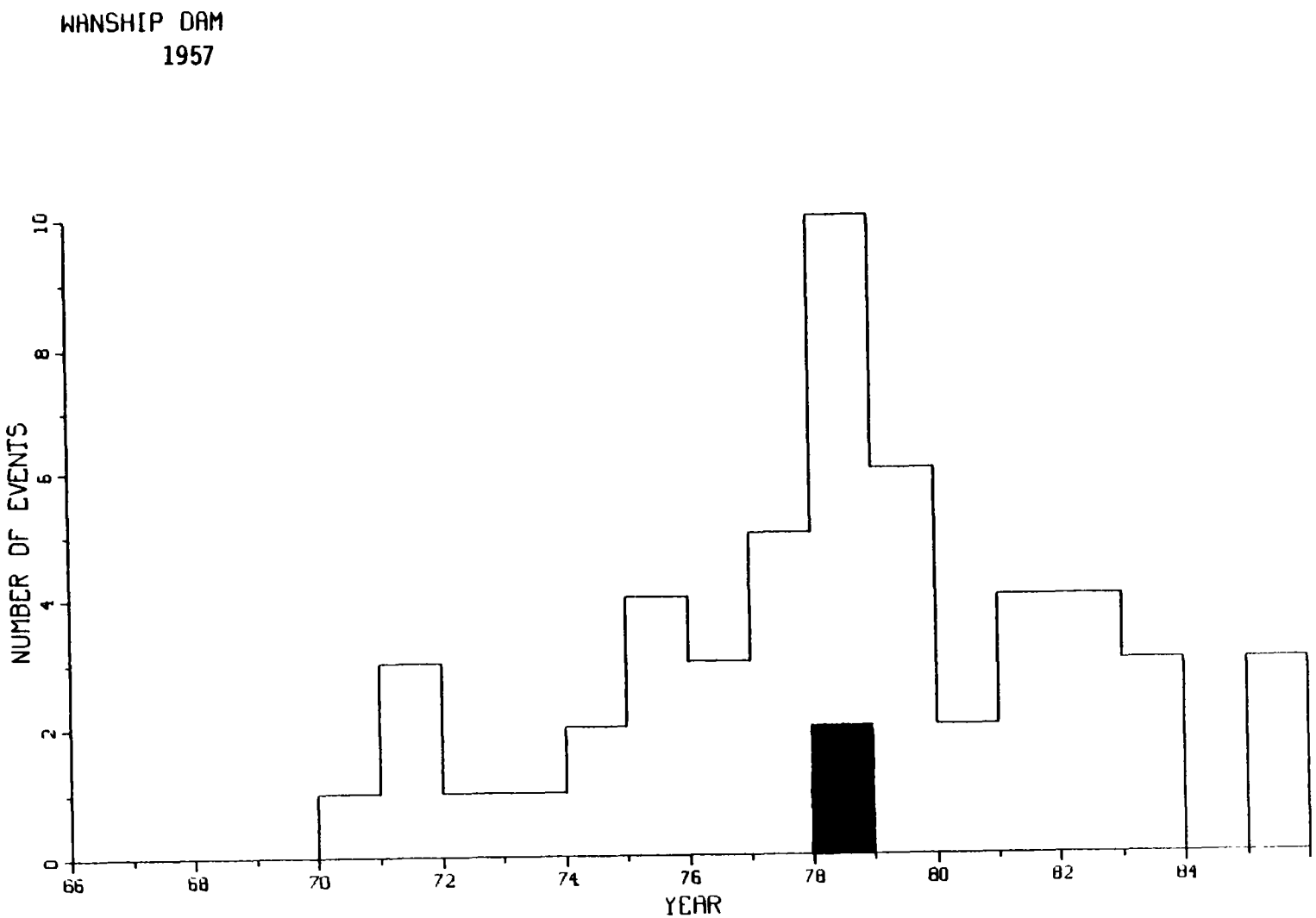

Figure B-2m. Yearly event count for Wanship Dam. Arrow signifies year of initial reservoir filling. Solid portions indicate events $\geq$ magnitude 2.3.

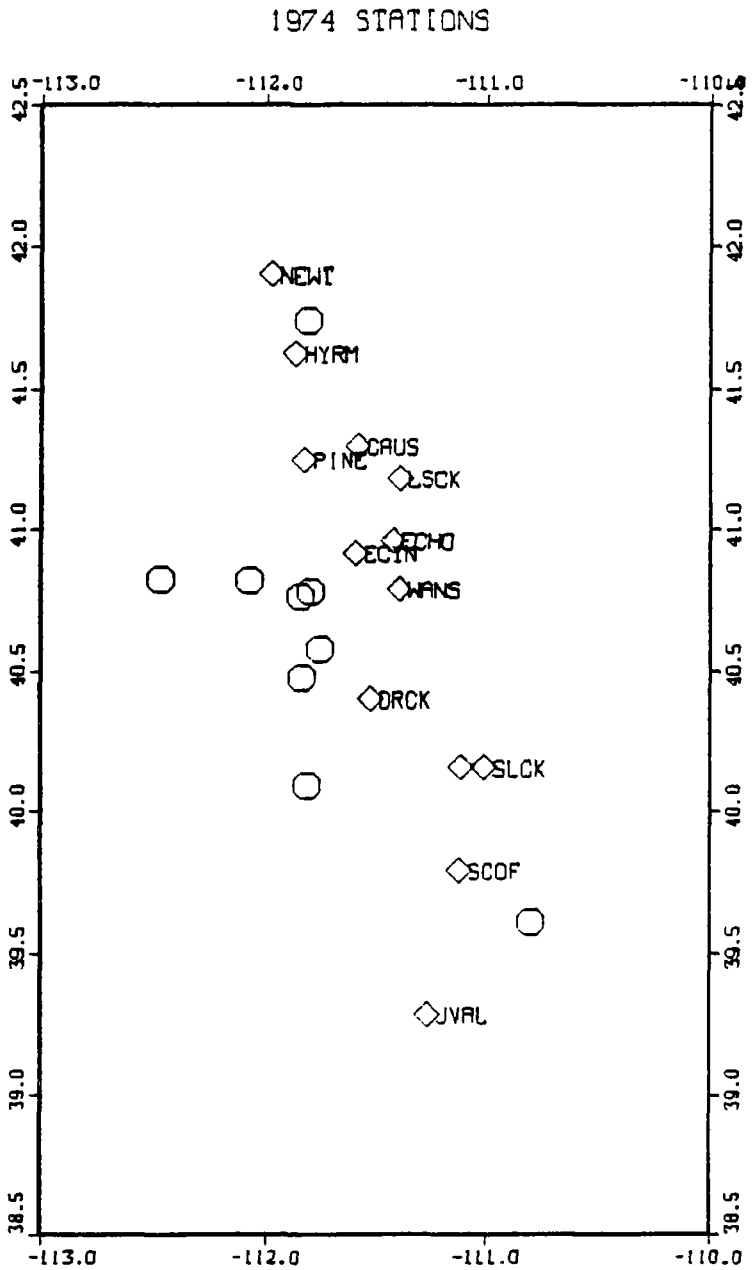

Dam	Code
Causey	CAUS
Deer Creek	DRCK
East Canyon	ECYN
Echo	ECHO
Hyrum	HYRM
Joes Valley	JVAL
Lost Creek	LSCK
Newton	NEWT
Pineview	PINE
Scofield	SCOF
Soldier Creek	SLCK
Strawberry	*
Wanship	WANS

*directly west of SLCK

Figure B-3a. Stations (octagons) operated for 7 or more months of 1974. Dams shown as diamonds.

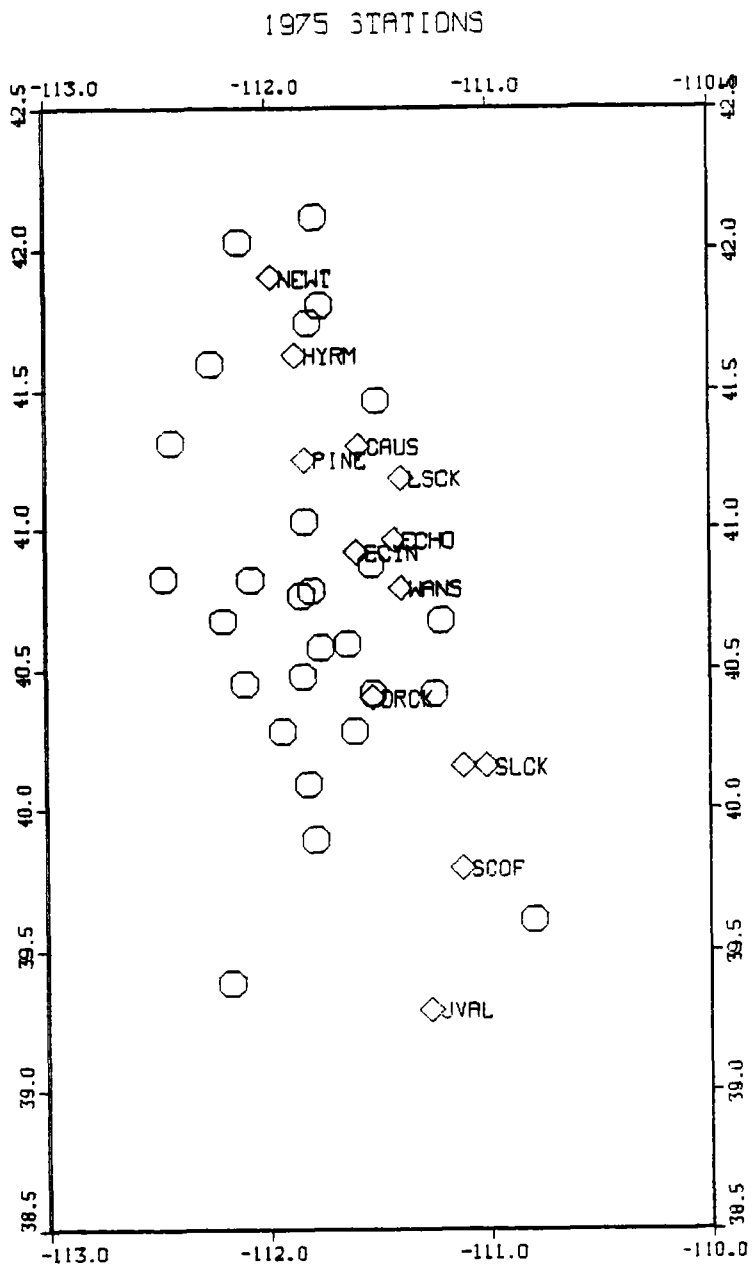

Figure B-3b. Stations (octagons) operated for 7 or more months of 1975. Dams shown as diamonds.

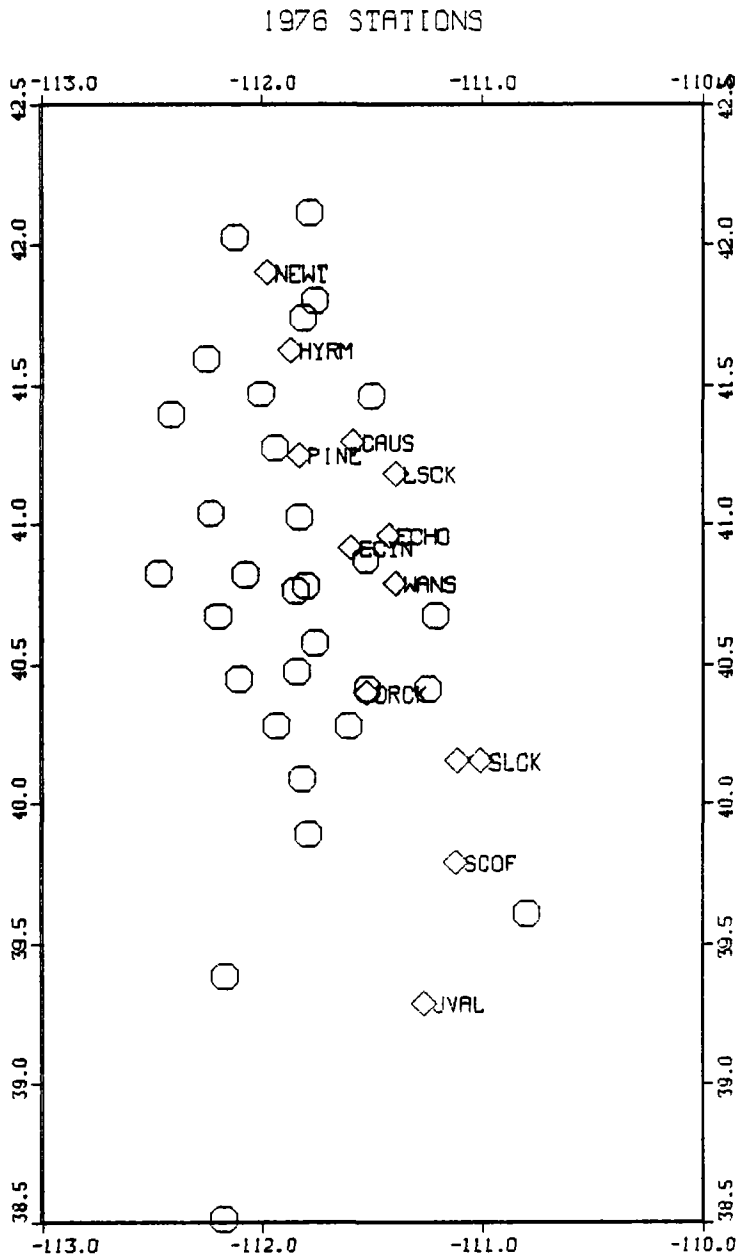

Figure B-3c. Stations (octagons) operated for 7 or more months of 1976. Dams shown as diamonds.

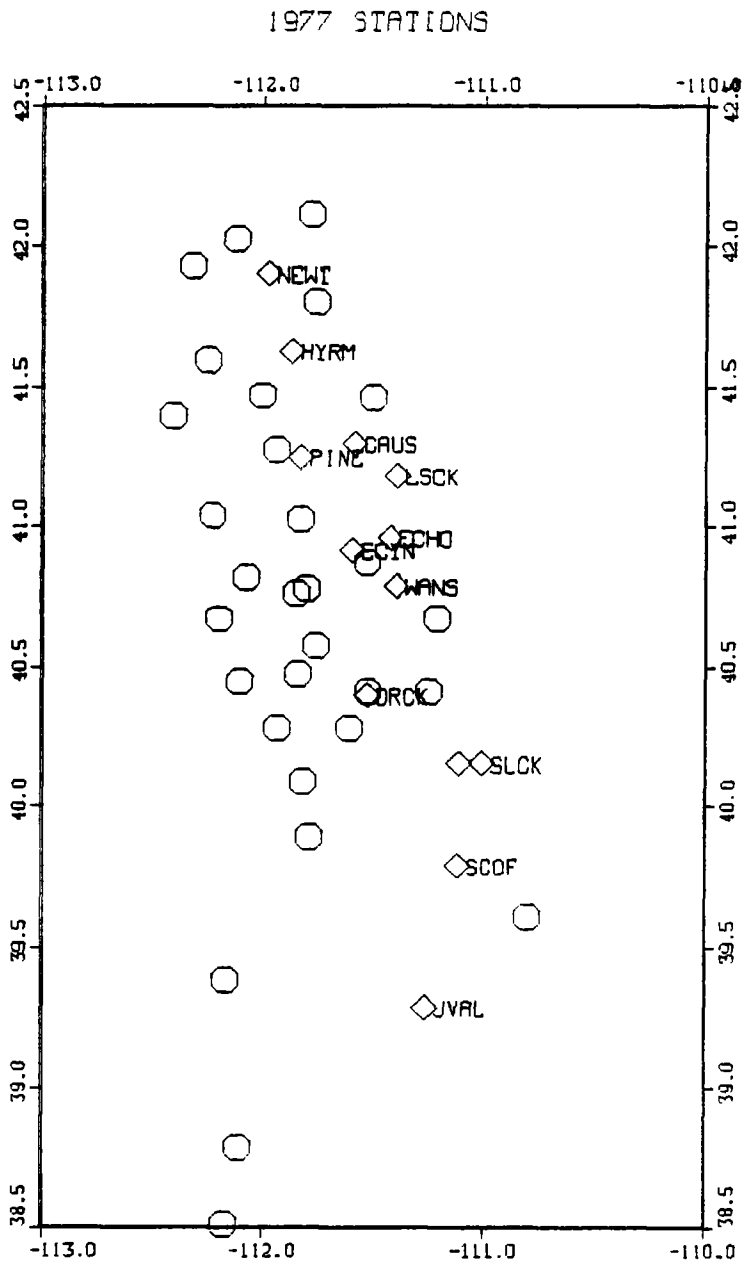

Figure B-3d. Stations (octagons) operated for 7 or more months of 1977. Dams shown as diamonds.

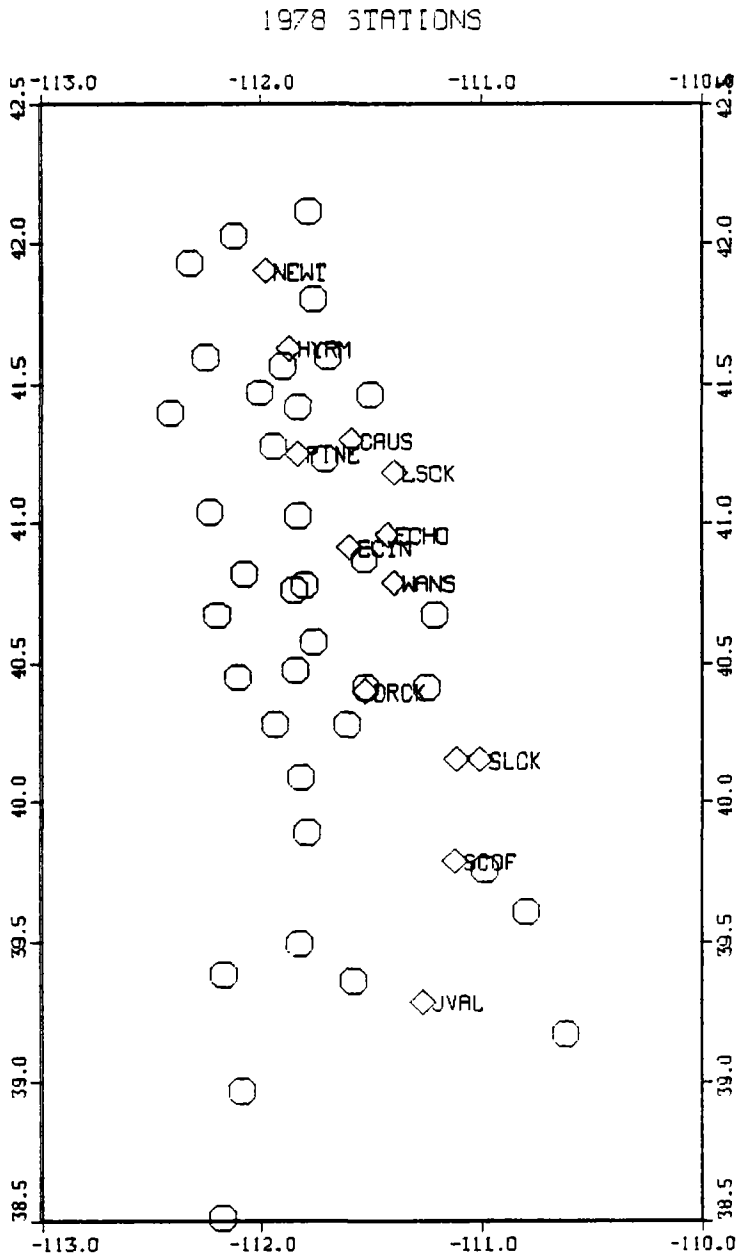

Figure B-3e. Stations (octagons) operated for 7 or more months of 1978. Dams shown as diamonds.

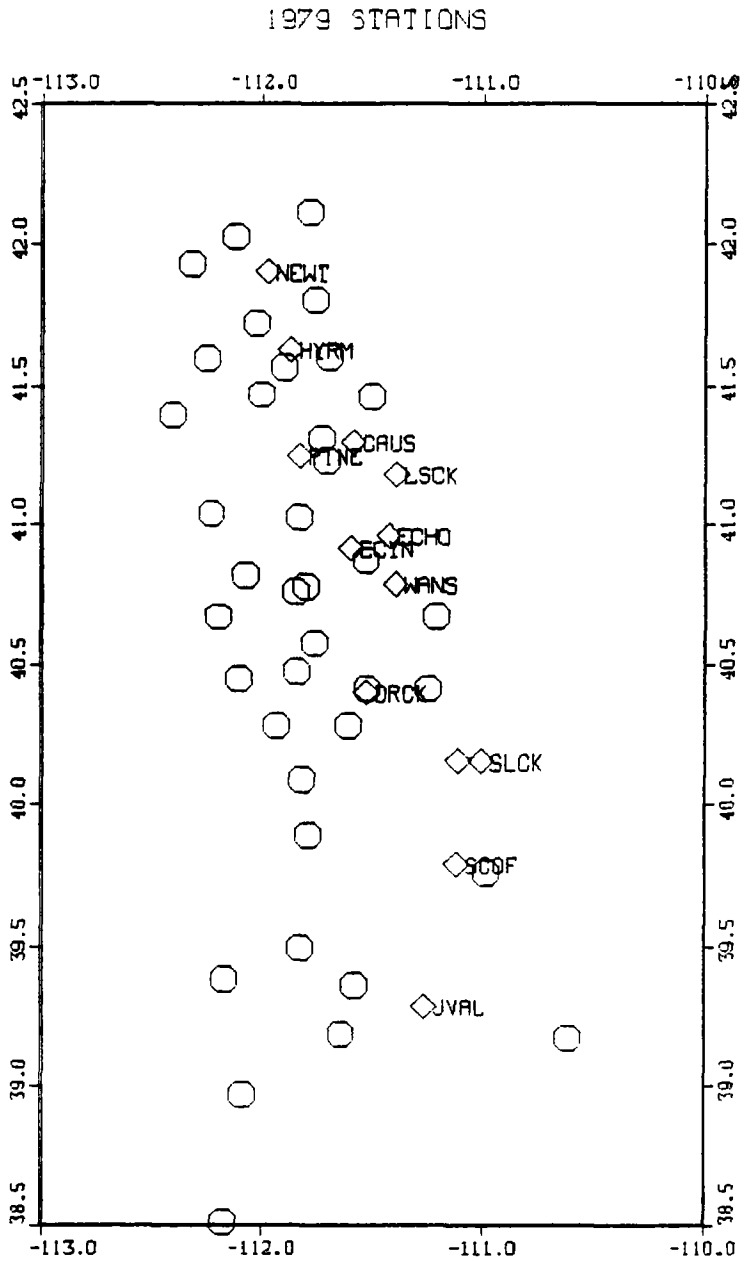

Figure B-3f. Stations (octagons) operated for 7 or more months of 1979. Dams shown as diamonds.

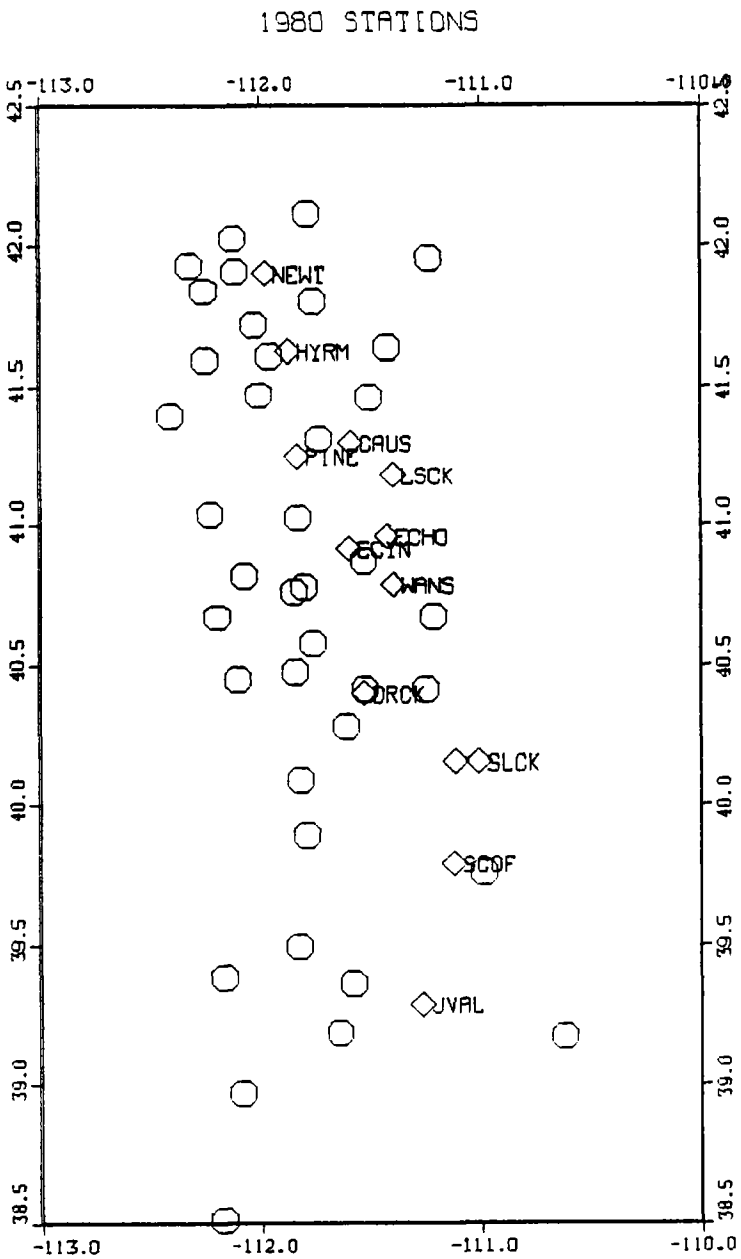

Figure B-3g. Stations (octagons) operated for 7 or more months of 1980. Dams shown as diamonds.

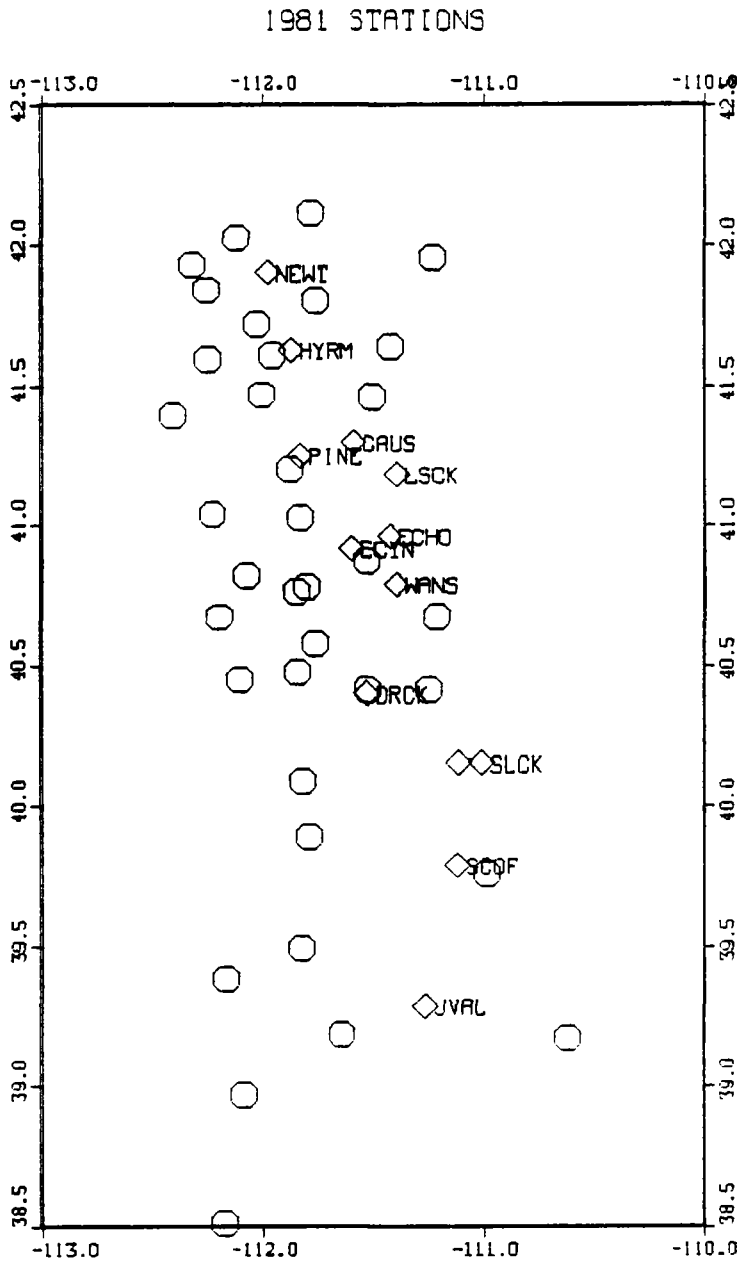

Figure B-3h. Stations (octagons) operated for 7 or more months of 1981. Dams shown as diamonds.

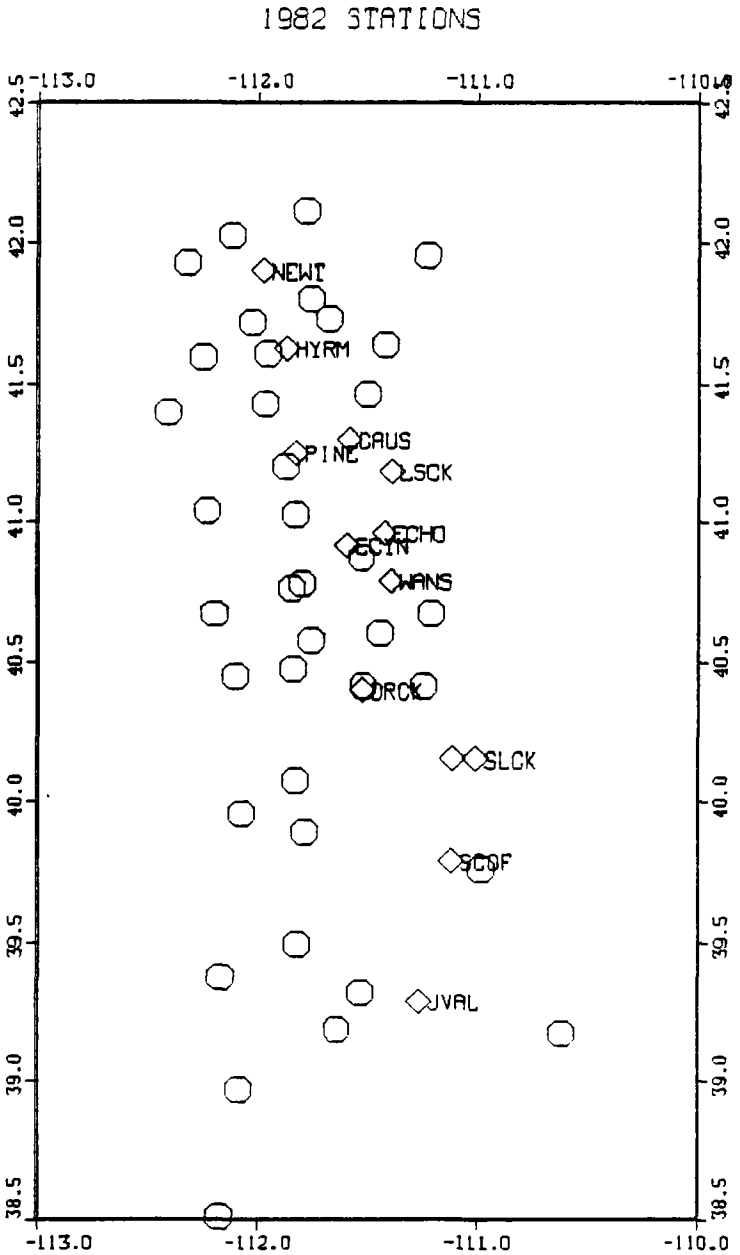

Figure B-3i. Stations (octagons) operated for 7 or more months of 1982. Dams shown as diamonds.

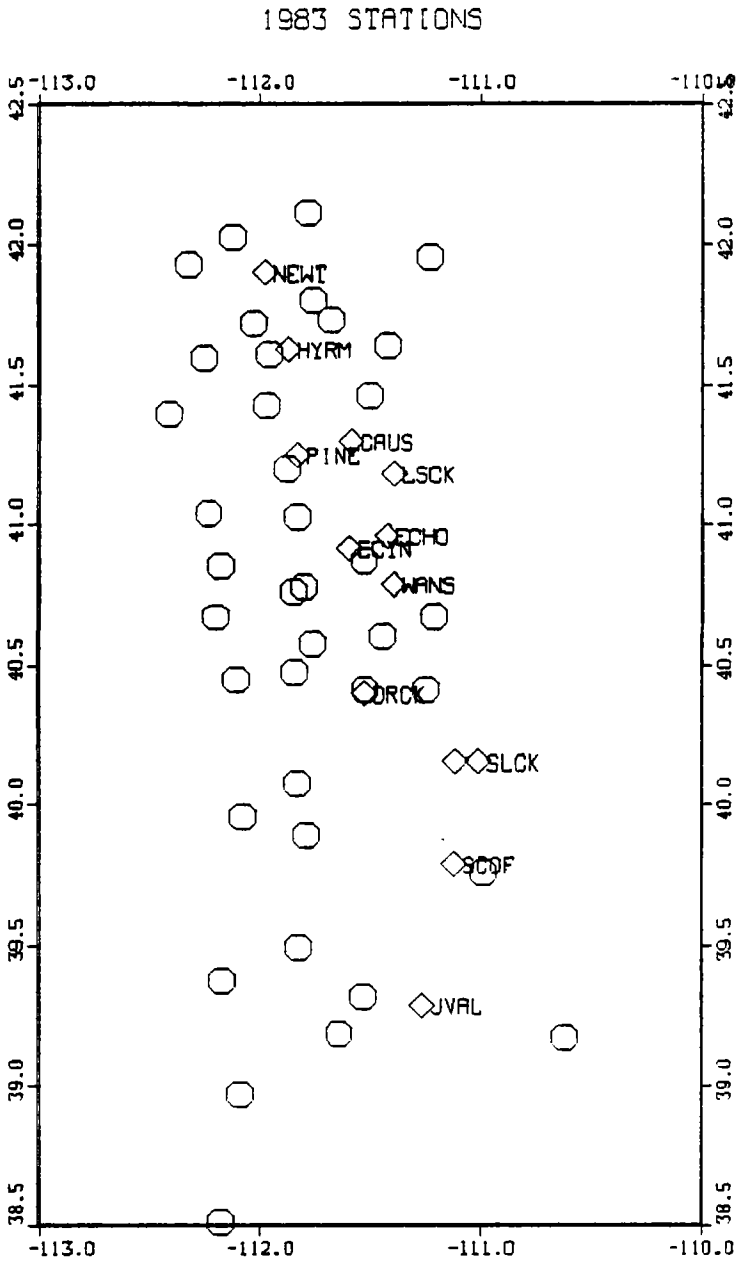

Figure B-3j. Stations (octagons) operated for 7 or more months of 1983. Dams shown as diamonds.

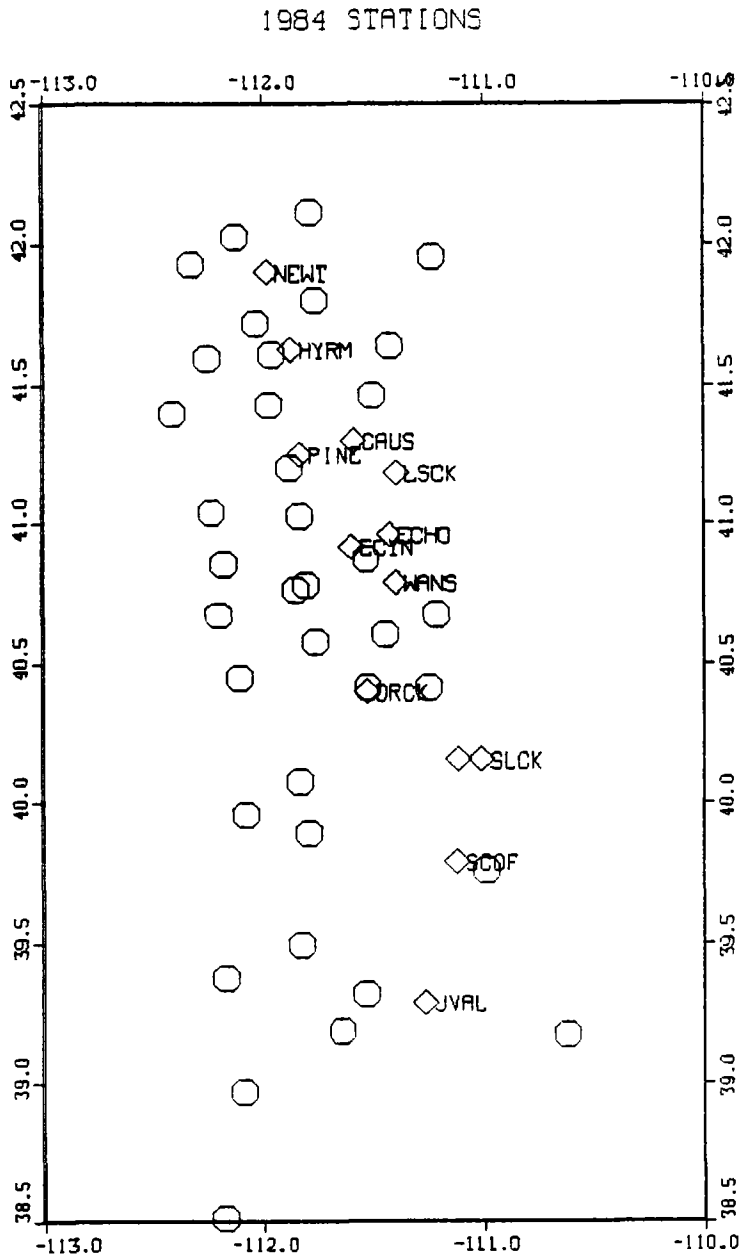

Figure B-3k. Stations (octagons) operated for 7 or more months of 1984. Dams shown as diamonds.

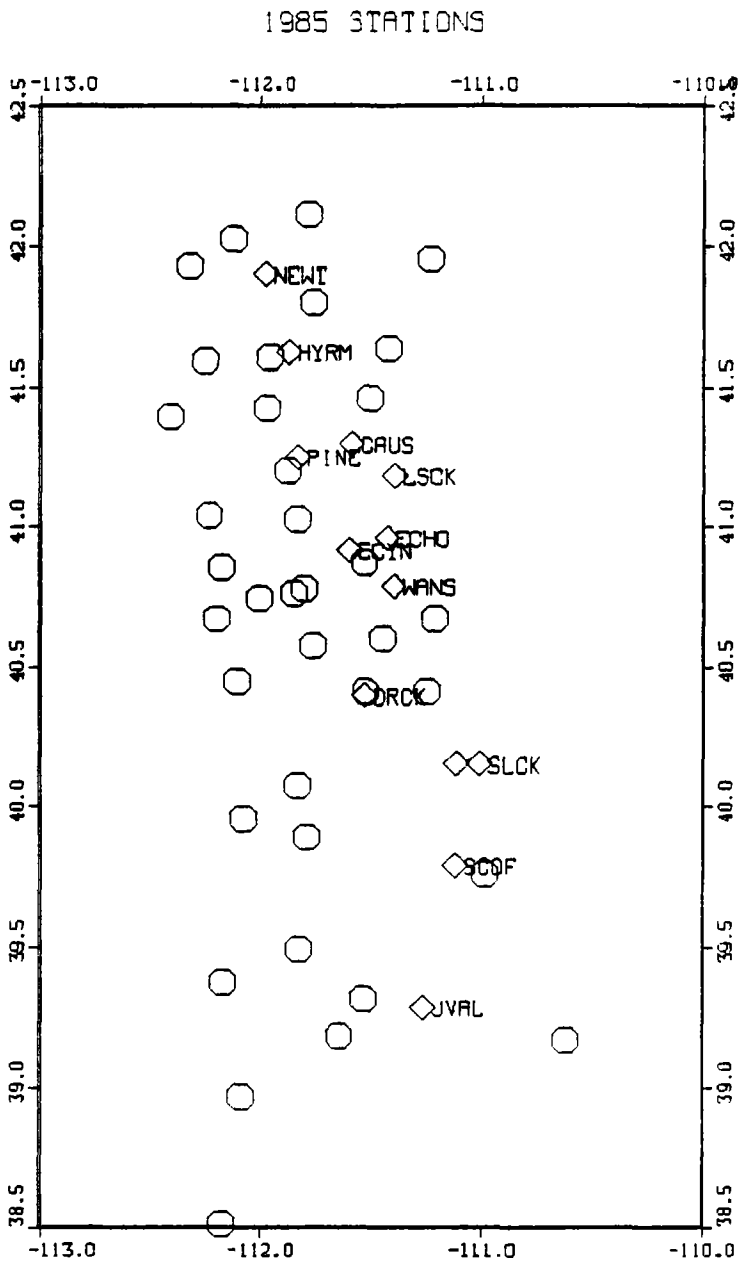

Figure B-31. Stations (octagons) operated for 7 or more months of 1985. Dams shown as diamonds.

References

Arabasz, W.J., R.B. Smith, and W.D. Richins, 1979, Earthquake studies along the Wasatch Front, Utah: Network monitoring, seismicity, and seismic hazards, in Arabasz, W.J., R.B. Smith, and W.D. Richins, eds., Earthquake studies in Utah, 1850-1978, University of Utah Seismograph Stations, Department of Geology and Geophysics, University of Utah, Salt Lake City, Utah, pp. 253-285.

_____, 1980, Earthquake studies along the Wasatch front, Utah: Network monitoring, seismicity, and seismic hazards, Bulletin of the Seismological Society of America, vol. 70, pp. 1479-1499.

Baecher, G.B., and R.L. Keeney, 1982, Statistical examination of reservoir induced seismicity, Bulletin of the Seismological Society of America, vol. 72, pp. 553-571.

Bones, D.G., 1978, Seismicity of the intermountain seismic belt in southeastern Idaho and western Wyoming, and tectonic implications, M.S. Thesis, Department of Geology and Geophysics, University of Utah, Salt Lake City, Utah, 131 pp.

Bufe, C.G., 1976, The Anderson Reservoir seismic gap - induced aseismicity?, Engineering Geology, vol. 10, pp.,255-263.

Carder, D.S., 1945, Seismic investigations in the Boulder Dam area, 1940-1944, and the influence of reservoir loading activity, Bulletin of the Seismological Society of America, vol. 35, pp. 175-192.

Foley, L.L., R.A. Martin, and J.T. Sullivan, 1986, Seismotectonic study for Joes Valley, Scofield, and Huntington north dams, Emery County and Scofield projects, Utah, Seismotectonic Report 86-7, U.S. Bureau of Reclamation, Denver, Colorado.

Gough, D.I., and Gough, W.I., 1970, Load-induced earthquakes at Lake Kariba, Geophysical Journal of the Royal Astronomical Society, vol. 21, pp. 79-101.

Guha, S.K., 1977, Premonitory crustal deformations, strains, and seismotectonic features (b-values) preceding Koyna earthquakes, Abstracts of the 1977 International Symposium on recent crustal movements, Stanford University, Palo Alto, CA.

Gupta, H.K., H. Narain, B.K. Rastogi, and I. Mohan, 1969, A study of the Koyna earthquake of December 10, 1967, Bulletin of the Seismological Society of America, vol. 59, pp. 1149-1162.

_____, B.K. Rastogi, and H. Narain, 1972, Common features of reservoir- induced seismic activities, Bulletin of the Seismological Society of America, vol. 62, pp. 481-492.

_____ and J. Combs, 1976, Continued seismic activity at the Koyna reservoir site, India, Engineering Geology, vol. 10, pp. 367-313.

_____ and B.K. Rastogi, 1976, Dams and Earthquakes, Elsevier Publishing, Amsterdam, 299 pp.

_____, C.V. Rama Krishna Rao, B.K. Rastogi, and S.C. Bhatia, 1980, Bulletin of the Seismological Society of America, vol. 70, pp. 1833-1847.

Jacob, K.H., W.D. Pennington, J. Armbruster, L. Seeber, and S. Farhatulla, 1979, Tarbela Reservoir, Pakistan: A region of compressional tectonics with reduced seismicity upon initial reservoir filling, Bulletin of the Seismological Society of America, vol. 69, pp. 1175-1193.

Kisslinger, C.K., 1976, A review of theories of mechanisms of induced seismicity, Engineering Geology, vol. 10, pp. 85-89.

Leith, W., D.W. Simpson, and C.H. Scholz, 1984, Two types of reservoir induced seismicity, presented at IASPEI Regional Assembly, Hyderabad, India.

Meade, R.B., 1982, The evidence for reservoir-induced macroearthquakes, State-of-the-art for assessing earthquake hazards in the United States, Report 19, U.S. Army Corps of Engineers, 194 pp.

Nuttli, O.W., 1979, The relation of sustained maximum ground acceleration and velocity to earthquake intensity and magnitude, State-of-the-Art for assessing earthquake hazards in the United States, Report no. 16, U.S. Army Engineer Waterway Experimental Station, Vicksburg, Miss., 74 pp.

Packer, D.R., J.R. Lovegreen, and J.L. Born, 1977, Reservoir-induced seismicity, vol. 6 (327 p.) in: Earthquake evaluation studies for Auburn dam, Woodward-Clyde Consultants, 8 v. NTIS report, PB-283 531/2GA, PC A15/MF A01.

_____, L.S. Cluff, P.L. Knuepfer, and R.J. Withers, 1980, Study of reservoir induced seismicity, U.S. Geological Survey Open-file Report 80-1092.

Piety, L.A., C.K. Wood, J.D. Gilbert, J.T. Sullivan, and M.H. Anders, 1986, Seismotectonic study for Palisades dam and reservoir, Palisades project, U.S. Bureau of Reclamation, Seismotectonic Report 86-3, 198 pp.

Rothé, J.P., 1970, Man-made earthquakes, Tectonophysics, vol. 9, pp. 215-238.

_____, 1973, Summary: Geophysics Report, in: Man-made lakes: their problems and environmental effects, Geophysical monograph 17, American Geophysical Union, Washington, D.C., pp. 441-454.

Schleicher, D., 1975, A model for earthquakes near Palisades reservoir, southeast Idaho, U.S. Geological Survey Journal of Research, vol. 3, pp. 393-400.

Simpson, D.W., 1976, Seismicity changes associated with reservoir loading, Engineering Geology, vol. 10, pp. 123-151.

_____, 1986, Triggered earthquakes, Annual Reviews of Earth and Planetary Science, vol. 14, pp. 21-42.

_____, and S.K. Negmatullaev, 1981, Induced seismicity at Nurek reservoir, Tadjikistan, USSR, Bulletin of the Seismological Society of America, vol. 71, pp. 1561-1586.

Smith, R.B., P.L. Winkler, J.G. Anderson, and C.H. Scholz, 1974, Source mechanisms of microearthquakes associated with underground mines in eastern Utah, Bulletin of the Seismological Society of America, vol. 64, pp. 1295-1317.

_____, and M.L. Sbar, 1974, Comtemporary tectonics and seismicity of the western United States with emphasis on the Intermountain seismic belt, Geological Society of America Bulletin, vol. 85, pp. 1205-1218.

Stuart-Alexander, D.E., and R.K. Mark, 1976, Impounding-induced seismicity associated with large reservoirs, U.S. Geological Survey Open-file Report 76-770.

Waldpole, R.E., and R.H. Meyers, 1985, Probability and Statistics for Engineers, MacMillan Publishing, New York, 639 pp.

Williams, D.J., and W.J. Arabasz, 1988, Mining related seismicity in the Wasatch Plateau, Utah, PAGEOPH, in press.

Appendix C

Static ground deformations for design earthquakes

Application to normal-faulting earthquakes in the Intermountain Seismic belt

by
Chris Wood

Seismotectonic Section
Geologic Services Branch
Division of Geology
Engineering and Research Center
Bureau of Reclamation
Denver, Colorado

April 1988

Table of Contents

1. Introduction 1
2. Historical earthquakes 4
    2.1. Surface faulting earthquakes 4
    2.2. Earthquakes on buried faults 8
3. Computation of displacements 13
    3.1. Previous work 13
    3.2. Description of models 15
    3.3. Examples from historic ISB earthquakes 17
4. Parametric analysis 24
    4.1. Point sources 24
    4.2. Finite sources 29
    4.3. Implications for design earthquakes 40
5. Discussion 41

References 43

List of Figures

1. Uniform slip planar fault model 16
2. Representation of a planar fault 18
3. Elevation change profile of the Hebgen Lake earthquake 20
4. Elevation change profile of the Borah Peak earthquake 21
5. Elevation change profile of the Pocatello Valley 22
6. Elevation change profile of the Yellowstone earthquake 23
7. Elevation change profiles for a point moment source 26
7a. Same as figure 7, but for a 60° dipping source 27
8. Effect of varying dip for a point moment source 28
9. Effect of varying depth for a finite dislocation surface 30
9a. Same as figure 9, but for 60° dip 31
10. Effect of varying dip for a finite dislocation surface 32
11. Elevation profile for planar source... at a depth of 1 km 34
12. Same as figure 11, but for burial depth of 2 km 35
13. Same as figure 11, but for burial depth of 3 km 36
14. Same as figure 11, but for burial depth of 5 km 37
15. Effect of curvature... average dip of 60° 38
15a. Effect of curvature... average dip of 45° 39

List of Tables

1. Historical (post-1910) surface faulting earthquakes 5
2. Historical $M \geq 6$ non-surface-faulting earthquakes 9
3. Faulting parameters used to model elevation changes 19

1. Introduction

Elastic behavior of the earth's crust has been used to explain deformation of the ground surface accompanying large earthquakes since at least Reid (1911). This study examines the static vertical displacements (elevation changes) of the ground surface resulting from slip on inclined faults by using results from elastic dislocation theory. Surface deformations are computed by modeling faults as planar dislocation surfaces in a uniform elastic medium. Studies of historic earthquakes are reviewed in an effort to determine appropriate values of faulting parameters to constrain the elastic models. The models are used to illustrate potential surface deformations resulting from two classes of earthquakes: earthquakes producing surface rupture (assumed to have M > 6-1/2), and earthquakes occurring on buried faults (M < 6-3/4). The treatment is intended to be primarily applicable to normal faulting earthquakes occurring within the ISB (Intermountain seismic belt), although the models are more general, and many historical examples of surface deformation are taken from other regions.

Static deformation of the ground surface accompanying the occurrence of large-magnitude (here defined as $M \geq 6$), normal-faulting earthquakes has been documented on several occasions within the Basin and Range and adjacent physiographic provinces. At least 20 $M \geq 6$ historical earthquakes have been reported in the western U.S. (excluding California, Oregon and Washington), primarily in the ISB, the central Nevada seismic belt, and the central Idaho seismic belt. Surface displacements (though not necessarily surface faulting) have been observed for many of these earthquakes. For example, surface faulting with more than 1 m of dip-slip offset was documented for the 1954 M 7.1 Fairview Peak, Nevada earthquake (Slemmons, 1957), the 1959 M_S 7.5 Hebgen Lake, Montana earthquake (Witkind, 1964), and the 1983 M_S 7.3 Borah Peak, Idaho earthquake (Crone and Machette, 1984). Displacements associated with these earthquakes were characterized by discrete surface offsets, and also by continuous surface deformation. In contrast, the 1925 M 6-3/4 Clarkston, Montana earthquake, the 1931 M 6.4 Valentine, Texas earthquake, and the 1975 M_L 6.0 Pocatello Valley, Idaho earthquake produced only ground cracking or subsidence (Pardee, 1926; Ni and others, 1981; Bucknam, 1976).

An important characteristic of historic earthquakes in the ISB (and elsewhere) is the association of surface offsets only for earthquakes above some threshold magnitude (Tocher, 1958; Fraser, 1964). Within the ISB, that magnitude is commonly assumed to be in the range of 6-1/2 to 6-3/4 (e.g. Doser 1985; Arabasz and others, 1987). Smaller magnitude historical ISB earthquakes have not been associated with surface rupture, although subsidence and secondary ground cracking have been observed. Precise geodetic leveling measurements have been made for few of the magnitude 6 to 6-3/4 earthquakes, but these data have indicated the occurrence of continuous, co-seismic surface deformation (typically manifested as a broad subsidence of the epicentral area). In principle, magnitude 5 and smaller earthquakes should also produce continuous surface deformation, with subsidence on the order of a cm or less, but such displacements are not significant for most engineering purposes.

The ultimate goal of this study is to estimate likely vertical surface displacements (elevation changes) for normal-faulting design earthquakes at sites within the ISB. The overall approach is to use observations from historical earthquakes to constrain simple theoretical faulting

models. The range of paramters thus obtained are then used to estimate the range of potential surface deformations resulting from $M \geq 6$ earthquakes. The basis for taking this approach is the relative success of a number of studies in applying theoretical models of faulting to geodetic data from historical earthquakes. These studies have indicated that elastic deformation is predominant, and that simple models can, in many instances, adequately explain the observed surface deformation.

Potential seismogenic surface displacements at particular sites in the ISB can be categorized as follows: 1) discrete offset on late Quaternary surface faults; 2) continuous deformation of the ground surface due to either slip on buried faults, or to surface faults which are located away from a site; and 3) discrete "secondary" breaks or cracking in the ground surface, resulting from near-surface readjustment to the predominant, continuous elastic deformation. The first category accounts for slip on active faults which extend to the surface. Such faults are likely to be characterized by multiple late Quaternary offsets (with slip ascribed to magnitude 6-1/2 or greater earthquakes), and should be identifiable from geologic studies (Arabasz and Julander, 1986; Arabasz and others, 1987). Continuous deformation of the ground surface away from the actual surface break, manifested as a broad subsidence of the epicentral area, represents a second category of deformation. For surface-faulting earthquakes, significant elevation changes possible at distances of 10-20 km from the fault trace. Smaller magnitude, non-surface faulting earthquakes, also produce subsidence of the epicentral area, which is also included in this category of deformation. If the historical record in the ISB can be used as a guide, such earthquakes will be of magnitude less than 6-1/2 to 6-3/4. The potential for surface cracks and secondary faulting at specific sites, the third category of deformation, is more difficult to assess. Factors such as the detailed near-surface structure, the relationship between favorably oriented joints or pre-existing faults and the causative fault, and the complicated interaction between the primary elastic deformation and the non-elastic surface cracking make quantitative estimates difficult.

Surface deformation observed for a number of large-magnitude ISB normal faulting earthquakes has been successfully explained using simple elastic dislocation models. For the particular case of normal faulting in the ISB, these models are commonly described as rectangular, inclined planar faults embedded within a homogeneous elastic half-space. For cases where well-distributed, precise leveling data has been obtained, these models have been able to predict the observations to within the error of measurement. This result is somewhat surprising given the simplicity of the models, but suggests that effects resulting from anelastic behavior, heterogeneity of the elastic properties, and deviation of the fault from a rectangular, planar surface are not dominant.

Elastic dislocation theory has been applied in this study to quantitatively estimate surface deformation which might accompany the occurrence of magnitude 6 and greater earthquakes within the ISB. The estimates have been constrained using available historic data for normal faulting earthquakes in the western U.S. (excluding California, Oregon and Washington). Two classes of models are presented: faults which penetrate the surface, and presumably result from large, magnitude 7-plus earthquakes; and faults which do not show discrete surface offset. A range of potential surface displacements are estimated, and the effects of varying model parameters are examined. Surface offsets due to cracking, settling of sediments, or other non-

elastic effects are not directly included in the models, but the models do suggest an upper bound for these effects.

2. Historical earthquakes

Vertical surface deformations associated with historic ISB and Basin and Range earthquakes provide the primary motivation for using elastic dislocation models, and also provide the most direct constraints for faulting parameters. Since 1900 there have been at least 10 earthquakes in the Basin and Range and adjacent provinces which have been associated with dip-slip surface faulting. Additionally, at least 19 (including aftershocks) magnitude 6 to 6-3/4 historic earthquakes with inferred normal faulting mechanisms, but not surface faulting, have been documented; for several of these events, minor subsidence and ground cracking has been reported. Historical western U.S. (excluding California, Oregon and Washington) earthquakes of $M \geq 6$ that were associated with significant amounts of dip-slip faulting are listed in **tables 1** and **2**, and are individually reviewed in this section. Focal mechanisms for many of the earlier earthquakes are poorly constrained, if known at all; these earthquakes have been classified as potential normal faulting events based on comparison to nearby earthquakes, or by location within regions showing geologic evidence for late Cenozoic normal faulting.

2.1. Surface faulting earthquakes

Most information relevant to evaluating the applicability of elastic dislocation models has been derived from observations of historic surface faulting earthquakes. Observed maximum vertical offsets from historic events have typically been on the order of 1 m or more; many detailed measurements of the associated deformation have been made. A brief review of these earthquakes is presented chronologically in this section, with the goal of estimating likely ranges of faulting parameters. Surface faulting earthquakes occurring prior to 1900 are not considered because relatively little detailed information data about the coseismic deformation is available. Several normal-faulting earthquakes in eastern California are also excluded because surface rupture appears to occur there at a considerably lower threshold magnitude (e.g., Bonilla, 1988).

October 2, 1915 Pleasant Valley, Nevada. M 7-1/2 to 7-3/4. Vertical surface offsets of up to 5.8 m were formed by this predominantly normal faulting earthquake (Jones, 1915; Page, 1934; Wallace, 1984; Wallace and Whitney, 1984). Four sets of en-echelon fault scarps were formed along a 60-km-long zone, but displacements were concentrated along the 35 km-long central zone consisting of two scarps; the average vertical displacement was about 3 m for this section. Faulting, as determined from the scarps, was predominantly dip-slip, with only 0.3 m of strike-slip movement. Dips of 50° to 80° were measured on the scarp face.

December 20, 1932, Cedar Mountain, Nevada. M 7.2. Geologic data indicated that faulting was predominantly strike-slip, with up to .86 m of right-lateral offset and 0.46 m of vertical offset (Gianella and Callaghan, 1934). Faulting occurred on a series of en-echelon rift and graben structures within a 60-km by 14-km zone, with individual faults lengths less than 6 km. The earthquake was felt over a 1.3-million-square-km area (Neumann, 1934).

Table 1. Historical (post-1910) surface-faulting earthquakes in the western U.S. (excluding California and the pacific northwest).

earthquake	earthquake parameters				fault parameters						references
	magnitude	moment (10^{25}dyne-cm)	focal depth (km)	offset* (cm)	depth (km)	dip (degrees)	length (km)	width (km)	slip (cm)	rake (degrees)	
Pleasant Valley, Nevada - 1915	M 7-3/4	50	-	460-580	0	50-80	35	-	-	-86	k,n,u,v
Cedar Mountain, Nevada - 1932	M 7.2	-	-	46	0		61	-	-	-150 - -175	i
Excelsior Mountains, Nevada - 1934	M 6.3	-	-	13	0	73	1.4-10	-	-	-	j
Hansel Valley, Utah - 1934	M 6.6	7.7	-	50	0	80	10-16	10?	145?	-24 - -90	d,g,h,p
Rainbow Mountain, Nevada - 1954	M 6.6	1.3-2.2	7-11	30	0	60-80	18	20	25	-90 - -140	f,l,r,t
Rainbow Mountain, Nevada - 1954	M 6.8	2.8-6.9	9-15	76	0	40-60	15-40	20	45	-90 - -145	a,f,l,r,t
Fairview Peak, Nevada - 1954	M 7.1	53-100	12-18	370	0	38-75	24-58	8-20	280-530	-140 - -160	f,l,o,q,r,v
Dixie Valley, Nevada - 1954	M 6.8	9.8-18	9-15	210	0	50-60	18-42	15	240-440	-83 - -90	f,l,o,q,r,v
Hebgen Lake, Montana - 1959	M_S 7.5	95-140	12-18	550-670	0-1.3	45-60	18-27	12-20	660-1080	-90 - -140	b,e,m,o,s,x
Borah Peak, Idaho - 1983	M_S 7.3	18-31	13-17	250-270	0	48-62	23-36	18	220	-42 - -83	b,c,s,w

* defined as maximum tectonic throw (corrected maximum scarp height), or maximum tectonic subsidence, when available. Otherwise, maximum scarp height.

code	reference	code	reference	code	reference
a	Baker and Doser (1988)	i	Gianella and Callaghan (1934)	q	Slemmons (1957)
b	Barrientos and others (1987)	j	Gianella and Callaghan (1935)	r	Snay and others (1985)
c	Crone and others (1987)	k	Jones (1915)	s	Stein and Barrientos (1985)
d	Dewey and others (1972)	l	Meister and others (1968)	t	Toucher (1956)
e	Doser (1985)	m	Meyers and Hamilton (1964)	u	Wallace (1984)
f	Doser (1986)	n	Page (1935)	v	Wallace and Whitney (1984)
g	Doser (1987)	o	Savage and Hastie (1966, 1969)	w	Ward and Barrientos (1986)
h	Doser and Smith (1982)	p	Shennon (1934)	x	Witkind (1964)

January 30, 1934 Excelsior Mountains, Nevada. M 6-1/4. This earthquake was felt over a 280-thousand-square-km area (Neumann, 1936). A single northeast trending 1.4-km-long en-echelon scarp was formed in bedrock, with a maximum vertical offset of 13 cm (Callaghan and Gianella, 1935). About 10 km northeast of the scarp, Callaghan and Gianella found slumping in alluvium for 100 m along the steep bank of a wash, and noted that the area seemed "to have been shaken with greater violence than near-by areas". While the observed slumping was not primary faulting, the 10-km distance between the bedrock scarp and the slumping may indicate the length of the buried part of the fault. Alternatively, the location of slumping may have simply been primarily determined by the distribution weak surface materials.

March 12, 1934 Hansel Valley, Utah. M 6.6. Shenon (1936) reported en-echelon ground cracks in weakly consolidated sediments on a 9-km-long fault zone; maximum vertical offsets of 50 cm were measured, but offsets of 5 to 25 cm were typical. Horizontal offsets were not believed to have occurred. No offsets were seen in fractures which cut bedrock. McCalpin and others (1987) found evidence for recurrent late Quaternary faulting on the bounding faults of Hansel Valley, including the fault on the southwestern margin of the valley which contained the 1934 scarp. Consistent with the observed scarps, Dewey and others (1972) found a steeply dipping normal faulting focal mechanism, but an oblique-slip mechanism was also possible. In contrast to Shennon's observations, Doser (1987) used teleseismic data to infer a significant component of strike-slip motion. Doser and Smith (1982) computed a moment of 7.7×10^{25} dyne-cm for this event, and estimated an average slip of 145 cm for a fault length of 16 km and width of 10 km.

July 6 - August 24, 1954 Rainbow Mountain, Nevada. M 6.8. The July 6 earthquakes began a sequence of five $M > 6$ earthquakes which occurred in the Fallon, Nevada area in 1954, and culminated with the Fairview Peak earthquake of December 16 (described below). Three M 6.4 to 6.8 earthquakes occurred on the Rainbow Mountain fault, forming up to 0.45 m vertical offsets on a group of several 10- to 20-km-long faults (Tocher, 1956; Byerly and others, 1956). The first event (M 6.6) ruptured a 18-km-long segment at the southern end of the Rainbow Mountain fault, producing up to 0.30 m of vertical offset. The second (M 6.4) earthquake occurred 11 hours later but produced only ground cracking in the epicentral region. The third (M 6.8) Rainbow Mountain earthquake occurred on August 24, and formed a new 15- to 20-km-long scarp extending from the July scarps, as well as producing additional offset on the July scarps. Doser (1986) suggested that rupture propagated unilaterally from the extreme southern end of Rainbow Mountain fault zone, and that significant components of right-lateral strike-slip motion occurred.

December 16, 1954 Fairview Peak and Dixie Valley. M 7.1 and 6.8. The Fairview Peak earthquake occurred about 4 minutes prior to the Dixie Valley earthquake, and the epicenters were separated by about 70 km (Tocher, 1957; Romney, 1957; Doser, 1986). Surface offsets occurred along many faults in four main zones within a 100-km-long by 30-km-wide belt located parallel to, and about 40 km west of, the scarps formed on the Rainbow Mountain fault earlier in the year (Slemmons, 1957; Wallace and Whitney, 1984). Scarps formed on the three fault zones in southern Dixie Valley and Fairview

Valley were probably related to the Fairview Peak earthquake, while the scarps formed along the central and northern part of Dixie Valley likely resulted from the second earthquake, although such an association may be too simplistic (Snay and others, 1985). The Fairview fault zone showed maximum vertical tectonic offsets of 3.7 m, and maximum horizontal offsets of 4 m, with typical vertical and horizontal offsets of 2.4 m and 3.7 m respectively. On the Dixie Valley fault zone, up to 2.2 m of apparently anomalous left-lateral offset, and a maximum 2.1 m of vertical offset was observed on a 43-km-long scarp; the average vertical offset was about 1 m for the 43-km-long scarp, but about 2 m for the 25-km-long central segment. Leveling and horizontal geodetic data indicated the distribution of surface displacements to be quite complex (Whitten, 1957; Reil, 1957; Meister and others, 1968). Dip angles of 55° to 75°, and rakes of −120° to −150° were commonly observed in striations measured in bedrock along the Fairview Peak fault zone. Re-examination of teleseismic waveforms by Doser (1985) detailed the complexity of this sequence of earthquakes, and suggested that the earthquakes occurred on high-angle faults dipping 40° to 80°, with significant components of right-lateral strike-slip movement. Review of geodetic investigations conducted for these earthquakes is deferred until a later section.

August 18, 1959 Hebgen Lake, Montana. M_S 7.5. This complex earthquake produced average vertical surface offsets of about 2 m over two parallel fault segments with an overall length of about 30 km (Witkind, 1964). While maximum vertical tectonic offsets of up to 5.5 m were determined from scarp height measurements, a somewhat greater value of maximum tectonic subsidence (6.7 m) was determined from leveling data (Myers and Hamilton, 1964). Several $M \geq 6$ aftershocks were associated with this event, but surface rupture was not reported. Fault plane solutions determined for the main shock indicated primarily dip-slip movement on 55° to 65° dipping plane (e.g., Ryall, 1962; Dewey and others, 1972). Doser (1985) re-examined waveform data from this event and suggested that rupture occurred during two sub-events with focal depths of 10 and 15 km, and having seismic moments of 2.8 and 92 $\times 10^{25}$ dyne-cm, respectively. Inversion of body-wave data suggested both normal- and oblique-slip movement on 40° to 60° dipping fault planes.

October 28, 1983 Borah Peak, Idaho. M_S 7.3. Numerous scientific investigations were initiated following this earthquake, and it is perhaps the most well-documented historic Basin and Range earthquake. Bucknam and Stein (1987) present an extensive bibliography listing most of these studies. A 36-km-long, Y-shaped scarp was formed, having a maximum net vertical tectonic offset of 2.7 m (Crone and Machette, 1984; Crone and others, 1987). The main fault zone consisted of a 21-km-long segment with average and maximum vertical throw of 1.1 m and 2.7 m, respectively. The two branches of the Y were 14 and 8 km long, with maximum vertical throws of 1.6 and 1 m. Faulting was predominantly dip-slip, but horizontal offsets of up to about 1 m were observed at several locations. Striations in colluvium indicated indicated a rake of −80°, in good agreement with seismologically determined values (see Richins and others, 1987, for a review).

With respect to predicting static deformations from future surface-faulting earthquakes in the ISB, several observations can be made about these historical earthquakes. Within the ISB, the threshold for surface rupture is often assumed to be about magnitude 6-1/2 to 6-3/4 (e.g., Doser, 1985), because: 1) the M 6.6 Hansel Valley earthquake is the smallest historic earthquake to produce surface offset, and 2) earthquakes such as the 1925 M 6-3/4 Clarkston, Montana and 1975 Pocatello Valley earthquakes had no reported surface rupture. Historic normal faulting earthquakes outside the ISB (but within the Basin and Range) provide counter-examples, with surface rupture for magnitudes as low as 6-1/4 (e.g., 1934 Excelsior Mountains, Nevada earthquake). Also, Bonilla (1988) presents evidence indicating a surface faulting threshold as low as M_L 5.0 for California and other areas. The interpretation of threshold magnitudes is complicated by lack of availability of a common magnitude scale, and by such effects as magma emplacement (suggested by Snay and others, 1985, to possibly explain inconsistencies in deformation models of the Fairview Peak earthquake sequence), or faulting which may be primarily strike-slip. Consideration of these effects, and allowance for differing tectonic environments, might allow for a more consistent interpretation of the threshold for surface rupture within the Basin and Range and ISB. Historic vertical surface offsets have typically been about 0.5 m or more, except for earthquakes which are predominantly strike-slip, so this number is probably a reasonable bound for the minimum value of vertical offset for surface faulting events in the ISB. Seismologic and geologic data from the better-recorded earthquakes indicate that slip occurs on steeply dipping fault planes which extend to depths of 10-15 km; listric fault models have not been supported by this data. The minimum fault length has been about 10 km, with typical lengths of 20 to 30 km for the zone of primary offset; fault lengths have been highly variable and not well correlated to magnitude.

2.2. Earthquakes on buried faults

Many historic earthquakes of magnitude 6 to 6-3/4 occurring in the western U.S. (excluding California, Oregon and Washington) did not form scarps on identified faults. To examine the ground deformation resulting from earthquakes below the threshold of surface rupture, a compilation of these earthquakes is made in **table 2**. Secondary ground cracking or slumping was observed for many of these events but was not continuous, or did not coincide with an identified fault zone. Geodetic leveling data has documented subsidence in the epicentral area of a few of these earthquakes, but such data has not generaly been available. The following is a review of the events listed in **table 2** for which some information is available about ground deformation. Leveling data from only two M 6 to 6-3/4 earthquakes in the ISB (and one in west Texas) has been presented in the literature. Considerably less data on ground deformation is available for earthquakes of this size than for surface faulting events; aside from observations of cracking and secondary faulting, geodetic measurements are required to document the relatively small deformations. Such measurements have rarely been made.

June 27, 1925 Clarkston, Montana. M 6-3/4. A one-word description of this event would be enigmatic. Clarkston Valley is a 20-km-long Cenozoic basin bounded on the east by faults of Miocene or Pliocene age, but with no documented Pleistocene or Holocene age movement (Quamar and Hawley, 1979; Stickney and Bartholomew, 1987). A strong shock was felt over an 800-thousand-square-km area, and was investigated in some

Table 2. Historical $M \geq 6$ non-surface faulting earthquakes in the western U.S. since 1925 (excluding aftershocks).

earthquake	earthquake parameters				fault parameters						references
	magnitude	moment (10^{25}dyne-cm)	focal depth (km)	subsidence* (cm)	depth (km)	dip (degrees)	length (km)	width (km)	slip (cm)	rake (degrees)	
Clarkston, Montana - 1925	M 6-3/4	-	-	60	1??	30-90	16	-	-	-38	g,h,i,k,p,s
Valentine, Texas - 1931	M 6.4	3.3	10	12.2	-	54	21	12.5	38	-155	k,o,m
Helena, Montana - 1935	M 6-1/4	-	-	-	-	-	-	-	-	-	n
Seafoam, Idaho - 1944	M 6.1	-	-	7?	-	-	-	-	-	-	d,i,j
Clayton, Idaho - 1945	M 6.0	-	-	-	-	-	-	-	-	-	e,i,j
Virginia City, Montana - 1947	M 6-1/4	-	-	-	-	80?	-	-	-	-44 - -90	k,i
Pocatello Valley, Idaho/Utah - 1975	M_L 6.0	0.7-2.2	9	13.6	5	30-60	18	8	23-50	-90	a,b,c,f,l
Yellowstone Park, Wyoming - 1975	M_L 6.1	0.75-2.6	5-8	12	1?	45-80	10	6-10	-	-51 - -90	b,c,q

* maximum tectonic subsidence, if known, or maximum vertical height of ground cracks (excluding obvious slumping).

code	reference	code	reference	code	reference
a	Arabasz and others (1981)	h	Byerly (1955)	n	Murphy (1950)
b	Bache and others (1980)	i	Dewey and others (1972)	o	Ni and others (1981)
c	Battis and Hill (1977)	j	Dewey (1987)	p	Pardee (1926)
d	Bodle (1946)	k	Doser (1987)	q	Pitt and others (1979)
e	Bodle and Murphy (1947)	l	Doser and Smith (1982)	r	Quamar and Hawley (1979)
f	Bucknam (1976)	m	Dumas and others (1980)	s	Smith and Sbar (1974)
g	Byerly (1926)				

detail by Pardee (1926). Pardee found several northwest-trending, newly formed ground cracks of up to 2 km in length at the northern end of Clarkston Valley. Based on Pardee's description, cracking was apparently occurred in two en-echelon zones, each 3 to 6 km in length, and horizontally separated by about 6 km. The maximum vertical offset in this area was about 0.6 m, and Pardee believed all movement to be dip-slip. In addition to the cracking found at the northern end of the Clarkston Valley, cracks were observed in road embankments 20 km southwest, along a creek bank about 10 km north, and in a slumped alluvial block about 65 km northwest; these areas of cracking were likely due to slumping or settling of alluvial material. Pardee stated that none of the cracks represented surface slip along a deep-seated fault, and this interpretation has been widely cited. Based on the magnitude and felt area, it seems surprising that surface faulting did not accompany this earthquake. Also, the 0.6 m maximum vertical offset of the cracks is comparable to the offsets observed for the M 6.6 Hansel Valley earthquake, which apparently did rupture along a late Quaternary fault. Detailed geologic investigations aimed at identifying Quaternary movement along the Clarkston Valley have apparently not been made, although Stickney and Bartholomew (1987) classify faulting in the area as pre-Quaternary based on "a literature review ...and selected field studies" for the entire Montana-Idaho basin and range.

Conflicting evidence for the type of faulting for this event is also apparent. Byerley (1955), Dewey and others (1972), and Smith and Sbar (1974) obtained apparently well-constrained fault plane solutions indicating strike-slip motion with a south-southeast direction of extension. In contrast, Quamar and Hawley (1979) found generally east-west extension on both normal and strike-slip fault plane solutions determined from contemporary $m_b \leq 4.4$ earthquakes located within Clarkston Valley. Thus the type of faulting determined from the 1925 event fault plane solution is inconsistent with both Pardee's normal faulting interpretation of the ground cracks, and with faulting determined from contemporary earthquakes. An additional interpretation was offered by Doser (1987), who reported preliminary results from a re-analysis of the teleseismic data indicating oblique slip on an east-northeast trending fault dipping to the northwest; this trend corresponds more closely with the strike of the southern end of the Clarkston Valley fault, but is perpendicular to the trend of the ground cracks at the northern end of the valley. To recapitulate, the Clarkston earthquake may have been either a normal or strike-slip event, which was near or at the threshold for surface rupture. An approximate upper limit on the vertical offset or deformation is 0.6 m.

August 16, 1931 Valentine, Texas. M 6.4. Surface faulting was not observed for this earthquake, and ground cracking was not reported (Sellards, 1932). Byerly (1934) located the earthquake in an area that fell outside the zone of greatest felt intensity. Recognizing this, Dumas and others (1980) used travel-time delays determined from a nearby nuclear explosion and relocated the epicenter into that zone. They determined a focal depth of 29 ± 25 km. Dumas and others also determined an oblique-slip faulting mechanism with west-southwest extension. Ni and others (1981) examined leveling line data, and noted that the epicenter of Dumas and others coincided with the area of maximum subsidence. Doser (1987) used regional and teleseismic body wave data to suggest that the earthquake occurred at a depth of 10 km, with a fault plane solution indicating oblique slip on a 54°

dipping plane.

October 18 and October 31, 1935 Helena, Montana. M 6-1/4 and 6. A damaging earthquake sequence with epicenters close to Helena, Montana, began on October 3, with strong shocks occurring through November, 1935 (Ulrich, 1936; Neumann, 1937). Based on S-P times from strong motion accelerographs installed after the October 18 shock, the epicenter of the October 31 shock was thought to be within a few km of Helena. The earthquakes were felt over areas of 590- and 360-thousand-square-km, respectively. Dewey and others (1972) found the relative location of the October 18 epicenter to be 22 km north of the October 31 epicenter, and suggested that the two earthquakes occurred on different faults.

June 12, 1944 and February 13, 1945 Seafoam, Idaho. M 6.1 and 6.0. Relatively little is known about these two earthquakes which occurred in Central Idaho. These events were the largest historic events in Idaho prior to the 1983 Borah Peak earthquake, and were felt over 180- and 150-thousand-square-km areas, respectively; several-hundred-meter-long cracks were formed along a road during the first event (Bodle, 1946; Bodle and Murphy, 1947). Relative locations of the earthquakes indicated that the 1944 event occurred about 20 km south-southwest of the 1945 event (Dewey and others, 1972; Dewey, 1987). Absolute locations of the earthquakes are poorly constrained, but appear to be 10 to 20 km within the Idaho batholith; the epicenters are about 75 km west of the rupture zone of the Borah Peak earthquake. Focal mechanisms have not been published, and the type of faulting is unknown.

November 23, 1947 Virginia City, Montana. M 6-1/4. Felt over a 380-thousand-square-km area, this earthquake formed mud springs and caused large boulders to roll down mountainsides, but ground cracking was not reported (Murphy, 1950). Dewey and others (1972) obtained a steeply dipping, normal faulting focal mechanism which indicated east-west extension. Doser (1987) suggested a mechanism with oblique slip, but with a strike similar to the north-trending Madison fault. Aside from an absence of reported surface scarps, very little information about ground deformation for this event is known.

March 27, 1975 Pocatello Valley, Idaho. M_L 6.0. Cracks in both snow and soil in the epicentral area were noted by Cook and Nye (1979) and Kaliser (1976). The cracks were primarily concentrated in a 5-km-long zone, and were attributed to differential compaction of the soil. Bache and others (1980) found a predominantly dip-slip fault plane solution from modeling of teleseismic P-waves, and obtained a preferred fault plane dipping 39°, and with a rake of −53°. Arabasz and others (1981) interpreted the main shock to have occurred on a buried fault obliquely transecting the east-bounding fault of the Pocatello Valley graben. They also used the leveling data of Bucknam (1976) to constrain a west-dipping dislocation model. This model, which is frequently referred to in subsequent sections, consisted of 50 cm of dip-slip movement on a 17.8-km-long by 8.1-km-wide rectangular fault with top edge buried 5 km, and dipping 60°. The up-dip projection of the fault model intersected the surface in the area were the most extensive ground cracks were observed. In contrast, McCalpin and Robison (1987) suggested that slip

occurred on the eastward-dipping, west-bounding fault of Pocatello Valley. Doser and Smith (1982) estimated an average slip of 23 cm from source modeling of body-wave spectra.

June 30, 1975 Yellowstone Park, Wyoming. M_L 6.1. Located on the margin of the Yellowstone caldera, this earthquake was felt over a 50-thousand-square-km area. Pitt and others (1979) reported on the main-shock and aftershock sequence, and also presented leveling data indicating 12 to 13 cm of tectonic subsidence in the epicentral area. No evidence of surface faulting was found, and surface cracking was not reported. The depth of the main-shock was not well-determined, but was suggested to be about 6 km based on the aftershock distribution. While Pitt and others determined a main-shock fault plane solution with nearly pure normal faulting, and dips of about 45°, Bache and others (1980) found an oblique faulting mechanism using teleseismic data. The preferred fault plane of Bache and others had a dip 71°, and rake of −51°.

Deformation manifested as ground cracking, slumping and tectonic subsidence, but not surface displacements on faults, has been observed for most M 6 to 6-1/2 historic ISB and Basin and Range earthquakes. Inferred fault lengths of 10 - 20 km have been suggested by aftershock distributions and geodetic data for a few of these earthquakes, but most have not been studied in detail. While normal-faulting mechanisms predominate, significant components of strike-slip motion have been inferred for several of these earthquakes.

3. Computation of displacements

Considerable success has been achieved using elastic dislocation theory to model observed vertical surface displacements from normal faulting earthquakes in the ISB and Basin and Range. Depending on the quality and extent of available leveling data, detailed interpretations of fault geometry and slip distribution have been made. Faults have typically been modeled by simple rectangular surfaces with uniform slip, but also have been modeled as curved surfaces with variable slip through superposition of planar sub-faults. In this section the development of these procedures is reviewed, and several examples are presented.

3.1. Previous work

Numerous investigators have applied elastic dislocation theory to model observed surface displacements associated with large-magnitude, dip-slip earthquakes. Savage and Hastie (1966, 1969) obtained closed expressions for the surface displacement due to slip on an inclined, rectangular fault in a homogeneous and isotropic elastic medium. Savage and Hastie (1966) modeled vertical displacements determined from level-line data for several earthquakes, including the 1954 Fairview Peak and 1959 Hebgen Lake earthquakes. By forward modeling, they obtained planar fault models with good qualitative agreement to the data. Savage and Hastie (1969) used a least-squares approach with both horizontal and vertical geodetic data to infer dislocation models of the Fairview Peak and Dixie Valley earthquakes. Koseluk and Bischke (1981) used numerical models of faulting to incorporate viscous effects, and estimated faulting parameters for the Fairview Peak and Hebgen Lake earthquakes. While the addition of viscous effects allowed for modeling interseismic doming, the fit of the coseismic deformation data was not significantly improved over the purely elastic dislocation models of Savage and Hastie (1966, 1969).

The occurrence of the 1983 Borah Peak, Idaho earthquake stimulated additional interest in theoretical modeling of surface displacements from dip-slip faulting. Several studies modeled deformation from that earthquake (e.g., Stein and Barrientos, 1985; Ward and Barrientos, 1986), and further studies of the Fairview Peak and Hebgen Lake earthquakes were also done for comparison (Snay and others, 1985; Barrientos and others, 1987).

High-quality leveling data in the vicinity of the Borah Peak earthquake permitted an unusually detailed investigation of possible modes of deformation and faulting. Stein and Barientos (1985), using a combination of least-squares and trial and error estimation, were able to find a planar, uniform-slip fault model which fit most of the geodetic observations within the expected random and systematic error. They also explored models of listric faulting by using three successive planar faults to simulate curvature, but found that all such listric models substantially increased model misfit. They concluded that the observed coseismic elevation changes were most compatible with a planar high-angle fault rupture.

Ward and Barrientos (1986) investigated more complicated models which allowed curvature of the fault surface, and variable slip by representing a fault as a large number of point dislocation sources. Applying the constraints of uniform slip direction and non-negative slip (i.e., slip

vectors for all subsources were parallel) with a novel gradient inverse technique allowed them to resolve the detailed slip distribution for a wide range of specified planar and curved faults. They found that a variable-slip planar fault reproduced the leveling data with considerably less error than uniform-slip planar models. Furthermore, any significant degree of curvature in the fault surface, at least for the active part of the fault, was found to be inconsistent with the data. They also noted that measurements of surface slip provided relatively little constraint on the slip distribution at depth, and suggested that surface slips measured on other Holocene scarps in the Basin and Range may also not be indicative of slip at depth.

Additional elevation-change data were examined for both the Hebgen Lake and Borah Peak earthquakes by Barrientos and others (1987) using uniform-slip planar and curved fault models. Curved fault models were not supported by these studies, and for the Borah Peak earthquake a planar fault model similar to that found by Stein and Barrientos (1985) and Ward and Barrientos (1986) was obtained. For the Hebgen Lake earthquake, Barrientos and others (1987) found that a two-plane model best represented the geodetic data. No significant improvement in fit was obtained by adding curvature, and, additionally, substantial curvature of the fault models was ruled out. They concluded that the geodetic observations for both earthquakes could be satisfactorily explained by planar, non-listric, uniform-slip fault models.

Further modeling of the Fairview Peak and Dixie Valley earthquakes was done by Snay and others (1985), using the horizontal displacement data of Whitten (1957). Their best-fitting model consisted of six uniform-slip planes distributed in the epicentral region, but the planes corresponding to the Rainbow Mountains fault required excessive amounts of slip. They suggested that incorporating an expanding dike in the model might explain the several inconsistencies with the data. Their model of the Fairview Peak earthquake consisted of two steeply dipping faults, the deepest of which extended to a depth of 20 km. Doser (1986) reexamined teleseismic data for this sequence of earthquakes and concluded that faulting occurred on steeply dipping (40° to 70°) planes, with no evidence for slip on listric or subhorizontal structures. The larger ($M > 6.5$) events had focal depths of 12-15 km, and were characterized by complex rupture processes. Doser noted that the Hebgen Lake earthquake also had a complicated rupture process, and suggested that rupture complexity may be associated with regions with high levels of volcanic and magmatic activity.

While various models of Basin and Range faulting which include slip on listric faults or normal faults soling into detachment surfaces have been presented based on geologic or seismic reflection data (e.g., Smith and Bruhn, 1984; Wernicke, 1981; Allmendinger and others, 1983; Arabasz and Julander, 1986), no support for such models has been found through geodetic analysis of crustal deformations of historic Basin and Range earthquakes. Furthermore, the many similarities between these earthquakes suggests that it is appropriate to consider such earthquakes as typical of future large-magnitude Basin and Range earthquakes. As a first approximation, deformations produced from surface breaking earthquakes may reasonably be modeled using a steeply dipping (45° to 60°) planar fault which extends from the surface to depths of 15 to 20 km. A uniform slip of 1 to 10 m and fault length of 15 to 50 km can then adequately represent the required amount of moment release for potential $M>7$ earthquakes, and is consistent with observed measurements of surface slip (notwithstanding the possible disparity between surface slip and slip at depth noted by Ward and Barrientos, 1986).

Leveling data have been presented in the literature for only two M 6 to 6-3/4 earthquakes in the ISB, and one in west Texas (Arabasz and others, 1981; Pitt and others 1979; Ni and others, 1981). These earthquakes did not produced surface rupture, and the amount of subsidence was substantially less than that observed for historic ISB surface faulting earthquakes. Compared to studies done for historic surface-faulting earthquakes, considerably less work has been done in using geodetic data to estimate faulting parameters for these non-surface-faulting events. Of the studies cited above, only Arabasz and others (1981) were able to infer a faulting model from the geodetic data.

3.2. Description of models

The problem of estimating vertical surface displacements due to slip on an extended dislocation source in a homogeneous elastic half-space can be treated generally by first obtaining the displacement field due to an elemental (or point) dislocation source. Horizontal deformations also result from a dislocation source (and can be similarly treated), but are not the focus here and so will not be further examined. An elemental fault source can be represented as an infinitesimal dislocation surface with uniform slip. Planar faults with simple geometrical shapes (in particular, rectangles) may be modeled as a single dislocation source, but with finite extent (the so-called uniform slip - planar, or USP model). An alternate approach is to model a finite fault as the superposition of many elemental point dislocation sources, each possibly having varying slip and orientation. The superposition is valid since displacements add linearly as long as the strains, at locations where the displacements are evaluated, remain small. Examples of models which can be constructed in this manner are planar faults with variable slip (VSP models), curved faults with uniform slip (USC models), and curved faults with variable slip (VSC models). USP models, despite being very simple, can often predict the gross features of the observed vertical displacement field, and available deformation data has typically been insufficient to constrain more complex models. Thus, USP models are a good first-order approximation for describing displacements due to a wide range of faulting configurations.

Several methods have been presented in the literature for calculating stress, strain and displacement fields due to dislocation sources in simple elastic media (Okada, 1985, presents a comprehensive review). Two of these methods, each derived independently, were implemented numerically for this study. For calculation of displacements due to slip on a planar fault with uniform slip, the results of Mansinha and Smylie (1971) were used. Their results were strictly valid only for the case of a poisson solid (equal Lamé constants λ and μ), but the relatively weak dependence of displacements on the Lamé constants makes the model sufficiently general. Faults are modeled as inclined rectangular surfaces of dimension $l \times w$, having a specified uniform slip **S**. Geometry and parameters of the USP fault model are shown in **figure 1**. The upper edge of the fault is parallel to the surface, and located at a depth d (zero for the case of surface faulting). The slip vector **S** is described in terms of scalar magnitude s and rake θ, where $\theta = -90^o$ is pure dip slip faulting, and $\theta = 0^o$ is left-lateral strike slip faulting. Vertical surface displacements result from both dip slip and strike slip faulting. Details of the calculation may be found in Mansinha and Smylie (1971).

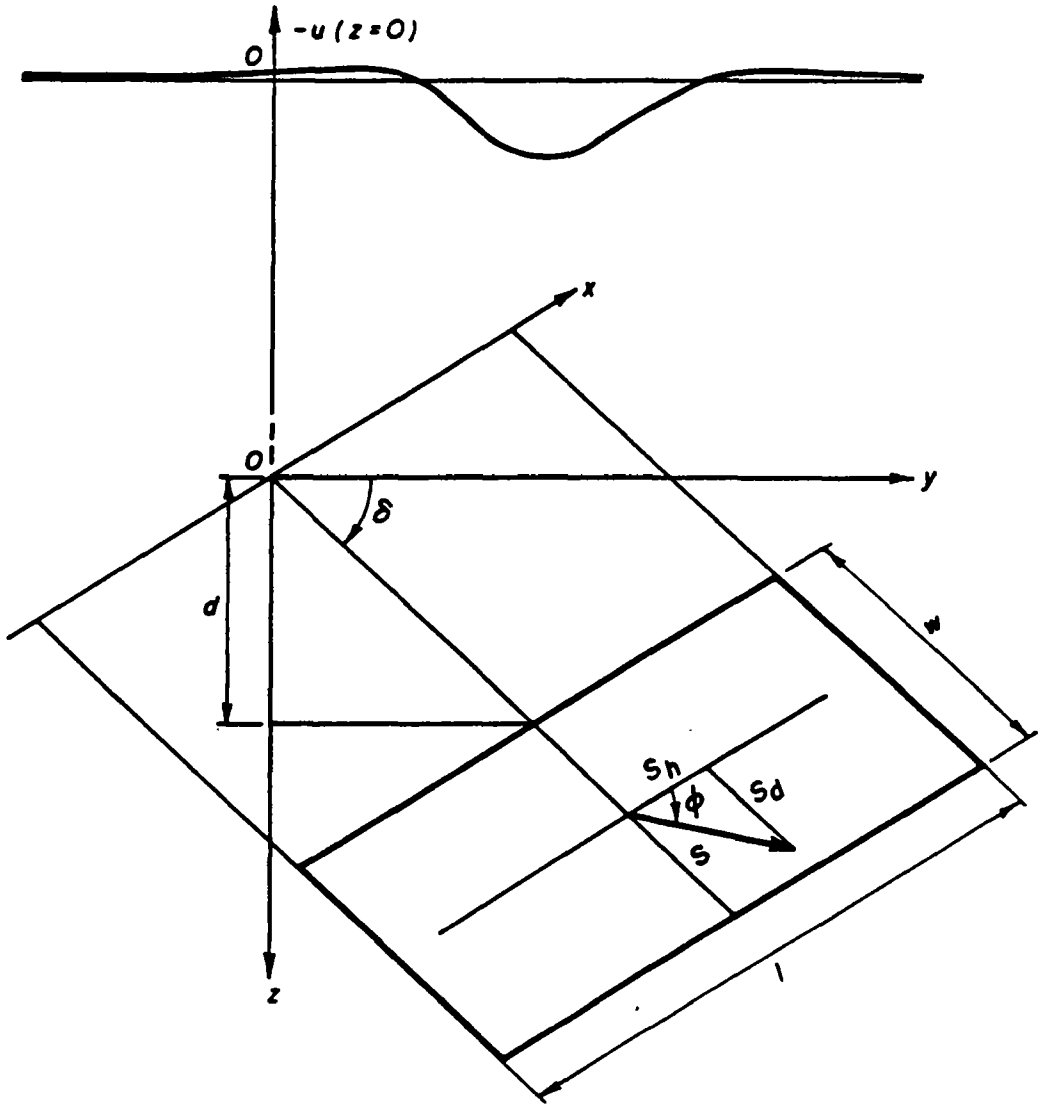

Figure 1. Uniform slip planar fault model. A fault is represented by a rectangular dislocation surface of length l and down-dip width w, with upper edge buried a depth d from the surface. The fault strikes parallel to the x-axis, and dips at an angle δ. A uniform slip vector **S** has strike-slip and dip-slip components S_h and S_d. Equivalently, slip is described by a magnitude $s = |\mathbf{S}|$, and rake $-\tan\phi = S_d/S_h$. Slip on the fault surface results in vertical (upper curve) and horizontal (not shown) displacements.

A second, more general approach is that of Comer (1977) who obtained relatively simple expressions for displacements resulting from a point double-couple source within a homogeneous half-space. Since the strength of a double couple M_0 can be expressed as $M_0 = \mu lws$, and the normalized elements of the moment tensor are directly related to the fault orientation and direction of slip, an elemental dislocation source may alternatively be described by a double-couple source. An arbitrary fault geometry and slip distribution may be specified by summing the contribution of sufficiently many of these elemental point sources. The modeling of a rectangular planar fault with variable slip (VSP model), is indicated schematically in **figure 2**. One important practical requirement for implementing this formalism is that the point source approximation be valid for each source point - evaluation point pair (i.e., the dimension of the individual source must be much less than the distance to the point where the surface displacement is to be evaluated). Typically, this is most significant only when the fault model extends near or to the surface, and there are evaluation points near the fault trace. One method to insure the requirement is to equally subdivide the fault surface into many sources, each with dimension much less than the smallest source - evaluation point pair. A considerably more efficient procedure is to subdivide the fault in such a way that the ratio of source dimension to source - evaluation point distance is roughly constant. The division of the fault surface required to meet the point source approximation must, of course, be at least as fine as the division required for introducing variable slip or a curved fault geometry.

Computer coding of each of the two approaches was done, and compared for the case of a rectangular planar fault with uniform slip. Code for the method of Mansinha and Smylie (1971) was obtained from H. Benz (University of Utah, personnel commun., 1987). Comparison of numerical results from the two methods was done as a verification of both the basic equations and the computer coding. Results of several trial runs indicated that the two methods yielded essentially the same surface displacements as long as the spacing between point sources was less than about one-fifth of the distance to the closest evaluation point.

3.3. Examples from historic ISB earthquakes

As a test of the computer code, and an illustration of the method, vertical elevation change profiles across planar fault models inferred for several historic ISB earthquakes were computed. The first two examples are from the 1983 (M_S) 7.3 Borah Peak and 1959 (M_S) 7.5 Hebgen Lake earthquakes, both of which produced extensive surface rupture as well as subsidence over large areas. These earthquakes serve as models of potential surface deformation resulting from M > 7 ISB earthquakes.

Barrientos and others (1987) inverted geodetic data measured from both the Hebgen Lake and Borah Peak earthquakes, and obtained best-fitting one- and two-plane USP models. Parameters for the single-plane models are listed in **table 3**. Elevation change profiles computed from the single-plane models of Barrientos and others are shown in **figures 3** and **4**. Note that the scales of the profiles differ. The profiles bisect and trend perpendicular to the strike of the model faults, and extend for 20 km on either side of the surface trace. While some component of strike slip faulting may have occurred, only dip-slip movement is modeled. The depth to the top of the single-plane fault model obtained by Barrientos and others for the Hebgen Lake

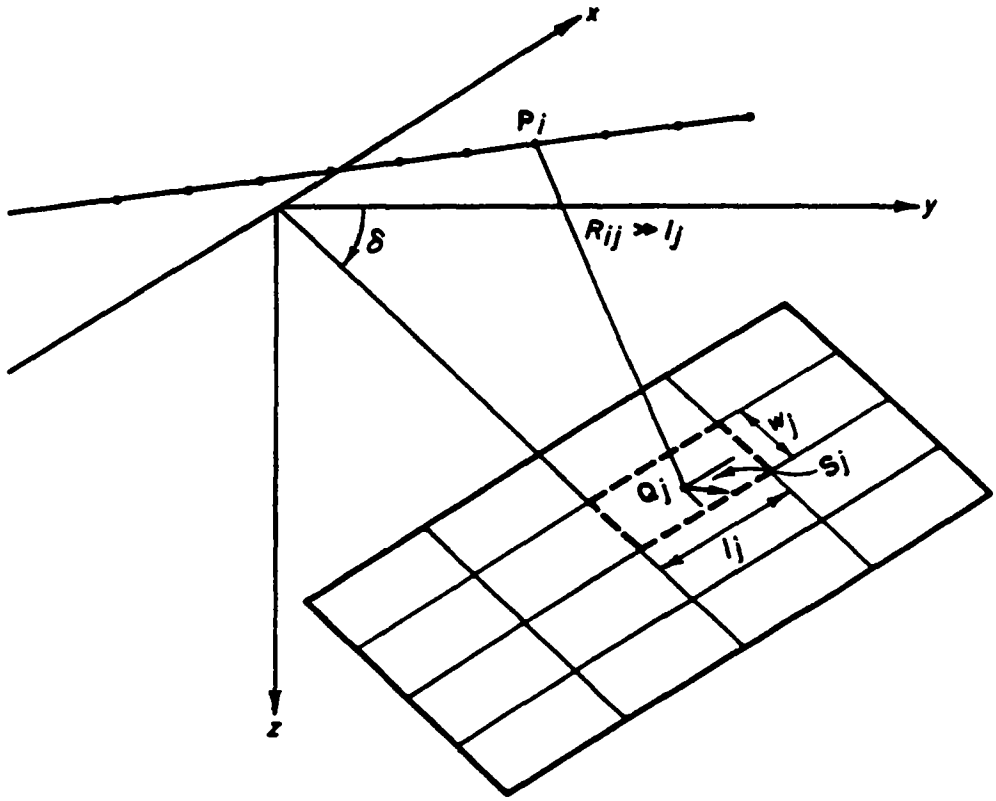

Figure 2. Representation of a planar fault as a superposition of subfaults. Vertical displacements are evaluated along a profile at points $\mathbf{P}_i$. The total displacement is the sum of the displacements caused by each sub-fault located at $\mathbf{Q}_j$. The subfault is equivalent to a moment point source with strength $M_0 = \mu l_j w_j s_j$ as long as the distance $R_{ij} = \overline{\mathbf{P}_i \mathbf{Q}_j}$ is much larger than a characteristic dimension l_j or w_j.

earthquake was greater than zero, even though surface faulting was observed. For the two-plane model (not shown), coinciding with the Hebgen and Red Canyon faults, a faulting depth closer to zero was obtained. Although Barrientos and others (1987) found the two-plane model to provide a significantly better fit to the geodetic data, for simplicity the single plane model is used here for illustration of the method. A faulting depth of zero was obtained by Barrientos and others for the single-plane model of the Borah Peak earthquake.

Table 3. Faulting parameters used to model elevation changes associated with selected $M_L \geq 6$ ISB earthquakes.

earthquake	length (km)	width (km)	dip (deg)	depth (km)	slip (cm)	moment (10^{25} dyne-cm)	reference
1959 Hebgen Lake M_S 7.5	23	16.4	50	1.2	1080	132	Barrientos and others (1987)
1983 Borah Peak M_S 7.3	23	18	49	0	220	29	Barrientos and others (1987)
1975 Yellowstone Park M_L 6.1	11.9	8.5	45	1	23.2	0.75	inferred from Pitt and others (1979)
1975 Pocatello Valley M_L 6.0	17.8	8.1	60	5	50	2.3	Arabasz and others (1981)

Two additional examples of surface deformation are from M < 6-1/2 earthquakes: the 1975 (M_L) 6.0 Pocatello Valley, and the 1975 (M_L) 6.1 Yellowstone earthquakes. These events produced only general subsidence in the epicentral area, and no evidence for surface faulting was observed. Leveling data for the Pocatello Valley and Yellowstone earthquakes was somewhat limited, and so detailed models of the subsurface geometry cannot be uniquely obtained from this data. Plausible interpretations have been made for the Pocatello Valley earthquake by Arabasz and others (1981) using leveling data from Bucknam (1976). Pitt and others (1979) presented leveling data from the vicinity of the Yellowstone earthquake, but did not explicitly model the observed deformations. They did suggest a qualitative model, which can partially be parameterized using the observed fault plane solution, moment, and hypocenter. Elevation change profiles from the resulting models of these earthquakes are shown in **figures 5** and **6**. While the model obtained from Arabasz and others (1981) for the Pocatello Valley earthquake has been faithfully reproduced, the model of the Yellowstone earthquake is only intended to represent the observed maximum subsidence, and no formal inversion of the leveling data has been attempted.

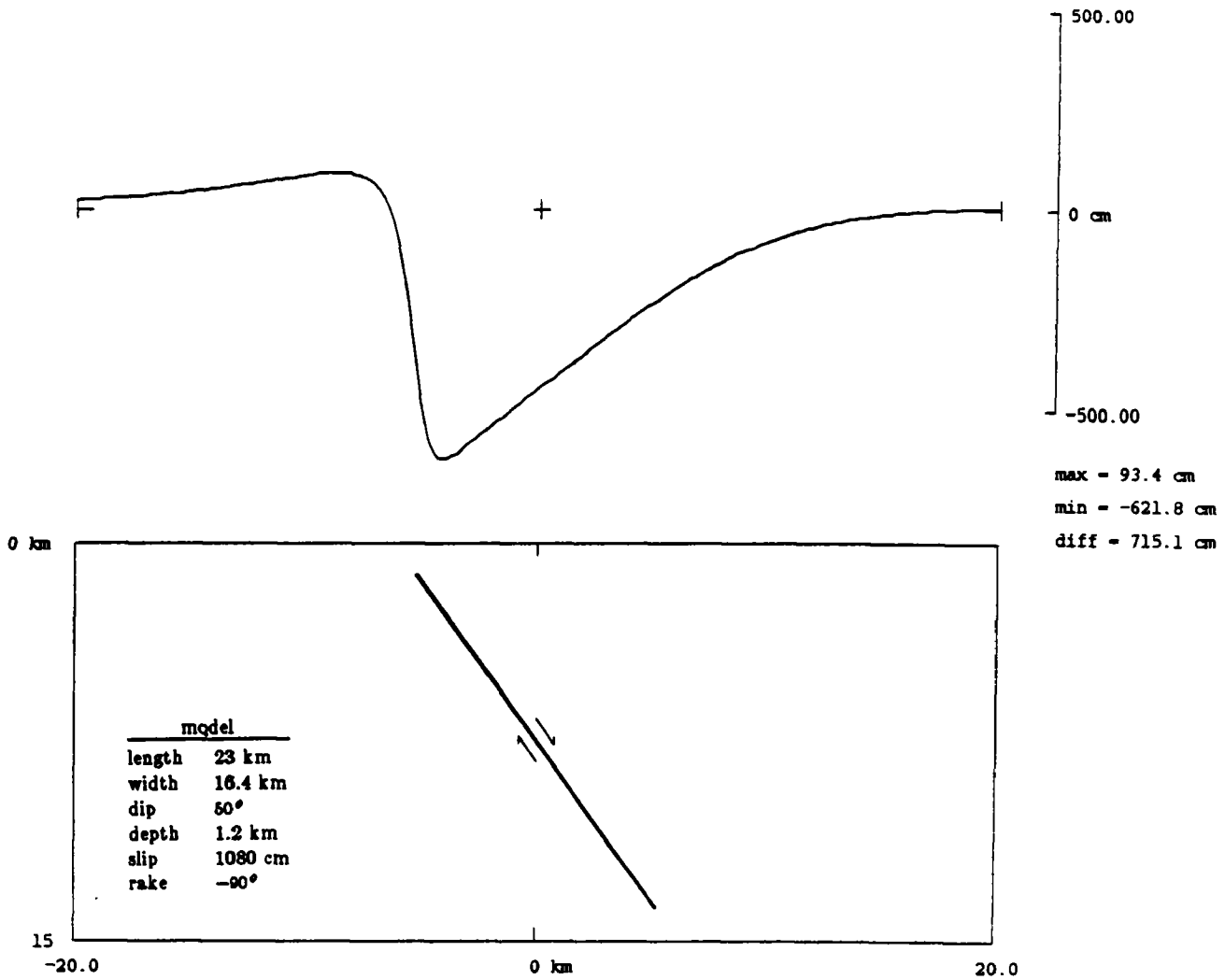

Figure 3. Elevation change profile of the Hebgen Lake earthquake (M_S 7.5) dislocation model obtained by Barrientos and others (1987). Profile trends perpendicularly to the strike of the fault model, and is centered on it. Vertical cross-section of fault model shown below profile (horiz. scale = vert. scale). Arrows indicate sense of movement on fault surface. For $\mu = 3.23 \times 10^{11}$ dyne/cm^2, this model yields $M_0 = 132 \times 10^{25}$ dyne-cm. Although the model shown does not extend to the surface, scarps with net tectonic throw of up to 5.5 m were observed (Witkind, 1964). Observed maximum subsidence was 6.7 m (Myers and Hamilton, 1964).

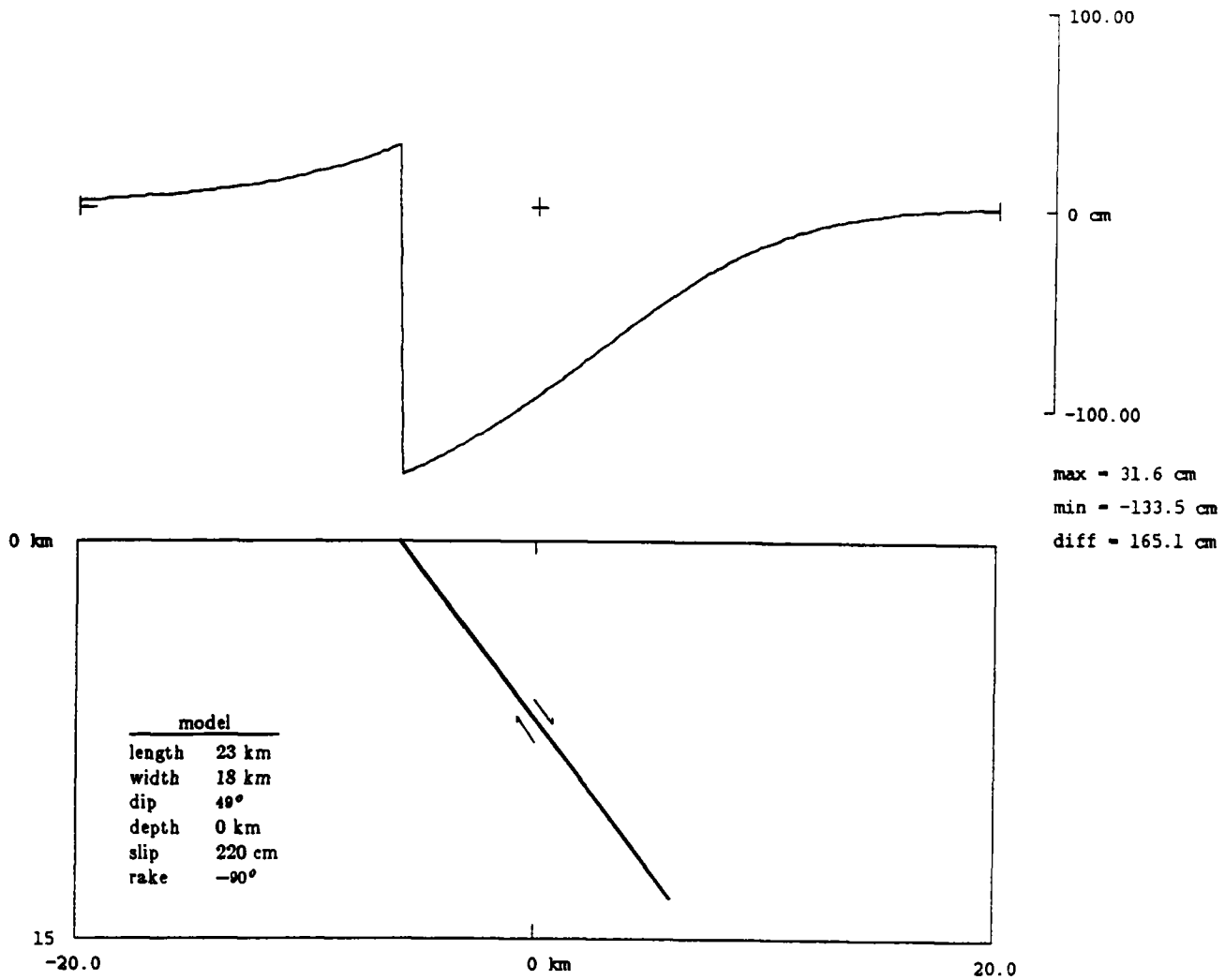

Figure 4. Elevation change profile of the Borah Peak earthquake (M_S 7.3) from model obtained by Barrientos and others (1987). For $\mu = 3.23 \times 10^{11}$ dyne/cm^2, this model yields $M_0 = 29 \times 10^{25}$ dyne-cm. The similarity in shape of this profile to that shown for the Hebgen Lake earthquake (previous figure - note difference in scale) is due primarily to similar dip-angles and maximum depth of faulting.

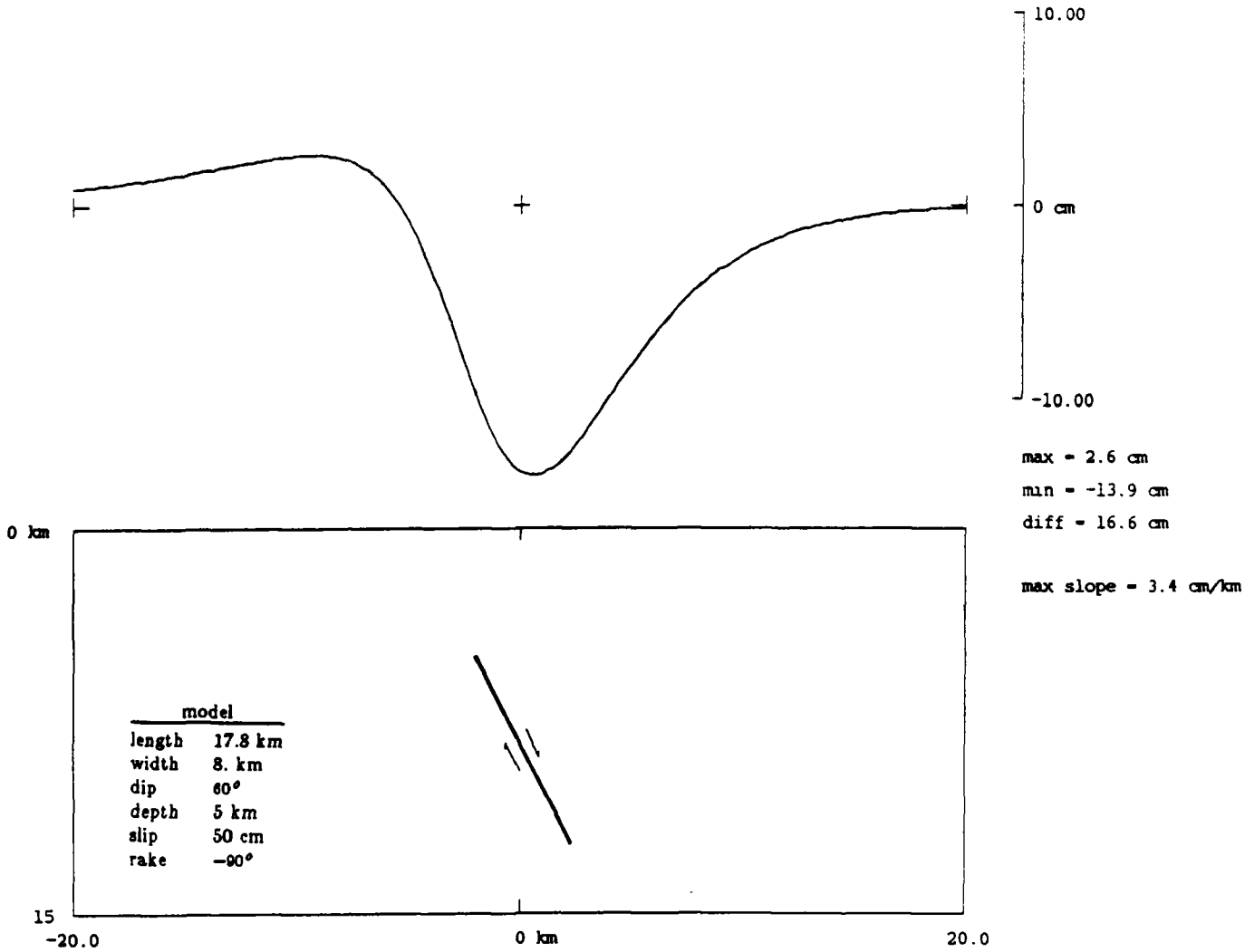

Figure 5. Elevation change profile of the Pocatello Valley earthquake (M_L 6.0) from model determined by Arabasz and others (1981). Using a shear modulus $\mu = 3.20\times10^{11}$ dyne/cm^2, this model yields a seismic moment $M_0 = 2.31\times10^{25}$ dyne-cm.

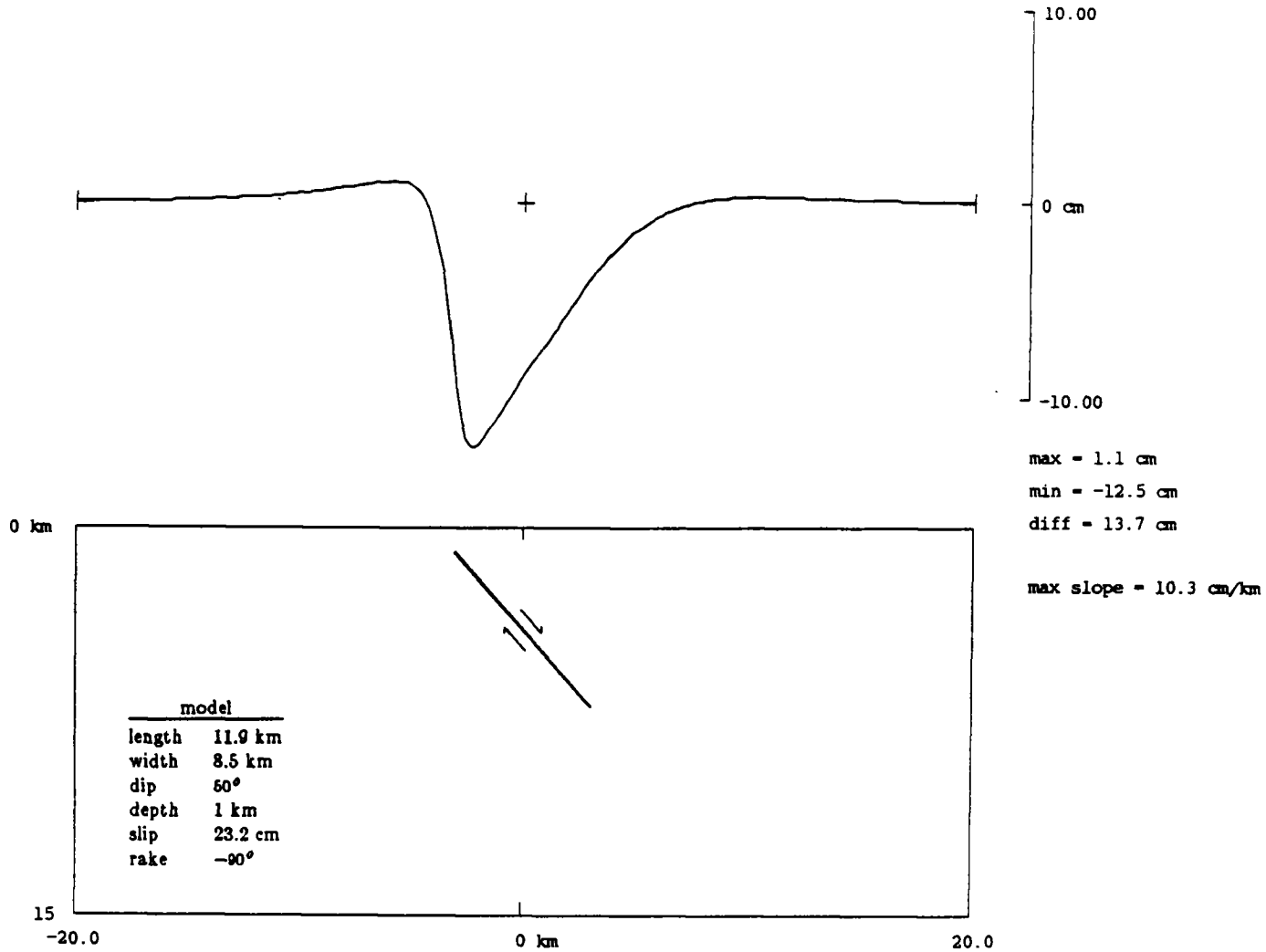

Figure 6. Elevation change profile of the Yellowstone earthquake (M_L 6.1). Model was inferred from data presented by Pitt and others (1979). Profile was adjusted to match the observed 12 - 13 cm maximum subsidence, but no attempt was made to match the actual level-line data. For shear modulus $\mu = 3.20 \times 10^{11}$ dyne/cm^2, this model yields $M_0 = 0.75 \times 10^{25}$ dyne-cm.

4. Parametric analysis

Previous examples have illustrated the general character of surface displacements observed for several historical M 6 to 6-1/2 and M 7 to 7-1/2 earthquakes. The next step in determining potential deformations for design earthquakes is to estimate a range of plausible faulting parameters, and to determine model sensitivity to those parameters. Surface displacements computed from dislocation models are sensitive to a number of faulting parameters, particularly to the depth of faulting and the fault plane dip angle. To illustrate that sensitivity, displacement profiles were computed for systematic variations of depth and orientation. In addition, the effect of curvature of the fault plane was examined. The effects of variable depth of faulting and orientation are more easily examined by first eliminating the effects due to the spatial dimensions of the fault. Thus, a number of elevation change profiles were computed for faults of extremely small size, but with variable position and orientation. These results then are used to help interpret similar variations in position and orientation on profiles computed for spatially extended fault models.

4.1. Point sources

To examine the effects of varying dip and depth, the effects of finite fault area were eliminated by examining the deformations produced by a point dislocation source. Deformations produced by a double-couple source are equivalent to those produced by slip on a fault plane: for a given dislocation source an equivalent distribution of double couples can be found, and described in terms of a symmetric 3×3 tensor (e.g, Aki and Richards, 1980, Chapter 3). For a vanishingly small fault plane the equivalence is particularly simple, with the elements of the moment tensor simply related to sines and cosines of the fault strike, dip and rake (e.g., Aki and Richards, 1980, Chapter 4). The strength of the double couple is the seismic moment $M_0 = \mu A s$. The point source models may be thought of as the shrinking of an extended fault plane such that M_0 remains constant in the limit of the area $A \rightarrow 0$ and slip $s \rightarrow \infty$. Equivalently, for distances large compared to the dimensions of a finite fault, the fault effectively behaves as a point double-couple source when computing static displacements. This representation then suggests that a finite dislocation source can always be modeled as the sum of a distribution of point sub-sources, such that the characteristic dimension of the equivalent fault area of the sub-sources is much less than the distance to the point where the displacements are computed. The point source representation then both provides a simplified means to qualitatively examine the effects of varying fault parameters, and a method for the computation of displacements due finite faults with complex shape and slip distribution.

Comer (1977) obtained the following expression for the vertical surface displacement $u(r,\phi)$ resulting from a point-source static moment tensor buried in a homogeneous and isotropic elastic half-space:

$$\frac{4\pi\mu}{M_0}\,u(r,\phi) = \frac{1}{2}\left(M_{xx}+M_{yy}\right)\left[\frac{-(\lambda+2\mu)}{(\lambda+\mu)}\frac{d}{R^3}+3\,\frac{d^3}{R^5}\right]$$
$$+\frac{1}{2}\left[(M_{xx}-M_{yy})\cos 2\phi + M_{xy}\sin 2\phi\right]\cdot\left[\frac{\mu}{\lambda+\mu}\frac{(R-d)(2+d/R)}{(R+d)R^2}-3\,\frac{r^2 d}{R^5}\right]$$
$$+M_{zz}\left[\frac{\lambda}{\lambda+\mu}\frac{d}{R^3}-3\,\frac{d^3}{R^5}\right]+\left(M_{xz}\cos\phi+M_{yz}\sin\phi\right)6\,\frac{rd^2}{R^5}$$

where d is the depth to the source, R is the distance to the source, $r=\sqrt{R^2-d^2}$ is the horizontal distance, ϕ is the azimuth of the evaluation point (ϕ=0 along the positive x-axis), M_{ij} are the normalized elements of the moment tensor, and λ and μ are the Lamé constants. From this relation, several important properties can be seen: 1) vertical displacements scale linearly with moment $M_0=\mu As$; 2) for the case of $\lambda=\mu$, substitution for M_0 shows the displacement to be independent of μ (i.e., for finite faults, displacements scale with slip, independently of μ); 3) symmetry of the moment tensor results in a fundamental ambiguity in determining from surface displacements which of the two double-couple nodal planes is the fault plane; and 4) displacements fall off as $1/R^2$ for distances large compared to the depth to the source, and as $1/d^2$ for horizontal distances small compared to that depth.

To illustrate these properties, elevation change profiles have been computed for point sources with varying orientation and depth. The point dislocation sources are oriented such that the profiles trend normal to strike, and only dip-slip movement is considered. **Figure 7** shows elevation changes for point dislocation sources buried at 1 to 9 km depths. The sources dip 45^0, and the moment varies from (0.022 to 1.6)$\times 10^{25}$ dyne-cm such that the resulting maximum subsidence is kept constant. From the above equation it can be shown that the moment required for constant maximum subsidence is proportional to d^2, which is verified in the profiles. The most prominent effects observed with decreasing depth to the source are the narrowing of the zone of subsidence (hereinafter called the *basin*), and the increase in the maximum horizontal gradient of elevation change. The gradient is proportional to $1/d$ for constant maximum subsidence, and hence the maximum horizontal gradient will scale as $1/d^3$ for a constant moment source positioned at variable depth. The displacement profiles of **figure 7** are symmetric, which reflects the ambiguity in nodal planes: sources dipping 45° in the opposite direction would produce identical displacements. Varying the dip of the point dislocation sources changes the shape of the dislocation profile, but the effects on maximum subsidence and gradient are not changed. **Figure 7a** shows profiles for dislocation sources dipping 60° (which are equivalent to profiles for point dislocation sources dipping 30° in the opposite direction).

The effect on maximum subsidence and maximum horizontal gradient from varying only dip angle is illustrated in **figure 8**. For these profiles, the point dislocation source was positioned at a depth of 7 km with a fixed moment of 10^{25} dyne-cm. While the overall shape of the resulting profiles are quite distinct, the maximum gradient changes less than 25 percent. Furthermore, the net subsidence, defined as the difference between the maximum uplift and maximum subsidence, changes by less than 5 percent. The profiles of sources with complimentary dips are seen to be mirror images, which again is the result of the ambiguity in nodal

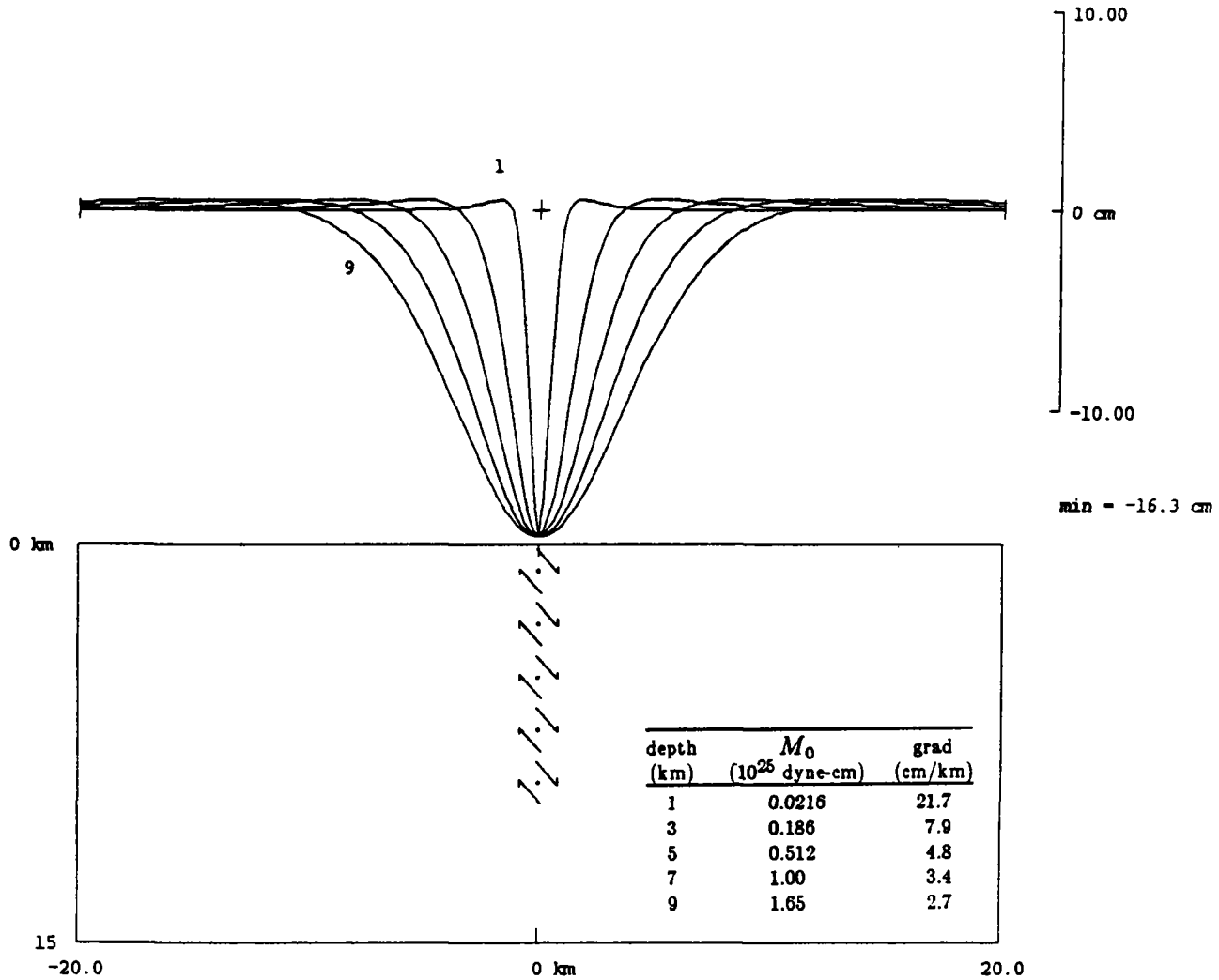

depth (km)	M_0 (10^{25} dyne-cm)	grad (cm/km)
1	0.0216	21.7
3	0.186	7.9
5	0.512	4.8
7	1.00	3.4
9	1.65	2.7

Figure 7. Elevation change profiles for a point moment source as a function of burial depth. Moment is adjusted to maintain constant subsidence in order to display how profile shape changes. Dip of point sources is 45°, and is indicated by arrows. Symmetry of profiles results from double-couple representation of dislocation, and is a fundamental property of moment tesor point sources. Shear modulus is $\mu = 3.20 \times 10^{11}$ dyne/cm^2 for this, and all subsequent profiles.

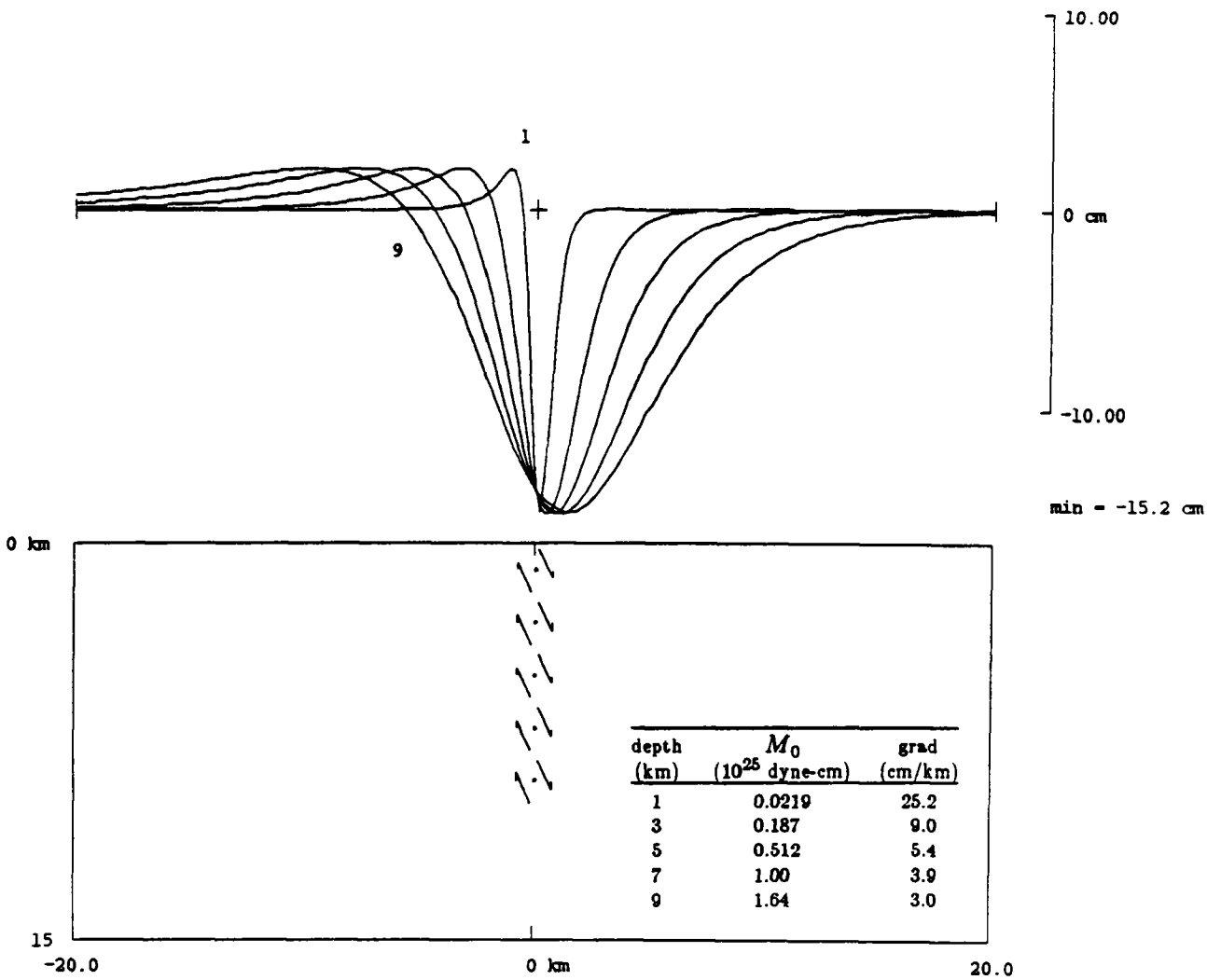

depth (km)	M_0 (10^{25} dyne-cm)	grad (cm/km)
1	0.0219	25.2
3	0.187	9.0
5	0.512	5.4
7	1.00	3.9
9	1.64	3.0

Figure 7a. Same as figure 7, but for a 60° dipping source.

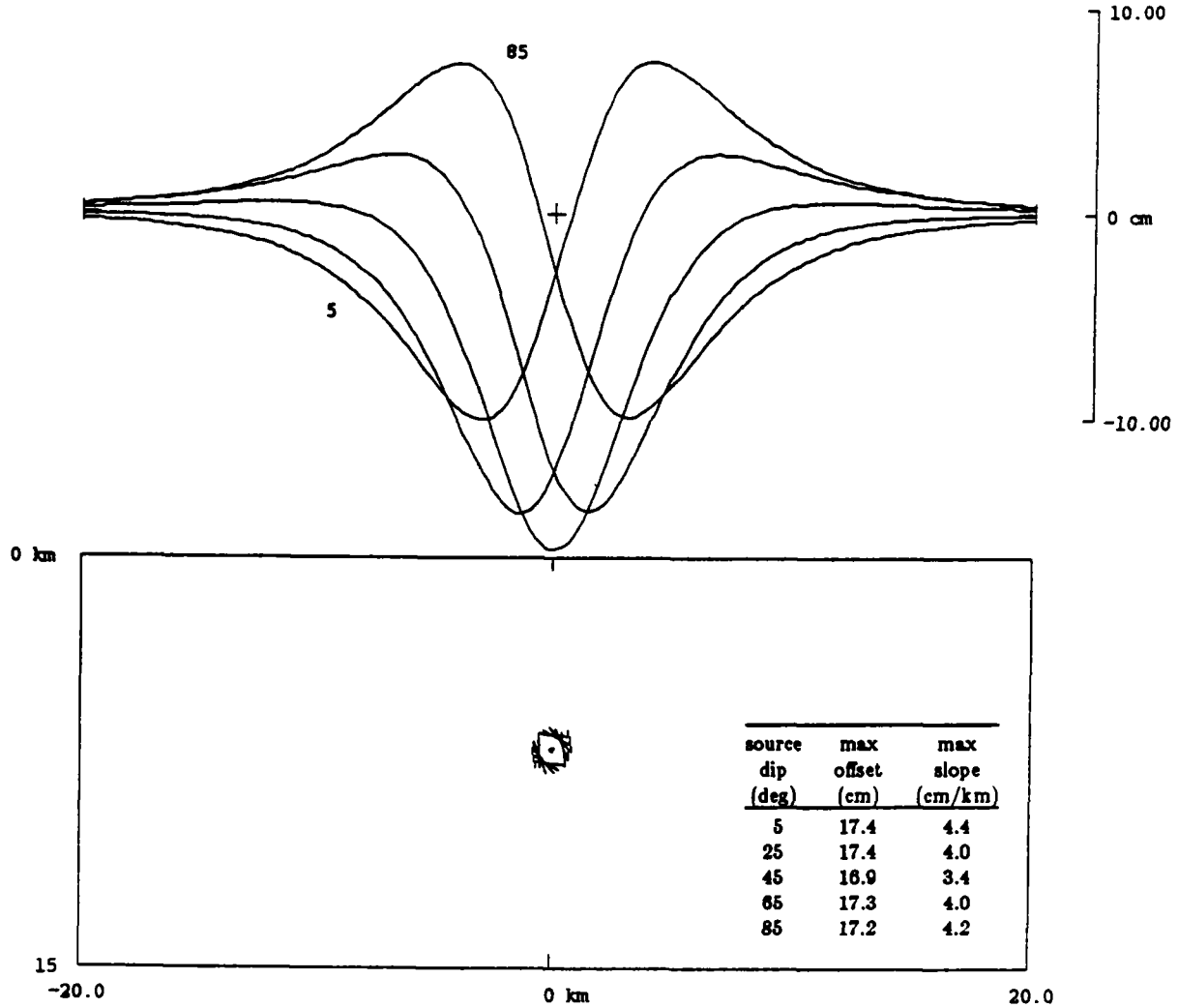

source dip (deg)	max offset (cm)	max slope (cm/km)
5	17.4	4.4
25	17.4	4.0
45	16.9	3.4
65	17.3	4.0
85	17.2	4.2

Figure 8. Effect of varying dip for a point moment source buried at depth of 7 km. Profiles of sources with complimentary dips are mirror images, which reflects the fundamental ambiguity in nodal planes from a double-couple source.

planes from a double couple source.

For point dislocation sources of constant moment, the predominant effect on net subsidence and horizontal gradient is burial depth. Dip angle also causes a significant, but considerably lesser effect. As burial depths decrease, the maximum subsidence increases as the square of burial depth, while the maximum gradient increases as the cube. The width of the basins is also a function of source burial depth; the the profiles in **figures 7** and **7a** suggest that the width of the basin is approximately proportional to twice the burial depth. While basin shape changes with varying dip angle, there is little change in basin width.

4.2. Finite sources

For dislocation sources with finite extent the effects of varying burial depth and dip angle are more complicated, but the general interpretation developed from the point source models is still a useful guide. For buried faults, the maximum horizontal gradient and maximum net subsidence are along a profile oriented normal to strike, and centered on the fault. **Figure 9** shows elevation profiles computed for a 45° dipping fault with dimensions equivalent to those obtained for the Pocatello Valley earthquake (length = 17.8 km, down-dip width = 8.1 km) by Arabasz and others (1981). As with the point source profiles, depth of burial has been varied while keeping the maximum subsidence constant by adjusting the amount of slip (unlike the point source profiles, the net subsidence is not also precisely constant). Dip is held constant. It is immediately apparent from **figure 9** that the profile shapes are not symmetric (as was the case for point source dislocations), and that the degree of asymmetry increases with decreasing burial depth. However, the effect of decreasing burial depth is still to decrease basin width and increase the values of net subsidence and maximum horizontal gradient. **Figure 9a** shows similar results for a 60° dipping plane. Basin width is seen from these profiles to decrease with decreasing depth, which suggests that the basin width is approximated by the maximum depth of faulting.

Figure 10 shows the effect of varying dip angle for a fault of finite extent, while fixing the depth to the center of the fault. The amount of slip is held fixed, and the dimensions are the same as the Pocatello Valley fault model. Relatively little change is seen in the net subsidence, from 14.3 cm at 5° to 17.7 cm at 85°, but the maximum horizontal gradient varies by about a factor of 2. Profiles with complimentary dip-angles are not precisely symmetric, but the symmetry is not greatly diminished at this burial depth. This illustrates the difficulty in determining fault planes from geodetic data when the fault does not come near the surface. In general, these examples indicate that for finite faults, net subsidence and basin width are primarily dependent on the depth extent of faulting. Maximum horizontal gradient is affected both by burial depth and dip angle, with the dip-angle effect increasing with decreasing burial depth. For finite faults, these effects can be visualized as resulting from the (sometimes competing) effects of moving moment sources closer to the surface, and changing the vertical projection of slip.

The length selected for the fault models has a relatively weak affect on these results as long as the slip remains constant. For fault lengths which are on the order of the dimension of the

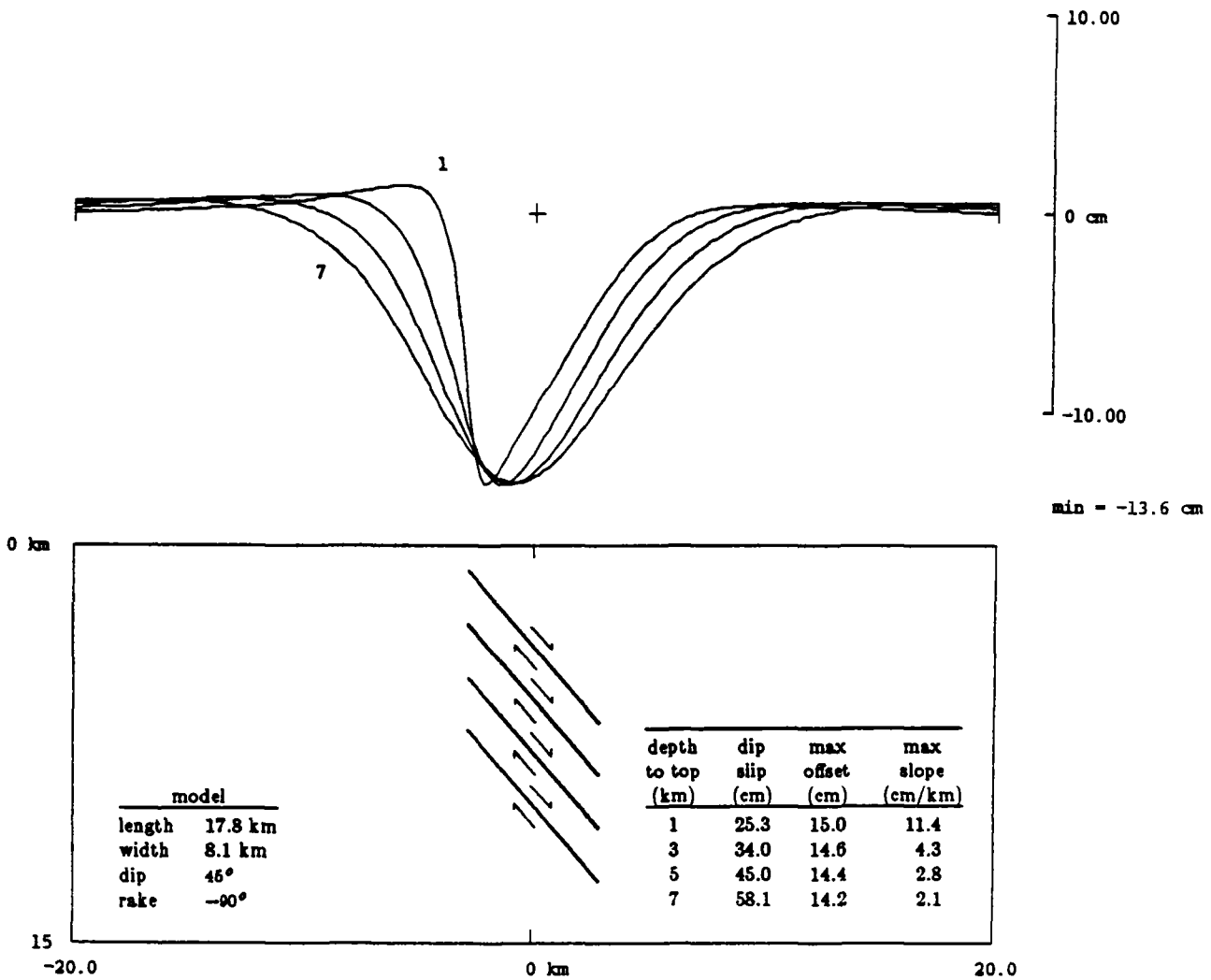

Figure 9. Effect of varying depth for a finite dislocation surface. Same fault dimensions as Pocatello Valley earthquake model. Dip is 45°. Note loss of symmetry in profile shape at shallow depths due to finite extent of source. Slip adjusted to maintain constant maximum subsidence of 13.6 cm.

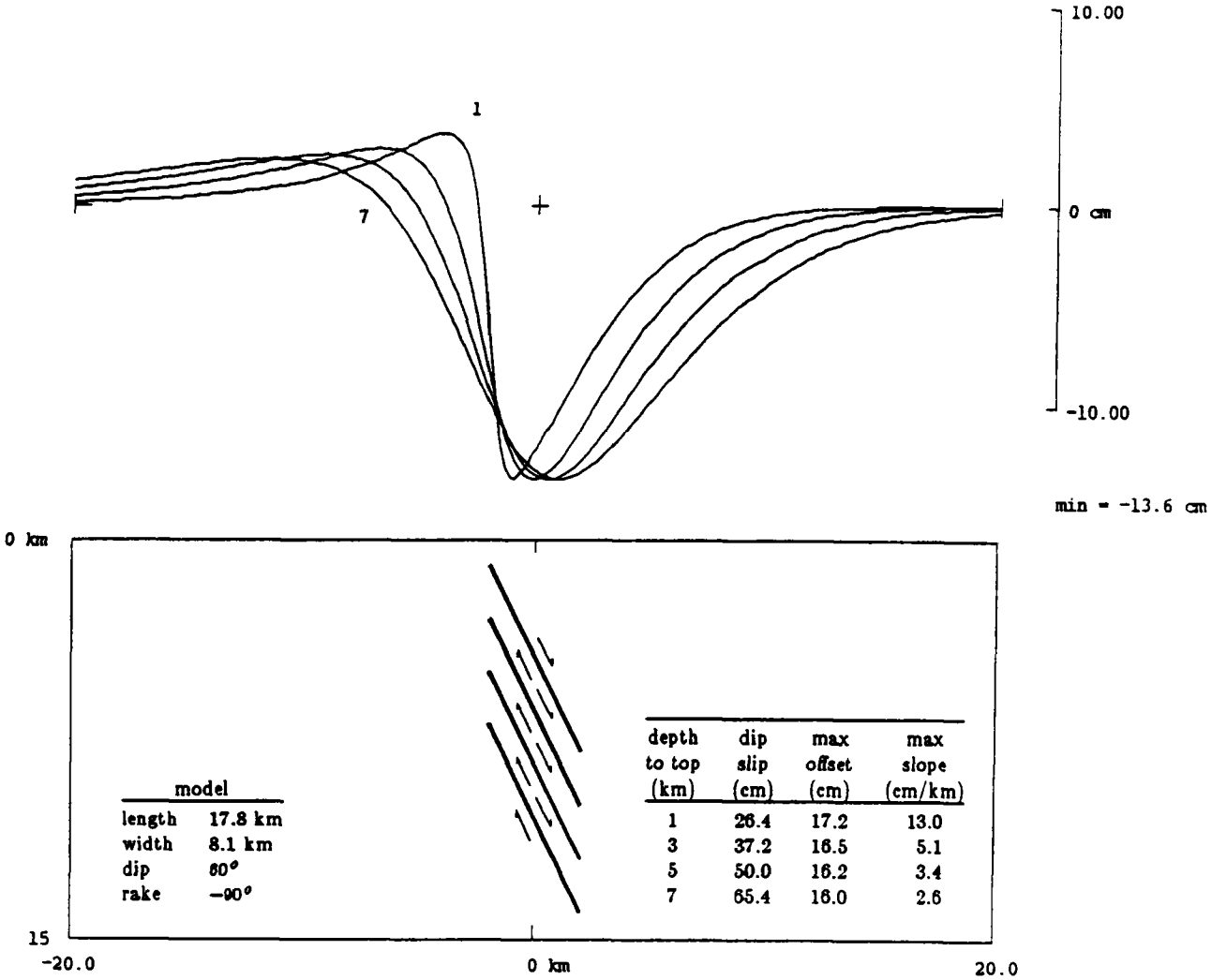

Figure 9a. Same as figure 9, but for 60° dip.

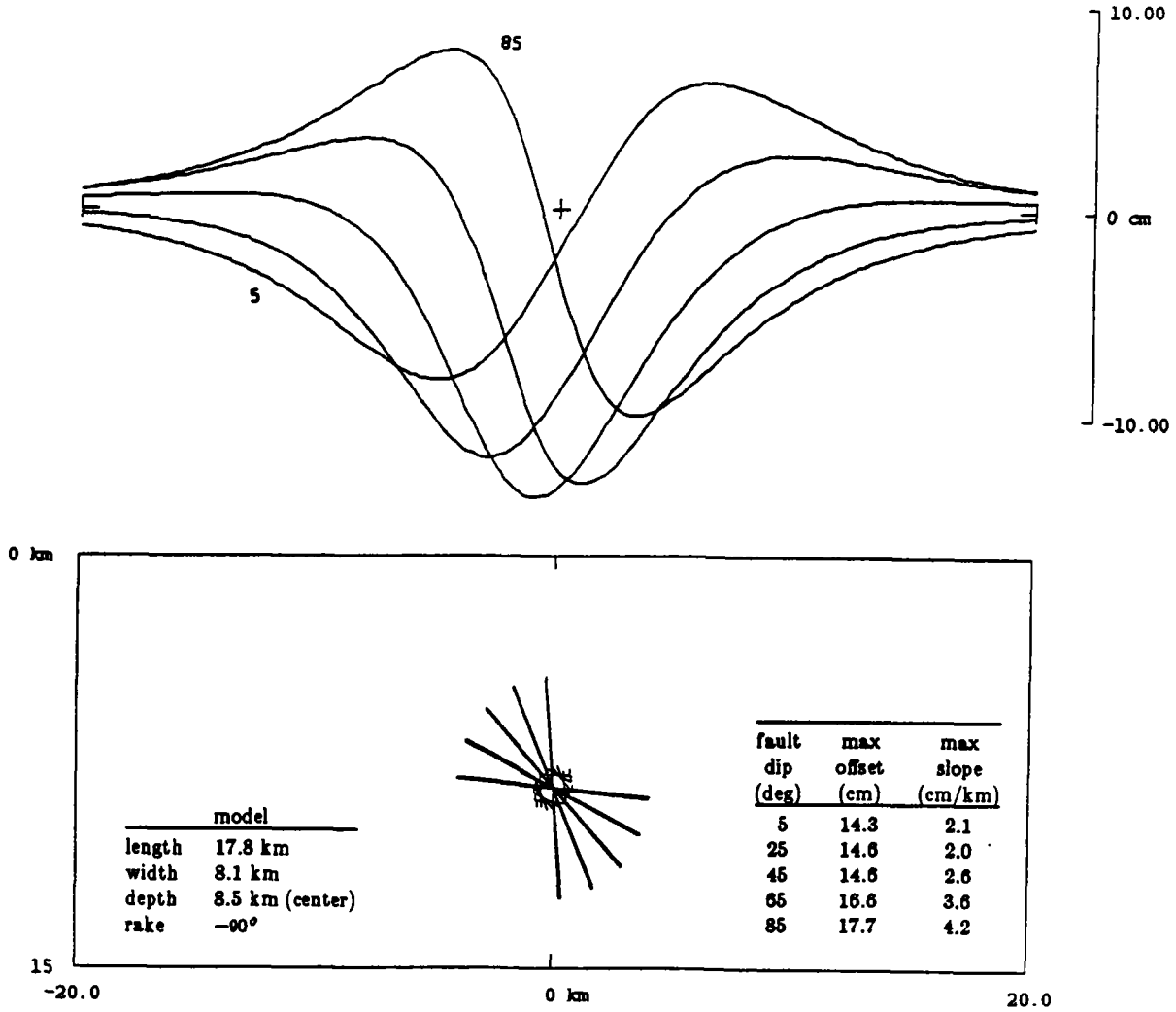

Figure 10. Effect of varying dip for a finite dislocation surface. Same fault dimensions as Pocatello Valley earthquake model. Slip fixed at 50 cm. Note that profiles from faults with complimentary dips are not precise mirror images, as for the case of point sources.

width, vertical displacements vary only by a small amount along strike near the center of the fault; the greatest effect of variable fault length is simply to change the moment, and therefore the amount of slip if other factors are held constant. Depth of burial and dip-angle remain the most sensitive parameters.

A number of profiles are shown in **figures 11** through **14** to estimate the range of surface displacements for hypothetical earthquakes assumed to be near or at the threshold of surface rupture. Each figure shows a set profiles with fixed depth to the top of the fault, but with varying dip. Depths of burial range between 1 and 5 km, which represents a plausible range for ISB earthquakes. The moment was set at about 4 x 10^{25} dyne-cm, and the dimensions of the fault chosen, within reason, to maximize slip. Profiles shown on **figures 11** through **14** are presented at this point primarily as further examples of the effect of variable slip and dip for finite faults. In later sections, they will be used as a suite of possible ground deformations for design earthquakes.

To evaluate the effects on surface displacements of curvature of the fault surface, deformations from a class of weakly curved faults were computed. Curvature of the fault was simulated by a quadratic in depth via the relation $y = d/tan(\delta) + c\,(z - d)^2$, where y is the horizontal distance from the up-dip projection of the fault at the surface, d is the depth to the top of the fault, δ is the dip angle at the top of the fault surface, c is the curvature parameter, and z is the depth to the corresponding point on the fault surface. The resulting elevation change profiles are shown in **figures 15** and **15a**. Superimposed on these profiles are those from planar models with equivalent dimensions, and with dips equal to the average dip of the curved faults. Several effects can be seen from these curved models: 1) The dip of the curved models is about 90° at the top the dislocation surface, and so the vertical projection of slip is greater there than for the 60° dipping planar models. This results in greater net subsidence for shallow burial depths; 2) At greater depths, the previous effect is overcome by the effect of the moment release being positioned below that for the corresponding planar model; 3) Basin width is narrower, particularly for shallow burial depths; 4) For surface faults, the relative uplift is much reduced on the upthrown block, and there is a large "bulge" on the downthrown block. The profiles indicate that these effects are fairly small, however, and there is also no evidence from historic seismicity faulting on curved faults. Given the numerous other simplifying assumptions in the modeling, the lack of observational evidence for curved faults, and the relatively small effect seen in the profiles, curved faults are not considered further for this study.

Factors which might have significant effects on computed elevation changes, but are not included in the simple faulting models, include: 1) possible variations in slip (and direction) over the fault plane; 2) multiple rupture planes; 3) non-faulting deformation sources (e.g. Fairview Peak); 4) anelastic, inhomogeneous or non-isotropic media; 5) stress singularities at the model fault edges; and 6) non-rectangular shaped faults (equivalent to variable slip). While some of these effects have been examined in the literature, sufficient data from historical earthquakes does not exist to allow for an evaluation of their engineering significance. Thus, lacking data to constrain more complicated models, results will be based only on the simple USP model.

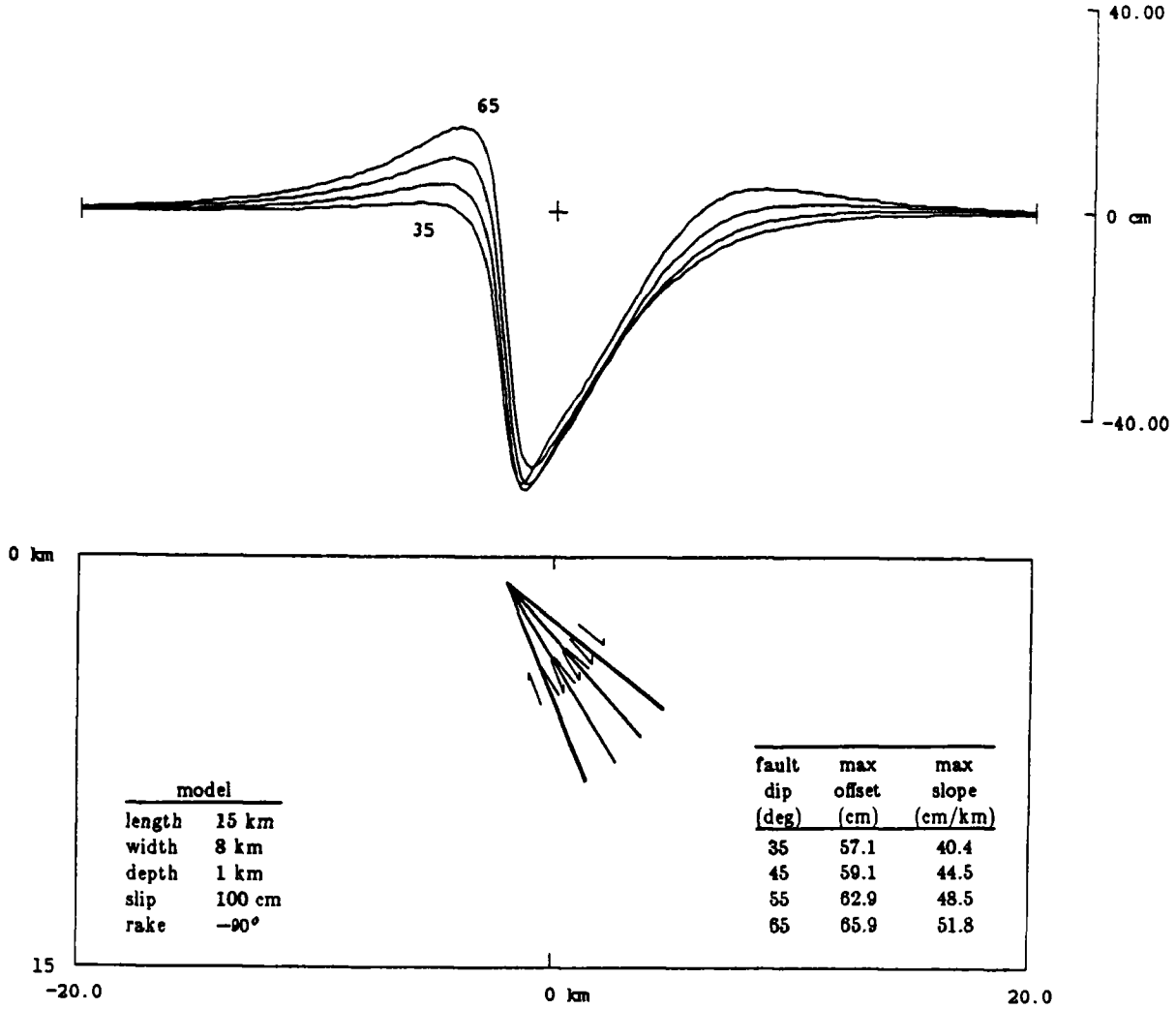

Figure 11. Elevation profile for planar source with 100 cm slip, 15 km length, and 8 km slip ($M_0 = 3.8 \times 10^{25}$ dyne-cm) buried at a depth of 1 km. Equivalent magnitude would be approximately M_L 6.5 (Doser and Smith, 1982).

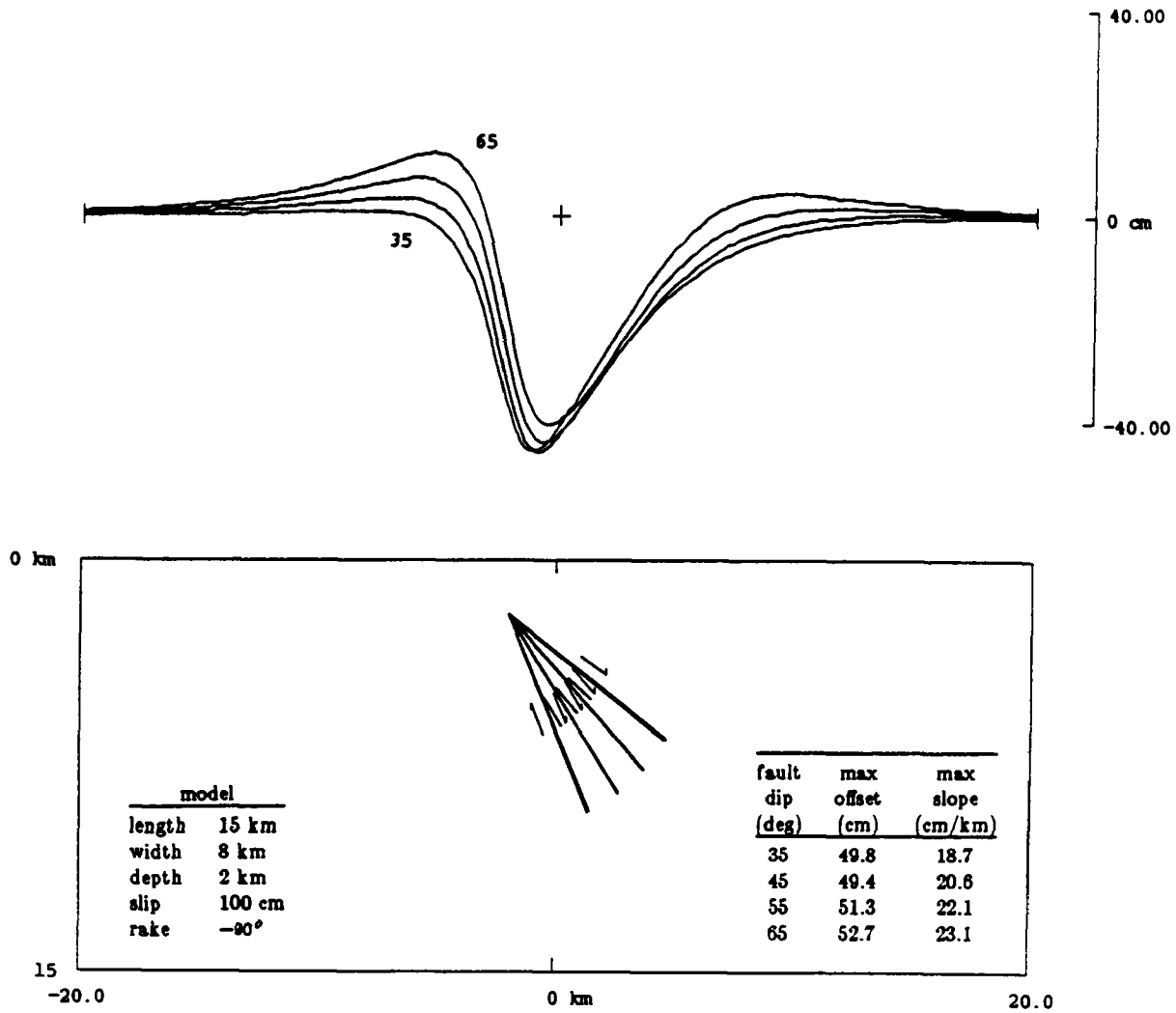

Figure 12. Same as figure 11, but for burial depth of 2 km.

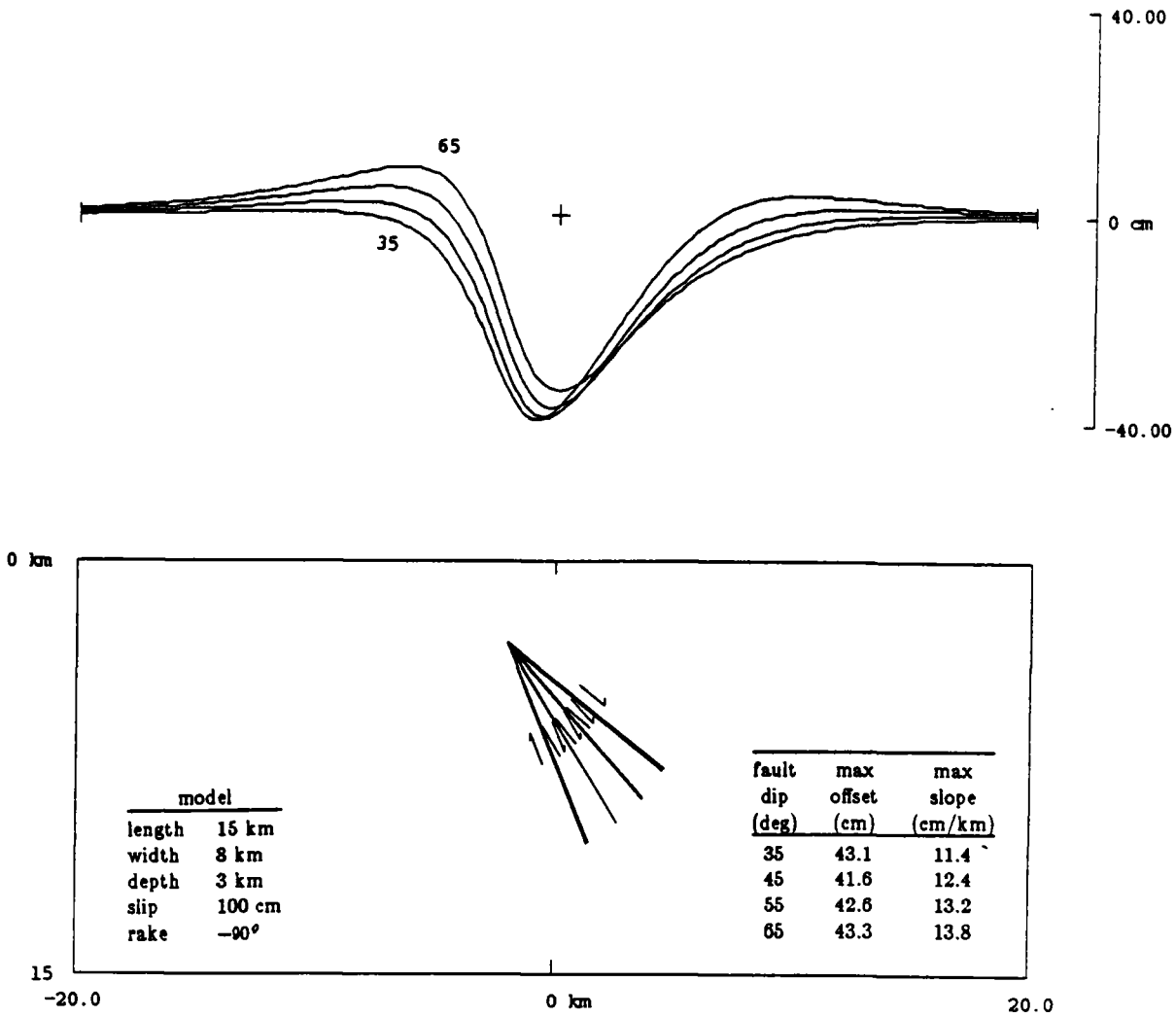

Figure 13. Same as figure 11, but for burial depth of 3 km.

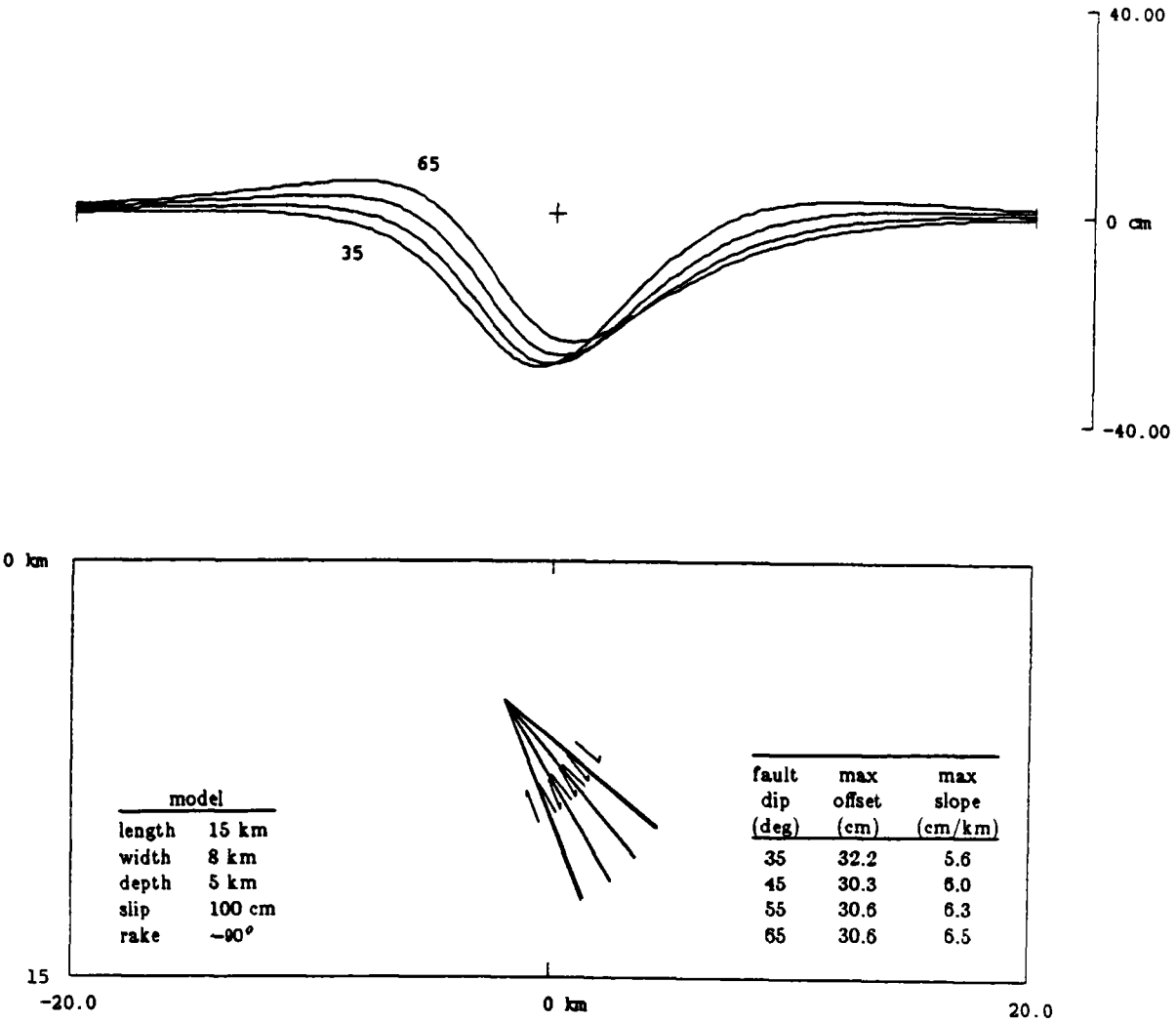

Figure 14. Same as figure 11, but for burial depth of 5 km.

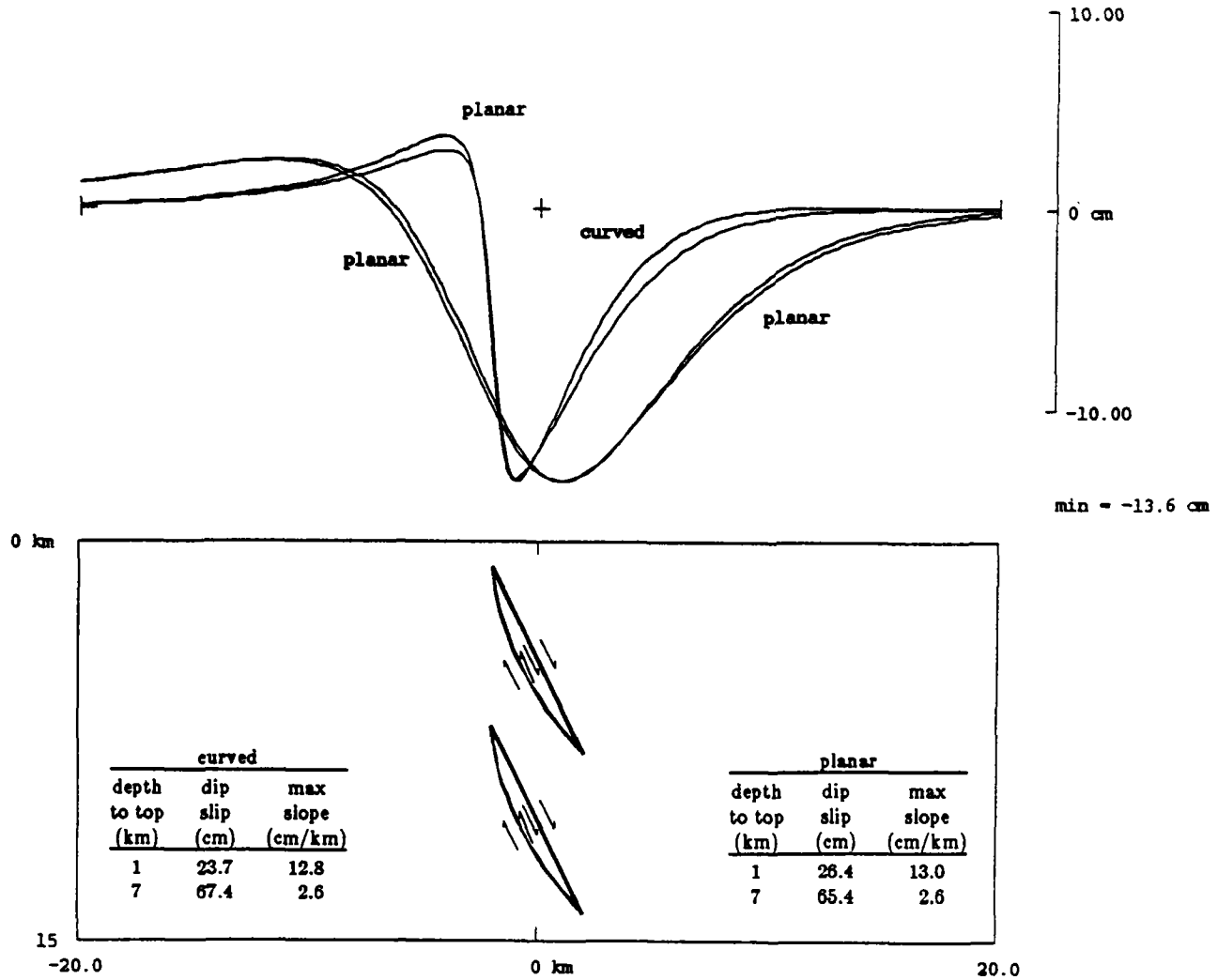

Figure 15. Effect of curvature. Curved faults have average dip of 60°, and produce profiles with slightly narrower zones of subsidence. Burial depths are 1 and 7 km, and dimensions are equivalent to Pocatello Valley model. Slip adjusted to maintain constant maximum subsidence. Curvature parameter was 0.07/km (see text). Curved faults yield slightly narrower basins than do planar models shown for comparison. See text for further discussion.

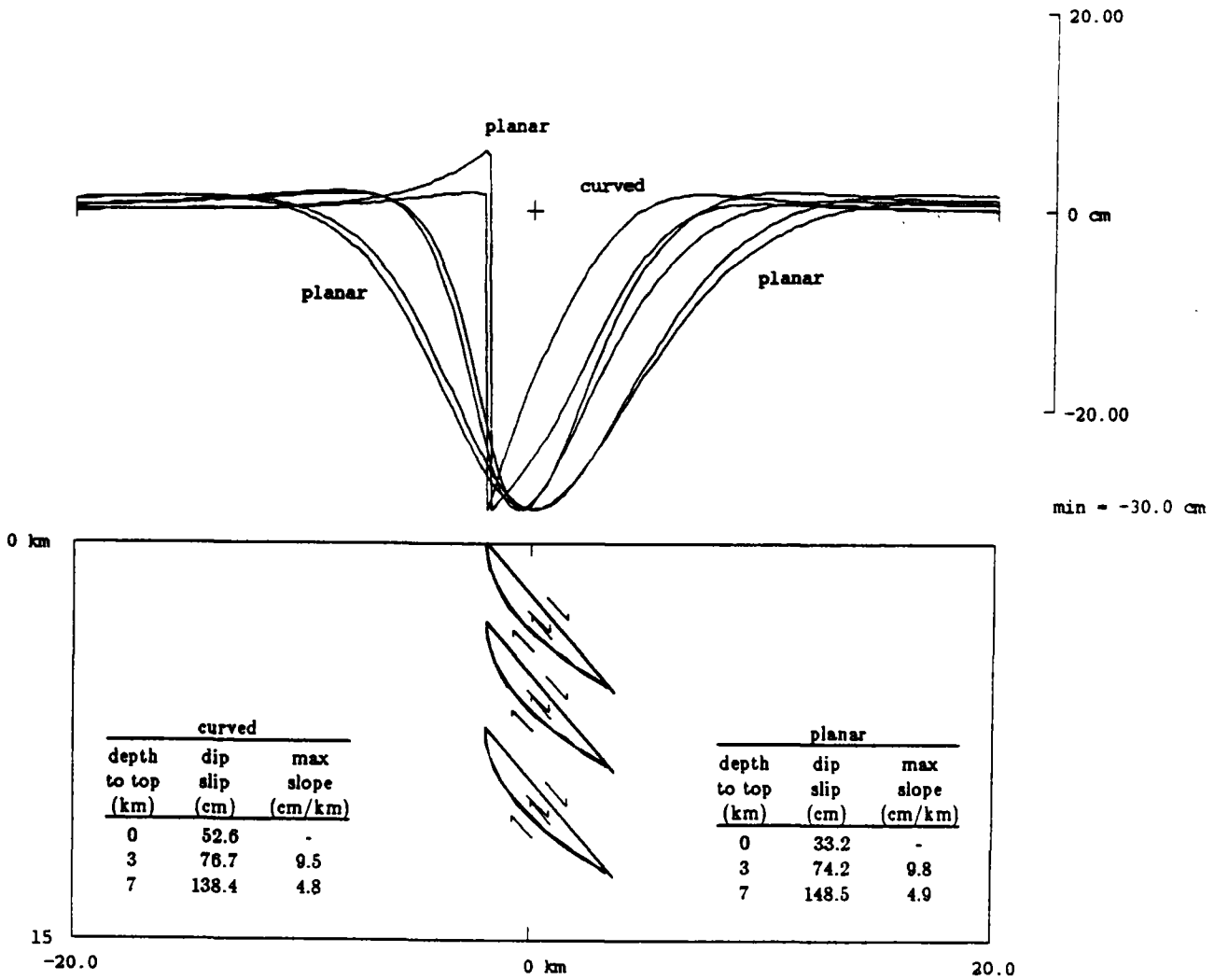

Figure 15a. Effect of curvature for faults with average dips of 45°. Fault dimensions are the same as in figures 11 through 14. Slip adjusted to give constant maximum subsidence. Curvature parameter was 0.18/km (see text).

4.3. Implications for design earthquakes

The profiles presented in **figures 5 - 15** provide an alternative perspective on deformations observed for historical non-surface-faulting earthquakes. For example, the Pocatello Valley earthquake has sometimes been used as an analogue for future, $M \geq 6$ earthquakes which are not associated with active surface faults. The profiles indicate, however, that for an earthquake of equivalent moment release, much greater surface deformations could result if the depth of faulting were significantly shallower than at Pocatello Valley.

Aftershock distributions of the 1975 Yellowstone earthquake suggests the possibility of faulting extending to within 1-2 km of the surface. Furthermore, if geologic deformations observed for the Clarkston earthquake were not due primarily to liquefaction or slumping effects, then (assuming that offsets on secondary cracks should not be greater than net tectonic subsidence) a maximum subsidence of up to 0.6 m may be possible for other non-surface faulting ISB earthquakes. Assuming that 0.6 m represents a plausible maximum net tectonic subsidence, and is just below the threshold of surface rupture, **figures 11** through **14** show a range of faulting models which could generate equivalent surface displacements. For the suite of faults buried at 1 km, and with dip-angles ranging between 35° and 65°, the resulting maximum net tectonic subsidences are about 60 cm, with maximum horizontal gradients of 45 cm/km. For 2 km depths, these values are 50 cm and 20 cm/km, respectively, and by 5 km depth the numerical values are 30 cm and 7 cm/km. If the minimum depth of faulting is somewhat arbitrarily selected to be 2 km, then potential net tectonic subsidence and maximum horizontal gradients which are several times that observed for the Pocatello Valley earthquake are possible for an $M \approx 6-1/2$ earthquake.

The parameters used in these models are not necessarily extreme values for M 6 to 6-1/2 earthquakes; changes in maximum subsidence or horizontal gradient by a factor of 2-4 are possible without changing the computed magnitude by more than a few tenths of a unit. This can occur for several reasons: 1) slip can be traded off with fault area to maintain a constant seismic moment; 2) many magnitude scales are proportional to the log of the seismic moment (e.g., Hanks and Kanamori, 1979; Doser and Smith, 1982), which allows small changes in magnitude for large changes in moment; and 3) there is uncertainty in precisely what the maximum moment of a non-surface-faulting earthquake should be. Thus, there remains considerable uncertainty in the selection of an appropriate upper bound model for non-surface-faulting earthquakes.

Determining appropriate model parameters for surface-faulting design earthquakes is considerably less ambiguous. Minimum depths of faulting may be taken to be zero (whether or not the surface scarps are assumed to be direct continuations of the fault plane at depth), and the range of dips based on observations of historical earthquakes is fairly well constrained. Aside from complications related to possible non-faulting deformation mechanisms (such as magma emplacement), the observations of historical earthquakes are well-represented by simple planar dislocation models. Planar models similar to that of the Hebgen Lake earthquake (**figure 3**) present reasonable upper bounds for the static deformation from surface-faulting, ISB design earthquakes.

5. Discussion

Modeling simulations suggest that maximum net tectonic subsidence of up to 50 cm is possible for non-surface rupturing earthquakes in the magnitude 6 to 6-1/2 range, if faulting extends to within about 2 km of the surface. Corresponding maximum horizontal gradients of up to about 20 cm/km are also predicted. Basin widths (width of the zone of deformation) of 10 to 15 km are possible, and may be numerically approximated by the maximum depth of faulting. Given a fault model having fixed width, length and slip, he most critical factor in evaluating potential subsidence is how close the dislocation approaches to the surface. Dip angle is also important, but is primarily of concern for evaluating maximum horizontal gradients; the effect of varying dip angle is reduced with increasing depth of burial. Other factors, such as curvature of the fault surface or non-uniform slip, may produce measurable differences in surface deformations from those predicted by uniform-slip planar (USP) models, but these effects are not large compared to to the effect of varying burial depth. Because of the many simplifying assumptions made in applying the USP model to predict potential maximum surface deformations, effects from these factors are not considered significant.

Deformation data from historic earthquakes provides the most direct constraints on parameters used in the dislocation models. Unfortunately, leveling data from non-surface-rupturing historic Basin and Range earthquakes has been available in only a few instances, and insufficient numbers of observations have prevented making detailed or unique interpretations. Evaluation of the minimum depth of faulting for non-surface rupturing ISB earthquakes is therefore difficult. Evidence for shallow minimum depths of faulting includes the aftershock distribution of the 1975 M_L 6.1 Yellowstone Park earthquake, with hypocentral depths ranging between 0 and 6 km; in comparison, aftershocks of the 1975 M_L 6.0 Pocatello Valley earthquake had focal depths, in the 5 - 11 km range. The focal depth distribution of the Yellowstone Park earthquake may, however, have been strongly influenced by the complex tectonic setting at the margin of the Yellowstone caldera. Geologic deformation observed related to the 1925 M 6-3/4 Clarkston, Montana earthquake may also suggest the possibility of faulting extending close to the surface, although insufficient data exists to make a confident evaluation.

Of the three M $>$ 6 earthquakes for which leveling data is available, remarkably similar values of maximum tectonic subsidence have been observed. Subsidence observed for the 1931 M 6.4 Valentine Texas, 1975 M_L 6.1 Yellowstone, and 1975 M_L 6.0 earthquakes were 12.2, 12.5, and 13.6 cm, respectively. Unfortunately, except for the Pocatello Valley earthquake, the positions of the fault planes with respect to the level lines is not well determined, and the actual maximum subsidence may have been somewhat greater. The general agreement in the observed maximum subsidence between these earthquakes might be interpreted to suggest that these numbers reflect reasonable deformations for potential future M 6 to 6-1/2 ISB earthquakes. However, theoretical modeling suggests that faults with equivalent moment release and size could, if positioned closer to the surface, produce vertical deformations which are significantly larger than the historical deformations.

Deformation data is substantially better for historical surface faulting earthquakes, and considerable success has been achieved in modeling the geodetic data with simple planar dislocations. These studies have indicated that complications such as curved faults and variable slip

distributions are not required by the data, and in some cases are not allowed by it. Maximum vertical offsets of up to 7 m are suggested for large-magnitude surface rupturing earthquakes in the ISB, although 2-5 m may be more typical. Basin widths of 17-20 km are suggested, and are largely controlled by the maximum depth of faulting. Maximum tilting of the basins may exceed 400-500 μrad. These studies have also indicated that the vertical surface offsets observed on fault traces may not be indicative of the average slip at depth, and in general underestimate slip determined from the geodetic models.

References

Aki, K. and P. G. Richards, *Quantitative Seismology: Theory and Methods, Volume 1*, p. 557, W. H. Freeman and Company, San Francisco, 1980.

Allmendinger, R. W., J. W. Sharp, D. Von Tish, L. Serpa, L. Brown, S. Kaufman, J. Oliver, and R. B. Smith, Cenozoic and Mesozoic structure of the eastern Basin and Range province, Utah, from COCORP seismic reflection data, *Geology, 11*, 532-536, 1983.

Arabasz, W. J. and D. R. Julander, Geometry of seismically active faults and crustal deformation within the Basin and Range - Colorado Plateau Transition in Utah, in *Extensional tectonics of the Basin and Range Province: A perspective*, edited by Mayer, L., Geological Society of America Special Paper no. 208, 1986.

Arabasz, W. J., J. C. Pechmann, and E. D. Brown, Observational seismology and the evaluation of earthquake hazards and risk in the Wasatch Front area, Utah, in *Assessment of Regional Earthquake Hazards and Risk Along the Wasatch Front, Utah*, vol. 1, edited by P. L. Gori and W. W. Hayes, pp. D1-D39, U. S. Geological Survey Open-File Report 87-585, 1987.

Arabasz, W. J., W. D. Richins, and C. J. Langer, The Pocatello Valley (Idaho-Utah border) earthquake sequence of March to April 1975, *Bulletin of the Seismological Society of America, 71*, 803-826, 1981.

Bache, T. C., D. G. Lambert, and T. G. Barker, A source model for the March 28, 1975 Pocatello Valley earthquake from time-domain modeling of teleseismic P-waves, *Bulletin of the Seismological Society of America, 70*, 405-418, 1980.

Barrientos, S. E., R. S. Stein, and S. N. Ward, Comparison of the 1959 Hebgen Lake, Montana and the 1983 Borah Peak, Idaho, earthquakes from geodetic observations, *Bulletin of the Seismological Society of America, 77*, 784-808, 1987.

Bodle, R. R., *United States Earthquakes -- 1944*, p. 43, U. S. Department of Commerce, Coast and Geodetic Survey, Serial No. 682, 1946.

Bodle, R. R. and L. M. Murphy, *United States Earthquakes -- 1945*, p. 38, U. S. Department of Commerce, Coast and Geodetic Survey, Serial No. 699, 1947.

Bonilla, M. G., Minimum earthquake magnitude associated with coseismic surface faulting, *Bulletin of the Association of Engineering Geologists, 25*, 17-29, 1988.

Bucknam, R. C., *Leveling data from the epicentral area of the March 27, 1975, earthquake in Pocatello Valley, Idaho*, p. 6, U.S. Geological Survey Open-File Report 76-52, 1976.

Bucknam, R. C. and R. S. Stein, Preface to collection of papers on the 1983 Borah Peak, Idaho, earthquake, *Bulletin of the Seismological Society of America, 77*, 691-693, 1987.

Byerly, P., The Montana earthquake of June 28, 1925, GMT, *Bulletin of the Seismological Society of America, 16*, 209-263, 1926.

Byerly, P., The Texas earthquake of August 16, 1931, *Bulletin of the Seismological Society of America, 24*, 81-99, 1934.

Byerly, P., Nature of faulting as deduced from seismograms, *Geological Society of America Special Paper, 62*, 75-86, 1955.

Byerly, P., D. B. Slemmons, D. Tocher, K. V. Steinbrugge, D. F. Moran, and W. K. Cloud, The Fallon-Stillwater earthquakes of July 6, 1954 and August 23, 1945, *Bulletin of the Seismological Society of America, 46*, 1-40, 1956.

Callaghan, E. and V. P. Gianella, The earthquake of January 30, 1934, at Excelsior Mountains, Nevada, *Bulletin of the Seismological Society of America, 25*, 161-168, 1935.

Comer, R. P., *Tsunami generation by earthquakes [Ph.D. Thesis]*, Massachusetts Institute of Technology, 232p., 1977.

Cook, K. L and R. K. Nye, Effects of the Pocatello Valley (Idaho-Utah border) earthquake of March 28, 1975 (UTC), in *Earthquake Studies in Utah: 1850 to 1978*, edited by Arabasz, W. J., R. B. Smith, and W. D. Richins, pp. 445-457, University of Utah Seismograph Stations, Salt Lake City, Utah, 1979.

Crone, A. J. and M. N. Machette, Surface faulting accompanying the Borah Peak earthquake, central Idaho, *Geology, 12*, 664-667, 1984.

Crone, A. J., M. N. Machette, M. G. Bonilla, J. J. Lienkaemper, K. L. Pierce, W. E. Scott, and R. C. Bucknam, Surface faulting accompanying the Borah Peak earthquake and segmentation of the Lost River fault, central Idaho, *Bulletin of the Seismological Society of America, 77*, 739-770, 1987.

Dewey, J. W., Instrumental seismicity of central Idaho, *Bulletin of the Seismological Society of America, 77*, 819-836, 1987.

Dewey, J. W., W. H. Dillinger, J. Taggart, and S. T. Algermissen, A Technique for seismic zoning: Analysis of earthquake locations and mechanisms in northern Utah, Wyoming, Idaho, and Montana, *Proceedings of the International Conference on Microzonation for Safer Construction Research and Application, II*, 879-895, Seattle, Washington, October 30 - November 3, 1972.

Doser, D. I., Source parameters and faulting processes of the 1959 Hebgen Lake, Montana, earthquake sequence, *Journal of Geophysical Research, 90*, 4537-4555, 1985.

Doser, D. I., Earthquake processes in the Rainbow Mountain - Fairview Peak - Dixie Valley, Nevada region, *Journal of Geophysical Research, 91*, 12572-12586, 1986.

Doser, D. I., The August 1931 Valentine, Texas, earthquake: Evidence for normal faulting in West Texas, *Bulletin of the Seismological Society of America, 77*, 2005-2017, 1987.

Doser, D. I., Source parameters of Intermountain earthquakes [abstract], *Eos, 68*, p. 1352, 1987.

Doser, D. I. and R. B. Smith, Seismic moment rates in the Utah region, *Bulletin of the Seismological Society of America, 72*, 525-551, 1982.

Dumas, D. B., M. J. Dorman, and G. V. Latham, A reevaluation of the August 16, 1931 Texas earthquake, *Bulletin of the Seismological Society of America, 70*, 1171-1180, 1980.

Fraser, G. D., Intensity, magnitude, and ground breakage, *The Hebgen Lake, Montana Earthquake of August 17, 1959*, 31-35, U.S. Geological Survey Professional Paper 435, 1964.

Gianella, V. P. and E. Callaghan, The earthquake of December 20, 1932, at Cedar Mountain. Nevada and its bearing on the genisis of Basin Range structure, *Journal of Geology, 42*, 1-22, 1934.

Jones, J. C., The Pleasant Valley, Nevada, earthquake of October 2, 1915, *Bulletin of the Seismological Society of America, 5*, 190-205, 1915.

Kaliser, B. N., Investigation and identification of potential earthquake hazards along the Wasatch Front, *Utah Geological and Mineral Survey, Investigation No. 108*, p. 231, 1976.

Koseluk, R. A. and R. E. Bischke, An elastic rebound model for normal fault earthquakes, *Journal of Geophysical Research, 86*, 1081-1090, 1981.

Mansinha, L. and D. E. Smylie, The displacement fields of inclined faults, *Bulletin of the Seismological Society of America, 61*, 1433-1440, 1971.

McCalpin, J., R. M. Robison, and J. D. Garr, Neotectonics of the Hansel Valley-Pocatello Valley corridor, northern Utah, and southern Idaho, in *Assessment of Regional Earthquake Hazards and Risk Along the Wasatch Front, Utah*, vol. 1, edited by P. L. Gori and W. W. Hayes, pp. G1-G44, U. S. Geological Survey Open-File Report 87-585, 1987.

Meister, L. J., R. O. Burford, G. A. Thompson, and R. L. Kovach, Surface strain changes and strain energy release in the Dixie Valley-Fairview Peak area, Nevada, *Journal of Geophysical Research, 73*, 5981-5994, 1968.

Murphy, L. M., *United States Earthquakes -- 1947*, p. 62, U. S. Department of Commerce, Coast and Geodetic Survey, Serial No. 730, 1950.

Myers, W. B. and W. Hamilton, Deformation accompanying the Hebgen Lake earthquake of August 17, 1959, in *The Hebgen Lake, Montana, Earthquake of August 17, 1959*, pp. 55-98, U.S. Geological Survey Professional Paper 435-I, 1964.

Neumann, F. K., *United States Earthquakes -- 1932*, p. 82., U. S. Department of Commerce, Coast and Geodetic Survey Serial No. 563, 1934.

Neumann, F. K., *United States Earthquakes -- 1935*, p. 93pp., U. S. Department of Commerce, Coast and Geodetic Survey Serial No. 600, 1937.

Ni, J. F., R. E. Reilinger, and L. D. Brown, Vertical crustal movements in the vicinity of the 1931 Valentine, Texas, earthquake, *Bulletin of the Seismological Society of America, 71*, 857-863, 1981.

Okada, Y., Surface deformation due to shear and tensile faults in a half-space, *Bulletin of the Seismological Society of America, 75*, 1135-1154, 1985.

Page, B. M., Basin-range faulting of 1915 in Pleasant Valley, Nevada, *Journal of Geology, 43*, 690-707, 1934.

Pardee, J. T., *The Montana earthquake of June 27, 1925*, U. S. Geological Survey Professional Paper 147-B, 17 p., 1926.

Pitt, A. M., C. S. Weaver, and W. Spence, The Yellowstone Park earthquake of June 30, 1975, *Bulletin of the Seismological Society of America, 69*, 187-205, 1979.

Quamar, A. and B. Hawley, Seismic activity near the Three Forks basin, Montana, *Bulletin of the Seismological Society of America, 69*, 1917-1929, 1979.

Reid, H. F., The ealstic rebound theory of earthquakes, *Bulletin of the Department of Geology, University of California, 6*, p. 413, 1911.

Reil, O. E., Damage to Nevada highways, *Bulletin of the Seismological Society of America, 47*, 349-352, 1957.

Richins, W. D., J. C. Pechmann, R. B. Smith, C. J. Langer, S. K. Goter, J. E. Zollweg, and J. J. King, The 1983 Borah Peak, Idaho, earthquake and its aftershocks, *Bulletin of the Seismological Society of America, 77*, 694-723, 1987.

Romney, C., Seismic waves from the Dixie Valley - Fairview Peak earthquakes, *Bulletin of the Seismological Society of America, 47*, 301-319, 1957.

Ryall, A., The Hebgen Lake, Montana, earthquake of August 18, 1959: P-waves, *Bulletin of the Seismological Society of America, 52*, 235-271, 1962.

Savage, J. C. and L. M. Hastie, Surface deformation associated with dip-slip faulting, *Journal of Geophysical Research, 71*, 4897-4904, 1966.

Savage, J. C. and L. M. Hastie, A dislocation model for the Fairview Peak, Nevada, earthquake, *Bulletin of the Seismological Society of America, 59*, 1937-1948, 1969.

Sellards, E. H., The Valentine, Texas, earthquake, in *Contribution to Geology, University of Texas Bureau of Economic Geology, Bulletin 3201*, pp. 113-138, 1932.

Shenon, P. J., The Utah earthquake of March 12, 1934, excerpts from an unpublished report of the U. S. Geological Survey, in *United States earthquakes 1934*, edited by Neumann, F., pp. 43-48, Washington, D. C., U. S. Department of Commerce, Coast and Geodetic Survey, 1936.

Slemmons, D. B., Geological effects of the Dixie Valley - Fairview Peak, Nevada earthquakes of December 16, 1954, *Bulletin of the Seismological Society of America, 47*, 353-375, 1957.

Smith, R. B. and R. L. Bruhn, Intraplate extensional tectonics of the eastern Basin-Range: Inferences on structural style from seismic reflection data, regional tectonics, and thermal-mechanical models of brittle-ductile deformation, *Journal of Geophysical Research, 89*, 5733-5762, 1984.

Smith, R. B., W. D. Richins, and D. I. Doser, The 1983 Borah Peak, Idaho, earthquake: regional seismicity, kinematics of faulting, and tectonic mechanism, in *Proceedings of Workshop XXVIII on the Borah Peak, Idaho, earthquake*, vol. A, edited by Stein, R. S., and Bucknam, R. C., pp. 236-263, U. S. Geological Survey Open File Report 85-290, 1985.

Smith, R. B. and M. L. Sbar, Contemporary tectonics and seismicity of the western United States with emphasis on the Intermountain seismic belt, *Geological Society of America Bulletin, 85*, 1205-1218, 1974.

Snay, R. A., M. W. Cline, and E. L. Timmerman, Dislocation models for the 1954 earthquake sequence in Nevada, in *Proceedings of Workshop XXVIII on the Borah Peak, Idaho, earthquake*, vol. A, edited by Stein, R. S., and Bucknam, R. C., pp. 531-549, U.S. Geological Survey Open File Report 85-290, 1985.

Stein, R. S. and S. E. Barrientos, Planar high-angle faulting in the Basin and Range: geodetic analysis of the 1983 Borah Peak, Idaho, earthquake, *Journal of Geophysical Research, 90*, 11355-11366, 1985.

Stickney, M. C. and M. J. Bartholomew, Seismicity and Late Quaternary faulting of the northern Basin and Range province, Montana and Idaho, *Bulletin of the Seismological Society of America, 77*, 1602-1625, 1987.

Tocher, D., Movement on the Rainbow Mountain fault, *Bulletin of the Seismological Society of America, 46*, 10-14, 1956.

Tocher, D., The Dixie Valley - Fariview Peak earthquakes of December 16, 1954: Introduction, *Bulletin of the Seismological Society of America, 47*, 299-300, 1957.

Tocher, D., Earthquake energy and ground breakage, *Bulletin of the Seismological Society of America, 48*, 147-153, 1958.

Ulrich, F. P., Helena earthquakes, *Bulletin of the Seismological Society of America, 26*, 323-339, 1936.

Wallace, R. E., *Faulting related to the 1915 earthquake in Pleasant Valley, Nevada,* U.S. Geological Surver Professional Paper 1274, 1984.

Wallace, R. E. and R. A. Whitney, Late Quaternary history of the Stillwater seismic gap. Nevada, *Bulletin of the Seismological Society of America, 74,* 301-314, 1984.

Ward, S. N. and S. E. Barrientos, An inversion for slip distribution and fault shape from geodetic observations of the 1983, Borah Peak, Idaho, earthquake, *Journal of Geophysical Research, 91,* 4909-4919, 1986.

Wernicke, B., Low-angle normal faults in the Basin and Range province: nappe tectonics in an extending orogen, *Nature, 291,* 645-648, 1981.

Whitten, C. A., Geodetic measurements in the Dixie Valley area, *Bulletin of the Seismological Society of America, 47,* 321-325, 1957.

Witkind, I. J., Reactivated faults north of Hebgen Lake, in *The Hebgen Lake, Montana, earthquake of August 17, 1959,* pp. 37-50, U. S. Geological Survey Professional Paper 435, 1964.

APPENDIX D

PALEOMAGNETISM OF QUATERNARY SEDIMENTS FROM THE JORDANELLE DAMSITE AND VICINITY, UTAH

By:

David R. Van Alstine
Sierra Geophysics, Inc.
15446 Bell-Red Road
Redmond, WA 98052

March, 1983

Final revisions by:

David R. Van Alstine
Applied Paleomagnetics, Inc.
1113 207th Place N.E.
Redmond, WA 98053

October, 1987

Prepared for the
U.S. Bureau of Reclamation
Denver, Colorado

SGI-R-83-085

TABLE OF CONTENTS

INTRODUCTION.....1
SAMPLE COLLECTION AND SCOPE OF INVESTIGATION.....2
LABORATORY AND DATA ANALYSIS.....4
RESULTS.....5
Trench JT-2.....5
Trench JT-7A and JT-7B.....7
Trench JT-8.....9
Trench JT-9.....11
Trench JT-10.....11
Trench JT-11.....12
Soil Pit J-4.....13
Soil Pit J-6A and J-6B.....13
Exposure J-13.....14
Soil Pit J-15.....15
Exposure J-16.....16
Exposure J-17.....17
Core Holes.....17
DH-R-101.....18
DH-R-104.....18
DH-R-110.....20
DH-R-111.....21
DH-R-114.....21
DH-R-115.....23
HV-1.....23
HV-2.....24
Exposure DC-1.....24
RV-1.....25
WD-1.....26
Soil Pit WV-16.....26
DISCUSSION.....27
CONCLUSIONS.....33
REFERENCES.....34
APPENDIX A: Paleomagnetic Sample Nomenclature.....35
APPENDIX B: Data Volume

INTRODUCTION

The purpose of this study was to investigate whether paleomagnetism might elucidate the age of Quaternary sediments at the Jordanelle damsite. Establishing the age of these sediments is particularly necessary in evaluating the recency of faulting at this planned facility. If these deposits are less than seven hundred thousand years old, they should contain only normal-polarity detrital remanent magnetization (DRM) or chemical remanent magnetization (CRM), because the present normal-polarity epoch began 730,000 years ago. On the other hand, if these sediments are greater than 730,000 years old, they might contain reversed-polarity magnetizations reflecting either deposition, weathering, or diagenesis in a reversed-polarity geomagnetic field.

Emphasis in this reconnaissance investigation was on establishing what units might contain reversed-polarity magnetization. Future studies could then be designed to determine the origin of reversed polarity magnetization in units that have particular relevance to recency-of-faulting investigations.

SAMPLE COLLECTION AND SCOPE OF INVESTIGATION

This study presents results of paleomagnetic analysis of 103 samples of Quaternary sediments from the Jordanelle damsite and vicinity, Utah. Sixty-five of these samples were from 6 trenches and 6 soil pits in the Keetley Valley (Figure 1). Another 20 samples were taken from 6 trenches and soil pits in adjacent valleys. The other 18 samples were from subsurface drillcore taken from 6 coreholes in the Keetley Valley. The sample site nomenclature and stratigraphy are presented in Appendix A.

All samples were ~6 cubic-centimeter cubes of sediment carved using stainless steel knives or (for drillcores) a hacksaw. Approximately one-third of the samples were collected in non-magnetic plastic boxes, and two-thirds of the samples were collected in fused quartz containers of the same volume. The quartz containers permit thermal demagnetization to be performed, so that secondary magnetizations residing in goethite or hematite can be separated from magnetizations residing in magnetite; this was important in this study, because many of the samples were noticeably hematitic or iron-stained. After placing each sample in its container, a 50% solution of sodium silicate was dripped onto the exposed surfaces to prevent grains from rotating during the laboratory analysis.

All oriented samples were collected by U.S. Bureau of Reclamation personnel following sampling procedures recommended by Sierra Geophysics. The majority of the samples were collected by Lucy Foley and Alan Nelson, who also selected the sampling sites. Generally, two or three oriented samples were collected for analysis from each stratigraphic horizon. Although care was taken to ensure accurate orientations and to investigate possible sampling errors, Sierra Geophysics assumes no responsibility for orientation errors made in the field.

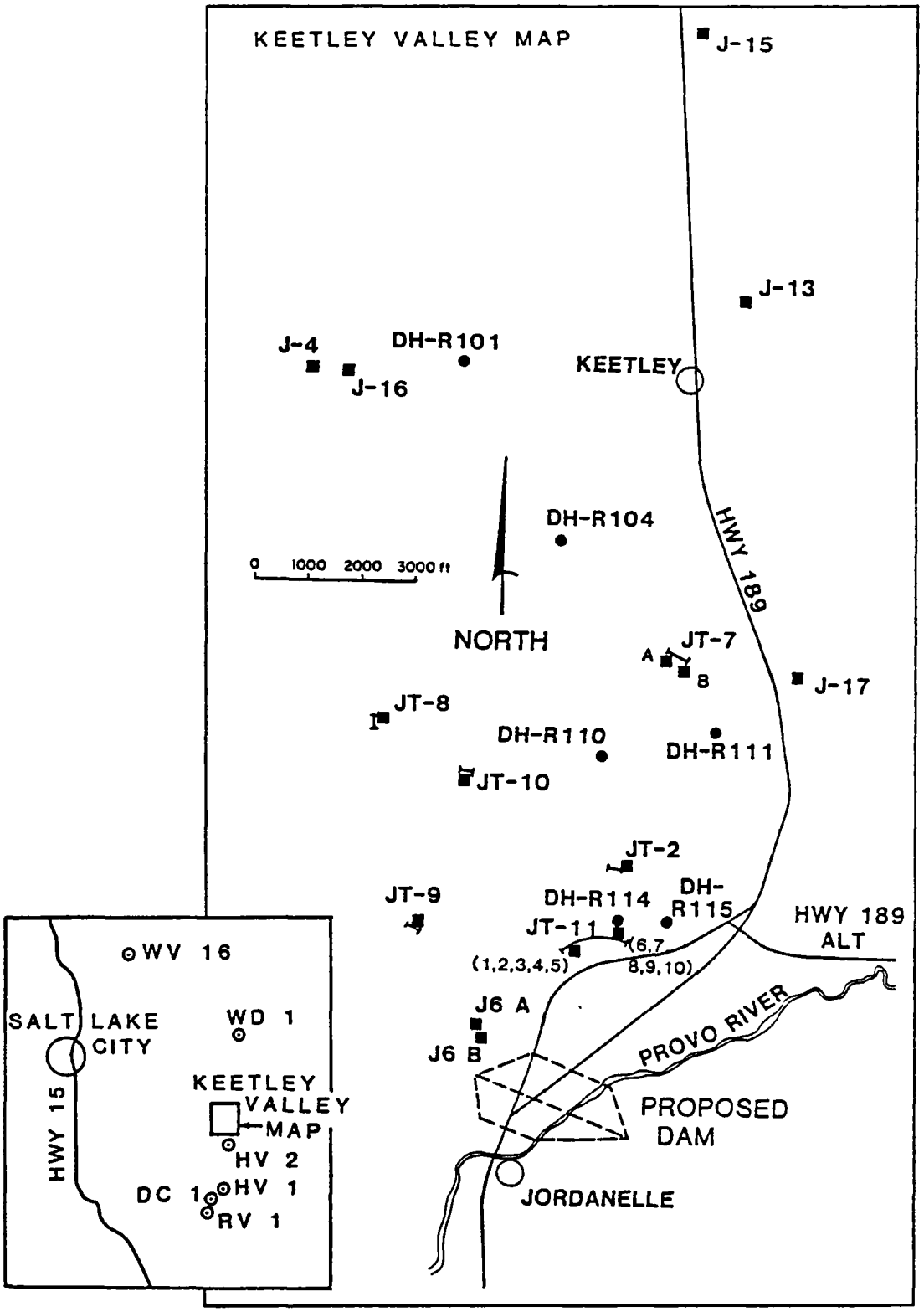

Figure 1: Map showing locations of paleomagnetic sampling sites. Solid circles = coreholes; solid squares = trenches and pits.

LABORATORY AND DATA ANALYSIS

In the Sierra Geophysics paleomagnetics laboratory, an effort was made to separate the primary detrital remanent magnetization (DRM) from any secondary magnetizations that might be present. This consisted of first measuring the natural remanent magnetization (NRM) of the samples and then subjecting them either to alternating-field (AF) demagnetization at 9 steps between 50 and 1,000 oersteds (1 oersted = 0.1 millitesla) or to progressive thermal demagnetization in at least 10 steps between 107° and 670°C.

All measurements of remanent magnetization were made on Sierra Geophysics' 3-axis, 6.3 cm-access superconducting (SQUID) magnetometer manufactured by Superconducting Technology, Inc. This instrument has a dynamic range between 10^{-8} and 10^{+1} emu. The magnetometer is interfaced to a mainframe computer, which permits real-time computation of magnetic directions, intensities, induced/remanent ratios, uniformity of magnetization parameters, structural corrections, and virtual geomagnetic poles.

Alternating-field demagnetization was performed using a Schonstedt Model GSD-5 demagnetizer, which provides 400 Hz fields up to 1,000 oersteds (Oe). The demagnetizer tumbles the samples around orthogonal axes while the peak field is decaying. During each decay cycle, the sense of rotation of the tumbler is periodically reversed; this cancels effects of rotational remanent magnetization (RRM) and results in smoother demagnetization paths.

Thermal demagnetization was performed using a custom-built, three-zone furnace with a very large isothermal region (thermal gradients <3°C). Samples are heated and cooled in a magnetic field of less than 5 gammas (nT).

All measurements and demagnetzation procedures were carried out in a 120-square-foot magnetically shielded room in which the ambient magnetic field is less than 0.3% of the Earth's magnetic field. This

improves the accuracy of the paleomagnetic analysis by minimizing the contribution of any viscous remanent magnetization (VRM) to the magnetization of the samples.

RESULTS

The paleomagnetic results from this study are presented in detail in Appendix B. This appendix includes tables and graphs showing the complete demagnetization history of each of the 103 samples. The tables list the magnetization directions, intensities as a function of demagnetization step, and subtracted vectors between demagnetization steps. The graphs show vector demagnetization information in the form of vector demagnetization diagrams, stereonet plots of directional change upon demagnetization, and normalized intensity versus demagnetization level.

The paleomagnetic data are now discussed separately by sample site. Results are first presented from the Keetley Valley (the site of the proposed Jordanelle reservoir) in the following order: (1) Data from trenches, in numerical order and designated by the prefix "JT-"; (2) Data from soil pits and other exposures (e.g., roadcuts), in numerical order and designated by the prefix "J-"; and (3) Data from drill cores, in numerical order and designated by the prefix "DH-R-". The Keetley Valley results are followed by results from Heber Valley and vicinity (north Heber Valley site HV-1, south Heber Valley site HV-2, Deer Creek site DC-1, and Round Valley site RV-1) and then by results from Weber River Valley (Wanship Dam site WD-1 and Weber River Valley site WV-16).

Trench JT-2

For paleomagnetic analysis, one specimen was cut from each of 10 fully-oriented block samples from the north face of trench JT-2. The cubical specimens were carved using a stainless steel knife and/or a hacksaw. The surfaces of the specimens were sanded to remove any steel-particle contamination resulting from sawing.

Results from AF and thermal demagnetization reveal that most of the samples contain both normal- and reversed-polarity magnetizations with overlapping coercivities but with different blocking temperatures. The normal-polarity component is approximately aligned with the direction of the present axial dipole field (PADF) at the site. This normal-polarity magnetization is probably in part a VRM residing in the coarser grains of magnetite and in part a chemical remanent magnetization (CRM) residing in "limonite" (cryptocrystalline iron oxides and oxyhydroxides which are probably predominantly goethite) produced by recent weathering. Because CRM residing in limonite has high coercivity (>1,000 Oe), it cannot be removed by AF demagnetization. On the other hand, because goethite is chemically unstable above ~120°C, the CRM residing in limonite can easily be removed by thermal demagnetization at relatively low temperatures. In most of the thermally demagnetized specimens, all traces of normal-polarity magnetization were removed by the 150° to 225°C demagnetization steps. Thus, thermal demagnetization appears to be more effective than AF demagnetization in isolating the reversed-polarity magnetization in these sediments.

This reversed-polarity magnetization probably resides partly in magnetite and partly in hematite. The AF demagnetization results from specimen JT-2-C2 best reveal the decay of a reversed-polarity magnetization in peak fields between 100 and 1,000 Oe. This is consistent with a magnetization carried by magnetite, especially since a magnetization residing in hematite would not be as affected by magnetic fields in this range. On the other hand, thermal demagnetization results (particularly of specimen JT-2-B3) reveal that as much as 50% of the NRM intensity remains after thermal demagnetization above the Curie point of magnetite (580°C). A significant fraction of the reversed-polarity magnetization is still present at temperatures as high as 660°C, consistent with a magnetization residing in hematite, which can retain a remanence to 680°C.

Trench JT-2 is the only site of this study from which a sufficient number of samples was analyzed to justify calculation of a mean

paleomagnetic direction. This mean was determined by first fitting least-squares lines to segments of the vector demagnetization diagrams that are linear in 3-space. The advantage of this technique, which we have refined after a method described by Kirschvink (1980) is that scatter of directions due to effects of VRM or anhysteretic remanent magnetization (ARM) are minimized in the final computation of the mean direction for a site.

These least-squares directions were then used to compute the mean paleomagnetic direction for trench JT-2, together with its estimated 95% confidence limits, α_{95} (e.g., McElhinny, 1973). The mean and α_{95} are derived from the statistics of Fisher (1953), which measure dispersion on a sphere. As shown in Figure 2, the mean reversed-polarity direction from JT-2 is statistically indistinguishable from being antiparallel to the PADF. This confirms that the reversed polarity magnetization has a geophysical origin, rather than reflecting spurious magnetizations imparted during sampling or laboratory analysis.

In summary, all 10 samples from JT-2 contain a reversed-polarity magnetization of high stability upon both AF and thermal demagnetization. This magnetization probably resides partly in magnetite and partly in hematite. Although the magnetization residing in hematite could be either a DRM or CRM (possibly acquired long after deposition), the magnetization residing in magnetite is probably a DRM acquired penecontemporaneously with deposition.

Trench JT-7A and JT-7B

Two samples (JT-7A-2, JT-7A-4) were collected for analysis from a depth of 2.35 meters below the surface in the west end (JT-7A) of a backhoe trench at the NE corner of section 30. The samples are of reddish-brown clay, with some iron-staining and some sand lenses, from

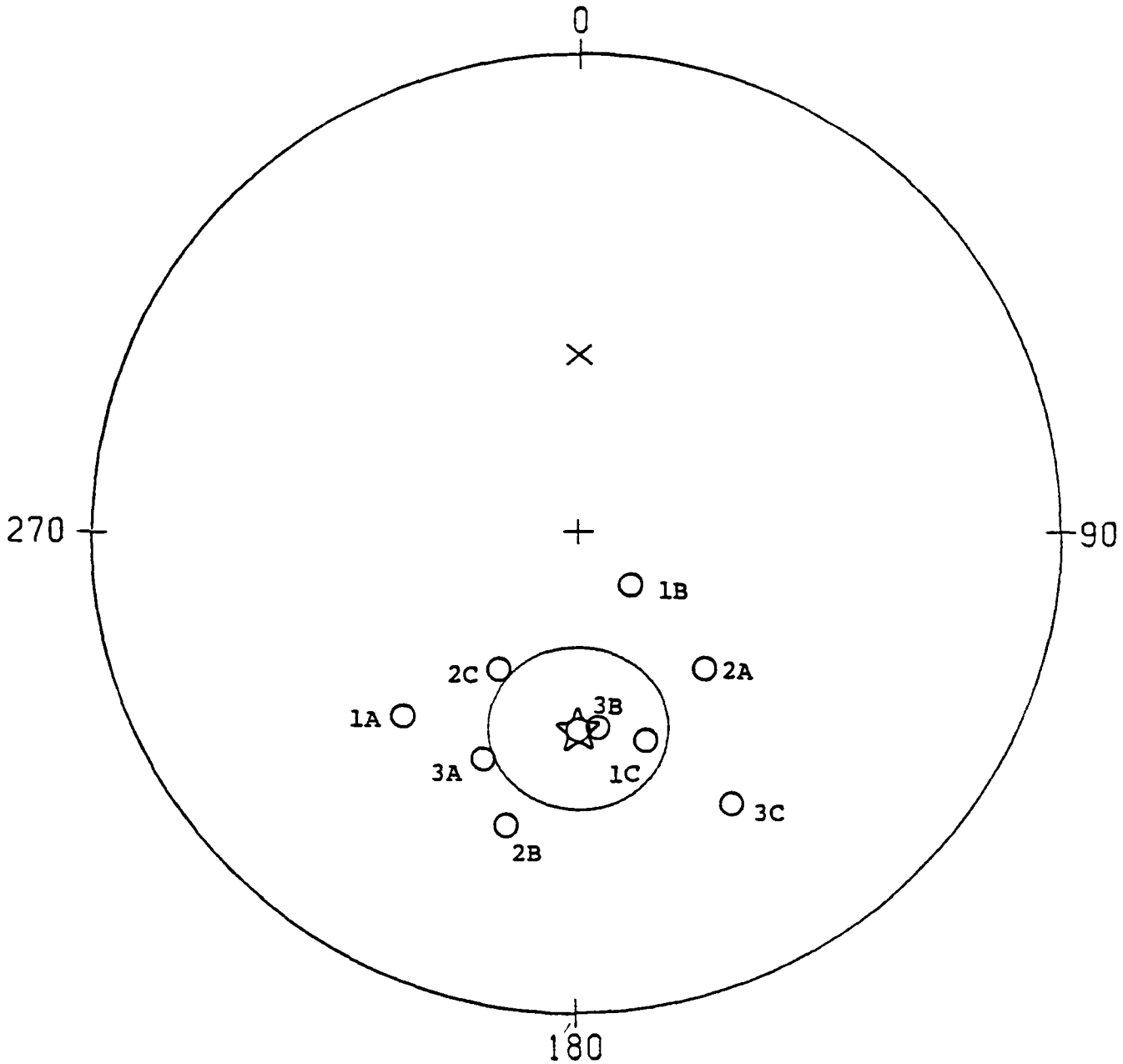

Figure 2: Stereographic projection showing least-squares-fitted magnetization directions representing the characteristic magnetization for trench JT-2 sediments. The X marks the direction of the present axial dipole field at the sampling site. Solid (open) circles are on the lower (upper) hemisphere, respectively (i.e., open circles have reversed polarity). The large circle around the star is the 95% confidence circle (Fisher, 1953) around the mean. The direction from one conglomeratic sample, which was unstably magnetized, has been excluded.

a unit mapped as older Pleistocene basin fill deposits. These samples apparently contain two magnetizations: (1) a normal-polarity magnetization residing in magnetite; and (2) a reversed-polarity magnetization probably residing in hematite. The normal-polarity magnetization could represent either a secondary, viscous remanent magnetization (VRM) or a primary, detrital remanent magnetization (DRM). In both samples, the reversed-polarity magnetization could be separated from the normal-polarity magnetization by the AF demagnetization treatment; both demagnetization paths pass within ~20° of being antiparallel to the PADF direction. The reversed-polarity magnetization could represent either a DRM or a secondary chemical remanent magnetization (CRM). The very high coercivity of the reversed component suggests that this magnetization resides in hematite or limonite (goethite). Thermal demagnetization would elucidate the magnetic mineralogy and hence the origin of this reversed component.

Two samples (JT-7B-2 and JT-7B-3) of clay from a depth of 0.70m at Station 7 were analyzed from the east end of trench JT-7B. Upon AF demagnetization, both samples trend toward reversed-polarity directions. The demagnetization path of sample JT-7B-3 terminates within ~30° of being antiparallel to the PADF direction. A normal-polarity magnetization predominating in the lower AF and thermal demagnetization steps could represent either VRM or DRM in magnetite. The reversed-polarity magnetization has very high coercivity; in sample JT-7B-3, for example, there was essentially no decay in remanence intensity between 550 and 1,000 Oe. This high-coercivity, reversed-polarity magnetization could represent either a DRM in very fine grains of magnetite or a CRM in authigenic hematite. In summary, the sampled sediments from the east and west ends of trench JT-7 contain an excellent record of reversed-polarity magnetization.

Trench JT-8

A trench was excavated down a hillside exposing a section of horizontally bedded alluvial deposits. The section alternated between

coarse (gravelly) and fine (clayey) strata, although only the finer units were sampled for paleomagnetism.

Initially, a pair of samples was collected from each of three different layers. Both samples (JT-8-2 and JT-8-3) from the upper layer apparently contain only normal-polarity magnetizations. Results of AF and thermal demagnetization suggest that 95% of the NRM resides in magnetite and about 5% in hematite; the hematite may carry either a DRM or CRM.

The two samples (JT-8-4 and JT-8-5) from the middle layer apparently contain a predominant normal-polarity magnetization residing in magnetite, as inferred from behavior during AF and thermal demagnetization. In these two samples, however, between 4% and 13% of the NRM resides in a mineral with a coercivity and blocking temperature typical of hematite; this hematite may reflect authigenesis during a reversed-polarity epoch, because the paleomagnetic directions at the highest demagnetization steps move away from the PADF and in the case of Sample JT-8-4 approach a direction nearly antiparallel to the PADF by ~660°C.

The two samples (JT-8-8 and JT-8-10) from the lowest stratum also suggest the presence of reversed-polarity magnetization. Both samples exhibit shallow-inclination, stable paleomagnetic directions, which may well indicate superposition of roughly equal amounts of normal- and reversed-polarity magnetizations with overlapping coercivity and blocking temperature spectra.

As a further check on the possibility of reversed polarity in trench JT-8, 5 additional samples (JT-8-11, -12, -13, -14, -15) were collected from the lower stratum. The NRM directions of all 5 samples deviated significantly from the PADF direction. The three samples with directions farthest from the PADF were subjected to thermal demagnetization up to 670°C; however, the remanence directions from none of these samples moved appreciably, toward a position parallel or

antiparallel to the PADF. The observation of scattered, but stable, remanence directions in these samples is consistent with the hypothesis that they contain roughly equal amounts of secondary CRM's (in authigenic hematite) with opposite polarities and with essentially identical blocking temperature spectra. Thus, the paleomagnetic evidence from the middle and lower units in trench JT-8 suggests that these sediments have been subjected to a reversed-polarity geomagnetic field at some time during their history.

Trench JT-9

Two samples (JT-9-1 and JT-9-2) were analyzed from trench JT-9 in yellow, clayey slopewash or colluvium. Both samples exhibit only normal-polarity magnetizations (within 10° of the PADF) upon both AF and thermal demagnetization. In both samples, about 10% of the normal-polarity magnetization resides in a species with coercivity and blocking temperature typical of hematite; most of the normal-polarity magnetization appears to be a stable DRM or VRM residing in magnetite. The strata sampled in trench JT-9, therefore, show no paleomagnetic evidence of having experienced a reversed-polarity geomagnetic field.

Trench JT-10

Five samples were collected from fine clayey sediments in trench JT-10. Most of the five samples had NRM directions close to (within ~20°) of the PADF. Results of thermal demagnetization on two samples (JT-10-3 and JT-10-5) and of AF demagnetization on one sample (JT-10-4) suggest that the NRM is a composite of a normal-polarity VRM or DRM in magnetite and a predominantly normal-polarity CRM or DRM in hematite. About 25% to 35% of the NRM has a coercivity and blocking

temperature typical of hematite, suggesting that these sediments contain significant amounts of hematite, probably of authigenic origin. Although the paleomagnetic results from trench JT-10 suggest that most of this hematite records a normal-polarity field, the possibility of a reversed-polarity component is suggested by: (1) negative-inclination remanence directions upon thermal demagnetization at 670°C; and (2) scatter of some of the NRM directions from the PADF direction. Thus, there is a suggestion that the JT-10 sediments may have experienced a reversed-polarity field at some time during their history.

Trench JT-11

Ten samples were collected from trench JT-11, five (JT-11-1, -2, -3, -4, -5) from the top and five (JT-11-6, -7, -8, -9, -10) from the bottom. This trench exposes horizontally bedded clayey and gravelly basin fill deposits. Most of the upper five samples had NRM directions that deviated by ~30° from the PADF; this suggests the possibility of a reversed-polarity component beneath a predominant normal-polarity magnetization. Thermal demagnetization of two of the upper samples (JT-11-3 and JT-11-4) provided even stronger indications of reversed polarity; below 360° to 540°C, the remanence directions consistently moved away from the PADF and approached within 30° to 70° of being antiparallel to the PADF; at higher temperatures, directions changed erratically. Between 15% and 21% of the NRM intensity remained at 600°C, suggesting an appreciable contribution from hematite. The one sample (JT-11-2) that was AF demagnetized also suggested the presence of a reversed-polarity component with moderate to high coercivity.

The lower five samples from JT-11 showed even more convincing evidence of reversed-polarity magnetizations. All five NRM directions deviated significantly (>45°) from the PADF. Upon thermal demagnetization of two samples (JT-11-7 and JT-11-8), the remanence directions were generally stable up to 600°C; between 25% and 50% of the NRM intensity remained at 600°C, again suggesting an appreciable contribution from hematite. The best example of a reversed-polarity

magnetization was in the one sample (JT-11-9) that was AF demagnetized; remanence directions progressively migrated away from the PADF and approached within ~45° of being antiparallel. Even after the 1000 Oe step, however, 45% of the NRM intensity remained, again suggesting a substantial contribution from high-coercivity hematite.

Thus, the paleomagnetic evidence from the upper and lower units in trench JT-11 is consistent in indicating the presence of reversed-polarity magnetization.

Soil Pit J-4

Two samples (J-4-1 and J-4-3) were analyzed from soil pit J-4 in clayey basin fill deposits. Both samples apparently contain only normal-polarity magnetizations, as evidenced by remanence directions remaining near the PADF upon both AF and thermal demagnetization. In both samples, about 5% of the NRM intensity has a coercivity or blocking temperature typical of hematite, consistent with either a DRM or CRM origin. Neither sample contains any paleomagnetic evidence, therefore, of deposition or diagenesis during a reversed-polarity epoch.

Soil Pits J-6A and J-6B

Three samples (J-6A-1, J-6A-2, J-6A-3) were collected and analyzed from 92 cm below the ground surface in soil pit J-6A. The samples are of fine, clayey, loessial colluvium which overlies older basin fill deposits at a 1.5 m depth. Directions of NRM were somewhat scattered about the PADF direction, suggesting the presence of an underlying reversed-polarity magnetization. A reversed-polarity magnetization was not clearly revealed, however, upon either AF demagnetization to 1000 Oe or thermal demagnetization to 670°C.

Five samples (J-6B-4, -5, -6, -7, -8) were collected from the underlying basin fill deposits in soil pit J-6B, adjacent to soil pit J-6A. Pit J-6B is farther downslope and exposes stratified silty sands and clays that underlie material exposed in pit J-6A. As in the samples from J-6A, the NRM directions of all five J-6B samples were scattered about the PADF direction, suggesting superposition of multiple components. Thermal demagnetization of three samples failed to isolate a reversed-polarity magnetization. All three samples, however, exhibited shallow-inclination directions that were relatively stable at even the highest temperatures. This behavior is commonly observed in samples that contain almost equal proportions of both normal and reversed-polarity magnetizations with similar blocking temperature spectra (cf. Larson et al., 1982). This phenomenon can occur in sediments containing authigenic hematite that grew over long ($\sim 10^6$ m.y) time scales and hence during normal and reversed-polarity epochs. The presence of abundant hematite in these samples is indicated by their containing up to 12% of their NRM intensity at 600°C, above the Curie point of magnetite. Thus, the sediments in Soil Pits J-6A and J-6B may contain a paleomagnetic record reflecting protracted diagenesis.

Exposure J-13

Two samples (J-13-1 and J-13-3) of tan, clayey basin fill deposits were analyzed from J-13. AF demagnetization of Sample J-13-1 revealed a reversed-polarity magnetization with high coercivity (>1,000 Oe) and with a direction within ~30° of being antiparallel to the PADF direction. A normal-polarity magnetization also residing in this sample was preferentially destroyed by the AF treatment and hence could reflect either DRM or VRM residing in magnetite. Thermal demagnetization of Sample J-13-3 also provided evidence for reversed-polarity magnetization; however, the multiple magnetizations that apparently reside in this sample (as evidenced by stable remanence directions intermediate between normal and reversed polarity) contain nearly identical blocking temperature spectra and hence cannot be separated by thermal

demagnetization. This paleomagnetic evidence strongly suggests that these sediments from J-13 have experienced a reversed-polarity geomagnetic field.

Soil Pit J-15

Six samples were collected for paleomagnetic analysis from soil pit J-15, which exposed a clay overlying sandy volcanic ash. Three samples (J-15-1, 2, 3) were collected from the clay at a depth of 1.25 m, and three samples (J-15-4, 5, 6) from the ash at a depth of 2.0 m.

The NRM directions from the clay were either parallel to (Sample J-15-2) or widely (>60°) deviant from (Samples J-15-1 and J-15-3) the PADF direction. Thermal demagnetization of the two deviant samples indicated that the remanence directions were essentially unchanged even at 670°C. In both samples, about 7% of the NRM intensity survived heating to 600°C, indicating that some fraction of the NRM resides in hematite. These paleomagnetic results suggest that the clay samples might contain authigenic hematite recording normal- and reversed-polarity CRM's with overlapping blocking temperature spectra.

In the underlying ash unit, NRM directions from all three samples also deviated significantly (~15° to 70°) from the PADF direction. In the one sample (J-15-4) that was thermally demagnetized, a remanence near the PADF predominated at low temperatures, and remanence directions changed erratically above 420°C. In the one sample (J-15-5) that was AF demagnetized, the widely deviating NRM direction (D = 268°, I = +29°) remained essentially unchanged even though the remanence intensity decayed to 90% of its NRM value by 1000 Oe. This response to AF demagnetization suggests that the scatter of remanence directions in the ash has some cause other than superimposed CRM's in hematite with overlapping blocking temperature spectra. It is possible that the scatter of remanence directions from the ash is caused by normal-polarity VRM in coarse-grained (sand-size) magnetite that has over-

printed reversed-polarity DRM or CRM. It is also possible that the grain size of the ash is too coarse to preserve an accurate record of the geomagnetic field at the time of deposition. Thus, although paleomagnetic results from the ash are equivocal, the ash does underlie sediments containing a suggestion of having experienced a reversed-polarity geomagnetic field.

Exposure J-16

Three samples (J-16-1, J-16-5, J-16-6) were analyzed from soil pit J-16 in a roadcut at Keetley Station. The samples, which are reddish-gray laminated clays from older basin fill deposits, are from 8.5 meters below the surface.

Alternating-field demagnetization of two of these samples suggests that they contain both normal- and reversed-polarity magnetizations. The normal-polarity magnetization has very high coercivity, suggesting that it resides in hematite or limonite (goethite). The presence of an underlying, reversed-polarity component is suggested by (1) the scatter of NRM directions (before demagnetization) away from the present axial dipole field (PADF) direction (Declination, D = 0°; Inclination, I = +61°) and (2) the movement of remanence directions upon demagnetization toward a reversed-polarity direction (D = 180°, I = -61°).

The presence of a reversed-polarity magnetization in J-16 was most clearly revealed in the single sample (J-16-6) that was thermally demagnetized. Inspection of the vector demagnetization diagram reveals that a normal-polarity magnetization was removed by 225°C; between 225°C and 660°C, the vector demagnetization path decays linearly to the origin with a reversed-polarity direction of D~155°, I~-35°. The presence of 19% of the NRM intensity at 600°C (20° above the Curie point of magnetite) indicates that a major fraction of the reversed-polarity component resides in hematite. Thus, the sediments sampled in J-16 seem to have been subjected to a reversed-polarity geomagnetic field either at the time of, or subsequent to, deposition.

Exposure J-17

Two samples (J-17-1 and J-17-3) were analyzed from exposure J-17. Both samples are from one meter beneath the ground surface in basin fill deposits of finely bedded silty clay with sand particles of rhyodacite. Both samples apparently contain only normal-polarity magnetizations, as evidenced by remanence directions near the PADF upon both AF and thermal demagnetization. In these samples, between 2% and 5% of the NRM intensity has a coercivity or blocking temperature typical of hematite. The sharp reduction in remanence intensity upon thermal demagnetization to 150°C could indicate the destruction either of VRM in coarse-grained magnetite or of CRM in goethite or fine-grained hematite. In any case, neither sample from exposure J-17 contains any evidence of deposition or diagenesis during a reversed-polarity epoch.

Core Holes

To complement the paleomagnetic study of surface trenches and exposures, 18 additional paleomagnetic samples were collected from six core holes. For all core holes, the sample numbers indicate the depth (in feet below the surface) from which the sample was derived.

Several factors make the paleomagnetism of drillcores far more difficult to interpret than from surface sites. First, very steep paleomagnetic inclinations are commonly observed in paleomagnetic studies of drillcores. This drilling-induced remanent magnetization (DIRM) points vertically downward in drillcores from the northern hemisphere (e.g., Van Alstine and Gillett, 1981, 1982; Johnson, 1979). Thus, in drillcore samples, a strong, normal-polarity DIRM is generally superimposed on any pre-existing paleomagnetic directions in a sample. On the one hand, this normal-polarity magnetization makes it increasingly difficult to recognize reversed-polarity magnetizations in drillcores. On the other hand, this DIRM can provide a useful indication of the true up-hole direction in cases where individual core segments have

inadvertently been placed in the core boxes upside-down. Indeed, it is estimated that about 20% of the core segments investigated in this study may well have been inverted at some time prior to sampling.

Core Hole DH-R-101

Two samples were collected from core hole DH-R-101. Both samples (#43.6 and #43.8) are from a single core segment of gray clay. The two samples were collected with the same relative azimuth, and hence they should yield the same NRM declination, as was observed. Both samples evidently contain anomalously shallow-inclination remanent magnetization (ASIRM) which is highly resistant to both AF and thermal demagnetization. Although ASIRM can in principle result from superimposed normal-and reversed-polarity components with overlapping stability spectra (e.g., Larson et al., 1982), it is unlikely that two different samples would exhibit the same magnetic directions (because they would probably contain different proportions of normal and reversed components). We have previously observed ASIRM in other drillcores of unconsolidated sediment, suggesting that ASIRM may be another artifact of drilling. An alternative explanation of these paleomagnetic results is that in both samples, the reference scribe lines on the samples were not marked according to the specified sampling conventions. The most likely sampling error would be to mark the core perpendicular to the convention. If this error is assumed and corrected for, however, then both samples would display nearly vertical NRM inclinations, typical of DIRM. In either case, both samples from core hole DH-R-101 are evidently too overprinted with drilling-induced magnetizations to permit reliable interpretations of the geomagnetic polarity.

Core Hole DH-R-104

Six samples were collected from core hole DH-R-104. At 132.0 feet, a single sample of light-gray clay yielded erratic behavior upon thermal

demagnetization. Thus, no geomagnetic polarity information could be obtained from this sample.

A sample at 271.8 feet contains two components of magnetization: (1) a magnetization pointing upward at an angle of at least -54°; and (2) a magnetization with a shallow, positive inclination of 35°. The negative-inclination component has a relativley low blocking temperature of ~300°C, and the positive-inclination component is essentially destroyed by 600°C. Two explanations can be proposed to account for the presence and thermal stability of these two components. (1) A reversed-polarity, low-blocking temperature magnetization residing in magnetite or hematite/limonite has been superimposed on a normal-polarity, high-blocking-temperature magnetization residing in magnetite or hematite. This hypothesis assumes that the core segment is rightside-up in the core box and that it was sampled following the orientation conventions. (2) The sample is inverted in the core box or was sampled incorrectly. In this case, a normal-polarity, low-blocking-temperature magnetization residing in magnetite or hematite/limonite has been superimposed on a reversed-polarity, high-blocking-temperature component residing in magnetite or hematite. In either case, there is a suggestion that sediments containing reversed-polarity magnetization were encountered at a depth of 271.8 feet in DH-R-104.

Two samples (#460.1 and 460.4) were collected from tan, finely bedded silty sand. Both samples contain essentially a single component of magnetization with very steep (~80°) inclinations. The steepness of this inclination, nearly 20° greater than the expected 61° axial-dipole-field inclination at this site, suggests that these samples probably contain pervasive DIRM. However, the negative inclination of Sm #460.1 suggests that there may be reversed-polarity sediments at a depth of 460.1 feet in DH-R-104.

Two samples, at 473.4 and 473.5 feet, also appear to contain multiple components of magnetization. One magnetization has a normal-polarity inclination of +66° and +81°, respectively. Vector demagnetization

diagrams from both samples reveal the presence of some additional magnetizaton, as evidenced by the fact that the demagnetization paths for both smaples do not trend to the origin. The second, unknown magnetization could have either a shallow (near 0°) or negative (reversed-polarity) inclination. Reversed polarity is indeed suggested, especially at 473.5 feet. The postulated reversed-polarity component probably resides in hematite because of its high coercivity (>1,000 Oe) and high blocking temperature (>600°C).

In summary, four of the six samples from DH-R-104 contain evidence of reversed-polarity magnetization, provided that all core marking and sampling instructions were followed correctly.

Core Hole DH-R-110

Two samples were collected from core hole DH-R-110. At 60.5 feet, a single sample of gray clay (with iron concretions) is dominated by a component with an inclination of +70°. The drop-off in the intensity-decay curve between 540° and 600°C suggests that this component resides in magnetite, which has a Curie point of 580°C. This component probably represents either a normal-polarity DRM or VRM. The demagnetization path does not trend to the origin, indicating the presence of some additional component of magnetization with shallow or perhaps negative (reversed-polarity) inclination. This component would be either ASIRM or perhaps a secondary chemical remanent magnetization (CRM) residing in hematite.

A single sample of tan silty clay at 79.8 feet exhibits two components of magnetization upon thermal demagnetization. The first component is removed by ~300°C and points steeply downward; this component probably represents DIRM or VRM. The second, characteristic magnetization yields a least-squares inclination of -70°; the survival of this component at 600°C (with 66% of the NRM intensity) indicates that this reversed-polarity magnetization resides in hematite, which could be

of either detrital or authigenic origin. Thus, there is paleomagnetic evidence that reversed polarity sediments are present between the 60.5 and 79.8 foot depths in DH-R-110.

Core Hole DH-R-111

Two samples were collected from core hole DH-R-111. A sample of tan sand at 30.2 feet contains a single, normal-polarity magnetization which has a coercivity typical of fine-grained magnetite. This component, which yields a least-squares inclination of +60°, probably represents a normal-polarity DRM.

A sample of gray clay at 81.5 feet contains two components of magnetization, as revealed by thermal demagnetizaton. A normal-polarity component (I=+65°) removed by 225°C probably represents secondary VRM residing in magnetite or CRM residing in goethite or fine-grained hematite. A stable, reversed-polarity characteristic magnetization (I=-46°) is isolated between 225° and 540°C; this component is destroyed by 600°C, at which point the demagnetization behavior becomes erratic. Thus, Sm #81.5 probably contains a reversed-polarity DRM residing in magnetite.

In summary, sediments containing reversed-polarity magnetization seem to be present at the 81.5-foot depth in DH-R-111.

Core Hole DH-R-114

Five samples were collected from core hole DH-R-114. A sample of brown silty clay at a depth of 4.1 feet contains a single, normal-polarity magnetization (I=+58°). Thermal demagnetization reveals that 16% of this magnetization survives above the Curie point of magnetite. Thus, Sm #4.1 probably contains a normal-polarity DRM residing chiefly in magnetite but partly in hematite.

A sample of tan silty clay at 9.5 feet displays normal-polarity magnetization (I=+57°) between NRM and 360°C; above this temperature, the demagnetization behavior becomes erratic. The normal-polarity magnetization observed below 360°C could be a primary, normal-polarity DRM in magnetite or secondary VRM, DIRM, or CRM in magnetite and/or hematite.

A sample of tan sandy silt at 35.9 feet also contains normal-polarity magnetizations. A steep, downward-pointing (I=+84°) component, which is removed by 100 Oe, is probably DIRM. Above 100 Oe, another normal-polarity magnetization is present, with a shallower inclination of +60°, similar to that of the present axial dipole field. The stability of this magnetization at the highest AF demagnetization steps suggests that ~10% of this characteristic magnetization resides in hematite, which has far higher coercivity than magnetite.

A sample of tan sandy silt at 56.2 feet exhibits two components of magnetization upon thermal demagnetization. The component with lower blocking temperature has an upward-pointing (reversed-polarity) inclination and is present up to 480°C. Between 540° and 660°C, a downward-pointing (normal-polarity) magnetization (I=+39°) seems to have been isolated. Two explanations can be proposed to account for the thermal demagnetization results from this sample. The first hypothesis is that a normal-polarity CRM residing in secondary hematite (with high blocking temperature) was superimposed on a reversed-polarity DRM residing primarily in magnetite (with lower blocking temperature). The second hypothesis is that the sample was derived from an upside-down core segment; in this case, normal-polarity VRM or DIRM in magnetite has apparently been superimposed on reversed-polarity DRM residing in magnetite and/or hematite. In either case, reversed-polarity sediments may be present at the 56.2-foot depth in DH-R-114.

A sample of tan silty clay at 133.5 feet exhibits two components of magnetization. A downward-pointing magnetization is removed upon AF demagnetzation to 150 Oe; this normal-polarity component probably

represents a combination of VRM and DIRM coexisting in the coarser grains of magnetite. The reversed-polarity (I=-77°) characteristic magnetization revealed between 150 and 1,000 Oe has a coercivity typical of fine-grained magnetite and may represent a reversed-polarity DRM.

In summary, reversed-polarity sediments may be present at depths between 56.2 and 113.5 feet in DH-R-114.

Core Hole DH-R-115

A sample of silt at 5.6 feet displays ambiguous thermal demagnetization behavior. These results could be interpreted as reflecting a small component of normal-polarity VRM/DIRM superimposed on a reversed-polarity DRM (note the slight increase in intensity between NRM and 107°C, suggesting the presence of two components of opposite polarity). Alternatively, the slight intensity increase at 107°C could reflect a spurious component acquired during sampling or transport, and the sample could have been derived from an upside-down core segment; in this case, the sample would contain a steeper normal-polarity component reflecting the present magnetic field and a shallower normal-polarity magnetization reflecting a normal-polarity DRM. In either case, no geophysically significant component appears to survive above the Curie point of magnetite, suggesting that the magnetization of this specimen resides chiefly in magnetite. The paleomagnetic results from the single DH-R-115 sample are therefore equivocal, and a reliable polarity interpretation cannot be made.

HV-1

Three samples (HV-1-1, -3, -4) from HV-1 in south Heber Valley exhibited only normal-polarity magnetization with directions nearly parallel to the PADF. These samples are in silty loessial colluvium or alluvium in a remnant of a dissected old alluvial fan on the south side of Heber Valley. Results of AF and thermal demagnetization suggest that the normal-polarity magnetization resides primarily in magnetite

(blocking temperature between 540 and 600°C; median destructive field ~250 Oe). The presence of ~5% of the NRM intensity at 600°C indicates that some fraction of the normal-polarity magnetizaton resides in hematite, representing either a DRM or CRM. In any case, no paleomagnetic evidence was found that the HV-1 sediments have ever been subjected to a reversed-polarity geomagnetic field.

HV-2

Two samples (HV-2-5 and HV-2-7) from HV-2 in north Heber Valley exhibited excellent reversed-polarity directions. These samples are from a lens of silty alluvium interbedded with fluvial gravels in a terrace ~100 feet above the Provo River. In both samples, a small normal-polarity component was removed upon AF demagnetization to 50 Oe. Between 50 Oe and 1000 Oe, a reversed-polarity magnetization decayed linearly to the origin of the vector demagnetization diagrams, and the observed direction was within 20° of being antiparallel to the PADF. The reversed-polarity magnetization was generally unaffected by AF demagnetization above 700 Oe, suggesting that part of the reversed-polarity component resides in a very high-coercivity species such as hematite. This was also indicated upon thermal demagnetization of one of the specimens (HV-2-7) that had already been AF demagnetized; presence of the reversed-polarity magnetization above 600°C suggests either a reversed-polarity DRM or CRM residing in hematite. Thus, the sediments sampled in HV-2 contain an excellent record of deposition or diagenesis in a reversed-polarity field.

Exposure DC-1

Two samples (DC-1-2 and DC-1-3) were analyzed from fine-grained (silty) alluvium in a roadcut through a terrace ~100 to 150 feet above Deer Creek Reservoir. Thermal demagnetization of Sample DC-1-2 indicated the presence of a reversed-polarity magnetization with a blocking temperature between 540° and 600°C. AF demagnetization of

Sample DC-1-3 also revealed a reversed-polarity magnetization with high coercivity (>1,000 Oe); a normal-polarity magnetization, which predominates through 250 Oe, could represent either a primary DRM or secondary VRM residing in coarser grains of magnetite. In both samples, the AF or thermal demagnetization treatments yielded remanence directions within ~40° of a direction antiparallel to the PADF direction. Thus, the two samples from DC-1 provide excellent evidence for a reversed-polarity magnetization of either primary (DRM) or secondary (CRM) origin.

RV-1

Initially, three samples (RV-1, -2, -3) were collected and analyzed from RV-1 in fine-grained (silt and clay) slopewash deposits in a large alluvial fan on the south side of Round Valley. Directions of NRM were somewhat scattered about the PADF direction, suggesting the presence of an underlying reversed-polarity magnetization. A reversed-polarity direction was not clearly revealed, however, upon either AF demagnetization to 1000 Oe or thermal demagnetization to 660°C.

As a further check on the possibility of reversed-polarity magnetization in RV-1, an additional 4 samples (RV-1-4, -5, -6, -8) were analyzed. As in the initial suite of samples, the NRM directions of all 4 resamples deviated significantly from the PADF direction, suggesting the possible superposition of normal- and reversed-polarity magnetizations. The normal-polarity magnetization probably resides chiefly in magnetite, because in sample RV-1-2 about 80% of the NRM intensity was destroyed by moderate peak AF fields of 400 Oe. This normal-polarity magnetization could represent VRM and/or DRM in grains of detrital magnetite. In contrast, the presence of a reversed-polarity magnetization was most strongly suggested by thermal demagnetization results from three samples (RV-1-1, -4, -6); remanence directions from all three samples approach within 90° of being antiparallel to the PADF. The reversed-polarity component must reside in hematite, because it is still present upon demagnetization at and above 600°C. A reversed-polarity magnetization residing in hematite could represent either a primary DRM or a secondary CRM produced by diagenesis or

weathering. In either case, the paleomagnetic evidence suggests that the sediments sampled in RV-1 have been subjected to a reversed-polarity geomagnetic field at some time during their history.

WD-1

Three samples were analyzed from WD-1 in a sand lens within fluvial gravels near Wanship Dam. These gravels form terraces 80 to 100 feet above the river channel. The NRM of all three samples was dominated by normal-polarity magnetization. This magnetization probably represents viscous remanent magnetization (VRM) and/or DRM in magnetite, because 70% of the NRM can be destroyed by AF demagnetization in a moderate peak field of 400 Oe. Between 10% and 17% of the NRM survives thermal demagnetization to 600°C and hence apparently resides in hematite. This hematite may record either a primary DRM or secondary CRM. The only hint of reversed polarity in these samples is the appearance of negative-inclination directions in the two thermally demagnetized samples at the highest (>600°C) demagnetization steps; these negative-inclination directions may merely reflect random, spurious magnetizations imparted during the demagnetization treatment. Considering the relatively coarse grain size of these sediments, however, it is likely that any primary reversed-polarity magnetization would have been heavily overprinted with normal-polarity VRM in the coarser grains of magnetite. Hence, the paleomagnetic evidence pertaining to the age of these sediments is equivocal.

Soil Pit WV-16

Three samples (WV-16-1, 2, 3) were analyzed from a loessial colluvium overlying pediment gravels in WV-16 on the west side of Morgan Valley. The surface soil is probably pre-Bull Lake, and WV-16 is hundreds of meters above the valley floor. The NRM directions of all three samples deviated from the PADF by amounts ranging from 60° to 150°; this distribution suggested that all three samples might contain superimposed normal- and reversed-polarity magnetizations. Two samples (WV-16-1

and WV-16-2) subjected to thermal demagnetization exhibited generally stable paleomagnetic directions, indicating that the normal- and reversed-polarity magnetizations have similar blocking-temperature spectra and probably reside in the same mineral (hematite?). Only 1.5% to 3.3% of the NRM intensity survived heating above the Curie point of magnetite; on this basis, any reversed-polarity magnetization could reside either in magnetite or hematite. In the one sample (WV-16-3) that was AF demagnetized, the reversed polarity component apparently has lower coercivity than the normal-polarity component; this suggests that the reversed-polarity magnetization could be a DRM residing in magnetite. In any case, the paleomagnetic results strongly suggest that these sediments in WV-16 have experienced a reversed-polarity geomagnetic field at some time during their history.

DISCUSSION

Sediments from the Jordanelle damsite and vicinity apparently have recorded a complex paleomagnetic history that should prove invaluable in determining recency of faulting. Originally, the NRM of these sediments was probably dominated by a primary DRM acquired penecontemporaneously with deposition. This DRM probably resided chiefly (~95%) in magnetite and partly (~5%) in hematite. Secondary magnetizations later overprinted this DRM, adding to the complexity of the paleomagnetic record. One common form of secondary magnetization is VRM in magnetite which, in sand-size particles, is magnetically "soft" and tracks the changes in the ambient magnetic field; VRM in coarse-grained magnetite would have normal polarity, low coercivity (<250 Oe), and low blocking temperature (<300°C). As the sediments undergo diagenesis or weathering, some of the detrital magnetite will become oxidized, forming authigenic hematite. The authigenic hematite will then record a secondary CRM, which can achieve very high coercivity (>1,000 Oe) and blocking temperature (up to 680°C) as the grains grow in size. Growth of authigenic hematite at the expense of detrital magnetite is accompanied by a significant reduction in NRM intensity, because magnetite is ~200 times more magnetic than an equivalent volume of hematite. If diagenesis proceeds over ~10^6 years, the CRM will

probably be a composite of both normal and reversed polarity, reflecting growth of hematite during several normal- and reversed-polarity epochs. Thus, a single sediment sample commonly contains many different magnetizations: (1) DRM of normal or reversed polarity residing in detrital grains of magnetite and hematite; (2) CRM of normal and/or reversed polarity residing in authigenic hematite; and (3) VRM of normal polarity residing in coarse-grained magnetite.

Recognizing and separating these multiple magnetizations can be a formidable challenge to the paleomagnetist, particularly when (as in this study) fewer than 5 samples are analyzed from any given unit. For example, if any one component dominates the others by greater than a factor of ~100, the weaker magnetizations would probably go undetected during a reconnaissance study. Moreover, neither identifying the magnetic mineralogy nor the stability to demagnetization treatments provides unambiguous proof as to which magnetizations are primary and which are secondary.

Nevertheless, by integrating the paleomagnetic, rock magnetic, and geologic evidence, it is commonly possible to derive a synthesis that is far more powerful than any given observation taken by itself. For example, finding an excellent, single-component, reversed-polarity magnetization in a sample can never establish an age >730,000 years at probability >97.4%, because it is now recognized that about 19,000 years of the most recent (Brunhes) normal-polarity epoch (730,000 years B.P. to present) was characterized by one or more short (10^3 - 10^4 yr) reversed-polarity "events" (Figure 3). On the other hand, finding a two-polarity CRM, replete with occasional stable, scattered remanence directions, can establish a >730,000 year age at close to 100% confidence, by the following reasoning. Authigenic growth of hematite probably occurs over very long time intervals, perhaps 10^7 years for continental red beds (cf. Larson et al., 1982). Thus, any two-polarity CRM probably would have been acquired over a timescale comparable to the entire length of the Brunhes (~10^6 years). It would be highly improbable for any paleomagnetic sample to exhibit a reversed-polarity CRM dating from the 19,000 years of reversed polarity within the

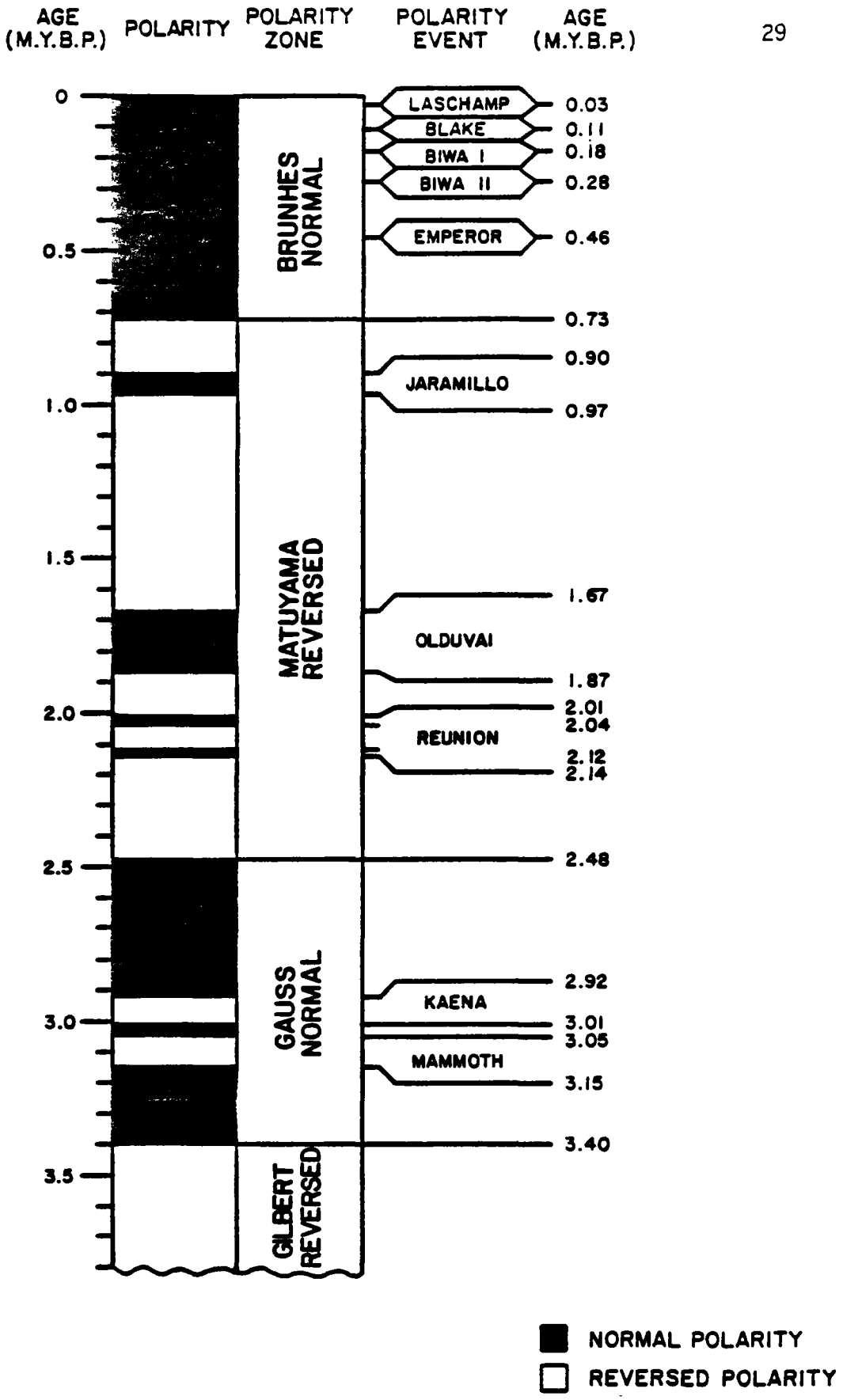

Figure 3: Geomagnetic polarity time scale for the past 3.8 million years. Compiled from Champion and others (1981) and Mankinen and Dalrymple (1979).

Brunhes, because this reversed-polarity component would be cancelled by a larger, normal-polarity component reflecting CRM acquired over the rest of the Brunhes.

In principle, therefore, discovering a two-polarity secondary CRM in a Quaternary sediment would provide far stronger evidence for an age >730,000 years than would discovery of a reversed-polarity DRM. Two-polarity CRM in secondary hematite has been documented by Roy and Park (1974) in Mississippian red beds of New Brunswick, by Larson et. al. (1982) in Triassic red beds of the Colorado Plateau, and by Van Alstine and Gillett (1979) in Precambrian siltstones and limestones from the southern Great Basin. Van Alstine (proprietary technical reports) has also found two-polarity CRM in Quaternary sediments from elsewhere in the western U.S. It should be emphasized that a sample containing two-polarity CRM will exhibit a paleomagnetic direction parallel or antiparallel to the PADF direction only if the ratio of normal- to reversed-polarity component is outside the range ~40% to 60%. As discussed by Larson et al. (1982), if this ratio is within the 40% to 60% range, then stable but scattered remanence directions can result. The stability of the deviating directions upon AF and thermal demagnetization reflects the fact that the normal- and reversed-polarity magnetizations, both of which reside in a similar generation of authigenic hematite, have the same blocking-temperature and coercivity spectra.

In summary, scattered, stable remanence directions that survive thermal demagnetization to 600°C suggest that two-polarity CRM may be present. Paleomagnetic analysis of additional samples from a suspected unit might yield a sample in which the proportion of reversed-polarity components is >60%, in which case a stable direction antiparallel to the PADF would be observed. Any Quaternary sediment sample exhibiting a remanence direction >30° from the PADF (i.e., outside the range of normal "secular variation" of the instantaneous geomagnetic field) might contain either a two-polarity CRM or reversed-polarity CRM or DRM.

Because the emphasis of this study was on establishing which sedimentary units near the Jordanelle damsite contain reversed polarity, a summary tabulation of the reversed-polarity occurrences is presented in Table 1. It must be emphasized that finding reversed polarity indicates that a unit was deposited >730,000 years ago with a probability >97.4%; failure to find reversed polarity in principle tells little about age, because a sediment could have been deposited during a normal-polarity epoch preceding the Brunhes or could have been completely remagnetized within the Brunhes. On the other hand, there is strong evidence that many of the older Quaternary basin fill sediments in the proposed Jordanelle reservoir contain authigenic hematite that grew during the Matuyama reversed epoch; thus, complete absence of reversed-polarity magnetizations would be highly suggestive of an age <730,000 years, unless a given unit were highly resistant to formation of authigenic hematite or perhaps contained a very strong VRM in coarse-grained magnetite.

Those sites included in the "excellent" to "good" columns of Table 1 yield at least some magnetization directions within 45° of being antiparallel to the PADF; these sites almost certainly contain sediments older than 730,000 years B.P.

The Round Valley site RV-1 is somewhat problematic because the directions remain almost exactly intermediate between normal and reversed polarity; additional sampling will probably be required to determine the exact cause of these intermediate directions.

Those sites showing a "suggestion" of reversed-polarity magnetization yield stable but scattered remanence directions, or remanence directions that trend away from the PADF upon demagnetization. One source of this scatter could be reversed-polarity magnetization reflecting great antiquity (>730,000 years). On the other hand, other sources of scatter include spurious magnetizations acquired during sampling or demagnetization, lightning strikes, rotations of coherent blocks, local tectonic rotations, and sample orientation errors. All units with a "suggestion" of reversed polarity should be resampled if they are especially important in evaluating the recency of faulting.

TABLE 1: Estimated Probability of Reversed-Polarity Magnetizations (by sample site)

Excellent†	Good††	Suggestion*	No Sign δ
JT-2	JT-7B	JT-8 (middle)	JT-8 (upper)
JT-7A	JT-11 (upper)	JT-8 (lower)	JT-9
DC-1	JT-11 (lower)	JT-10	J-4
HV-2	J-13	J-6A	J-17
	J-16	J-6B	HV-1
	WV-16	J-15 (upper)	
		J-15 (lower)	
		DH-R-104	
		DH-R-110	
		DH-R-111	
		DH-R-114	
		RV-1	
		WD-1	

Notes:

† Most samples exhibit remanence directions within 45°of being antiparallel to the present axial dipole field (PADF) direction.

†† Some samples exhibit remanence directions within 45° of being antiparallel to the PADF direction.

* The presence of a reversed-polarity component is suggested by either (1) scattered remanence directions (deviating from the PADF) that do not change appreciably upon AF or thermal demagnetization; or (2) remanence directions migrating away from the PADF upon demagnetization.

δ All remanence directions are within 30° of the PADF. If reversed-polarity components are present, they are overprinted by normal-polarity magnetization by ~ two orders of magnitude.

The five sites showing "no sign" of reversed-polarity magnetization yield remanence directions that are within 30° of the PADF direction and that trend toward the origin of vector demagnetization diagrams. As discussed earlier, caution must be exercised in interpreting absence of reversed polarity as evidence for deposition <730,000 years B.P.; this is especially true for sediments containing sand-size magnetite which could record a predominant normal-polarity VRM.

CONCLUSIONS

Nearly half of 18 trenches and pits in Quaternary basin fill sediments and colluvium near the Jordanelle damsite contain good to excellent records of reversed-polarity magnetization that almost certainly (P>97.4%) was acquired prior to 730,000 years B.P. Some of this reversed-polarity magnetization probably represents detrital remanent magnetization acquired penecontemporaneously with deposition. Much of this reversed-polarity magnetization, however, may reflect chemical remanent magnetization acquired during prolonged growth of authigenic hematite at the expense of detrital magnetite. Thus, even units deposited during normal-polarity epochs prior to the Brunhes may contain a paleomagnetic record of diagenesis or weathering during reversed-polarity times. The widespread occurence of reversed-polarity magnetization in the Quaternary basin fill deposits of Keetley Valley and vicinity indicates that much of the proposed Jordanelle reservoir is probably underlain by sediments deposited more than 730,000 years ago.

REFERENCES

Champion, D.E., Dalrymple, G.B., and Kuntz, M.A., 1981, Radiometric and paleomagnetic evidence for the Emperor reversed polarity event at 0.46 + 0.05 m.y. in basalt lava flows from eastern Snake River Plain, Idaho: Geophys. Res. Lett., v. 8. p. 1055-1058.

Fisher, R.A., 1953, Dispersion on a sphere: Proc. Roy. Soc. Lond., v. A125, p. 54-59

Johnson, H.P., 1979, Paleomagnetism of igneous rock samples--DSDP Leg 45: Initial Repts. Deep Sea Drilling Project, v. 45, P. 387-395.

Kirschvink, J.L., 1980, The least-squares line and plane and the analysis of palaeomagnetic data: Geophys. Jour. Roy. Astron. Soc., v. 62, p. 699-718.

Larson, E.E., Walker, T.R., Patterson, P.E., Hoblitt, R.P., and Rosenbaum, J.G., 1982, Paleomagnetism of the Moenkopi Formation, Colorado Plateau: Basis for long-term model of acquisition of chemical remanent magnetism in red beds: Jour. Geophys. Res., v. 87, p. 1081-1106.

Mankinen, E.A., and Dalrymple, G.B., 1979, Revised geomagnetic polarity time scale for the interval 0-5 m.y.B.P.: Jour. Geophys. Res., v. 84, p. 615-626.

McElhinny, M.W., 1973, Palaeomagnetism and plate tectonics: Cambridge Univ. Press, 358 pp.

Roy, J.L., and Park, J.K., 1974, The magnetization process of certain red beds: Vector analysis of chemical and thermal results: Can. Jour. Earth Sci., v. 11, p. 437-471.

Van Alstine, D.R., and Gillett, S.L., 1979, Two-polarity late Tertiary CRM in some upper Precambrian sedimentary rocks from the southern Great Basin (abstract): Trans. Am. Geophys. Un. (Eos), v. 60, p.816.

Van Alstine, D.R., and Gillett, S.L., 1981, Magnetostratigraphy of the Columbia River Basalt, Pasco Basin and vicinity, Washington: Rockwell Hanford Operations, Richland, Washington, RHO-BWI-C110, 60 pp.

Van Alstine, D.R., and Gillett, S.L., 1982, Magnetostratigraphy of the Wanapum and Grande Ronde Basalts, Pasco Basin, Washington: Rockwell Hanford Operations, Richland, Washington, in press.

APPENDIX A: Paleomagnetic Sample Nomenclature

This appendix documents the sample nomenclature used during the course of this paleomagnetic study. The samples were received and analyzed in 8 batches, designated BuRec #1 to #8 in column 1 of this Appendix. The preliminary site name is designated in column 2. Later in this investigation, a consistent terminology was implemented for naming (and renaming) the sites. Trenches in the Keetley Valley were prefixed by "JT-"; soil pits and other exposures in the Keetley Valley were prefixed by "J-". Data from drillcores (all from BuRec #2 and #3) are designated by the prefix "DH-R-". Other final site designations are as follows: HV = Heber Valley; DC = Deer Creek; RV = Round Valley; WD = Wanship Dam; WV = Weber Valley. Also listed are the relative stratigraphic positions (if more than one horizon was sampled at a site) and the geologic units from which the samples were derived.

JORDANELLE PALEOMAGNETIC SAMPLES

BuRec #	Preliminary Name	Final Name	Sample #	Rel. Strat. Pos.	Geologic Unit
1	Jord. Trench 2	JT-2	A1,A2,A3	upper	Pao
1	"	JT-2	B1,B2,B3,B4	middle	Pao
1	"	JT-2	C1,C2,C3	lower	Pao
3	B	JT-7A	2,4		Pao
6	WT	JT-7B	2,3		Pao
5	CT	JT-8	2,3	upper	Pa or Pao
5	CT	JT-8	4,5	middle	Pa or Pao
5	CT	JT-8	8,10	lower	Pao
8	CT	JT-8	11,12,13,14,15	lower	Pao
7	JT-8	JT-9	1,2		~~Qc/O~~ Qc or Qaf
8	JT-10	JT-10	1,2,3,4,5		Pao or younger slopewash?
	JT-11	JT-11	"		
6	J-4	J-4	1,3		Pao
4	J-6	J-6A	1,2,3	upper	Qc/Pao
8	J-6	J-6B	4,5,6,7,8	lower	Pao
6	J-13	J-13	1,3		Pao
8	J-15	J-15	1,2,3	upper	Pao
8	J-15	J-15	4,5,6	lower	tephra in Pao
3	C	J-16	1,5		Pao
4	C	J-16	6		Pao

EXPLANATION

QUATERNARY — HOLOCENE: Ha, Haf; PLEISTOCENE: Pay, Pa, Pao, ?; Qc, ?

HOLOCENE
- Ha- floodplain alluvium
- Haf-alluvial fan deposits

PLEISTOCENE
- Pay-younger alluvium
- Pa-alluvium
- Pa/ao-alluvial fan deposits overlying older basin fill
- Pao-older basin fill

QUATERNARY, undifferentiated
- Qc-colluvium
- Qc/Pao-colluvium overlying older basin fill
- Qls-landslide deposits

LOWER TERTIARY (Tkj, Tm, Tpp, Tv, Tki; Tksc, Ts, Tkcb, Tku)
- Tkj-Jordanelle stock: andesite porphyry
- Tpp-Park Premier stock: rhyodacite porphyry
- Tm-Mayflower stock: granodiorite porphyry
- Tv-Valeo stock: granodiorite porphyry
- Tki-intrusive andesite and andesite autobreccia
- Tg-unconsolidated alluvial and colluvial deposits
- Tku-Keetley volcanics, undivided
- Tksc-volcanic breccia of Silver Creek: light grey rhyodacitic to andesitc volcanic breccia
- Tkcb-volcanic breccia of Coyote Canyon: rhyodacitic to andesitic tuff breccia, rubble breccia, and lapilli tuff

MESOZOIC AND PALEOZOIC (TRIASSIC: Rt, Rw, Ru; PENNSYLVANIAN, PERMIAN: PRpc, Pw, Prv)
- Rt-Thaynes Formation: brown-weathering, fine-grained, limey sandstone, siltstone, shale, and grey limestone
- Rw-Woodside Shale: dark and purplish-red shale, siltstone, and grey fine-grained sandstone
- Ru-sedimentary rocks, undivided
- PRpc-Park City Formation: grey limestone and tan sandstone
- Pw-Weber Quartzite: grey-weathering and tan-weathering quartzite and sandstone with some interbedded white limestone and dolomite
- Prv-Round Valley Limestone pale grey limestone

- ●R4 5977Tkj (220) — drill hole with elevation of the base and the thickness of basin fill in feet
- ▲ soil pit
- ■ paleomagnetic sample location
- d mine dump
- J-13 exploratory trench
- contact, dashed where approximately located
- fault, dashed where approximatley located, dotted where concealed, queried where existence and location are uncertain

Bedrock geology slightly modified from Bromfield and others (1970), Bromfield and Crittenden (1971), and Bridges (1984).

See Table 3.1 for detailed description of Quaternary units.

0 METERS 500 1000 1500
0 FEET 1000 2000 3000 4000 5000

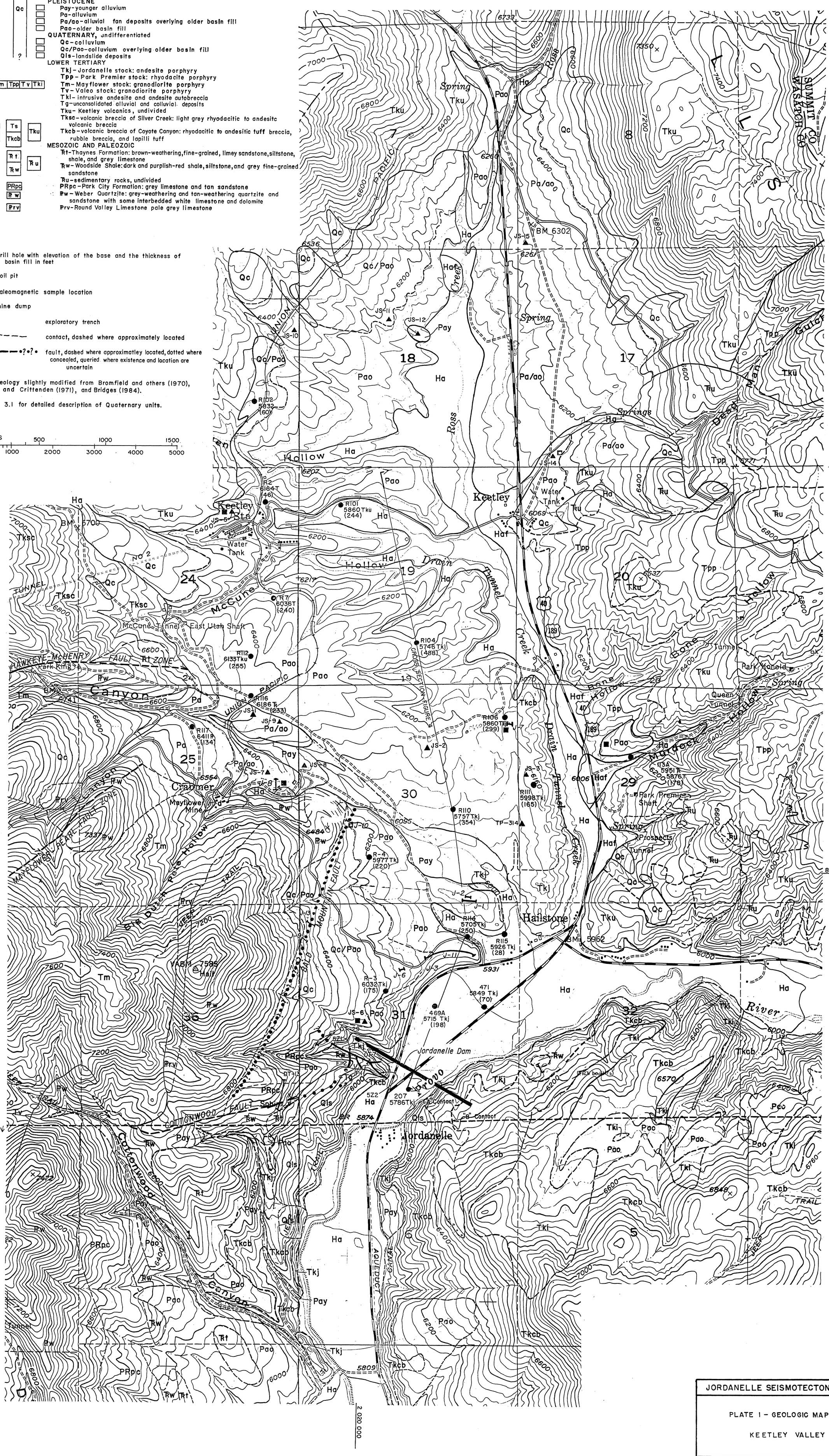

JORDANELLE SEISMOTECTONIC STUDY

PLATE 1 - GEOLOGIC MAP OF KEETLEY VALLEY